Design of polymer materials for innovative foams

Liutong Hou

N°d'ordre NNT : 2023ISAL0052

THESE de DOCTORAT DE L'INSA LYON,
Membre de l'Université de Lyon

Ecole Doctorale N° 34
Ecole Doctorale de Matériaux de Lyon

Spécialité/ discipline de doctorat : Matériaux Polymères et Composites

Soutenue publiquement le 19/07/2023, par :
Liutong HOU

Design of polymer materials for innovative foams

Devant le jury composé de :

KOTEK Jiri	Professeur (Czech Academy of Sciences)	Examinateur
NANNI Francesca	Professeur (University of Rome Tor Vergata)	Rapporteuse
LEROY Eric	Directeur de recherche (Nantes Université)	Rapporteur
DUCHET-RUMEAU Jannick	Professeur (INSA Lyon)	Directrice de thèse
GÉRARD Jean-François	Professeur (INSA Lyon)	Co-Directeur de thèse
LIVI Sébastien	Professeur (INSA Lyon)	Co-Encadrant

Département FEDORA – INSA Lyon - Ecoles Doctorales

SIGLE	ECOLE DOCTORALE	NOM ET COORDONNEES DU RESPONSABLE
CHIMIE	**CHIMIE DE LYON** **https://www.edchimie-lyon.fr** Sec. : Renée EL MELHEM Bât. Blaise PASCAL, 3e étage secretariat@edchimie-lyon.fr	**M. Stéphane DANIELE** C2P2-CPE LYON-UMR 5265 Bâtiment F308, BP 2077 43 Boulevard du 11 novembre 1918 69616 Villeurbanne **directeur@edchimie-lyon.fr**
E.E.A.	**ÉLECTRONIQUE, ÉLECTROTECHNIQUE, AUTOMATIQUE** **https://edeea.universite-lyon.fr** Sec. : Stéphanie CAUVIN Bâtiment Direction INSA Lyon Tél : 04.72.43.71.70 secretariat.edeea@insa-lyon.fr	**M. Philippe DELACHARTRE** INSA LYON Laboratoire CREATIS Bâtiment Blaise Pascal, 7 avenue Jean Capelle 69621 Villeurbanne CEDEX Tél : 04.72.43.88.63 **philippe.delachartre@insa-lyon.fr**
E2M2	**ÉVOLUTION, ÉCOSYSTÈME, MICROBIOLOGIE, MODÉLISATION** **http://e2m2.universite-lyon.fr** Sec. : Bénédicte LANZA Bât. Atrium, UCB Lyon 1 Tél : 04.72.44.83.62 secretariat.e2m2@univ-lyon1.fr	**Mme Sandrine CHARLES** Université Claude Bernard Lyon 1 UFR Biosciences Bâtiment Mendel 43, boulevard du 11 Novembre 1918 69622 Villeurbanne CEDEX **sandrine.charles@univ-lyon1.fr**
EDISS	**INTERDISCIPLINAIRE SCIENCES-SANTÉ** **http://ediss.universite-lyon.fr** Sec. : Bénédicte LANZA Bât. Atrium, UCB Lyon 1 Tél : 04.72.44.83.62 secretariat.ediss@univ-lyon1.fr	**Mme Sylvie RICARD-BLUM** Institut de Chimie et Biochimie Moléculaires et Supramoléculaires (ICBMS) - UMR 5246 CNRS - Université Lyon 1 Bâtiment Raulin - 2ème étage Nord 43 Boulevard du 11 novembre 1918 69622 Villeurbanne Cedex Tél : +33(0)4 72 44 82 32 **sylvie.ricard-blum@univ-lyon1.fr**
INFOMATHS	**INFORMATIQUE ET MATHÉMATIQUES** **http://edinfomaths.universite-lyon.fr** Sec. : Renée EL MELHEM Bât. Blaise PASCAL, 3e étage Tél : 04.72.43.80.46 infomaths@univ-lyon1.fr	**M. Hamamache KHEDDOUCI** Université Claude Bernard Lyon 1 Bât. Nautibus 43, Boulevard du 11 novembre 1918 69622 Villeurbanne Cedex France Tél : 04.72.44.83.69 **hamamache.kheddouci@univ-lyon1.fr**
Matériaux	**MATÉRIAUX DE LYON** **http://ed34.universite-lyon.fr** Sec. : Yann DE ORDENANA Tél : 04.72.18.62.44 yann.de-ordenana@ec-lyon.fr	**M. Stéphane BENAYOUN** Ecole Centrale de Lyon Laboratoire LTDS 36 avenue Guy de Collongue 69134 Ecully CEDEX Tél : 04.72.18.64.37 **stephane.benayoun@ec-lyon.fr**
MEGA	**MÉCANIQUE, ÉNERGÉTIQUE, GÉNIE CIVIL, ACOUSTIQUE** **http://edmega.universite-lyon.fr** Sec. : Stéphanie CAUVIN Tél : 04.72.43.71.70 Bâtiment Direction INSA Lyon mega@insa-lyon.fr	**M. Jocelyn BONJOUR** INSA Lyon Laboratoire CETHIL Bâtiment Sadi-Carnot 9, rue de la Physique 69621 Villeurbanne CEDEX **jocelyn.bonjour@insa-lyon.fr**
ScSo	**ScSo*** **https://edsciencessociales.universite-lyon.fr** Sec. : Mélina FAVETON INSA : J.Y. TOUSSAINT Tél : 04.78.69.77.79 melina.faveton@univ-lyon2.fr	**M. Bruno MILLY** Université Lumière Lyon 2 86 Rue Pasteur 69365 Lyon CEDEX 07 **bruno.milly@univ-yon2.fr**

*ScSo : Histoire, Géographie, Aménagement, Urbanisme, Archéologie, Science politique, Sociologie, Anthropologie

Acknowledgements

How time flies! I still remember the 30th September 2019, the first day I arrived in France. Until now, with this doctoral thesis finished, 42 months have passed and my journey as a PhD student comes to its end. When I look back in IMP, in Lyon, and in France, I feel so lucky to have such a beautiful journey with so many kind people by my side. Without their help, support and encouragement, my thesis work would not have been possibly finished.

I would like to express my sincerest gratitude to my supervisors, who accepted as their PhD student and accompanied me all the work along the beautiful journey in France. Thank Prof. Jannick DUCHET-RUMEAU for her guidance and kind help on my research. With no doubt that I have learned so much from her, especially her solid experience of composite materials, her insight into the polymer science and her vision of a good work. Her smile, "well done" and "good job" have always inspired and warmed me, no matter the challenges of my research and life. I also appreciate her patience in guiding and understanding me, especially when I am impatient and need help. She can always give me invaluable insights into my research. Without her, I even cannot imagine how to overcome the problems time and time again. Thank Prof. Jean-François GÉRARD for his kind guidance and for sharing his knowledge. In every discussion, I got a lot out of it. I have benefited a lot from his rigorous academic attitude and open-minded attitude towards research and life. I also express my great thanks to Prof. Sébastien LIVI for his kind help during these years, whenever I need him. His rich knowledge in structuration of polymers by adding ionic liquids, his passionate enthusiasm for research, and his constant good mood for work always motivate me to be strong, be positive and be professional with our work.

In addition to my supervisors, I would like to thank the members of my defense committee who have accepted to review and examine this work. I would like to thank Prof. Francesca NANNI and Dr. Eric LEROY for reviewing the manuscript, and Prof. Jiri KOTEK for examining this work. Thanks for their time, interest, insightful remarks, and helpful comments. It is a great honor to have you as my defense jury.

This work was supported by China Scholarship Council (CSC) and done in the laboratory

Ingénierie des Matériaux Polymères in INSA Lyon (IMP@INSA). Thanks for the financial support from CSC and all the members in IMP@INSA. Thank Pierre ALCOUFFE for the TEM and SEM analysis, Guilhem QUINTARD for the rheology property and Xavier MORELLE for the mechanical property, Ahmed BELHADJ for the thermal properties, and Carlos FERNANDEZ DE ALBA, Patrick GOETINCK, Fernande BOISSON for the help of NMR analysis. Thank Isabelle POLO, Mallaouia BENGOUA, and Sylvain BAUDU for their kindly help in the lab. Thank Gabriel PERLI for the help of synthesis. Thank Victor HADDAD, Adrien TOPALIAN, Laurent REMY, Carolina Helena FRANZON for sharing the time in the lab. Thank especially Ting SHI for helping me adapt to the lab quickly. Thank all the professors, technicians, PhD students, and postdoc researchers for your welcome, kindness, and sharing of knowledge during the past three years.

Thank all my best office members. It is really lucky for sharing the same office with you. Thank Dr. Younes EL OMARI and Dr. Raissa GALLU for all the help from the very first day when I arrived in France, I will never forget your kindness, your advice, and discussions. Especially thank you for all the help and all the praises every day. Thank Dr. Celso Yassuo Okada Junior for helping on the chemistry. Thank all the Chinese students in the lab. Jixiang LI, Hu QIAO and Yiping CHEN for your help and kindness, thank you for all the exciting moments and experiences together.

I would like to express all my appreciation to my Chinese friends, Jiqing HUANG, Yulei QIN, Cong YOU, Xiaorui WANG, Wenxiang SUN, Feng WANG, Haosheng LIANG, Qilin XIN, Hao HONG. It is all of you that make my life in France happier, more enriched and fulfilled. I do believe it is a kind of special fate that allows us to meet in France and become friends.

The deepest thanks and love to my beloved family and my girlfriend. It is your support that keeps me bravely pursuing my dream and becoming the person that I want to be. Especially, I would like to thanks my girlfriend, Yufei WANG, it must have been a special fate that made us meet, fall in love and get to know each other in Lyon, France, a city 100,000 miles away from our homeland. Thank you for being the one who made me feel at home. We have snuggled up to each other and took care of each other throughout the years, especially when we contracted the COVID-19. Thank you for being understanding and tolerant of my quick temper, you taught me to reconcile with myself. In the past three years, we have set foot in more than ten countries on the European continent together, among which my most favorite days in Northern Europe were as if the whole world was just the two of us. As we are about to

fall in love for three years, I would like to ask if you will marry me? From now on, a day with two souls, three meals through four seasons, seven emotions, six desires, five flavors, a lifetime.

Finally, thank myself for never giving up even when facing all the difficulties during my PhD, just like all the medical workers in the pandemic COVID-19. Thank myself for always working hard to be a strong, independent, free and better person. There is a long journey to go, I will always keep going forward, always staying true to myself, and let my heart be my guide.

Thank you all and love you all.

Liutong HOU

Lyon, France

July, 2023

Acknowledgements

献给我的法兰西青春岁月

Dédié à mes jeunes années en France

Stay true to yourself, and let your heart be your guide

Reste fidèle à toi-même et laisse ton cœur te guide

Abstract

By combining polypropylene grafted (PPgMA) and ionic liquids (ILs), the new generation of ionomers (denoted as LIonomers) has been designed and tailored for the first time in this work. The LIonomers owing best properties are then used to prepare lightweight materials considering supercritical carbon dioxide ($scCO_2$) as the physical agent. In the first section, four phosphonium-based ionic liquids (PhILs) and two imidazolium-based ionic liquids (ImILs) have been mixed with PPgMA to prepare LIonomers via the interactions between cation/anion pairs and polar groups of PPgMA. The structuration of ILs in LIonomers occurs from a nano/microphase separation process. The existence of strong ionic-ionic and ionic-dipolar interactions could be activated in several conditions. Such IL/polymer combinations prove the existence of interactions between the maleic anhydride group and the cation or anion composing the ionic liquid and then generating an ionic network highlighted by the improved molten strength. These interactions can be tuned by the nature of cation and anion, but also depend on the IL content and MA content. ILs could also affect the crystallization process according to different pathways. Thanks to the maleic anhydride/IL interactions, an excellent compromise between stiffness and stretchability could be achieved under some specific conditions, paving the way for processing new polyolefin-based materials. In the second section, one functional imidazolium-based ionic liquid is cooperated with PPgMA to realize another new kind of LIonomers. The effect of four factors, *i.e.* maleic anhydride (MA) and IL content, dispersion of ionic liquid and the length of “liquid-like branches” assembling from the cation/anion pairs of IL, on the solid and melt state properties have been studied. The reactivity of this amino functionalized IL could not only enhance the compatibility with the PPgMA matrix and as a result dispersion (nanoscale), but also impact the relaxation behavior, particularly rigid amorphous fraction (RAF) where they locate. Thanks to the presence of the

terminated amino group, the intensity of generated ionic network within such LIonomer tends to be stronger than others obtained in previous work. In addition, the properties of several prepared LIonomers have been compared with that of traditional Zn-Ionomers. The LIonomers display considerable tunability thanks to the characteristic-limitless anion-cation combinations of ILs. The application of lightweight materials is realized using supercritical carbon dioxide ($scCO_2$) as the physical agent. In the last section, the foaming strategy has been conducted on some selected LIonomers owning outstanding overall performance. The foamability and compressive properties of pure PPgMA have been improved significantly thanks to the successful design of LIonomers. Therefore, this work focused on the designing new generation of ionomers, *i.e.* LIonomers, by combining polypropylene grafted maleic anhydride and ionic liquids, investigating and understanding the interactions and structurations as a function of the tunability of cation and anion of ionic liquids, as well as studying their potential application on lightweight materials. Thanks to the special components of ionic liquids and outstanding comprehensive properties, numerous research routes and technological applications will be offered based on our results.

Keywords: LIonomers, ionic liquids, polypropylene grafted maleic anhydride, microcellular foams, supercritical CO_2

Résumé

En combinant du polypropylène greffé (PPgMA) et des liquides ioniques (ILs), la nouvelle génération d'ionomères (appelés LIonomers) a été conçue et adaptée pour la première fois dans ce travail. Les LIonomères ayant les meilleures propriétés seront ensuite utilisés pour préparer des matériaux légers en utilisant du dioxyde de carbone supercritique (scCO2) comme agent physique. Dans la première section, quatre liquides ioniques à base de phosphonium (PhIL) et doux liquides ioniques à base d'imidazolium (ImIL) ont été mélangés avec du PPgMA pour préparer des LIonomères via les interactions entre les paires cation/anion et les groupes polaires du PPgMA. La structuration des LI dans les LIonomères se produit à partir d'un processus de séparation nano/microphase. L'existence d'interactions ioniques-ioniques et ioniques-dipolaires qui pourraient être activées dans plusieurs conditions. De telles combinaisons IL/polymère prouvent l'existence d'interactions entre le groupe anhydride maléique et le cation ou l'anion composant le liquide ionique. Ces interactions peuvent être accordées par la nature du cation et de l'anion mais dépendent également de la teneur en IL et en MA. Les ILs peuvent également affecter le processus de cristallisation selon différentes voies. Grâce aux interactions anhydride maléique/IL, un excellent compromis entre la rigidité et l'étirabilité a pu être obtenu dans certaines conditions spécifiques, ouvrant la voie au traitement de nouveaux matériaux à base de polyoléfines. Dans la deuxième section, un liquide ionique fonctionnel à base d'imidazolium a coopéré avec le PPgMA pour réaliser un autre nouveau type de LIonomères. L'effet de quatre facteurs, à savoir la teneur en anhydride maléique (MA) et en IL, la dispersion du liquide ionique et la longueur des "branches de type liquide" assemblées à partir des paires cation/anion de l'IL sur les propriétés à l'état solide et à l'état fondu, a été étudié. La réactivité de ce liquide ionique amino-fonctionnalisé pourrait non seulement améliorer la compatibilité avec la matrice

PPgMA et par conséquent la dispersion (à l'échelle nanométrique), mais aussi avoir un impact sur le comportement de relaxation, en particulier sur la fraction amorphe rigide (RAF) où ils sont situés. Grâce à la présence d'un groupe amino terminé, l'intensité du réseau ionique généré dans ce LIonomère tend à être plus forte que celle obtenue dans les travaux précédents. En outre, les propriétés de plusieurs LIonomères préparés ont été comparées à celles du Zn-Ionomer traditionnel. En conclusion, les LIonomères montrent une tunabilité considérable grâce aux combinaisons anion-cation caractéristiques et illimitées des ILs. L'application sur des matériaux légers est réalisée en utilisant du dioxyde de carbone supercritique ($scCO_2$) comme agent physique. Dans la dernière section, la stratégie de moussage a été menée sur certains LIonomères sélectionnés en raison de leur performance globale exceptionnelle. La capacité de moussage et les propriétés de compression du PPgMA pur ont été considérablement améliorées grâce à la conception réussie de LIonomères. Par conséquent, ce travail s'est concentré sur la conception d'une nouvelle génération d'ionomères, c'est-à-dire des LIonomères, en combinant de l'anhydride maléique greffé au polypropylène et des liquides ioniques, en étudiant et en comprenant les interactions et les structurations en fonction de l'accordabilité des cations et des anions des liquides ioniques, ainsi qu'en étudiant leur application potentielle sur des matériaux légers. Grâce aux composants spéciaux des liquides ioniques et à leurs propriétés globales exceptionnelles, de nombreuses voies de recherche et applications technologiques seront proposées sur la base de nos résultats.

Mots clés: LIonomères, liquides ioniques, anhydride maléique greffé sur du polypropylène, mousses microcellulaires, CO_2 supercritique

Table of contents

List of Figures

List of Schemes

List of Tables

List of Abbreviations and Symbols

Nomenclature

Zn	Zinc
Na	Sodium
K	Potassium
Li	Lithium
Cu	Copper
Ba	Barium
Cs	Caesium
E/AA	Ethylene-acrylic acid
E/MAA	Ethylene/methacrylic acid
PE	Polyethylene
B/MAA	Butadiene methacrylate copolymer
PP	Propylene
PPgMA	Polypropylene grafted maleic anhydride
MA	Maleic anhydride
PU	Polyurethane
PLA	Polylactic acid
PS	Polystyrene
P^+TMP	Trihexyl(tetradecyl) phosphonium bis(2,4,4-trimethylpentyl) phosphinate
P^+DEP	Tributyl(ethyl)phosphonium Diethyl Phosphate
P^+Ac	Trihexyl (tetradecyl) phosphonium chloride
P^+Cl	Trihexyl (tetradecyl) phosphonium acetate
EMIM Ac	1-Ethyl-3-methylimidazolium acetate

EMIM DEP	1-Ethyl-3-methylimidazolium diethyl phosphate
[AEMIM] Br	1-aminoethyl-3-methylimidazolium Bromide
ZnO	Zinc oxide
PAs	polyacrylate latexes
PEMAA	Polyethylene-co-methacrylic acid
MPER	Maleic anhydride grafted polypropylene-based thermoplastic elastomers
AlSt	Aluminum stearate
MgSt	Magnesium stearate
CaSt	Calcium stearate
ZnSt	Zinc stearate
NaSt	Potassium stearate
KSt	Sodium stearate
ZnS	Zinc sulfide
MH	Magnesium hydroxide
m-EPDM	Maleated EPDM rubber
CPVC	Cchlorinated poly(vinyl chloride)
NaOH	Sodium hydroxide
$Al(OH)_3$	Aluminium hydroxide
THF	Tetrahydrofuran
PA6	Polyamide 6
LDPE	Low-density polyethylene
P (EA-co-AA)	Ethyl acrylate/acrylic acid copolymer
DCP	Diisopropyl peroxide
$AlCl_3$	Aluminium chloride
$FeCl_3$	Iron(III) chloride
$ZnCl_2$	Zinc chloride
BF_4^-	Tetrafluoroborate
PF_6^-	Hexafluorophosphate

OTf^-	Trifluoromethanesulfonate
$N(CN)_2^-$	Cyanide
NTf_2^-	Bis(trifluoromethylsulfonyl)azanide
$CF_3CO_2^-$	Trifluoroacetate
ILs	Ionic liquids
RTILs	Room temperature ionic liquids
ImILs	Imidazolium-based ionic liquids
PyILs	Pyridinium-based ionic liquids
PhILs	Phosphonium-based ionic liquids
PTFE	Poly (tetrafluoro ethylene)
P(VDF-CTFE)	Poly (vinylidene fluoride-co-chloro trifluoro ethylene)
PBAT	Poly (butylene adipate-co-terephthalate)
IL-Cl	Trihexyltetradecylphosphonium chloride
IL-TFSI	Trihexyltetradecyl phosphonium bis (trifluoromethylsulfonyl) imide
IL-TMP	Trihexyltetradecyl phosphonium bis 2,4,4-(trimethylpentyl) phosphinate
MCDEA	4,4’-methylenebis(3-chloro-2,6-diethylaniline)
Dmim NTf_2	1-dodecyl-3-methylimidazolium bis (trifluoromethylsulfonyl) imide
PBS	Polybutylene succinate
RS	Rice starch
mPEG-ILs	Polyethylene glycol-dicationic imidazolium-based ionic liquids
[EMIM] Br	1-ethyl-3-methylimidazolium bromide
MMT	Montmorillonites
LDH	Layered double hydroxide
$CoFe_2O_4$	Cobalt ferrite
MNP	Magnetic nanoparticles
PET	Polyethylene terephthalate

BHET	Bis (hydroxyethyl) terephthalate
POSS	Polyhedral oligomeric silsesquioxane
GNP	Graphene nanoplatelets
PMMA	Poly (methyl methacrylate)
DMF	N, N-dimethylformamide
$C_{12}Py$	Ndodecyl-pyridinium
$C_{12}mim$	1-methyl-3-dodecyl imidazolium
Br	Bromide
$C_{12}ViPy$	GNP/N-dodecyl-4-vinyl-pyridinium
TFSI	Bis(trifluoromethyl-sulfonyl) imide
$scCO_2$	Supercritical carbon dioxide
Tcritical	Critical temperature
Pcritical	Critical pressure
CF	Crystalline fraction
RAF	Rigid amorphous fraction
MAF	Mobile amorphous fraction

Characterization

T_g	Glass transition temperature
σ	Surface energy of cells
ΔP	Difference between the internal and surrounding pressure of a bubble
f_0	Frequency factor of gas molecules entering the nucleus of a bubble
ΔG^*_{hom}	Gibbs free energy required for homogeneous nucleation
k	Boltzmann constant
ΔG^*_{het}	Gibbs free energy required for heterogeneous nucleation
DMA	Dynamic mechanical analysis
DSC	Differential scanning calorimetry
FTIR	Fourier transform infrared spectroscopy
NMR	Nuclear magnetic resonance
ATG	Thermogravimetric analysis
POM	Polarizing Optical Microscope
SEM	Scanning Electron Microscope
T_α	α Relaxation temperature
T_β	β Relaxation temperature
$T_{\alpha'}$	α' Relaxation temperature
tan δ	Loss factor
TEM	Transmission Electron Microscope
D	Crystal size
T_m	Melting temperature
T_c	Crystallization temperature
X_c	Crystallinity
$t_{1/2}$	Half-crystallization time

Φ	Cooling rate
Z_t	Crystallization kinetic constant
n	Avrami' exponent
X_t	Relative crystallinity
T_0	Onset crystallization temperature
T_∞	End crystallization temperature
η^*	Complex viscosity
K	Crystalline shape parameter
λ	The Cu Kα wavelength
θ	Diffraction angle
β	Sample diffraction peak half-height width
s	Instrument factor calibration
N	Nuclei factor
V	The average crystallization rate
A	The average crystal size
WAXD	Wide Angle X-Ray Diffraction
$P_{saturation}$	Foaming pressure
$P_{foaming}$	Foaming pressure
$T_{infiltration}$	Infiltration temperature
$T_{foaming}$	Foaming temperature
R_V	Volume expansion ration
p^0	The density of the unfoamed samples
p'	The density of the foamed samples
p_w	The density of water
N	Cell density

General Introduction

Since the 1980s, academic and industrial researchers have had a growing interest in the processing of polymer/fillers nanocomposites due to their excellent barrier, electrical and mechanical properties which are conferred by the unique advantages of nanoparticles such as their high surface area, aspect ratio, shape and size. More recently, the market for lightweight materials very present in the industry is oriented towards the development of polymer nanocomposite foams in order to improve the compressive properties, mechanical strength and dimensional stability of unmodified foams. If processing parameters (temperature-pressure-soaking time-depressurization rate) have a clear impact on the foams morphology, materials parameters can also be tuned to tailor the foams structuration. For this reason, the strategy of the introduction of chemical or physical heterogeneities into the polymer matrix has been planned to increase the viscosity of the polymer and limit cell growth. The objective of this thesis focuses on designing a new generation of ionomers (denoted LIonomers) by combining polypropylene grafted maleic anhydride and ionic liquids, and investigating their perspective application on lightweight materials.

Based on the kinds of literature and our research objectives, this PhD work is divided into the following five chapters.

The first chapter is dedicated to reporting the state of art concerning ionomers, ionic liquid, and foaming. The first section reviewed the ionomer history as well as their impact on the physical properties of the resulting polymer materials, and finally, their different applications. The second section focuses on the combination of ionic liquid and polymer. Ionic liquids are recently founded to be attractive compounds because of their outstanding characteristic-limitless anion-cation combinations, and the dispersion of ILs in polymer could change the nanostructuration structure and impact the overall properties. The third section describes the foaming processing under supercritical CO_2,

as well as their methods. Herein, our study brings new insight into ionic liquids use, *i.e.* designing new generation of ionomers (denoted as LIonomers) as well as investigates their potential applications on foamed materials.

The second chapter focuses on the designing new generation of ionomers (denoted LIonomers) by combing polypropylene-grafted maleic anhydride (PPgMA) and four phosphonium-based ionic liquids (PhILs) and two imidazolium-based ionic liquids (ImILs), as well as understanding their interactions between polar groups of polymer backbone and cation/anion pairs of ionic liquids (ILs), and the structuration as a function of the tunability of cation and anion. The results show that all ionic liquids seem not play as the plasticizer, but improve the property of pure polymer to different extent owing to the difference in their nature, steric hindrance and as a result interaction strength. Then due to the outstanding performance of three LIonomers containing tributyl (ethyl) phosphonium diethyl phosphate (P^+DEP), 1-ethyl-3-methylimidazolium diethyl phosphate (EMIM DEP) and1-ethyl-3-methylimidazolium acetate (EMIM Ac), they have been selected to explore the role of anion and cation according to the nature of these three ionic liquids. The results show that the property of prepared LIonomer could be tailored by changing the anion/cation combinations, for example the achieved compromise between stiffness and stretchability when considering EMIM Ac or EMIM DEP, rather than P^+DEP thanks to their different interactions with the grated groups on the polymer backbone.

The third chapter is divided into two sections including designing and understanding of LIonomers-2.0 generation ionomer: the effect of generated “ionic-branched chains” consisting of cation/anion pairs of ionic liquids, and Understanding and Compressive Investigation between Conventional and the next generation of Ionomers: Zn-Ionomer versus LIonomers. One functional imidazolium-based ionic liquid has cooperated with PPgMA to obtain stronger interactions between these two phases, *i.e.* a covalent bond. Such 2.0 generation of ionomer indicates unprecedented improvement in solid and melt state properties of virgin polymer, which could be affected by four factors including maleic anhydride (MA) and amino-terminated IL

content, dispersion of ionic liquid and the length of “liquid-like branches” assembling from the cation/anion pairs of amino-terminated IL. On the other side, in order to explore the role of anion and functional group, such 2.0 generation ionomer has been compared to LIonomers processed with EMIM Ac and EMIM DEP (prepared previously), and the comparison with traditional Zn-Ionomer to look for the effect of different microstructure and interactions on the final property. The results demonstrate that the generated imide group and ionic network within such a 2.0 generation ionomer is much stronger than that among PPgMA/EMIM DEP or PPgMA/EMIM Ac blends, the compromise between stiffness and stretchability could be obtained from LIonomers under specific combinations, while not received from traditional Zn-Ionomer.

The fourth chapter shows the preparation of lightweight materials using supercritical carbon dioxide ($scCO_2$) as the foaming agent. Thanks to the improved properties (especially on the molten property), the foamability has increased significantly, even with some differences because of the effect of various cation/anion pairs. The average cell diameter could decrease to around 40 μm, and the expansion ratio, as well as cell density, are strongly influenced by the absorption ability of ionic liquids on CO_2. On the other side, in addition to the effect of cell size on the compressive property, the porosity seems to charge the compressive stress, *i.e.,* the low porosity makes great contributions to the compressive stress, while the samples owning big cell size displays the potential for good impact absorption property.

To summarize the work done in this study, different types of ionic liquids and cation/anion combinations are blended with polypropylene grafted maleic anhydride for designing the new generation of ionomer, as well as the application on lightweight materials is investigated. The prepared LIonomers show great improvement in physical properties. The interactions between ionic liquids and polar groups on polymer backbone have been studied deeply, and such interactions could be tailored as a function of the tunability of cation and anion, as a result the structuration. The first result of this work can be considered as the proof of concept and more works could be proposed. For example, multiple ionic liquid combinations could be applied to design

other functional LIonomers. On the other side, this class of new materials is very promising for processing functional materials such as foams, and the absorption ability of different ionic liquids on CO_2 should be further explored, especially at high temperature and high pressure.

Résumé Etendu

Chapitre 1 : Etudes bibliographiques

- **Ionomère**

Au cours des dernières décennies, une grande attention a été portée à l'étude des ionomères. L'ionomère est considéré comme une macromolécule contenant jusqu'à 15 % molaire de groupes ioniques qui sont fréquemment des anions d'acides carboxyliques, phosphoriques ou sulfoniques neutralisés par des sels métalliques, c'est-à-dire des cations de zinc, de sodium ou de potassium [1,2]. Ces matériaux présentent une structuration multi-échelle : les paires d'ions formées entre les anions d'acides et les sels métalliques, s'assemblent généralement pour former des états multiples et participent à des clusters ioniques. Cette structuration ionique conduit à un mouvement restreint des chaînes de polymère [3,4]. Par conséquent, une amélioration significative des propriétés à l'état fondu et solide est réalisée grâce aux points de réticulation physique générés par les interactions ioniques [5–11]. En outre, le type et la concentration des ions peuvent également entraîner certaines différences.

Ces matériaux présentent de nombreuses applications. Par exemple, les agents de compatibilité, en raison de la présence de composants polaires (groupes polaires et ions ajoutés) et non polaires (principalement dans les chaînes de polymères), entraînent une compatibilité avec les substances polaires et non polaires ; les agents de nucléation, c'est-à-dire les agrégats séparés par des microphases, riches en substances, sont formés à la suite de fortes interactions attractives entre les unités monomères ioniques, qui peuvent agir comme des sites de nucléation, déclenchant une nucléation hétérogène et accélérant la vitesse de cristallisation du polymère.

- **Liquides ioniques**

Les liquides ioniques (LIs), également appelés liquides ioniques à température ambiante, sont des sels organiques qui sont liquides au voisinage de la température ambiante. Le premier d'entre eux, le nitrate d'éthylammonium LI [$EtNH_3$][NO_3], a été découvert par Paul Walden en 1914 [12]. Depuis cette date, les liquides ioniques ont été largement utilisés comme solvants propres, électrolytes ou additifs dans les matériaux polymères [13–16] en raison de leurs excellentes caractéristiques, notamment une pression de vapeur nulle, une large gamme de fonctionnement, une stabilité thermique élevée et une bonne conductivité ionique, etc. Grâce aux nombreuses approches d'anions et de cations, les propriétés physiques et chimiques finales des mélanges polymères/ILs peuvent être ajustées en changeant les paires d'ions.

- **Moussant**

Grâce aux avantages des mousses de polymères, notamment une résistance aux chocs élevée, une grande ténacité, une stabilité thermique élevée, une faible conductivité thermique, etc. [17–19], les matériaux moussés ont fait l'objet d'une attention croissante en tant que matériaux légers et peu coûteux. La préparation de ces matériaux comprend la nucléation, la croissance, le refroidissement et la mise en forme [20,21], et ils conviennent à un large éventail d'applications, depuis les équipements de protection, l'isolation, le rembourrage et l'amortissement jusqu'aux absorbeurs d'ondes acoustiques et électromagnétiques [22,23]. Au cours du processus de moussage, on a constaté que la force du liquide fondu influençait considérablement les cellules finales, puisque les petites bulles peuvent s'effondrer en une grosse bulle si la viscosité ne peut pas supporter la croissance des cellules. En particulier, la conception d'ionomères ou l'utilisation d'allongeurs de chaîne pourraient améliorer ces propriétés.

D'autre part, compte tenu des nombreux points forts du dioxyde de carbone

supercritique [24–27] ($scCO_2$) *i)* il est respectueux de l'environnement, non toxique, ininflammable et bon marché ; *ii)* sa température critique est basse, sa pression critique est basse [28] ($T_{critique}$=31,1 ºC et $P_{critique}$=7.37 MPa), équipement de réaction simple, adapté à l'industrialisation ; *iii)* faible polarité moléculaire, capable de dissoudre des polymères non polaires ou moins polaires ; *iv)* taux de diffusion élevé et efficacité de production élevée ; *v)* solubilité élevée dans la plupart des polymères, il a été considéré comme l'agent moussant vert idéal à l'heure actuelle, en particulier compte tenu des problèmes environnementaux. Le $scCO_2$ est donc considéré comme l'agent moussant physique idéal pour préparer des matériaux légers.

- **References**

[1] Kirkmeyer B P, Weiss R A, Winey K I. Spherical and vesicular ionic aggregates in Zn-neutralized sulfonated polystyrene ionomers[J]. Journal of Polymer Science Part B: Polymer Physics, 2001, 39(5): 477-483.

[2] Zhang L, Brostowitz N R, Cavicchi K A, et al. Perspective: Ionomer research and applications[J]. Macromolecular Reaction Engineering, 2014, 8(2): 81-99.

[3] Datta S, De P P, De S K. Blends of ionomers[J]. Journal of Applied Polymer Science, 1996, 61(10): 1839-1846.

[4] Eisenberg A, Hird B, Moore R B. A new multiplet-cluster model for the morphology of random ionomers[J]. Macromolecules, 1990, 23(18): 4098-4107.

[5] Ling G H, Wang Y, Weiss R A. Linear viscoelastic and uniaxial extensional rheology of alkali metal neutralized sulfonated oligostyrene ionomer melts[J]. Macromolecules, 2012, 45(1): 481-490.

[6] Longworth R, Vaughan D J. Physical structure of ionomers[J]. Nature, 1968, 218(5136): 85-87.

[7] Kim J S, Yoshikawa K, Eisenberg A. Molecular weight dependence of the viscoelastic properties of polystyrene-based ionomers[J]. Macromolecules, 1994, 27(22): 6347-6357.

[8] Dalmas F, Leroy E. New insights into ionic aggregate morphology in Zn-neutralized sulfonated polystyrene ionomers by transmission electron tomography[J]. Macromolecules, 2011, 44(20): 8093-8099.

[9] Aitken B S, Buitrago C F, Heffley J D, et al. Precision ionomers: Synthesis and thermal/mechanical characterization[J]. Macromolecules, 2012, 45(2): 681-687.

[10] Weiss R A, Zhao H. Rheological behavior of oligomeric ionomers[J]. Journal of Rheology, 2009, 53(1): 191-213.
[11] Qiao X, Weiss R A. Nonlinear rheology of lightly sulfonated polystyrene ionomers[J]. Macromolecules, 2013, 46(6): 2417-2424.
[12] Liu J fu, Chi Y guang, Jiang G bin, et al. Ionic liquid-based liquid-phase microextraction, a new sample enrichment procedure for liquid chromatography[J]. Journal of Chromatography A, 2004, 1026(1-2): 143-147.
[13] Yang J, Pruvost S, Livi S, et al. Understanding of versatile and tunable nanostructuration of ionic liquids on fluorinated copolymer[J]. Macromolecules, 2015, 48(13): 4581-4590.
[14] Livi S, Duchet-Rumeau J, Pham T N, et al. A comparative study on different ionic liquids used as surfactants: Effect on thermal and mechanical properties of high-density polyethylene nanocomposites[J]. Journal of Colloid and Interface Science, 2010, 349(1): 424-433.
[15] Rahman M, Brazel C S. Ionic liquids: New generation stable plasticizers for poly(vinyl chloride)[J]. Polymer Degradation and Stability, 2006, 91(12): 3371-3382.
[16] Yousfi M, Livi S, Duchet-Rumeau J. Ionic liquids: A new way for the compatibilization of thermoplastic blends[J]. Chemical Engineering Journal, 2014, 255: 513-524.
[17] Suh K W, Park C P, Maurer M J, et al. Lightweight cellular plastics[J]. Advanced Materials, 2000, 12(23): 1779-1789.
[18] Tomasko D L, Li H, Liu D, et al. A review of CO_2 applications in the processing of polymers[J]. Industrial & Engineering Chemistry Research, 2003, 42(25): 6431-6456.
[19] Xu Z M, Jiang X L, Liu T, et al. Foaming of polypropylene with supercritical carbon dioxide[J]. The Journal of Supercritical Fluids, 2007, 41(2): 299-310.
[20] Colton J S, Suh N P. Nucleation of microcellular foam: Theory and practice[J]. Polymer Engineering & Science, 1987, 27(7): 500-503.
[21] Reverchon E, Cardea S. Production of controlled polymeric foams by supercritical CO_2[J]. The Journal of Supercritical Fluids, 2007, 40(1): 144-152.
[22] Krause B, Sijbesma H J P, Münüklü P, et al. Bicontinuous nanoporous polymers by carbon dioxide foaming[J]. Macromolecules, 2001, 34(25): 8792-8801.
[23] Doroudiani S, Park C B, Kortschot M T. Effect of the crystallinity and morphology on the microcellular foam structure of semicrystalline polymers[J]. Polymer Engineering & Science, 1996, 36(21): 2645-2662.
[24] Arora K A, Lesser A J, McCarthy T J. Synthesis, characterization, and expansion of poly (tetrafluoroethylene-co-hexafluoropropylene)/polystyrene blends processed in supercritical carbon dioxide[J]. Macromolecules, 1999, 32(8): 2562-2568.
[25] Watkins J J, McCarthy T J. Polymerization in supercritical fluid-swollen polymers: a new route to polymer blends[J]. Macromolecules, 1994, 27(17): 4845-4847.

[26] Kumar V, Suh N P. A process for making microcellular thermoplastic parts[J]. Polymer Engineering & Science, 1990, 30(20): 1323-1329.

[27] Kung E, Lesser A J, McCarthy T J. Morphology and mechanical performance of polystyrene/polyethylene composites prepared in supercritical carbon dioxide[J]. Macromolecules, 1998, 31(13): 4160-4169.

[28] Nalawade S P, Picchioni F, Janssen L. Supercritical carbon dioxide as a green solvent for processing polymer melts: Processing aspects and applications[J]. Progress in polymer science, 2006, 31(1): 19-43.

Chapitre 2 : LIonomères - nouvelle génération d'ionomères : en combinant le PPgMA et différents liquides ioniques

- **Introduction**

Les ionomères sont considérés comme des macromolécules contenant un type de groupes ioniques/ionisables qui sont composés d'anions d'acides (comme les acides carboxyliques et phosphoriques) et de sels métalliques (comme Zn^{2+} et Na^{+}) [1–4]. Ces matériaux présentent une structuration multi-échelle : les paires d'ions, formées entre les anions d'acides et les sels métalliques, s'assemblent généralement pour former des états multiples impliqués eux-mêmes dans des clusters ioniques. Non seulement les réseaux ioniques générés par les interactions de paires d'ions entre les cations métalliques et les anions acides, mais aussi les domaines ioniques agrégés peuvent créer des régions confinées où la mobilité des chaînes polymères est limitée [5]. Ces zones de restriction des mouvements agissent comme des points de réticulation favorisant la cristallisation et améliorant les propriétés thermo-mécaniques et rhéologiques [6–11].

Les liquides ioniques (LIs) sont des composants prometteurs en raison de leurs caractéristiques intrinsèques et de leurs caractères ioniques [12–15]. Grâce à leurs combinaisons particulières, ils ont été appliqués comme agents interfaciaux dans des mélanges de polymères ou des hybrides organiques-inorganiques, ou comme réactifs pour concevoir de nouveaux réseaux IL-époxy. La composition de cations et d'anions pourrait favoriser les interactions avec les groupes polaires. Jusqu'à présent, aucun autre chercheur n'a étudié leur nouvelle utilisation, c'est-à-dire leur combinaison avec des polymères pour concevoir une nouvelle génération d'ionomères (appelés LIonomères). Ce chapitre comprend trois sections : *i)* LIonomères - rôle des liquides ioniques à base de phosphonium dans la fabrication d'une nouvelle génération d'ionomères : Comprendre l'accordabilité de l'anion et son effet sur la structuration et

les propriétés ; *ii)* LIonomer - la nouvelle génération d'ionomères : Understanding the tunability of ImILs cation and anion and effect on structuration and performance ; *iii)* LIonomers-New Generation of Ionomer : Compréhension de leur interaction et de leur structuration en fonction de l'accordabilité du cation et de l'anion.

- **Préparation et caractérisations de LIonomères traités avec des liquides ioniques à base de phosphonium ou d'imidazolium**

Le mélange PPgMA/ILs a été mélangé pendant 5 minutes à l'aide d'une micro extrudeuse DSM à 180 °C, et injecté à 30 °C. Ensuite, huit LIonomères différents, en fonction de la nature du couple (cation/anion), à savoir PhILs Bis (2,4,4-triméthylpentyl) phosphinate de tétradécyl (trihexyl) phosphonium (P^+TMP), diéthyl phosphate de tributyl (éthyl) phosphonium (P^+DEP) et chlorure de trihexyl (tétradécyl) phosphonium (P^+Cl), acétate de trihexyl (tétradécyl) phosphonium (P^+Ac), phosphate diéthylique de 1-Ethyl-3-méthylimidazolium (EMIM DEP), acétate de 1-Ethyl-3-méthylimidazolium (EMIM Ac), et de teneur en IL sont préparés (Figure 1).

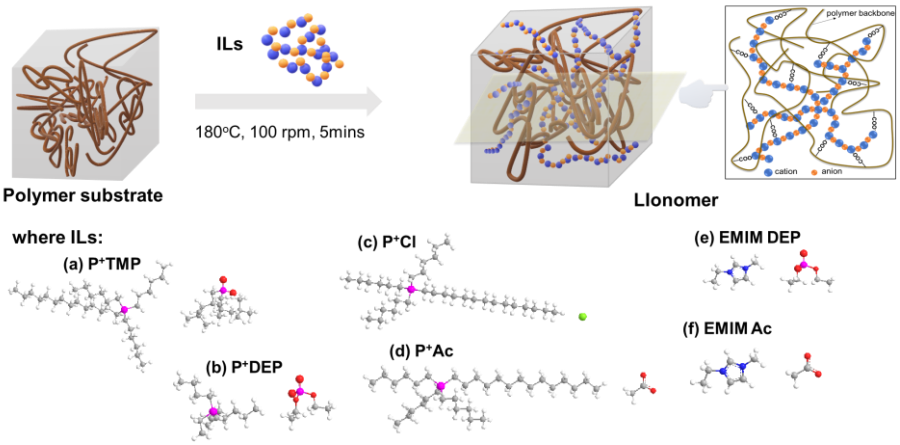

Figure 1 Le schéma de préparation proposé pour les Lionomers

La structure chimique des mélanges PPgMA/ILs obtenus est caractérisée par ^{31}P et ^{1}H NMR, comme le montrent les Figures 2 et 3. En combinaison avec l'augmentation de la viscosité à l'état fondu à haute température et de la température de relaxation de la RAF (fraction amorphe rigide) (voir les Figures 4 et 5 en considérant le PPgMA pur comme la conférence), ces IL coopérés pourraient s'auto-assembler dans de

nouveaux arrangements comme indiqué dans le Schéma 1.

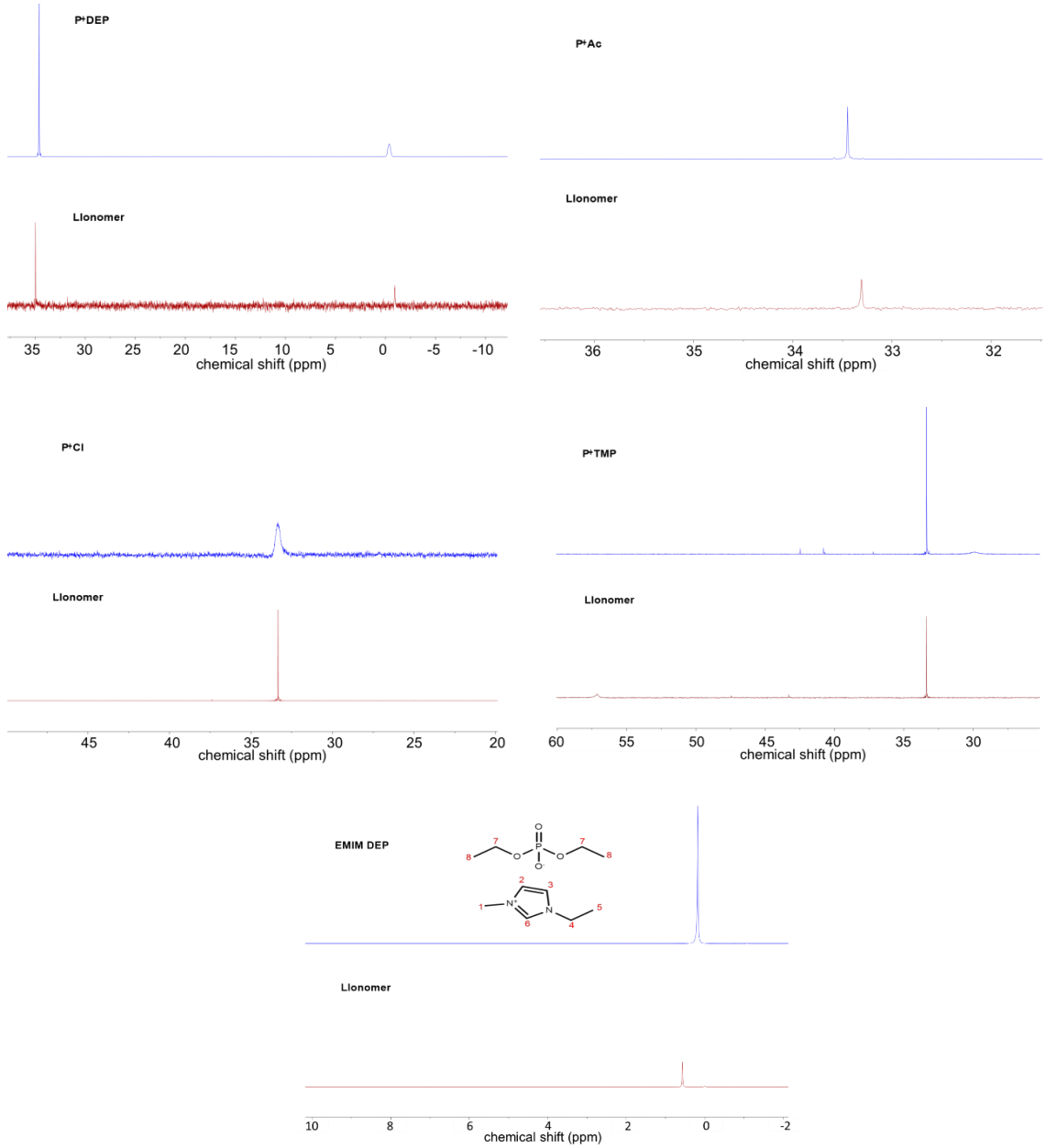

Figure 2 Spectres de RMN ^{31}P (400 MHz ; solvant C_6D_5Cl) de P^+DEP, P^+Ac, P^+Cl, P^+TMP, EMIM DEP et leurs Llonomères (10 % en poids)

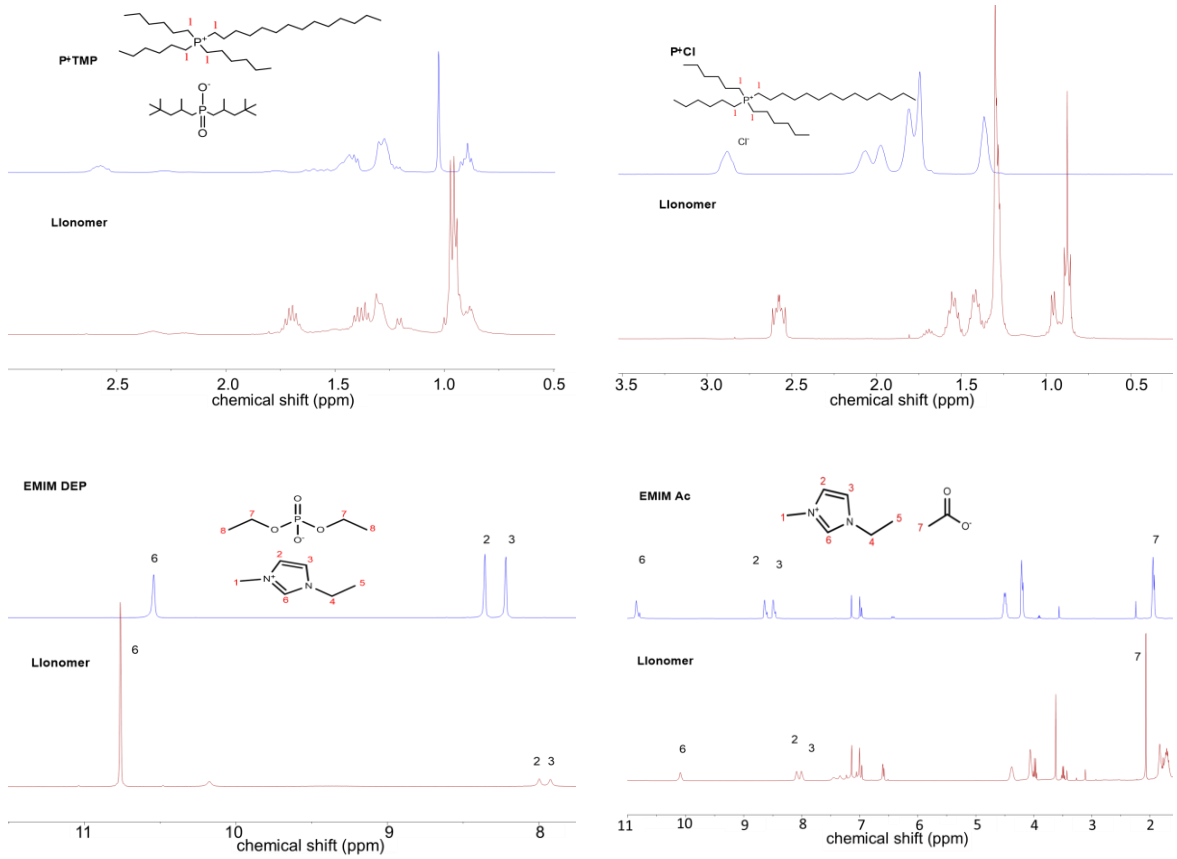

Figure 3 Spectres de RMN ^{1}H (400 MHz ; solvant C_6D_5Cl) de P^+TMP, P^+Cl, EMIM DEP, EMIM Ac, et des LIonomères correspondants (10 % en poids).

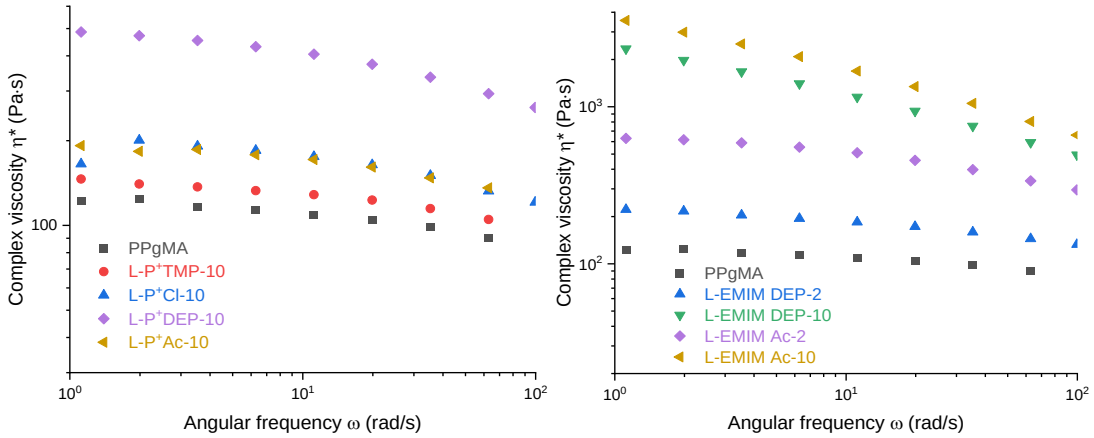

Figure 4 La viscosité de la matrice polymère et des LIonomères en fonction du type et du teneur en LI.

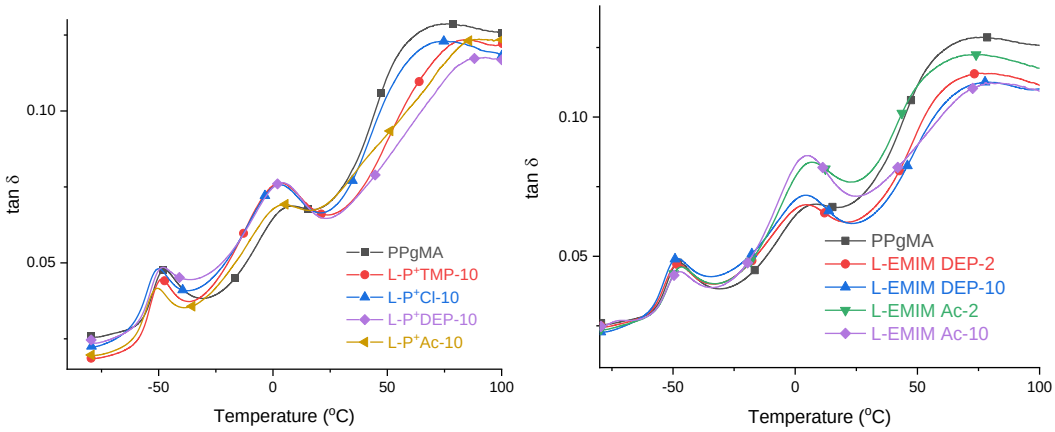

Figure 5 Courbes de la tangente de la perte mécanique dynamique (tan δ) en fonction de la température

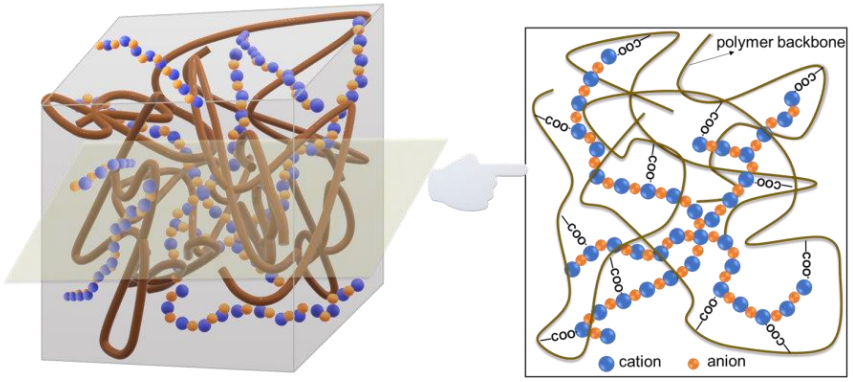

Schéma 1 Schéma proposé pour les LIonomères au sein de PPgMA

La morphologie de la dispersion (Figure 6) des liquides ioniques dans la matrice PPgMA varie en fonction des différentes interactions entre les paires cation/anion et les groupes polaires de la matrice polymère, selon la nature des liquides ioniques.

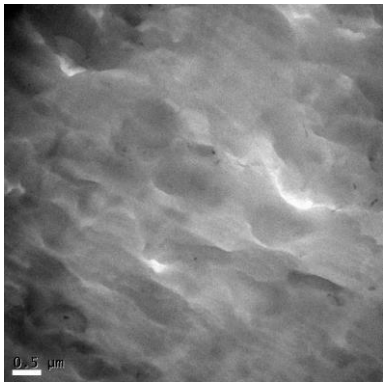

PPgMA (a)

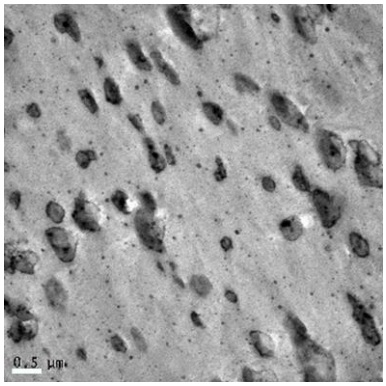

L-EMIM DEP-10 (b)

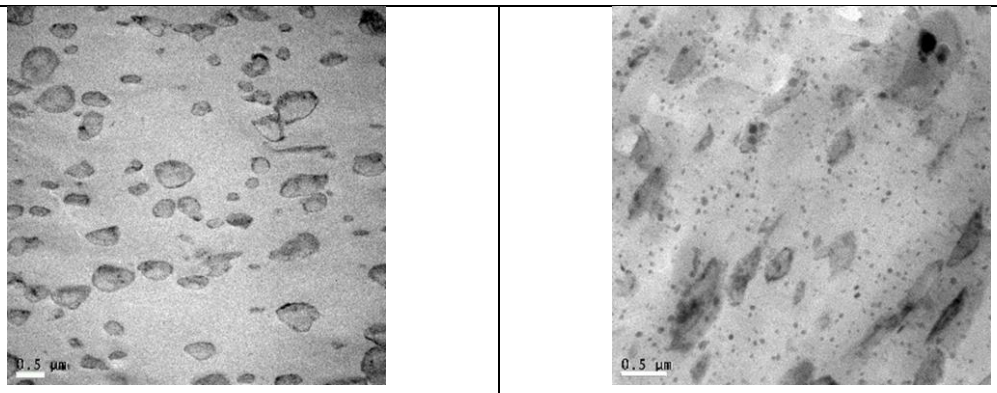

L-P⁺DEP-10 (c) | L-EMIM Ac-10 (d)

Figure 6 Images par microscopie électronique à transmission (MET) de PPgMA et de LIonomers apparentés contenant 10 % en poids de IL.

- **Principaux résultats**

Ce chapitre a permis de synthétiser une série d'ionomères de nouvelle génération (appelés LIonomers), dont les propriétés peuvent être adaptées en fonction de la nature cation/anion des liquides ioniques régissant les interactions au sein des mélanges PPgMA/LIs. Les conclusions révèlent que la présence d'anhydride maléique greffé sur le squelette du polypropylène en tant que "groupe de tête", combinée à des paires de liquides ioniques, pourrait conduire à la formation de nouvelles nanostructures via la génération d'interactions ioniques et polaires (voir Schéma 1). Dans cette étude, tous les liquides ioniques ont pu renforcer les performances à l'état solide et à l'état fondu, plutôt que d'agir comme un plastifiant affaiblissant la viscosité et le module [16]. En particulier, en ce qui concerne les LIonomères traités par P⁺DEP, EMIM Ac et EMIM DEP présentant les trois meilleures performances globales, différentes morphologies peuvent être conçues, c'est-à-dire d'une séparation de phase résultant en une structuration à une seule échelle (nano) composée d'une distribution de clusters ioniques lorsque les LIonomères concernent des LIs à base de phosphonium, à une structure multi-échelle combinant des clusters ioniques mais aussi une phase séparée riche en IL comme pour les IL à base de cation imidazolium

(voir Figure 6). Ces distributions d'IL sont très liées à l'interaction avec les groupes polaires du PPgMA. La plus petite taille des phases séparées riches en IL est susceptible d'établir des interactions LI/polymère plus fortes. Le cation imidazolium combiné à l'anion acétate apparaît comme la LI la plus pertinente pour optimiser les interactions avec le groupe anhydride maléique greffé sur le squelette du polypropylène. Les propriétés physiques à l'état fondu et solide semblent être fortement influencées par ces interactions [8,17–20]. En effet, l'augmentation de la viscosité complexe met en évidence l'existence d'interactions IL/polymère et la capacité dans ce cas à former un réseau ionique. En relation avec leur morphologie, leur cristallinité et l'existence d'une phase ionique percolée, les LIonomères présentent à la fois un module d'Young amélioré et la capacité de supporter de grandes déformations avant rupture. Par conséquent, ces LIonomères sont très prometteurs pour le traitement de matériaux fonctionnels tels que les mousses ou les membranes soufflées à l'état fondu.

- **References**

[1] Eisenberg A, Hird B, Moore R B. A new multiplet-cluster model for the morphology of random ionomers[J]. Macromolecules, 1990, 23(18): 4098-4107.

[2] Datta S, De P P, De S K. Blends of ionomers[J]. Journal of Applied Polymer Science, 1996, 61(10): 1839-1846.

[3] Zhang L, Brostowitz N R, Cavicchi K A, et al. Perspective: Ionomer research and applications[J]. Macromolecular Reaction Engineering, 2014, 8(2): 81-99.

[4] Kirkmeyer B P, Weiss R A, Winey K I. Spherical and vesicular ionic aggregates in Zn-neutralized sulfonated polystyrene ionomers[J]. Journal of Polymer Science Part B: Polymer Physics, 2001, 39(5): 477-483.

[5] Ma Y, Yang G, Xie L. Morphology, nonisothermal crystallization behavior and mechanical properties of polypropylene modified by ionomers[J]. Journal of Macromolecular Science, Part B, 2014, 53(12): 1829-1845.

[6] Kim J S, Yoshikawa K, Eisenberg A. Molecular weight dependence of the viscoelastic properties of polystyrene-based ionomers[J]. Macromolecules, 1994, 27(22): 6347-6357.

[7] Dalmas F, Leroy E. New insights into ionic aggregate morphology in Zn-neutralized

sulfonated polystyrene ionomers by transmission electron tomography[J]. Macromolecules, 2011, 44(20): 8093-8099.

[8] Aitken B S, Buitrago C F, Heffley J D, et al. Precision ionomers: Synthesis and thermal/mechanical characterization[J]. Macromolecules, 2012, 45(2): 681-687.

[9] Weiss R A, Zhao H. Rheological behavior of oligomeric ionomers[J]. Journal of Rheology, 2009, 53(1): 191-213.

[10] Qiao X, Weiss R A. Nonlinear rheology of lightly sulfonated polystyrene ionomers[J]. Macromolecules, 2013, 46(6): 2417-2424.

[11] Ling G H, Wang Y, Weiss R A. Linear viscoelastic and uniaxial extensional rheology of alkali metal neutralized sulfonated oligostyrene ionomer melts[J]. Macromolecules, 2012, 45(1): 481-490.

[12] Chen Y, Zhang Y, Ke F, et al. Solubility of neutral and charged polymers in ionic liquids studied by laser light scattering[J]. Polymer, 2011, 52(2): 481-488.

[13] Hajipour A R, Rafiee F. Recent progress in ionic liquids and their applications in organic synthesis[J]. Organic Preparations and Procedures International, 2015, 47(4): 249-308.

[14] Yue C, Fang D, Liu L, et al. Synthesis and application of task-specific ionic liquids used as catalysts and/or solvents in organic unit reactions[J]. Journal of Molecular Liquids, 2011, 163(3): 99-121.

[15] Livi S, Duchet-Rumeau J, Pham T N, et al. A comparative study on different ionic liquids used as surfactants: Effect on thermal and mechanical properties of high-density polyethylene nanocomposites[J]. Journal of Colloid and Interface Science, 2010, 349(1): 424-433.

[16] Yang J, Pruvost S, Livi S, et al. Understanding of versatile and tunable nanostructuration of ionic liquids on fluorinated copolymer[J]. Macromolecules, 2015, 48(13): 4581-4590.

[17] Weiss R A, Yu W C. Viscoelastic behavior of very lightly sulfonated polystyrene ionomers[J]. Macromolecules, 2007, 40(10): 3640-3643.

[18] Li Y, Yao Z, Chen Z hua, et al. High melt strength polypropylene by ionic modification: Preparation, rheological properties and foaming behaviors[J]. Polymer, 2015, 70: 207-214.

[19] Page K A, Park J K, Moore R B, et al. Direct analysis of the ion-hopping process associated with the α-relaxation in perfluorosulfonate ionomers using quasielastic neutron scattering[J]. Macromolecules, 2009, 42(7): 2729-2736.

[20] Castagna A M, Wang W, Winey K I, et al. Influence of cation type on structure and dynamics in sulfonated polystyrene ionomers[J]. Macromolecules, 2011, 44(13): 5420-5426.

Chapitre 3 : 2.0 Génération d'ionomères à base de PPgMA-LIonomers : introduction de liquides ioniques fonctionnels à base d'imidazolium et comparaison avec l'ionomère Zn traditionnel.

- **Introduction**

En plus de la nouvelle génération d'ionomères préparés dans le chapitre précédent, un liquide ionique à base d'imidazolium à terminaison amino a coopéré avec le PPgMA pour réaliser une interaction plus forte, c'est-à-dire une liaison covalente. Ce chapitre se compose de deux sections : *i)* conception et compréhension de LIonomers-2.0 génération d'ionomères : l'effet des chaînes ramifiées ioniques générées constituées de paires cation/anion de liquides ioniques ; *ii)* LIonomer-nouvelle génération d'ionomères : compréhension de leur interaction et de leur structuration en fonction de la nature du liquide ionique à base d'imidazolium, et comparaison avec le traditionnel Zn-Ionomer.

- **Préparation et caractérisations d'ionomères de la génération LIonomers-2.0 traités avec un liquide ionique à base d'imidazolium à terminaison amino**

Les mêmes conditions de traitement que celles du chapitre 2 ont été appliquées pour obtenir la génération 2.0 d'ionomère en combinant le bromure de 1-aminoéthyl-3-méthylimidazolium ([AEMIM] Br) et le PPgMA, ainsi que l'ionomère Zn traditionnel avec l'acétate de zinc (Figure 7).

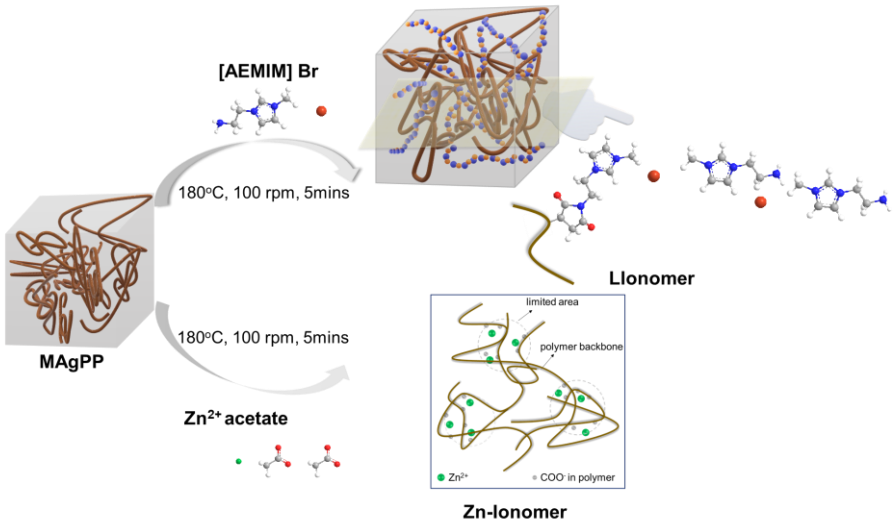

Figure 7 Les différentes structures d'interaction dans les différents mélanges

Les échantillons préparés ont été caractérisés par ATR-FTIR à température ambiante, comme le montre la Figure 8. La structure d'interaction proposée dans la Figure 7, et l'introduction de [AEMIM] Br pourraient également se réorganiser en branches "liquides" (voir Schéma 1) en considérant le groupe imide généré [1–3] comme la "tête" et en utilisant les combinaisons cation/anion des liquides ioniques comme les composants.

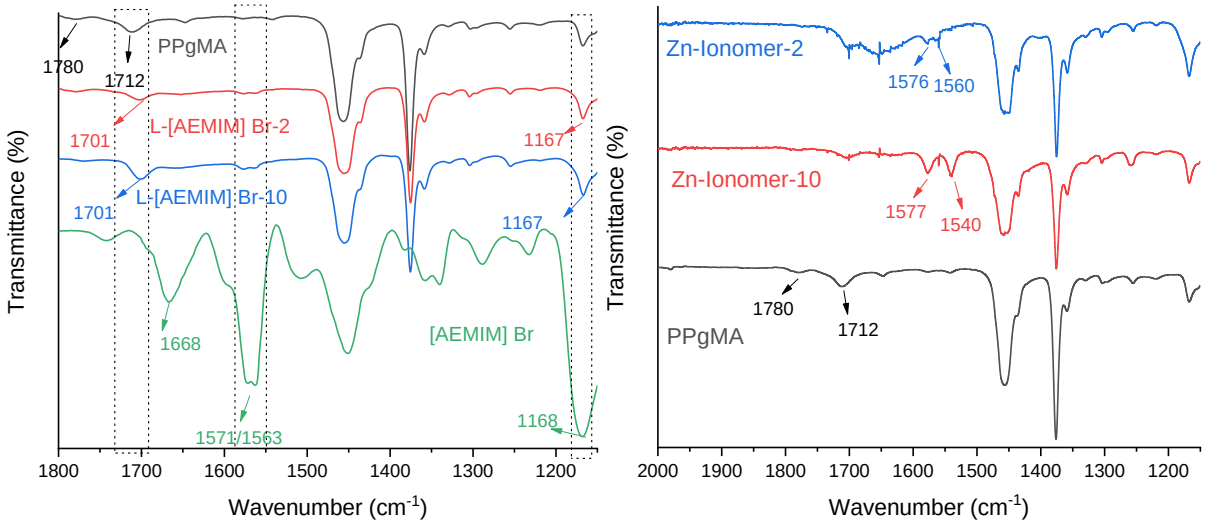

Figure 8 Courbes ATR-FTIR des Llonomères traités avec l'[AEMIM] Br (a) et les ionomères Zn (b).

- **Principaux résultats**

La génération 2.0 d'ionomères a été synthétisée dans ce chapitre, en combinant un liquide ionique fonctionnel à base d'imidazolium, c'est-à-dire le bromure de 1-aminoéthyl-3-méthylimidazolium, avec de l'anhydride maléique greffé au polypropylène. Les résultats révèlent que trois facteurs ***a*** le nombre de points de réaction chimique (la teneur en MA), ***b*** la longueur des chaînes ioniques ramifiées, ***c*** les interactions ioniques-ioniques entre les longues chaînes ioniques ramifiées et/ou les points de réticulation entre les chaînes ioniques ramifiées et les chaînes polymères, pourraient avoir un impact sur l'état solide et l'état fondu. D'autre part, en combinant les LIonomères traités avec EMIM Ac et EMIM DEP dans les chapitres précédents, les propriétés des LIonomères pourraient être adaptées en changeant les paires cation/anion de l'ImIL, et être comparées à celles du traditionnel Zn-Ionomer. La RMN et l'IRTF prouvent que les interactions (ionique-ionique, dipolaire-ionique et liaison chimique) entre l'ImIL et le groupe polaire du PPgMA varient selon la nature de l'ImIL. Les différentes forces et modèles d'interaction régissent la distribution de l'ImIL dans le LIonomère correspondant. Par conséquent, la morphologie des LIonomères traités avec [AEMIM] Br présente une structuration à l'échelle nanométrique due au groupe imide généré, tandis que ceux traités avec EMIM DEP et EMIM Ac présentent des distributions à plusieurs échelles, c'est-à-dire des multiplets ioniques et une phase séparée d'ImIL dans les LIonomères. En même temps, la valeur de la viscosité complexe à haute température révèle le classement de la force d'interaction dans les LIonomères, et la capacité de générer un réseau ionique continu contribuant à la viscosité fondue [4–9]. Le Zn-Ionomer présente une valeur similaire à celle du LIonomer traité avec l'[AEMIM] Br. Tous les additifs sont susceptibles de se trouver dans la phase amorphe, en particulier dans la fraction amorphe rigide (RAF), ce qui entraîne une valeur de relaxation significativement élevée. En plus de l'effet des paires cation-anion sur le processus de cristallisation, la β-phase cristalline est également produite. En

outre, en relation avec la microstructure et la cristallinité, un excellent compromis de rigidité et d'étirabilité est obtenu, affichant un module élevé accompagné d'une déformation de rupture élevée. Alors que ni un tel compromis ni la formation de cristaux de phase β ne sont obtenus dans les ionomères de Zn. En conclusion, ces LIonomères sont très prometteurs pour le traitement de matériaux hautement fonctionnels, tels que les mousses ou les films soufflés à l'état fondu dans lesquels la capacité d'étirement est requise.

- **References**

[1] Zhou X, Zhang Y, Huang Z, et al. Ionic liquids modified graphene oxide composites: a high efficient adsorbent for phthalates from aqueous solution[J]. Scientific Reports, 2016, 6(1): 1-10.

[2] Létoffé A, Hoppe S, Lainé R, et al. Resilience improvement of an isotactic polypropylene-g-maleic anhydride by crosslinking using polyether triamine agents[J]. Polymer, 2019, 179: 121655.

[3] Suckow M, Zschoche S, Heinrich G, et al. New reactive poly (ionic liquid) s synthesized by polymer analogous conversion of maleic anhydride containing polymers[J]. Polymer, 2016, 96: 20-25.

[4] Aitken B S, Buitrago C F, Heffley J D, et al. Precision ionomers: Synthesis and thermal/mechanical characterization[J]. Macromolecules, 2012, 45(2): 681-687.

[5] Weiss R A, Yu W C. Viscoelastic behavior of very lightly sulfonated polystyrene ionomers[J]. Macromolecules, 2007, 40(10): 3640-3643.

[6] Li Y, Yao Z, Chen Z hua, et al. High melt strength polypropylene by ionic modification: Preparation, rheological properties and foaming behaviors[J]. Polymer, 2015, 70: 207-214.

[7] Page K A, Park J K, Moore R B, et al. Direct analysis of the ion-hopping process associated with the α-relaxation in perfluorosulfonate ionomers using quasielastic neutron scattering[J]. Macromolecules, 2009, 42(7): 2729-2736.

[8] Castagna A M, Wang W, Winey K I, et al. Influence of cation type on structure and dynamics in sulfonated polystyrene ionomers[J]. Macromolecules, 2011, 44(13): 5420-5426.

[9] Eisenberg A, Hird B, Moore R B. A new multiplet-cluster model for the morphology of random ionomers[J]. Macromolecules, 1990, 23(18): 4098-4107.

Chapitre 4 Comportement de la mousse en utilisant le dioxyde de carbone supercritique comme agent moussant physique

- **Introduction**

Les mousses de polypropylène (PP) ont fait l'objet d'un intérêt croissant en tant que matériaux légers et peu coûteux adaptés à une variété d'applications allant de l'équipement de protection, l'isolation, les coussins, l'amortissement aux absorbeurs d'ondes acoustiques et électromagnétiques [1,2]. Ces matériaux moussés présentent de nombreux avantages, notamment une grande résistance aux chocs, une grande ténacité, une grande stabilité thermique, etc. [3–5]. Cependant, l'opération de moussage sur le PP n'est pas facile en raison de deux facteurs principaux [6–9]. D'une part, le PP étant un polymère semi-cristallin, les gaz ne se dissolvent pas dans les zones cristallines. Par conséquent, le contrôle de la structure cellulaire du PP est plus difficile que celui d'un polymère amorphe. Parallèlement, en raison de l'hétérogénéité du polymère semi-cristallin, la nucléation cellulaire est hétérogène. D'autre part, en raison de la faible force de fusion du PP, les parois séparant les cellules n'ont pas assez de force pour supporter la force d'extension et plusieurs petites cellules peuvent s'effondrer en une grande pendant le moussage. De nombreuses stratégies ont été mises en œuvre pour obtenir des mousses de PP exceptionnelles, comme les mélanges de polymères [10] et les composites [11,12]. Dans le cas présent, nous avons l'intention de sélectionner plusieurs LIonomers présentant une excellente viscosité de cisaillement, préparés dans les chapitres précédents, et de les faire mousser en utilisant un processus de moussage par lots. Compte tenu des préoccupations environnementales, le dioxyde de carbone supercritique (scCO2) est utilisé comme agent moussant physique [13–17].

- **Moussage par scCO₂ et caractérisations**

Selon le nouveau procédé de moussage par lots [18], les LIonomères sélectionnés ont été immergés dans une atmosphère de scCO₂ pendant une heure sous 158 °C ($T_{infiltration}$) et 150 bar ($P_{saturation}$), puis en diminuant la température et la pression en 135 °C ($T_{foaming}$) et 135 bar ($P_{foaming}$) pendant encore une heure. Ensuite, le CO_2 a été rapidement libéré (> 10 bar/s) pour induire la nucléation et la croissance de la mousse, et l'échantillon moussé a été rapidement transféré dans l'azote liquide pour stabiliser la structure cellulaire. Le schéma du moussage par lots et de l'ensemble de la procédure est présenté dans le Schéma 2.

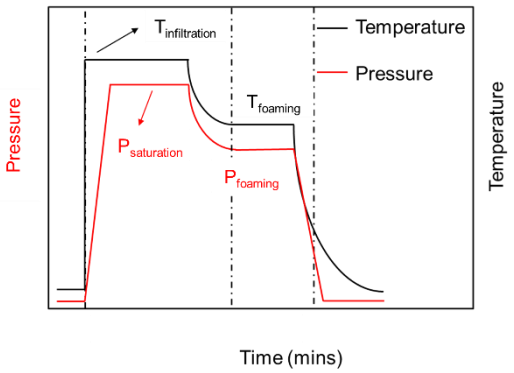

Schéma 2 Schéma du montage expérimental pour le processus de moussage par lots ($P_{saturation}$ et $P_{foaming}$: pression de saturation et de moussage, $T_{infiltration}$ et $T_{foaming}$: température d'infiltration et de moussage)

Le rapport d'expansion volumique (R_V) [19] et la porosité [20] des échantillons moussés sont déterminés par les équations 1 et 2, comme le montrent les Figures 9 et 10.

$$R_V = \frac{p^0}{p'} \quad \text{(équation 1)}$$

$$Porosity = 1 - \frac{1}{R_v} \quad \text{(équation 2)}$$

où p^0 et p' sont les densités des échantillons non moussés et moussés reçues de la balance de densité. Et la valeur (p') a été définie par la méthode de drainage

selon ASTM D792 (par l'équation 3) :

$$p' = \frac{a}{a+b-c} \times p_w \qquad \text{(équation 3)}$$

où p_w est la densité de l'eau à la température d'essai, a est la masse apparente de l'échantillon dans l'air sans la platine, tandis que b est la masse apparente d'une platine complètement immergée (si elle est utilisée), c est la masse apparente de l'échantillon et de la platine (si elle est utilisée) totalement immergés dans l'eau.

La morphologie des cellules a été observée par MEB (voir Figure 11), et la densité cellulaire (N, voir Figure 9), définie comme le nombre de cellules par unité de volume par rapport au polymère non expansé, a été déterminée à partir de l'équation 4 [21]:

$$N = \left(\frac{nM^2}{A}\right)^{3/2} R_V \qquad \text{(équation 4)}$$

où n est le nombre de cellules dans l'image MEB, M est le facteur de grossissement et A est la surface de l'image.

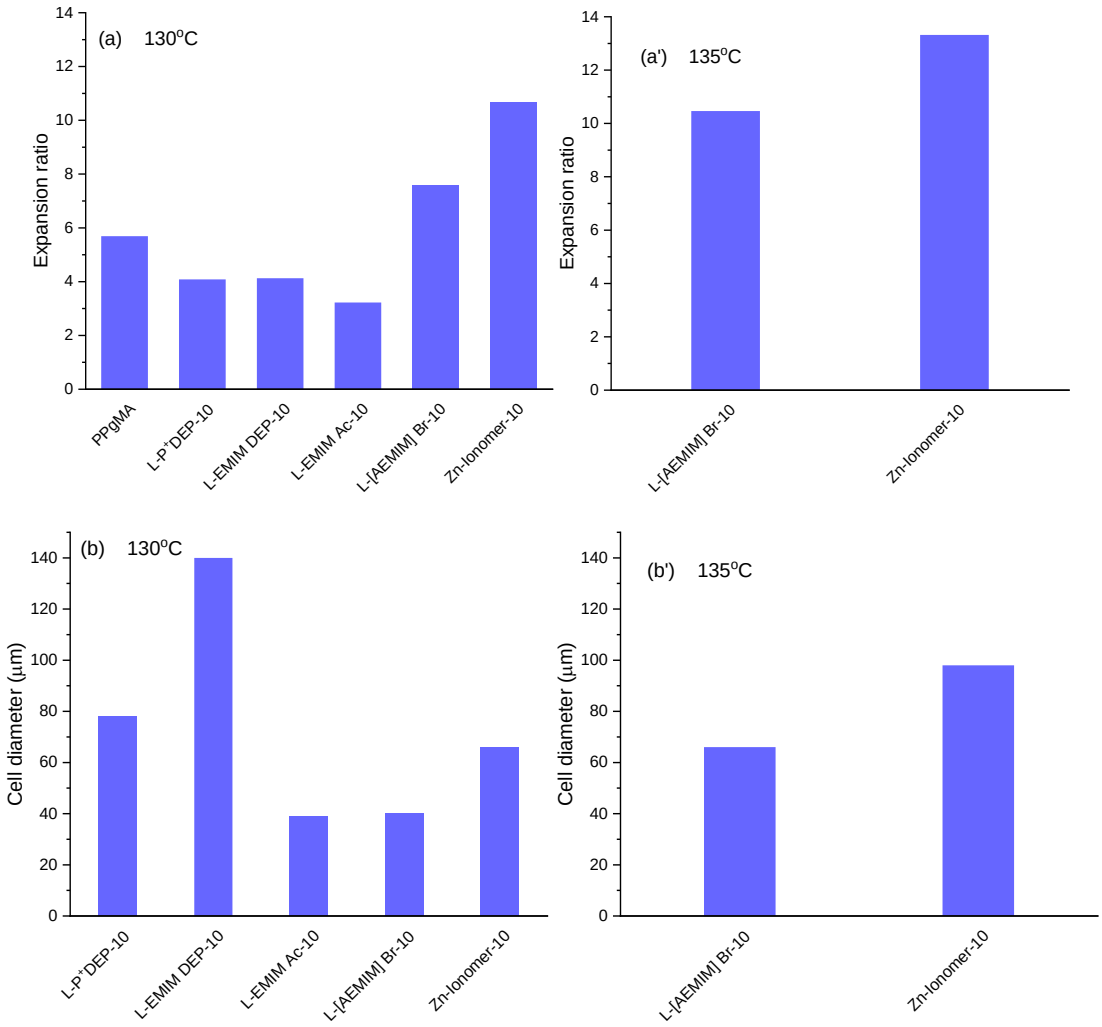

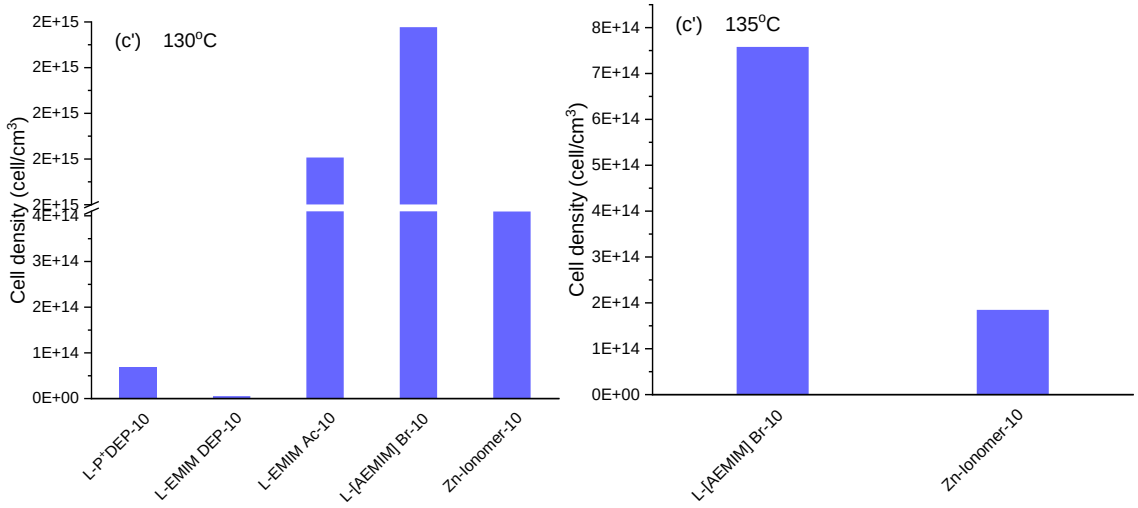

Figure 9 (a) Taux d'expansion cellulaire, (b) diamètre des cellules et (c) densité cellulaire de tous les substrats et des échantillons correspondants moussés au LIonomer.

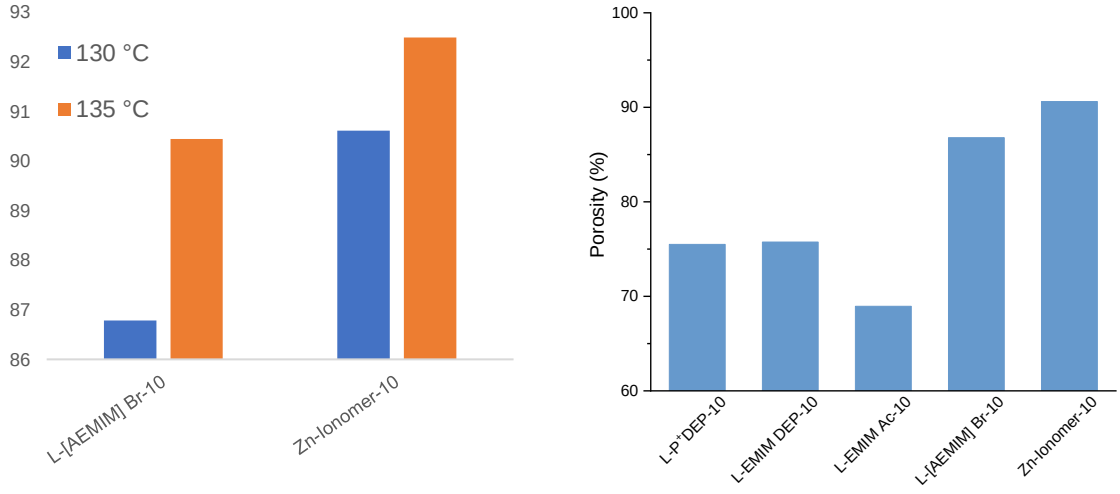

a b

Figure 10 La porosité des LIonomers moussés (a) et des échantillons à différentes températures de moussage (b).

130 ºC PPgMA

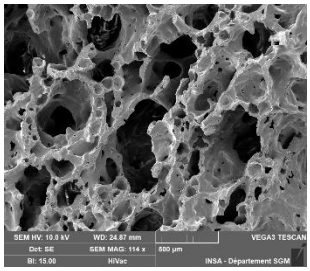

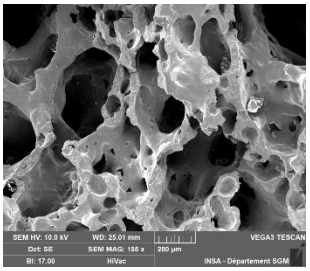

L-P^{+}DEP-10	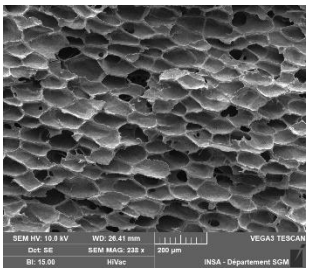	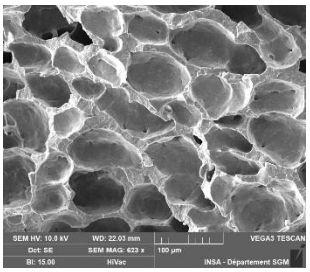
L-EMIM DEP-10	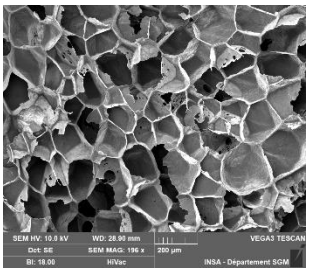	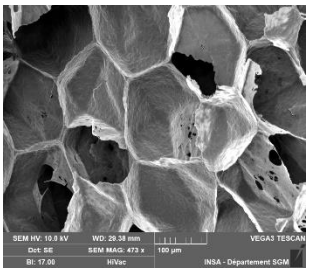
L-EMIM Ac-10	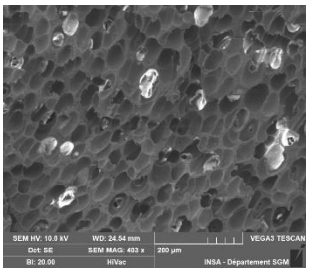	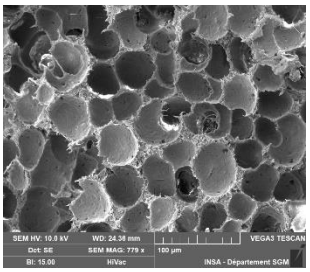
L-[AEMIM] Br-10	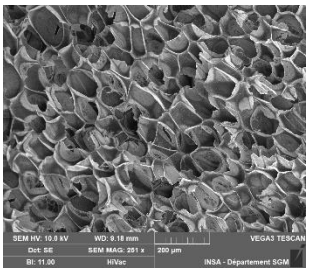	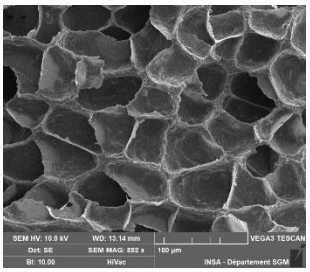
Zn-Ionomer-10	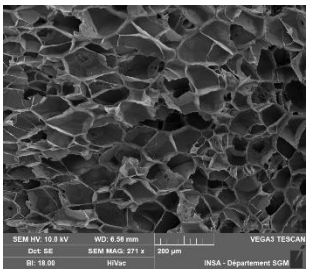	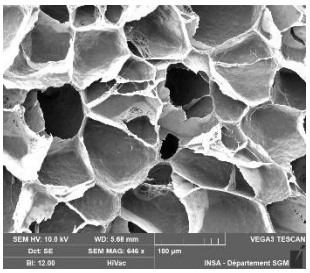
135 ºC L-[AEMIM] Br-10	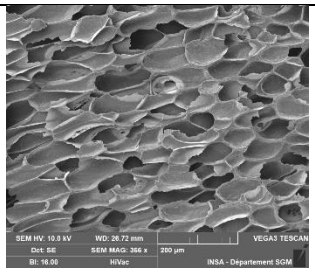	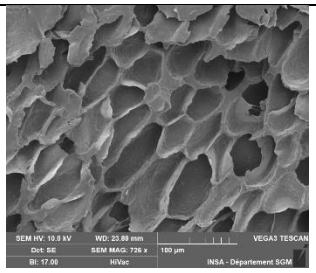

Zn-Ionomer-10

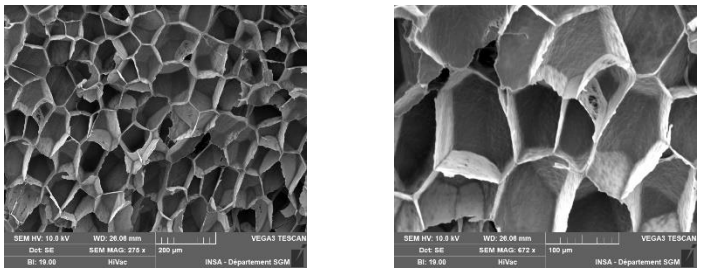

Figure 11 Morphologie cellulaire des échantillons de mousse de PPgMA et de ses LIonomères

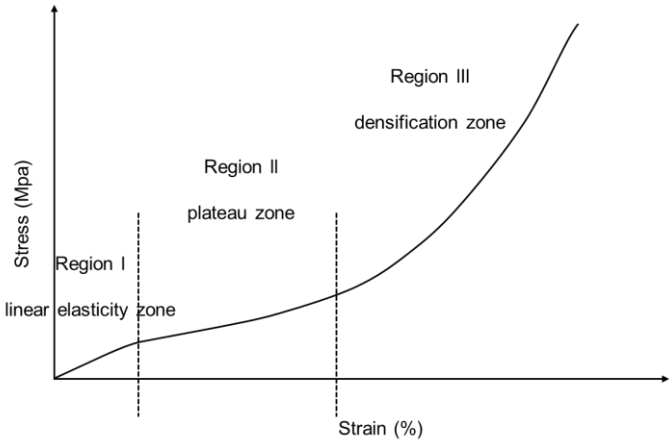

Figure 12 Courbes typiques de contrainte-déformation obtenues lors d'essais mécaniques de compression montrant les trois principaux régimes différents.

- **Principaux résultats**

L'uniformité améliorée de la morphologie, de la taille et de la densité des cellules est obtenue avec les LIonomers et les Zn-Ionomers. Ces modifications sont déterminées par la force élevée de la fusion, puisque la force extrême de la fusion supprime la coalescence et la rupture des cellules, et empêche la génération de grosses mousses [22–24] (voir Figure 11). En même temps, pendant la croissance des cellules, le substrat subit une extension biaxiale [28]. L'amélioration de la viscosité à haute température grâce aux réseaux ioniques des LIonomères peut être la principale cause de l'amélioration de la capacité de moussage du substrat polymère. Le comportement moussant des LIonomères traités avec divers liquides ioniques diffère.

Cette variété est très liée aux schémas d'absorption des liquides ioniques correspondants [29–33] (voir Figure 12). En outre, les LIonomères expansés traités avec 10 % en poids de P+DEP, EMIM DEP ou EMIM Ac présentent une densité supérieure à celle du PPgMA pur. Ces conclusions peuvent être attribuées à l'impact d'une température et d'une pression élevées et continues sur la capacité d'absorption du CO_2 des LI, le processus d'absorption pouvant être achevé en quelques minutes [34].

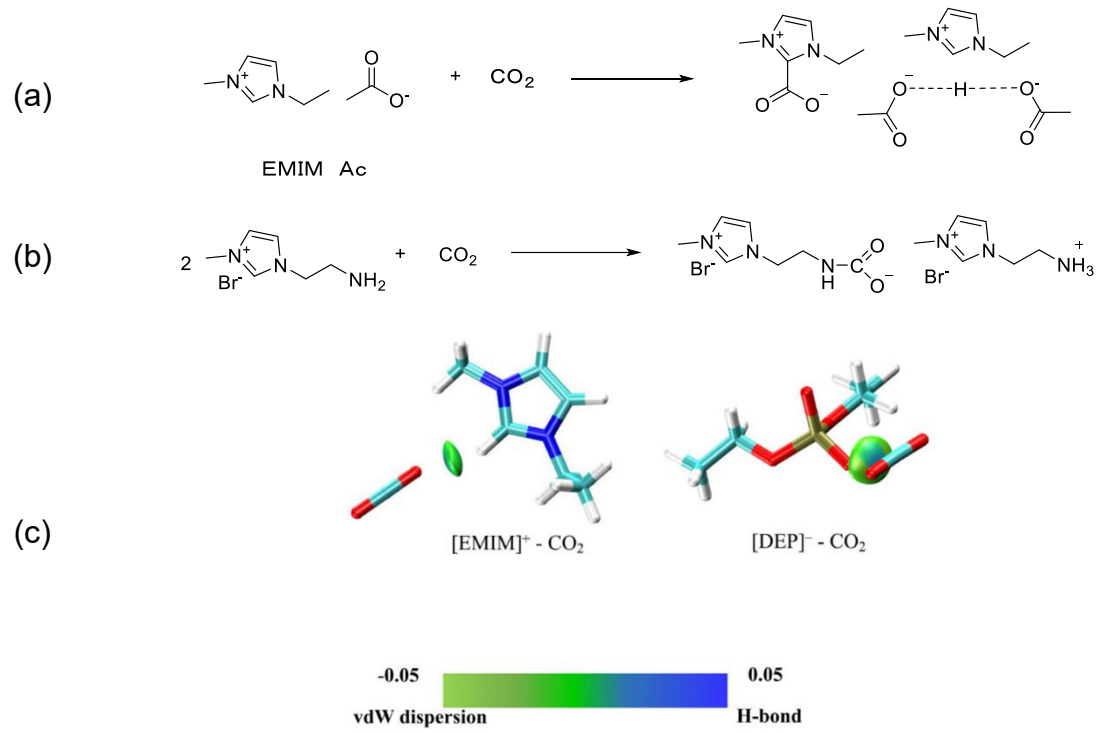

Figure 13 Les diagrammes d'absorption de CO_2 de différents liquides ioniques

Outre le fait de renforcer la résistance de la fusion, une teneur élevée en [AEMIM] Br pourrait également augmenter la solubilité du CO_2. Une dissolution élevée du CO_2 facilite la nucléation et la densité des cellules et favorise la croissance des bulles [35] et la finesse des parois des vésicules. Par conséquent, le L-[AEMIM] Br-10 présente une porosité, un taux d'expansion et une densité cellulaire supérieurs à ceux du L-[AEMIM] Br-2. En même temps, les mélanges de polymères contenant des groupes amino présentent une plus grande solubilité dans le CO_2 que les ionomères de zinc, dont la solubilité est comparable à celle du PPgMA parent [36]. Par conséquent, le L-[AEMIM] Br-10 indique une densité cellulaire plus élevée que celle du Zn-Ionomer-10. En outre, le Zn-Ionomer peut faciliter la nucléation des cellules en fournissant une

quantité substantielle de sites de nucléation dans le processus de moussage [37,38], ce qui entraîne une grande amélioration de la morphologie des cellules.

D'autre part, l'augmentation de la température de moussage conduit à l'augmentation du diamètre moyen des cellules, du taux d'expansion et à la diminution des cellules. La diminution de la densité cellulaire et l'augmentation du diamètre cellulaire interprètent l'effondrement des petites cellules en raison d'une température de moussage plus élevée [5,18,25,26].

Conformément à la théorie de Gibson-Ashby, le processus de contrainte-déformation en compression peut être divisé en trois étapes : l'étape d'élasticité linéaire, l'étape de plate-forme et l'étape de compression [39] (voir Figure 13). Les échantillons de mousse possédant une taille de cellule moyenne plus importante présentent une capacité d'absorption d'énergie plus importante que ceux possédant une taille de cellule plus petite, tandis que la faible porosité est le principal facteur contribuant à la contrainte de compression élevée.

- **References**

[1] Krause B, Sijbesma H J P, Münüklü P, et al. Bicontinuous nanoporous polymers by carbon dioxide foaming[J]. Macromolecules, 2001, 34(25): 8792-8801.

[2] Doroudiani S, Park C B, Kortschot M T. Effect of the crystallinity and morphology on the microcellular foam structure of semicrystalline polymers[J]. Polymer Engineering & Science, 1996, 36(21): 2645-2662.

[3] Suh K W, Park C P, Maurer M J, et al. Lightweight cellular plastics[J]. Advanced Materials, 2000, 12(23): 1779-1789.

[4] Tomasko D L, Li H, Liu D, et al. A review of CO_2 applications in the processing of polymers[J]. Industrial & Engineering Chemistry Research, 2003, 42(25): 6431-6456.

[5] Xu Z M, Jiang X L, Liu T, et al. Foaming of polypropylene with supercritical carbon dioxide[J]. The Journal of Supercritical Fluids, 2007, 41(2): 299-310.

[6] Fu D, Chen F, Kuang T, et al. Supercritical CO_2 foaming of pressure-induced-flow processed linear polypropylene[J]. Materials & Design, 2016, 93: 509-513.

[7] Naguib H E, Park C B, Panzer U, et al. Strategies for achieving ultra low-density polypropylene foams[J]. Polymer Engineering & Science, 2002, 42(7): 1481-1492.

[8] Naguib H E, Park C B, Reichelt N. Fundamental foaming mechanisms governing the volume expansion of extruded polypropylene foams[J]. Journal of Applied Polymer Science, 2004, 91(4): 2661-2668.

[9] Pop-Iliev R, Rizvi G M, Park C B. The importance of timely polymer sintering while processing polypropylene foams in rotational molding[J]. Polymer Engineering & Science, 2003, 43(1): 40-54.

[10] Li H, Zhang X M, Zhu S Y, et al. Preparation of polypropylene and polystyrene with -NCO and -NH2 functional groups and their applications in polypropylene/polystyrene blends[J]. Polymer Engineering & Science, 2015, 55(3): 614-623.

[11] Kuo C C, Liu L C, Liang W C, et al. Preparation of polypropylene (PP) composite foams with high impact strengths by supercritical carbon dioxide and their feasible evaluation for electronic packages[J]. Composites Part B: Engineering, 2015, 79: 1-5.

[12] Gong W, Yu J, Fu H, et al. Strengthening and toughening mechanisms for polypropylene/glass fiber composite foams under three-phase coexistence[J]. Polimery, 2015, 60(7-8): 457-461.

[13] Bhamidipati M, Scurto A M, Detamore M S. The future of carbon dioxide for polymer processing in tissue engineering[J]. Tissue Engineering Part B: Reviews, 2013, 19(3): 221-232.

[14] White L J, Hutter V, Tai H, et al. The effect of processing variables on morphological and mechanical properties of supercritical CO_2 foamed scaffolds for tissue engineering[J]. Acta biomaterialia, 2012, 8(1): 61-71.

[15] Sheng S J, Hu X, Wang F, et al. Mechanical and thermal property characterization of poly-L-lactide (PLLA) scaffold developed using pressure-controllable green foaming technology[J]. Materials Science and Engineering: C, 2015, 49: 612-622.

[16] Montjovent M O, Mathieu L, Hinz B, et al. Biocompatibility of bioresorbable poly (L-lactic acid) composite scaffolds obtained by supercritical gas foaming with human fetal bone cells[J]. Tissue engineering, 2005, 11(11-12): 1640-1649.

[17] Dlouhá J, Suryanegara L, Yano H. The role of cellulose nanofibres in supercritical foaming of polylactic acid and their effect on the foam morphology[J]. Soft Matter, 2012, 8(33): 8704-8713.

[18] Ding J, Shangguan J, Ma W, et al. Foaming behavior of microcellular foam polypropylene/modified nano calcium carbonate composites[J]. Journal of Applied Polymer Science, 2013, 128(6): 3639-3651.

[19] Hani E. Naguib, Chul B. Park, Patrick C. Lee. Effect of Talc Content on the Volume Expansion Ratio of Extruded PP Foams[J]. Journal of Cellular Plastics, 2003, 39(6): 499-511.

[20] Kwon Y, Cooke R E, Park C. Representative unit-cell models for open-cell metal foams

with or without elastic filler[J]. Materials Science and Engineering: A, 2003, 343: 63-70.

[21] Wang X, Max R Salick, Guo Y, et al. Interconnected porous poly(ε-caprolactone) tissue engineering scaffolds fabricated by microcellular injection molding[J]. Journal of Cellular Plastics, 2018, 54(2): 379-397.

[22] Zhai W, Wang H, Yu J, et al. Cell coalescence suppressed by crosslinking structure in polypropylene microcellular foaming[J]. Polymer Engineering & Science, 2008, 48(7): 1312-1321.

[23] Zheng W G, Lee Y H, Park C B. Use of nanoparticles for improving the foaming behaviors of linear PP[J]. Journal of Applied Polymer Science, 2010, 117(5): 2972-2979.

[24] Park C B, Cheung L K. A study of cell nucleation in the extrusion of polypropylene foams[J]. Polymer Engineering & Science, 1997, 37(1): 1-10.

[25] Corre Y M, Maazouz A, Duchet J, et al. Batch foaming of chain extended PLA with supercritical CO_2: Influence of the rheological properties and the process parameters on the cellular structure[J]. The Journal of Supercritical Fluids, 2011, 58(1): 177-188.

[26] Li Y, Yao Z, Chen Z hua, et al. Numerical simulation of polypropylene foaming process assisted by carbon dioxide: Bubble growth dynamics and stability[J]. Chemical Engineering Science, 2011, 66(16): 3656-3665.

[27] Huang H X, Wang J K. Improving polypropylene microcellular foaming through blending and the addition of nano-calcium carbonate[J]. Journal of Applied Polymer Science, 2007, 106(1): 505-513.

[28] Arefmanesh A, Advani S G. Diffusion-induced growth of a gas bubble in a viscoelastic fluid[J]. Rheologica Acta, 1991, 30(3): 274-283.

[29] Sistla Y S, Khanna A. CO_2 absorption studies in amino acid-anion based ionic liquids[J]. Chemical Engineering Journal, 2015, 273: 268-276.

[30] Said R B, Kolle J M, Essalah K, et al. A Unified Approach to CO_2 –Amine Reaction Mechanisms[J]. ACS Omega, 2020, 5(40): 26125-26133.

[31] Huang Z. Study on Supported Triamino-functionalized Ionic Liquids for Carbon Dioxide Capture[J]. 114.

[32] Chen F F, Huang K, Fan J P, et al. Chemical solvent in chemical solvent: A class of hybrid materials for effective capture of CO_2[J]. AIChE Journal, 2018, 64(2): 632-639.

[33] Zhu R, Huang S, Gui C, et al. Capturing low-carbon alcohols from CO_2 gas with ionic liquids[J]. Chemical Engineering Science, 2022, 258: 117745.

[34] Wang J, Petit C, Zhang X, et al. Simultaneous measurement of CO_2 sorption and swelling of phosphate-based ionic liquid[J]. Green Energy & Environment, 2016, 1(3): 258-265.

[35] Low B T, Xiao Y, Chung T S, et al. Simultaneous occurrence of chemical grafting, cross-

linking, and etching on the surface of polyimide membranes and their impact on H_2/CO_2 separation[J]. Macromolecules, 2008, 41(4): 1297-1309.

[36] Li Y, Yao Z, Chen Z hua, et al. High melt strength polypropylene by ionic modification: Preparation, rheological properties and foaming behaviors[J]. Polymer, 2015, 70: 207-214.

[37] Jiang X L, Bao J B, Liu T, et al. Microcellular foaming of polypropylene/clay nanocomposites with supercritical carbon dioxide[J]. Journal of Cellular Plastics, 2009, 45(6): 515-538.

[38] Yu K, Jiang H, Zhou H, et al. Evolution of double crystal melting peak in polypropylene foam assisted by β-nucleating agent and supercritical CO_2[J]. Journal of Applied Polymer Science, 2018, 135(12): 46007.

[39] Gibson L J, Ashby M F. Cellular Solids: Structure and Properties[M]. 2nd ed. Cambridge: Cambridge University Press, 1997.

Chapitre 5 Conclusions et Perspectives

- **Conclusions**

En résumé, ce travail a permis de synthétiser avec succès une nouvelle génération d'ionomère (appelé LIonomer) en combinant pour la première fois des liquides ioniques et de l'anhydride maléique greffé au polypropylène, et d'étudier son application potentielle sur des matériaux légers. Cette nouvelle utilisation des liquides ioniques pourrait enrichir la communauté des composites. Les principaux résultats sont les suivants :

- En ce qui concerne les liquides ioniques à base de phosphonium, le faible encombrement stérique contribue de manière significative aux fortes interactions au sein des LIonomères (mélanges PPgMA/P^{+}DEP). D'autre part, le cation imidazolium peut créer plus de points d'interaction avec les groupes polaires du squelette du polymère si le contre-anion a une polarité suffisante (comme le phosphate, l'acétate). Ces interactions générées conduisent à une amélioration des propriétés de la matière solide et de la matière fondue, plutôt que le rôle du plastifiant qui affaiblit la viscosité et le module. En plus de l'effet des interactions entre le liquide ionique et les groupes polaires dans les LIonomères, la performance du polymère pourrait également être influencée par les branches "liquides" qui en résultent en utilisant le COO^{-} généré par le polymère ou le groupe imide formé comme "groupe de tête" et les paires cation/anion comme composants, ainsi que sa longueur. Ce nouveau réengagement des paires ioniques dans les mélanges conduit à de nouveaux types de réseaux ioniques.
- La propriété sur mesure du LIonomer pourrait être réalisée en changeant les combinaisons cation/anion des liquides ioniques coopérés. Par exemple, la rigidité pure et la viscosité extrêmement élevée pourraient être obtenues en introduisant le bromure de 1-aminoéthyl-3-méthylimidazolium, tout en envisageant le

phosphate diéthylique de 1-Ethyl-3-méthylimidazolium (EMIM DEP) ou l'acétate de 1-Ethyl-3-méthylimidazolium (EMIM Ac) lorsque le compromis entre rigidité et extensibilité est souhaité. Ce compromis n'a pas pu être obtenu avec l'ionomère de zinc traditionnel.

- L'aptitude à la mousse et la propriété de compression de la matrice polymère ont été considérablement améliorées par l'ajout de liquides ioniques spéciaux. La taille moyenne des cellules du LIonomère expansé a pu atteindre 40 μm grâce à la coopération de 10 % en poids de bromure de 1-aminoéthyl-3-méthylimidazolium, alors que le PPgMA pur n'a pas pu être expansé en raison de sa très faible viscosité. Les échantillons moussés possédant une taille de cellule moyenne plus importante présentent une capacité d'absorption d'énergie plus importante que ceux possédant une taille de cellule plus petite, tandis que la faible porosité est le principal facteur contribuant à la contrainte de compression élevée. Dans le même temps, ces propriétés sont fortement liées à la capacité des liquides ioniques à absorber le dioxyde de carbone lorsqu'on utilise du dioxyde de carbone supercritique comme agent moussant physique.

- **Perspectives**

Ce travail propose pour la première fois le concept de LIonomer - nouvelle génération d'ionomères - et les a synthétisés en combinant des liquides ioniques et de l'anhydride maléique greffé au polypropylène, et a étudié leur application potentielle sur des matériaux légers. Afin de poursuivre ce premier travail, plusieurs autres études pourraient être envisagées :

- L'universalité de ces trois liquides ioniques (bromure de 1-aminoéthyl-3-méthylimidazolium, phosphate diéthylique de 1-Ethyl-3-méthylimidazolium, et acétate de 1-Ethyl-3-méthylimidazolium) dans différents polymères doit encore être étudiée. Ce travail a prouvé l'effet de ces trois liquides ioniques dans l'anhydride maléique greffé au polypropylène (polymère à semi-cristallisation), cependant,

l'étude dans les polymères amorphes (par exemple le polystyrène, le plastique acrylonitrile-butadiène-styrène) et dégradables (par exemple l'acide polylactique) doit être approfondie.

- Face à la propriété fonctionnelle souhaitée, par exemple une surface hydrophobe, les combinaisons de différents liquides ioniques peuvent être envisagées si de fortes interactions ne peuvent être obtenues entre l'anhydride maléique et un seul liquide ionique fluoré (comme le tétrafluoroborate de 1-butyl-3-méthylimidazolium, l'hexafluorophosphate de 1-butyl-3-méthylimidazolium).
- La capacité d'absorption du CO_2 par les liquides ioniques doit être étudiée de manière plus approfondie, notamment à haute température et à haute pression. Car cette capacité est très liée à la propriété finale des matériaux légers préparés.

Chapter 1: Literature Review

Table of contents

Chapter 1: Literature Review

1.1 Ionomers

1.1.1 Introduction

During the last decades, polymers containing ionized groups have received growing attention. Among them, ionomers are polymers containing both electrically neutral and ionized groups that are frequently carboxylic, phosphoric or sulfonic acid anions fully or partially neutralized by metal salts [1,2], such as zinc (Zn^{2+}), sodium (Na^{+}) or potassium (K^{+}) cations. These ionic groups may produce phase-separated morphologies (ionic aggregates) due to the Columbic interactions between ions embedded in the matrix with a low dielectric constant [3]. Meanwhile, the interactions among ionic groups improve and reinforce the intermolecular forces, resulting in kind of physical cross-linking points. These formed ionic aggregates are also able to modify the viscoelastic properties of ionomers. At a certain level of entanglement density caused by the increased interactions between ion pairs, the mechanical properties such as tensile strength and impact resistance can also be improved [4].

The subsequent sections will focus on providing an overview of the current state-of-the-art in ionomers research, including its history, their impact on the physical properties of the resulting polymer materials, and finally, their different applications.

1.1.2 Historical features

The study of ionomers dates back to the 1950s. In 1946, Ambrose *et al* [5] discovered that chlorosulphonated and chlorinated polyethylene could be vulcanized with metal oxides to give an ionic covalently crosslinked elastomer. DuPont Co produced these elastomers ionomers on an industrial scale in the early 1950s under the trade name Hypalon®. In 1954, Brown and his colleagues [6] developed an "ionically crosslinked" material from terpolymer of butadiene, acrylonitrile, and methacrylic acid as backbone. Their later terpolymers have a carboxyl content of 0.01 mol (per 100 parts of rubber) and 0.02 mol (per 100 parts of rubber) of zinc oxide after vulcanisation.

The tensile strength and the strain at beak are 62 MPa and 550%, respectively. The vulcanised rubber undergoes a high permanent compression deformation and a fast stress relaxation. Later in 1957 and 1963, they [7,8] investigated the ionic crosslinking effect of metal salts on butadiene/methacrylic acid copolymers. In the mid-1960s, DuPont [9] produced an ethylene/methacrylic acid copolymer partially neutralized with sodium or zinc ions under the trade name Surlyn®. This first industrial Surlyn® product demonstrated the technological advances that DuPont has made in vinyl polymers for over 40 years. These materials displayed better toughness, transparency, elasticity, and polar characteristics than traditional polyethylene and they could be melt-processed for important applications, such as coating and packaging. In 1964, Rees *et al* [2] published a paper naming these types of materials as "ionomers" and believed that the strong intermolecular forces result from electrostatic interactions between negatively charged groups "hang" from the hydrocarbon chain and positively charged groups. They proposed two ways to explain such resulting molecular structures and the forces at work, *i.e. i)* the ions are located between the molecular chains and the distance between them is large and beyond the control of electrostatic forces, unless there are "clusters" of ions. A positive ion can attract not just one carboxylate ion but several. When the ions are clustered together, also they exhibit a similar structure to the crystallization of inorganic materials and this structure may act as a cross-linking point; *ii)* there is hydrogen bonding between the metal ion and the free acid ion, where the hydrogen atom can be considered as a "bridge" and leads to crosslinking. However, there was no evidence to support this.

In 1968, the first qualitative structure model of the random ionomers (ethylene-acrylic acid (E/AA) copolymer salts) was presented (see Figure 1-1) [10]. According to their work, a small number of ionic clusters illustrated an efficient multifunctional crosslinking effect on the ionomer molecular chains (particularly the amorphous region), *i.e. i)* there were short hydrocarbon chains (for example carboxyl groups) that may be hydrogen-bonded, and ionised carboxyl groups; *ii)* the presence of multiple ionic regions, such as one or two monovalent ions surrounded by several carboxyl groups

dragged out of the crystalline region; *iii)* a trivalent ion in the ionic region was equivalent to two monovalent ions, also surrounded by the same number of carboxyl groups; *iv)* the "clusters" of polar groups inhibiting the growth of polymer chain crystals acted as a kind of block, embedded in the polymer matrix; *v)* the ionic bonding was dispersive and non-directional. In the same year, Longworth *et al* [11] proposed a structural model based on the results of small angle X-ray scattering (SAXS) analysis of E/MAA (ethylene/methacrylic acid) sodium ionomers (see Figure 1-2). This model suggested three phases existing in E/MAA ionomers, *i.e*. ion cluster phase, crystalline phase, and PE amorphous phase containing a small number of discrete sodium carboxylate ion pairs. The ion-related peaks on SAXS were argued to be generated by the ordered hydrocarbon chain segments between the ion clusters rather than by scattering from the aggregates themselves. However, this model displays some drawbacks, *i.e.* neither explains the lack of difference in melting point and crystallinity between the copolymer and its ionomer, nor the experimental fact that the cesium salt ionomer has a stronger ion peak than the lithium salt ionomer.

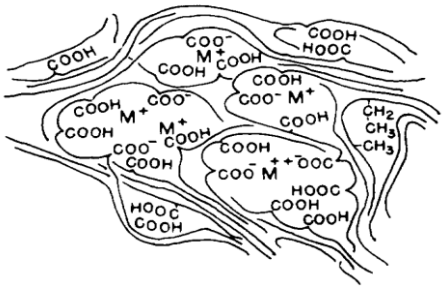

Figure 1- 1 Proposed model for E/AA ionomers morphology [10]

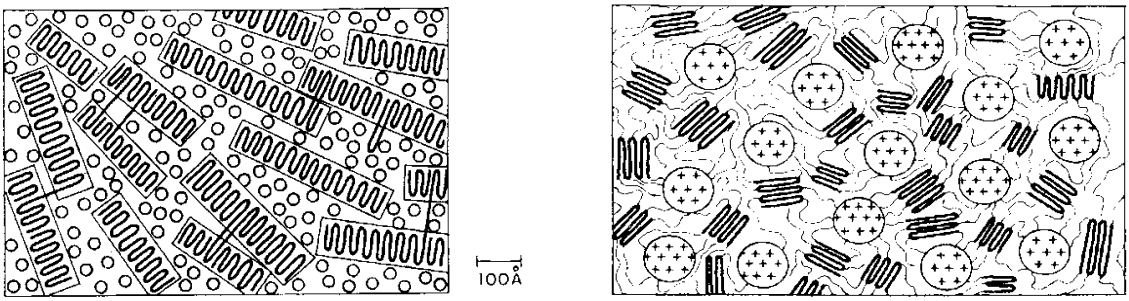

a b

Figure 1- 2 Schematics of (a) E/MAA; and (b) E/MAA sodium ionomer [11]

In 1970, A. Eisenberg *et al* [12] proposed a theoretical model for ionic clusters of random ionomers. According to their model, due to the low dielectric properties of hydrocarbon chains and the electrostatic interactions between charges, ions mostly exist in the form of ion pairs or "multiplets" (even at high temperatures). Such ion-rich zones did not contain hydrocarbon chain components but were surrounded by hydrocarbon chains. The theoretical model concluded that the amorphous phase of polymer contained up to 8 ion pairs. At a certain characteristic temperature, the isolated aggregates form "ionic clusters". Three major factors may govern the formation of multiple ion pairs: ***(a)*** the size of the polymer chains and ion pairs; ***(b)*** the amount of tension along the macromolecular chains as the ion pairs aggregate; ***(c***) the electrostatic energy released during the formation of the multiple ion pairs.

In 1973 Marx *et al* [13] established a model suggesting that the ion-related peaks on SAXS patterns are related to the curves were due to the difference of electron density between the metal cation and the hydrocarbon chains. Their model explained the small size of the ion-pair aggregates in the E/MAA and B/MAA (butadiene methacrylate copolymer) ionomers. In addition, they demonstrated that the number of ion-pairs in the aggregates is supposed to be less than six (even at a very high ion content). It also proposed the existence of multiple ion pairs within ionomers, rather than the existence of ion clusters or phase separation phenomenon. This model explains SAXS results in a better, but is not consistent with the glass transition temperatures (T_g) and mechanical properties of the ionomers.

In 1974, MacKnight *et al* [14] derived the "nucleus-shell" model from the formula for the radial distribution of X-ray scattering from partially neutralised poly (ethylene-butyrate) acid ionomers. According to the model, the ionomers included ionic clusters of ion pairs dozens with radii of about 0.8-1.0 nm, denoted as the 'nucleus'. This ‘nucleus’ was surrounded by a 'shell' of hydrocarbon chains. Such a model could explain the higher T_g close to the nucleus. In 1980, Roche *et al* [15] proposed a model similar to the 'core-shell' model but considering a different geometric distribution of ionic clusters. In their research, the ‘core’ was lamellar flanked by regions with counter

ions determining the closest distance to other ion pairs, rather than spherical as previously. The spatial structure of the 'nucleus' and 'shell' could explain the ion-related peaks on SAXS patterns, while the size of the ion clusters resulted from a phase separation phenomenon.

In 1982, Forsman *et al* [16] proposed a theoretical model suggesting the formation of ionic clusters via the direct aggregation of adjacent molecular chains containing ion pairs (Figure 1-3). This model is applicable to ionomer melts and solutions rather concentrated solutions. However, this model doesn't take into account the presence of isolated ion pairs and assumed that the ion pairs were all located in the ion clusters. According to this model, the macromolecular chains between ionic groups could be considered to able to a Gaussian chain distribution. Therefore, such a model is only applicable to amorphous polymer-based ionomers with low ion pair content.

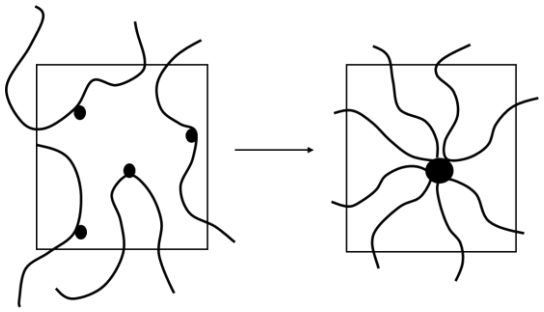

Figure 1- 3 Schematics of the formation of a ionic cluster according to Forsman's model [16]

In 1983, Yarusso *et al* [17] proposed the 'hard sphere model' considering that aggregates within ionomers existed in a regular liquid-like arrangement and interference between aggregated hard sphere particles lead to ion-related peaks on SAXS patterns. In 1985, the 'modified hard sphere model' was proposed (Figure 1-4) [18] suggesting that aggregates surrounded by hydrocarbon chains could neither develop into ionic clusters nor produce micro-phase separation. This model could fit well with the SAXS patterns of sulphonated polystyrene ionomers but did not explain the mechanical properties of these ionic materials. The model proposed by Ding *et al* [19] (Figure 1-5) in 1988 also proposed that the SAXS patterns could be interpreted by the interference between the ion cluster particles.

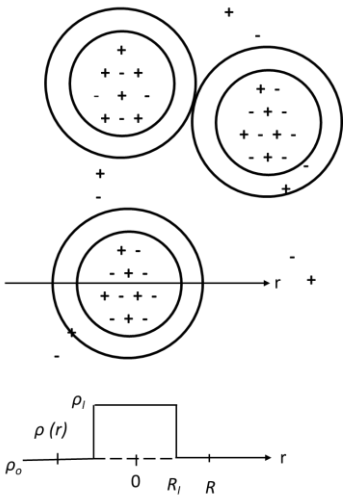

Figure 1- 4 Schematics of modified hard sphere model and corresponding electron density profile for one of the ionic cluster [18]

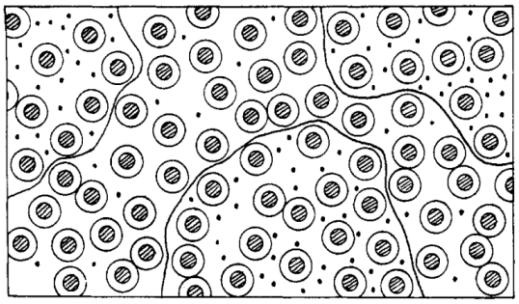

Figure 1- 5 Possible model for the source of zero-angle scattering. Dots represent dissolved cations. Solid line boundaries are drawn to visualize the non-homogeneous distribution of dissolved cations [19]

In 1984, Dreyfus *et al* [20] proposed a theoretical crystallization-like model. These authors referred to the electrostatic interactions that drive the aggregation of ion pairs to form multiple ion pairs as the basic electrostatic energy. Then, the residual electrostatic interaction energy between the ion pairs impelled the further aggregation of multiple ion pairs, generating ion clusters. Two features of this crystallization-like model included ***a)*** the ion clusters were internally ordered and could be considered as small crystals; ***b)*** the ion clusters themselves were also ordered over a larger size range. During the same year, Datye *et al* [21] also proposed a similar theoretical structural model based on electrostatic and elasticity theory.

In 1990, Eisenberg *et al* [22] modified their previously proposed model of ionic

clusters and proposed the 'motion-limited' model, also known as the Eisenber-Hird-Morre (EHM) model. According to the existence of multiple ion pairs and keeping the original definition of multiple ion pair clusters, EHM model assumed ***a)*** the appearance of a layer of motion-limited polymer chains around the multiple ion pair and ***b)*** the thickness of the motion-restricted layer around the multiple ion pair was of the same order of magnitude as the relative chain length of the polymer backbone. The multiple ion pairs acting as crosslinkings increase T_g. As the ion concentration increases, a larger continuous region may be formed due to the superposition of each multiple ion pair on each other in the surrounding motion-limited region. But as the ion concentration is large enough, a phase separation could occur. This model also demonstrates that ***a)*** ion clusters did not have a specific geometry and ***b)*** there is no specific size or number of ion pairs or multiple ion pairs in each cluster. The conclusions from this model are in agreement with experimental data such as SAXS and DMA (dynamic mechanical properties) analyses for many ionomers. A. Eisenberg argued that phase separation of ionomers could occur if several conditions must be present: *i)* the ion pairs must be aggregated to produce ionic multiplets; *ii)* the multiple ion pairs must be rigid, *i.e.* the ionic groups must be tightly bound together, reducing the mobility of the surrounding polymer chains; *iii)* the multiple ion pairs must be close enough to overlap the motion-limited layers surrounding the multiple ion pairs; *iv)* when the temperature is higher than the T_g of the non-ionic cluster phase, even though the ion pairs in the multiple ion pair migrate to each other, the multiple ion pair must still exist. The authors demonstrated that for the St/MAA (styrene/methacrylic acid copolymer) sodium ionomers the structure of a multiple ion-pair core and its surrounding is composed of motion-limited polymer chains (see Figure 1-6).

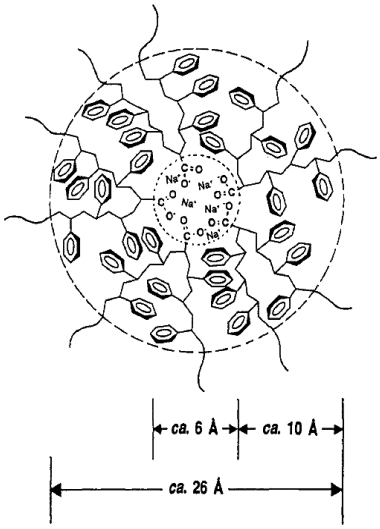

Figure 1- 6 Schematics of a ionic multiplet and the surrounding region of restricted mobility of polymer chains for a St/MAA sodium ionomer [22]

The previous studies of ionomers and the developed models concerned mainly random ionomers. With the development of ionomer synthesis, the investigation of ionomers nano/micro structures has been extended from established ionomers to other types of ionomers. Register [23] had systematically studied remote claw ionomers of polyisoprene and confirmed the exacerbated inter-chain entanglement due to the aggregation of chain end groups. The ion aggregation in block ionomer occurred only within the block where the ionic groups are located [24], and the ionised regions of the block polymer often exhibited a specific behaviour of "phase within a phase" due to the inherent block phase separation therein [25].

All of the models related previously have limitations, since ion-pair aggregates have sizes of only few nanometre and could be convinced easily by TEM on SAXS. The presence and shape of ion-pair aggregates cannot be directly observed by conventional methods such as electron microscopies. The consensus for the presence of ion-pair aggregates in ionomers leading to a physical crosslinking of macromolecular chains is now there. A breakthrough in the experimental study of ionomer morphology was achieved in 1998, when Laurer [26] directly observed ion-pair aggregates of E/MAA copolymer neutralized by zinc salt using scanning transmission electron microscopy (SEM) equipped with both a high-angle ring dark-field and bright-field scintillation

detectors. These ion-pair aggregates were approximately spherical in shape with diameters from 2.5 to 2.8 nm and a uniform size. Their work provided direct evidence for the existence of ion-pair aggregates within ionomer.

1.1.3 Ionomer properties

Due to the presence of ionic pairs and clusters, as well as the difference in polarity between the ionic groups and the hydrocarbon backbone, ionomers have properties completely different from those of their parent polymers. At the same time, these unique features result in dramatic improvement on the solid and molten properties, such as mechanical properties, T_g and thermal stability, etc.

1.1.3.1 Thermal beaviour

According to Eisenberg's theoretical model (EHM model), the restricted movement of the polymer chains due to the presence of multiple ion pairs and ion clusters within ionomers leads to enhance thermal properties and T_g (glass transition temperature) value.

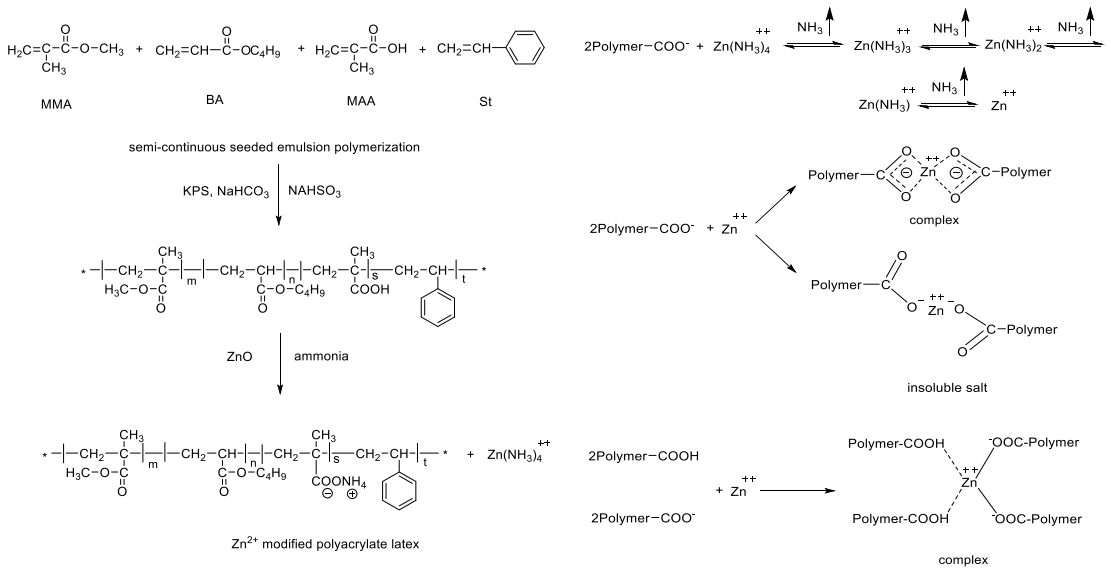

(a) (b)

Scheme 1- 1 Synthetic route of (a) Zn^{2+} self-crosslinkable PAs and (b) their crosslinking reactions [27]

Yan *et al* [27] considered Zn-ionomers with using ZnO as crosslinker, *i.e.* to

neutralize polyacrylate latexes (PAs) (see Scheme 1-1). From thermal analyses, *i.e.* by DSC (Differential Scanning Calorimetry) and TGA (Thermogravimetric Analysis), these authors showed that T_g increases with increasing of the apparent crosslinked structure. The addition of ZnO could also significantly improve the thermal stability (the initial degradation temperature increases from 297 to 314 °C).

Ghosh *et al* [28] analysed a sulfonated maleated EPDM rubber (m-EPDM) (see Scheme 1-2), neutralized by Na^+ and Zn^{2+} cations to prepare different ionomers containing both carboxylate and sulfonate anions on the same polymer backbone. These two ionomers displayed both cylindrical and spherical ionic domains, from the ionic-type crosslinking. Therefore, the Zn^{2+}-based ionomer exhibited higher T_g value than the Na^+-based one.

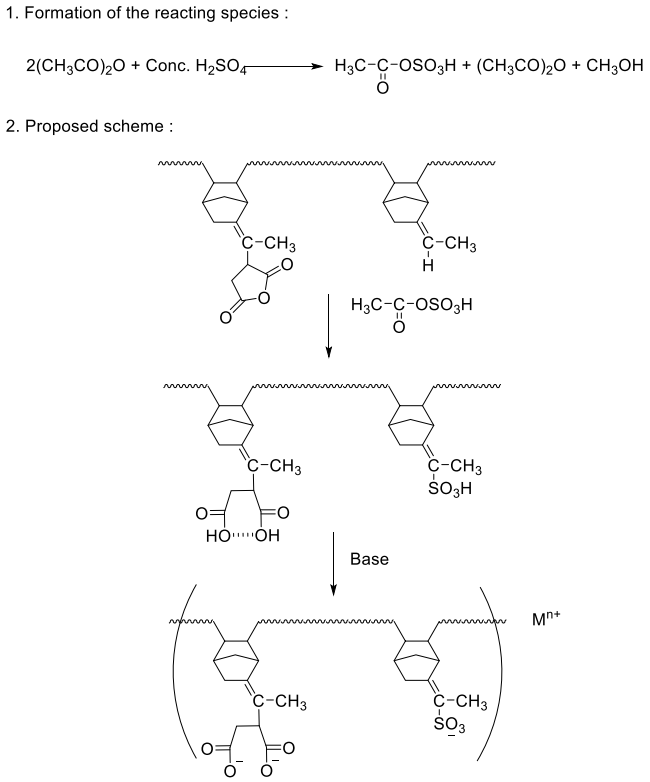

Scheme 1- 2 Schematics of the sulfation of m-EPDM rubber [28]

1.1.3.2 Crystallization behaviour

The presence of ionic clusters may prevent crystallization. In fact, as segmental motions are restricted due to the neighbouring ions. As a consequence, a less ordered crystalline structure with thinner lamellae and lower crystallinity yield could be

observed. In parallel, the introduced metal ions may disrupt the regularity of the molecular chain segments of the matrix. The usually crystallinity also influenced. Therefore, a high degree of neutralization within ionomers which leads to larger ionic clusters conducts to a lower crystallinity of the nanocomposites(see Figure 1-7) [29].

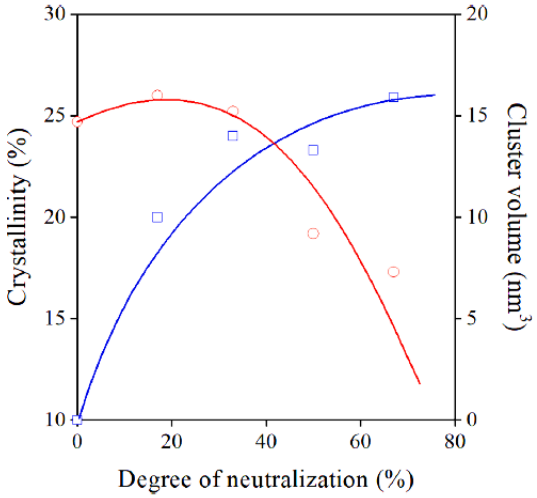

Figure 1- 7 Changes in crystallinity and size the clusters as a function of the degree of neutralization. Symbols: (o) crystallinity (%), (□) cluster volume (nm^3) [29]

1.1.3.3 Mechanical properties

The resulting (ionically) crosslinked structures of ionomer can effectively transfer mechanical stress. As enhanced strength of the material leading to the improvement of mechanical properties. It is worth noting that the mechanical properties of the ionomers depend on the nature of metal ions and preparation methods.

Gao *et al* [30] investigated the effect of metal ions (*i.e.* Na^+, Zn^{2+}, and Al^{3+}) on the mechanical properties of the ionomers based on the ethylene-acrylic acid copolymers. The resulting mechanical properties varied due to the different steric effects of the added metal ions. The mechanical properties of the Na-ionomer and Zn-ionomer increase with the addition of the corresponding salt, while the ones of Al-ionomer decrease with increasing the Al^{3+}-salt content.

Thanks to the involvement of sodium element, Sampath *et al* [31] observed an increase of both yield stress and elastic modulus compared to neat polyethylene-co-methacrylic acid (PEMAA). These two physical characteristics increase with increasing

the ion content due to the highest cohesion within ionomers according to ionic groups. On the other hand, the generated ionic aggregates could re-aggregate (becoming very stringy as they were pulled) when modified from the application of an external electric field (see Figure 1-8).

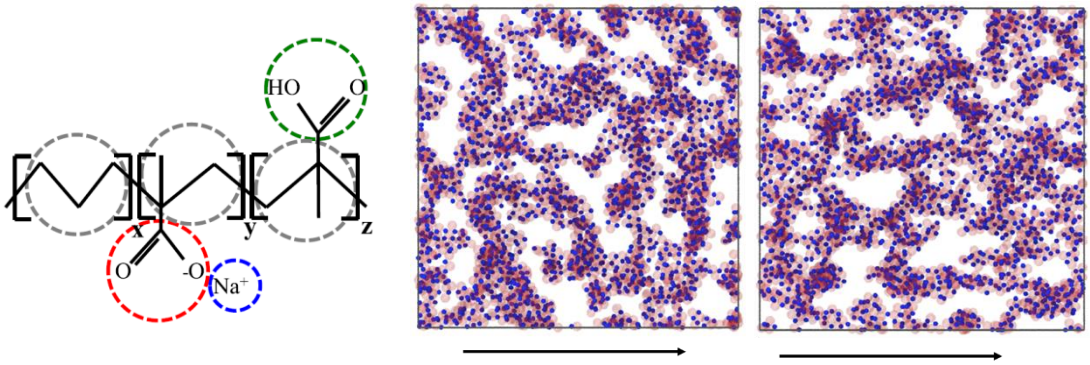

(a) (b)

Figure 1- 8 (a) Chemical structure of the ionomer considered in the study (PEMAA) with pendant groups placed randomly along the chain (coarse grained mapping of the system with the anion shown in red, counterion in blue, sticker in green, and neutral monomers in grey); (b) snapshots showing ions in the $N_{bb}7$ - 50% Na system (with the anions red and translucent, and counter ions blue and opaque, before (left) and after (right) the application of the field (the initial and final snapshots of the E = 2, T* = 1.25 simulation run); the arrow indicates the direction of the field) [31]

1.1.3.4 Rheological behavior

The ion-pair aggregates in the ionomer may undergo reversible crosslinking. Consequently, the viscosity and modulus of the ionomer tracked for the one of a glassy polymer state over crosslinked rue to a thermoplastic-like material.

The nature and concentration of cation/anion pairs have a significant effect on solid and molten properties. Using a twin-screw reactive extruder, Fujiyama *et al* [32] prepared maleic anhydride grafted polypropylene-based thermoplastic elastomers (MPER), which were then ionically cross-linked with nine different metal compounds including aluminum stearate (AlSt), magnesium stearate (MgSt), calcium stearate (CaSt), zinc stearate (ZnSt), potassium stearate (KSt), sodium stearate (NaSt),

magnesium hydroxide (MH), zinc oxide (ZnO), and zinc sulfide (ZnS). The processing properties of the ionomers were analysed by the capillary flow rheology and dynamic mechanical spectrometry. The degree of crosslinking of the gel fraction followed this ranking: AlSt, MgSt, CaSt, ZnSt > NaSt, KSt > MH > ZnO, ZnS > MPER. The viscosity of ionomers and the neat polymer matrix at low shear rate followed the same order. Therefore, the higher the ionic charge, the higher the viscosity building effect of stearic acid, while the lower the viscosity building effect of other compounds compared to stearic acid.

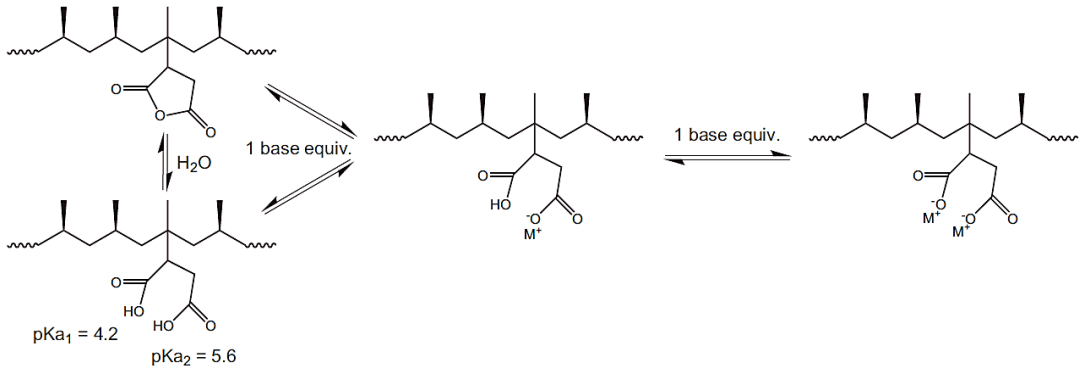

Scheme 1- 3 PPgMA neutralization steps [33]

In the presence of N-bromosuccinimide, two types of carboxylic-based ionomers were produced by adding sodium hydroxide and sodium acetate into PPgMA [33] (Scheme 1-3). The rheological properties showed that the shear modulus and complex viscosity of the ionomer increased significantly with increasing the neutralization level.

1.1.3.5 Swelling abilities

A physically crosslinked structure is generated in the ionomers as they are insoluble in non-polar solvents, and not easily soluble in water and polar solvents. The degree of ion aggregation in ionomer solutions varies with the polarity of the solvent. In low polarity solvents, ionic groups are aggregated, and increasing polarity of the solvent causes the decreasing degree of ion aggregation. As a consequence of the existing solemnization effect, in highly polar solvents the ionic groups are more dispersed from one to another. On the other hand, the physically crosslinked structures are very different as a function of metal ions.

Wang *et al* [34] used NaOH and $Al(OH)_3$ to neutralize the chlorinated poly(vinyl chloride) (CPVC) carboxylated ionic copolymers. According to the swelling state, the Na-ionomer could be dissolved in tetrahydrofuran (THF), whereas the Al-ionomer could be only swelled (Figure 1-9).

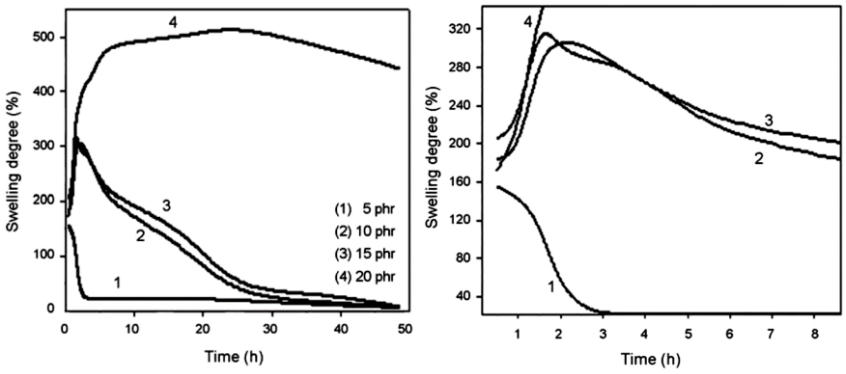

Figure 1- 9 Swelling degree of the Al-ionomers (the neutralization degree 100%) [34]

1.1.4 Ionomer applications

Blended containing ionomers have complex morphologies. Eisenberg *et al* [35] have found that at least six specific interactions could be generated, including ion-ion interactions, ion pair-ion pair interactions, ion-dipole interactions, metal complexation interactions, hydrogen bonding interactions, and hydrophobic interactions. Interactions within ionomers are complex and their internal interactions are likely to be a combination of one or more of the previously cited forces. Therefore, they have gained a wide range of attentions and applications.

1.1.4.1 As compatibilizers

Compatibilization is the most widespread application for ionomers. Ionomers have both polar (polar groups on polymer backbone and added ions) and non-polar (mainly in polymer chains) groups as described above. Therefore, they can be used as compatibilizers to facilitate the blending of polar and non-polar substances as they are compatible with both. In addition, they may improve the rheological, mechanical, and crystallization properties of the blends.

Sodium-, zinc-, and lithium-neutralized ethylene-methacrylic acid ionomers were considered as compatibilizers in polyamide 6/low-density polyethylene (PA6/LDPE)

blends, Sinthavathavorn *et al* [36] investigated the effect of ionomers with different neutralization levels on the melt rheology of the blends. They found that the shear viscosity of the blends is enhanced significantly with the addition of compatibilizers (see Figure 1-10) due to the generation of a grafted copolymer from the reaction of the original amine with free acid groups. In addition, the tailoring of the viscosity of polymer blends by using ionomers as compatibilizers leads to smaller sizes of the dispersed phase (decrease of the interfacial tension) and improved tensile strength of the resulting blends [37,38].

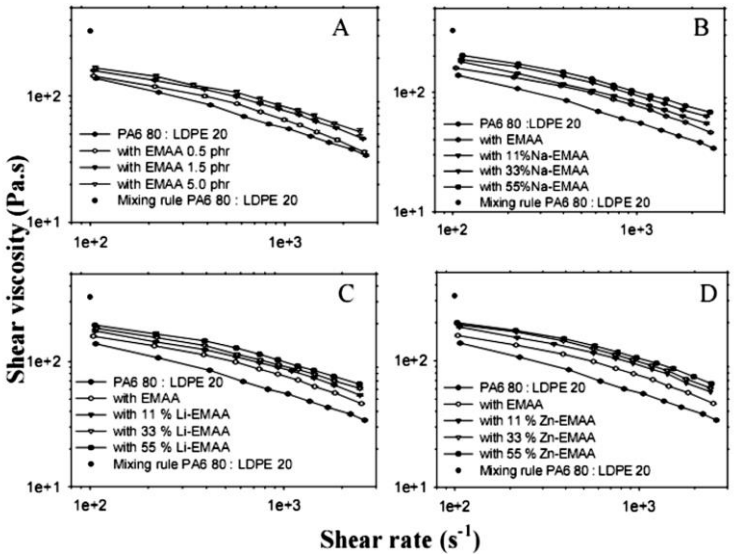

Figure 1- 10 Shear viscosity *vs.* shear rate of PA6 80: LDPE 20 blends with ionomers as compatibilizers (A: E-MAA, B" Na-EMAA at 1.5 phr, C: Zn-EMAA at 1.5 phr, D: Li-EMAA at 1.5 phr) [36]

1.1.4.2 As nucleating agents

Ionomers can also be used as nucleating agents to promote crystallization. In many ionomers, microphase-separated aggregates rich zones in the polymer matrix are formed as a result of the strong attractive interactions between ionic monomer units. The ionic clusters may act as nucleation sites, triggering heterogeneous nucleation and accelerating the rate of crystallization of the polymer. Thankappan *et al* [39] reported the special role of block ionomers by accelerating nucleation and crystallization, *i.e.* the ionic groups located at the end of the polymer chain could act as nucleation sites,

leading to faster crystallization.

However, not all ionomers could contribute to crystallization. Wu *et al* [40] obtained an ionomer from polymethacrylic acid and the reaction of methacrylate group with sodium and zinc ions. By studying the effect of such ionomer on the crystallization behaviour of polyamide (PA6), they showed a decreasing of the crystallinity of the blend after the addition of the ionomer. The added ionomer was believed to influence the PA6 molecular chain, making difficult for these chains to crystallize in the isothermal crystallization process.

1.1.4.3 As conductive materials

The ions in ionomers have good electrical conductivity. So ionomers can also be used as conductive materials, including applications in batteries, membrane electrolysis, capacitors, etc.

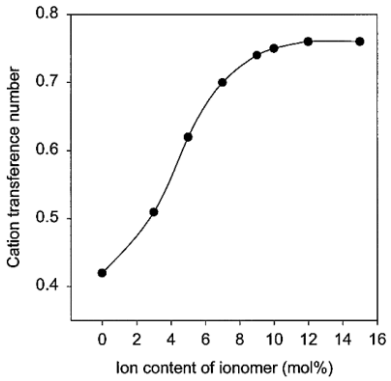

Figure 1- 11 Cation transference number of the plasticized ionomer based polymer electrolytes as a function of the ion content of the ionomer at room temperature [42]

Zhu *et al* [41] produced a film using poly (styrene/acrylic acid) and poly (styrene-butyl acrylate) zinc ionomers. Such film was wrapped around the surface of the zinc electrode, preventing soluble zinc discharge material from entering the solution, and avoiding a change in the shape of the zinc electrode without weakening the conductivity of the electrode. As a result, the life of the zinc electrode in batteries was improved. In addition, a poly (methyl methacrylate-lithium maleate) ionomer was synthesized and used as an electrode [42]. In this study, ion aggregation in ionomers appeared to significantly affect the electrochemical behaviour of ionomer-based

polymer electrolytes (see Figure 1-11).

1.1.4.4 As self-healing materials

The specific intrinsic chemical structures and morphologies of ionomers give them self-healing ability. The self-healing property is not spontaneous but rather transfers the energy from the impact to the polymer. It stores the energy elastically before dissipating it in the form of heat, causing the local temperature of the ionomer to rise above the melting point upon impact. This, in turn, breaks the ionic cross-link. In the molten state, however, the ionic regions in the ionomer allow the polymer to undergo large tensile strains. Spring back when the stored energy is not successfully released, stretching to such an extent that the polymer cavities can close to their original state. The degree of viscoelasticity and physical crosslinking of the ionomer determine the ultimate level and strength of healing. Finally, the key to healing is that ***a)*** the ionomer has enough elastic strength and ***b)*** the ionomer must be able to melt well enough to allow chemical spread at the interface boundary.

Generally, self-healing materials can only heal themselves once. On the opposite, ionomers can heal multiple times [43,44]. The application of self-healing properties of ionomers was first used for military applications to reduce the corrosive of fuel tanks to prevent combustion [43,45,46].

1.1.5 Conclusions

To conclude, the ionomers have been invented and studied for several decades. With the development of characterization tools, researchers have developed a deep understanding on the generation of especially the microstructures of ionic pairs/multiplets in ionomers from STEM in 1998, gave a direct proof of the existence of ion-pair aggregates within ionomers. The generated ion multiplets in ionomers act as crosslinking points to restrain the motions of polymer chains, leading to modifications of overall performances compared to the original polymer matrix. By changing the nature of metal ions for a given polymer could broaden its applications.

1.2 Ionic Liquids

1.2.1 Introduction

Ionic liquids (IL) are composed entirely of ions, *i.e.* an organic cation and organic/inorganic anion [47]. Nowadays, they have been the subject of many academic and industrial studies and becoming one new type of solvents thanks to their unique physical and chemical properties. Their origins refer to 1914 when Walden [48] synthesized the first IL, named ethyl ammonium nitrate. According to the sequence discovery of ILs, it could be roughly divided into three generations. The first generation refers of $AlCl_3$ and halogenated ethyl pyridine ionic liquids [49,50]. These ones were mainly used in electroplating applications. After that, researchers successively developed other metal chloride salts (such as $FeCl_3$, $ZnCl_2$) of alkylimidazoles and alkylpyridines [51]. This type of ILs could adjust the acidity and alkalinity of the substance by changing the mole fraction. Nevertheless, they are very unstable in the air and readily decomposes in the presence of water. In the 1980s, more stable ILs with dialkylimidazolium chloroaluminate cations were developed by Wilkes and Hussey [52]. They received plenty of attention in both academic and industrial fields and opened one new way for electrochemistry. In 1990s, series of dialkylimidazolium ionic liquids were developed, such as hexafluorophosphoric (PF_6^-) and tetrafluoroboric (BF_4^-), etc. [53]. Such ionic liquids exhibit low viscosity, broad electrochemical window, and stable chemical properties. They could be considered as the second generation of room temperature ionic liquids (RTILs) materials. Since 2000, the ionic liquids are further enriched in terms of types and functions. By introducing functional groups with specific functions in the imidazole side chain, the design capabilities of ionic liquids can be fully exploited to give them specific functions and applications, generating "functionalized ionic liquids", *i.e.* the third-generation ionic liquids. The variability of cations and anions results in numerous combinations and then the tunability of ILs properties. Figure 1-12 reports some widely used cations and anions.

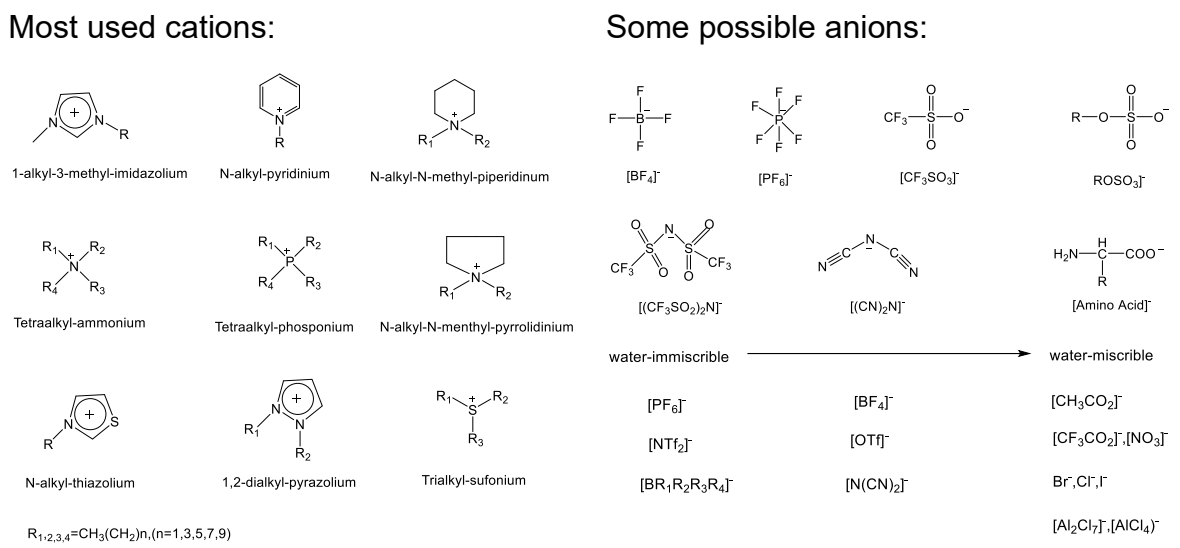

Figure 1- 12 Some of commonly used cations and anions of ionic liquids

1.2.2 Properties of ionic liquids

As mentioned previously, ionic liquids have a unique structure composed entirely of anions and cations. Compared with solid substances, they are in a liquid state at moderate temperatures, while compared with conventional liquid substances, they are ionic. Combining diverse combinations, they exhibit plenty of advantages, such as ***i)*** high solubility [54] could be used as a capacitive or catalytically active carrier for chemical reactions; ***ii)*** high viscosity as the viscosity of ionic liquids is mainly governed by hydrogen bonds and van der Waals forces. The longer the carbon chain on the cationic side chain, the greater the viscosity [55]; ***iii)*** high electrical conductivity leading to unique advantages in the field of electrochemistry [56,57]; ***iv)*** non-volatile and non-flammable [58]; ***v)*** good thermal stability and wide application window [57,59,60]. Compared with other organic salts, ionic liquids have a high thermal and chemical stabilities. Their thermal stability are linked with the interactions between heteroatoms and carbon atoms, and between heteroatoms and hydrogen bonds. Therefore, the stability of ionic liquids is closely related to the structure, nature of anions and cations; ***vi)*** as green solvents, due to their ability to dissolve many substances and their ability to be reused and recycled [61]; ***vii)*** a wide variety of artificial design according to actual requirements [62].

Thanks to these performances [63], ILs have been used in organic synthesis [64–66],

separation and purification, and polymer modification [58,67–72].

1.2.3 Applications in polymers

A century after since the birth of the first ionic liquid, their application in polymers was not reported until 2002. In the past, they have been mainly used in catalysis, analytical chemistry and physical chemistry, rather than being combined with polymers [73]. Actually, they could also be applied in polymerization [74], poly-condensation reaction [75], etc. For example, Strehmel *et al* [76] used ILs as solvents to operate the radical polymerization and obtained a higher polymerization degree than that in toluene. Thanks to the tunable structures and properties of ILs, the desired interactions with polymer could be tailored. The following sections collect some of the works describing the roles of ILs (such as imidazolium-based ILs (ImILs), pyridinium-based ILs (PyILs) and phosphonium based ILs (PhILs), etc.) in various polymer matrices.

1.2.3.1 As (nano)structuration agents

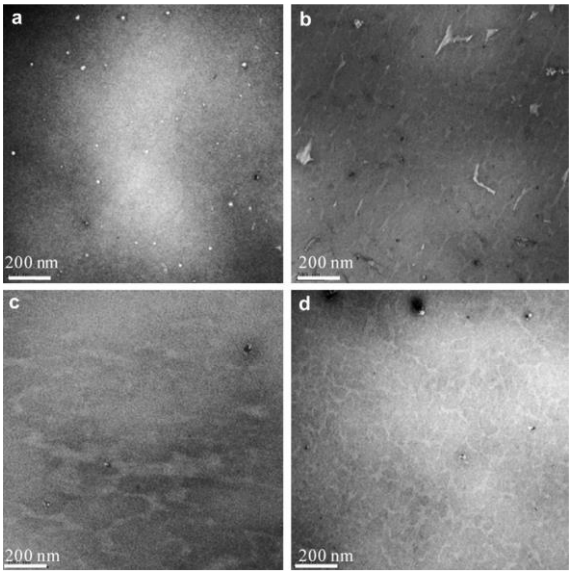

Figure 1- 13 TEM micrographs of neat PTFE (a) and blends with ImILs (b), PyILs (c), PhILs (d)

According to the cation/anion combinations of ionic liquids, some researchers have considered them as structuration agents to design the proper nanostructures of polymers, such as poly (tetrafluoro ethylene) (PTFE), poly (vinylidene fluoride-co-chlorotrifluoro ethylene) (P(VDF-CTFE)), poly (butylene adipate-co-terephthalate)

(PBAT), and epoxy networks [77–79]. In fact, the various chemical natures of ILs added in polymer have an effect on the structuration (nano- to micro-) which control the overall physical properties. For example, co-continuous morphologies obtained by introducing ImILs and PyILs into PTFE resulted in stiffer materials. A “spider web”-like morphology of PhILs leads to a dramatic compromise between stiffness and deformation (see Figure 1-13) [80,81]. The authors supposed that the nature of ILs pairs plays a critical role on its spatial distribution and structured morphology within polymer medium.

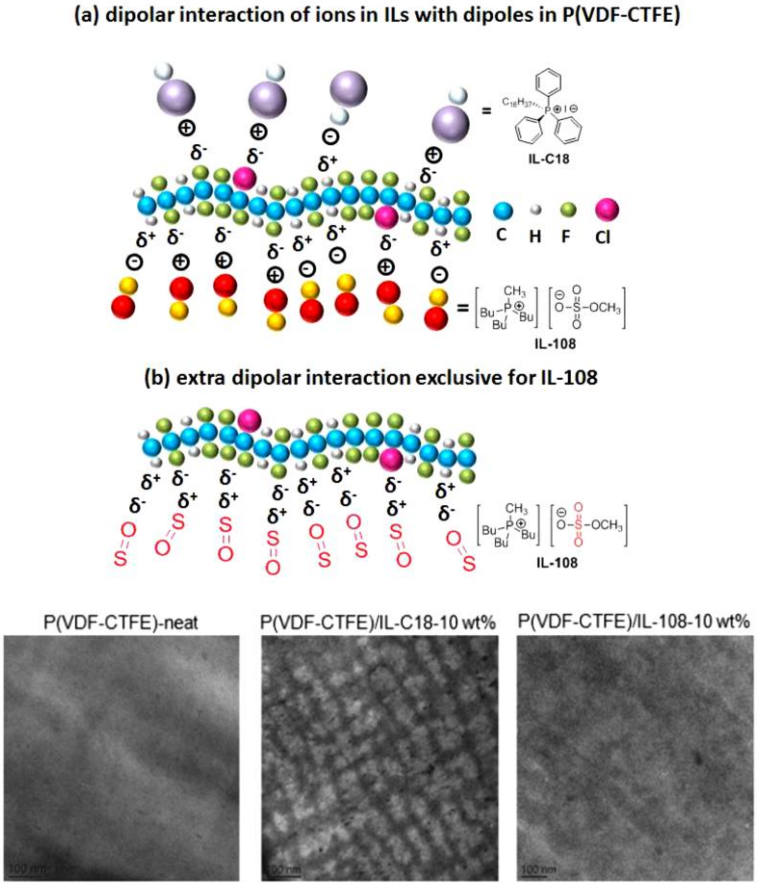

Figure 1- 14 Morphologies of P(VDF-CTFE)/PhILs blends and the schematic presentation of dipolar interactions

The combination of PhILs with P(VDF-CTFE) could affect the original structuration structures via the dipolar-dipolar interactions generated between PhILs and matrix. The nanostructurations varied with the chemical structure of added PhILs and their interaction strength (see Figure 1-14) [82]. In this reported study, the low content of PhILs caused the complete transition of nonpolar α-phase into polar- and/or β-phase,

resulting in the decrease of melting and crystallization temperatures. Higher content of PhILs (10 wt.%) could restrain the change of conformations and the rearrangement of polymers chains into ordered ones leading to reduce crystallinity rate and crystal size [83,82].

The hydrophobic nature of three PhILs added to PBAT (polybutylene adipate terephthalate), *i.e.* trihexyltetradecylphosphonium chloride (IL-Cl), trihexyltetradecyl phosphonium bis (trifluoromethylsulfonyl) imide (IL-TFSI), and trihexyltetradecyl phosphonium bis 2,4,4-(trimethylpentyl) phosphinate (IL-TMP), as well as the generated ionic clusters within PBAT films could delay the diffusion of water molecules into the polymer matrix by creating “tortuous path”, leading to a significant reduction in vapor water permeability (see Figure 1-15) [84].

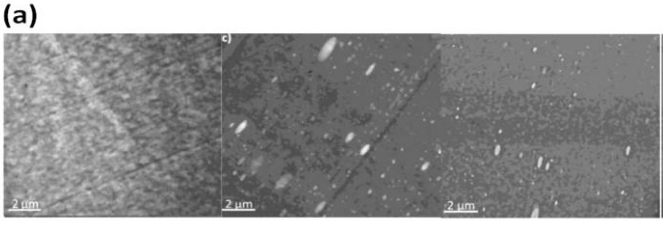

(b)

Sample	Water sorption C_{eq} (g per 100 g)	Water diffusion D (cmq s^{-1})	Water permeability (cc(STP) cm^{-3} atm^{-1}) (cm^2 s^{-1})
PBAT	2.37	2.26×10^{-8}	3.32×10^{-8}
PBAT/IL-TMP	0.84	2.50×10^{-8}	1.30×10^{-8}
PBAT/IL-TFSI	0.47	3.80×10^{-8}	1.10×10^{-8}
PBAT/IL-Cl	1.45	2.10×10^{-8}	1.90×10^{-8}

Figure 1- 15 Generated ionic clusters within PBAT/IL films (a) and resulting water permeability (b)

An acceleration curing kinetics of thermoset resins could be obtained by introducing ILs into reactive systems such as MCDEA (4,4’-methylenebis(3-chloro-2,6-diethylaniline) [85,77] and Jeffamine (Poly(propylene glycol) bis(2-aminopropyl ether)) [86,87]. Depending on the combinations of ILs, PyILs and ImILs act as catalytic curing agents leading to faster reaction kinetics of epoxy/amine polymerization while PhILs could not [85]. In addition, the plasticizing effect varies with the corresponding anion.

For example, the PhILs owning dicyanamide (IL-DCA) and sulfonate (IL-DBS) leads to a plasticization effect without any change of glass transition temperature when the anion was replaced by trifluoro methane sulfonyl imide (IL-TFSI) [86]. This difference could be interpreted from the generated different morphologies (see Figure 1-16), the low miscibility of IL-TFSI in epoxies.

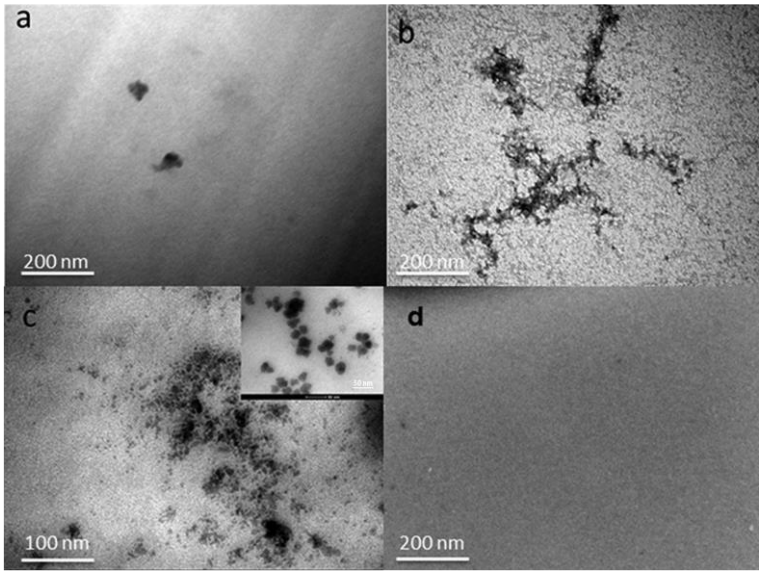

Figure 1- 16 TEM morphologies of epoxy networks modified by 10 wt.% of (a) IL-DCA, (b) IL-DBS, (c) IL-TFSI and (d) neat epoxy matrix

1.2.3.2 As compatibilizers

Ionic liquids have been also used as compatibilizers for thermoplastic and/or biopolymer blends. For example, some PhILs [88] could be used as compatibilizer agents in biopolymer-based blends, *i.e.* poly (butylene adipateco-terephtalate)/poly (lactic acid), PBAT/PLA with PLA as minor component. These PhILs are located in an interphase around the disperse phase leading to a decrease of the interfacial tension and as a consequence to reduce PLA domain sizes. The outstanding thermal and mechanical properties could be tuned by changing the anion nature. On the other hand, 1-dodecyl-3-methylimidazolium bis (trifluoromethylsulfonyl) imide (Dmim NTf_2) was used as compatibilizer for polybutylene succinate/rice starch (PBS/RS) blends [89]. According to this study, both thermal and mechanical properties are strongly affected. The high degradation temperature of Dmim NTf_2 and the generated intermolecular

interactions between the matrix chains and Dmim NTf_2 contribute to the improved thermal stability of the resulting blends. The tensile and flexural strain at break of PBS/RS blends were improved by up to 233% and 17%, respectively.

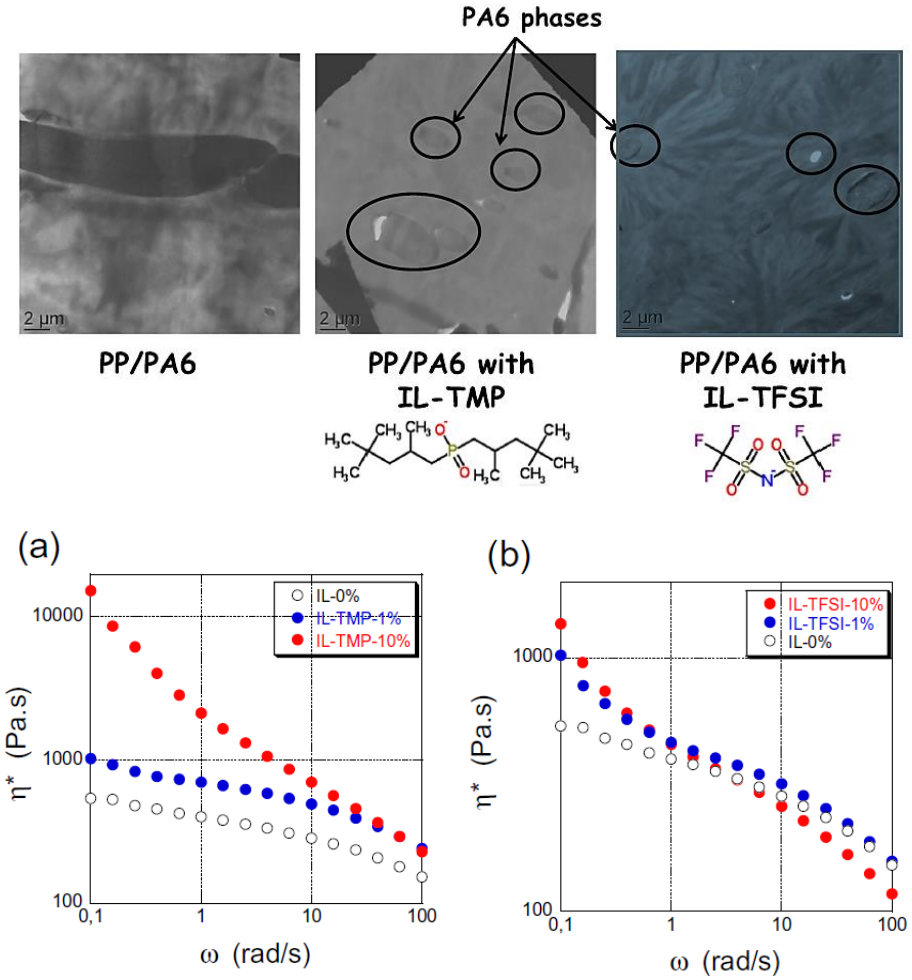

Figure 1- 17 Effect of ILs on the morphology and complex viscosity of polypropylene/polyamide 6 blends [90]

For polypropylene/polyamide 6 (PP/PA6, 80/20/wt/wt) blends, the IL-TFSI and IL-TMP could migrate into the interphase [90]. As a consequence, these ILs play the role of barrier to prevent the coalescence of dispersed phase (PA6) resulting in a significant domain reduction from 27µm to 1-2µm (see Figure 1-17). In addition to the improved thermal stability and mechanical properties, the generated ionic interactions between ILs and matrix could therefore restrain the large-scale polymer relaxation motions within these binary blends, leading to considerably improved complex viscosity (see Figure 1-17).

1.2.3.3 As plasticizers

Some PhILs in P(VDF-CTFE) matrix may play the role of plasticizers leading to large decrease of the glass transition temperature [83] (see Figure 1-18). Meanwhile, the strain at break was increased dramatically, *i.e.* from 23 into 122% and 838% with 10 wt.% IL-C18 and IL-108, respectively. On the other hand, their Young's modulus were reduced from 866 to 318 MPa and 276 MPa correspondingly.

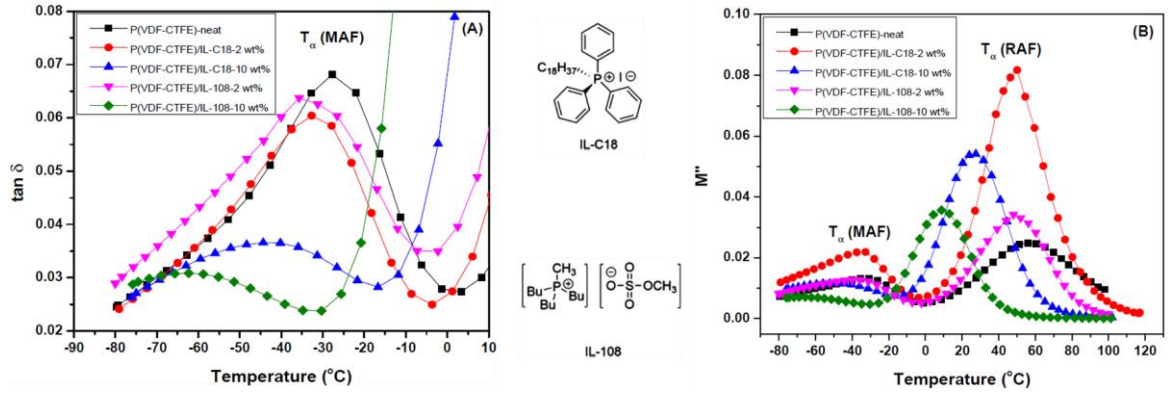

Figure 1- 18 Dielectric loss tangent (tan δ) (A) and imaginary part of the dielectric modulus (M″) (B) as a function of temperature within P(VDF-CTFE)/PhILs systems (frequency: 1Hz) [83]

Similarly, in addition to the effect on mechanical properties due to the plasticizing effect of ionic liquid (see Figure 1-19), the compatibility between synthesized polyethylene glycol-dicationic imidazolium-based ionic liquids (mPEG-ILs) and PLA could be improved thanks to the generated ion-dipole and hydrogen bond interactions [91]. In accordance to the literature [92], adding 10 wt.% of 1-ethyl-3-methylimidazolium bromide ([EMIM] Br) into biopolymer electrolytes led to the depression of the glass transition temperature (T_g) by 8 K, and further decreased by 12 K for 30 wt.% [EMIM] Br, since the cooperative [EMIM] Br could enhance the chain flexibility of the polymer substrate.

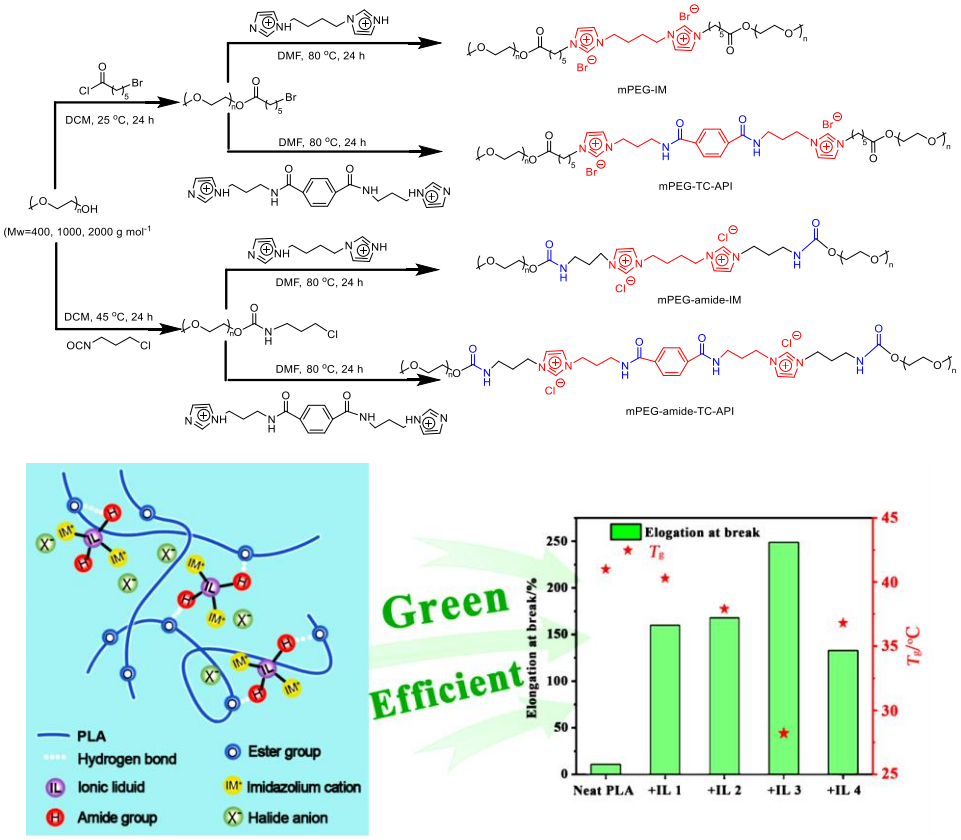

Figure 1- 19 Synthesis of mPEG-ILs and interactions within mPEG-ILs/PLA blend [91]

1.2.3.4 As reactants and/or catalysts

Thanks to the ionic pair nature of ILs, the numerous cation/anion combinations could allow to promote the interactions with polar groups. Thus, regarding the ionic polymerization mechanisms with epoxy monomer as the theoretical evidence, researches have paid a lot of attention to investigate the IL-epoxy networks and their resulting properties. According to the literatures, both imidazolium-based [85,93,94] and phosphonium-based [73,95,96] ILs could be considered as the candidates for polymerization of epoxy prepolymers. Scheme 1-4 [85] and Scheme 1-5 [96] show the reaction mechanisms of imidazolium ILs and phosphonium ILs for opening of the epoxide rings leading to new type of IL-epoxy networks.

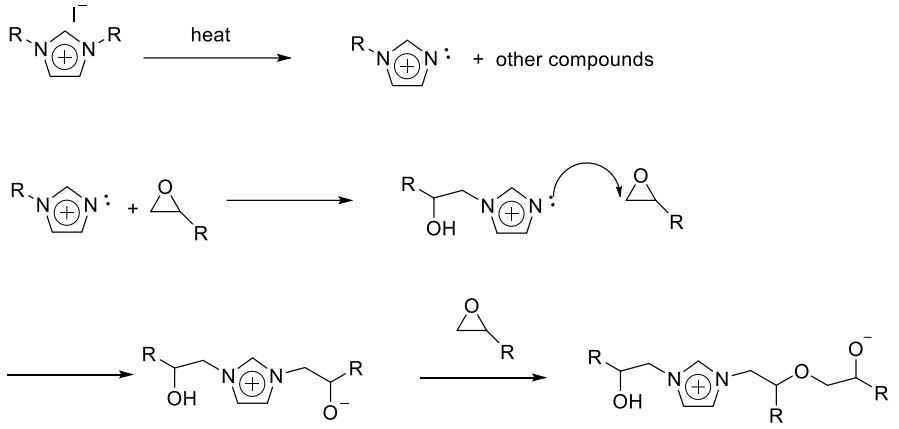

Scheme 1- 4 Proposed mechanism for curing initiated by imidazolium IL of epoxy monomer [85]

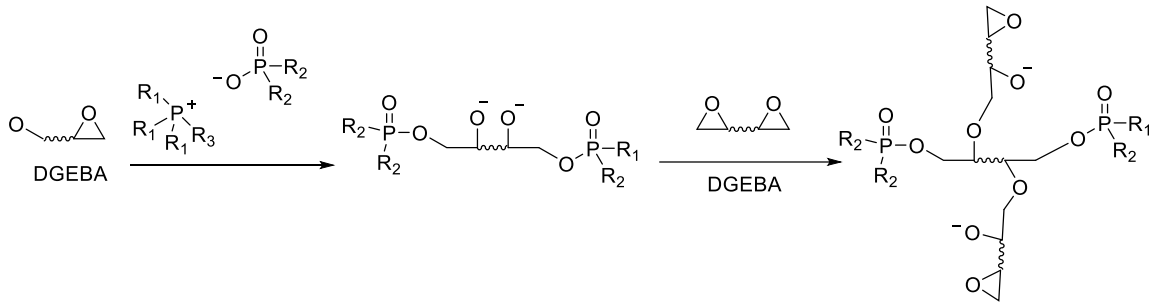

Scheme 1- 5 Proposed mechanisms for the polymerization of epoxy resin components in the presence of phosphonium-based IL [96]

More recently, ILs have been reported to be efficient as catalysts activating maleic anhydride groups for esterification reactions [97] (see Scheme 1-6). The authors found that reaction rate of the diesterification of maleic anhydride (MA) could be quantitatively tailored from a proper selection of the nature of ILs. Such a deep understanding of the relationships between the nature of ILs and the reactivity and rate of diesterification of MA groups could provide further insights to guide other esterification reactions and the rational design of IL catalysts.

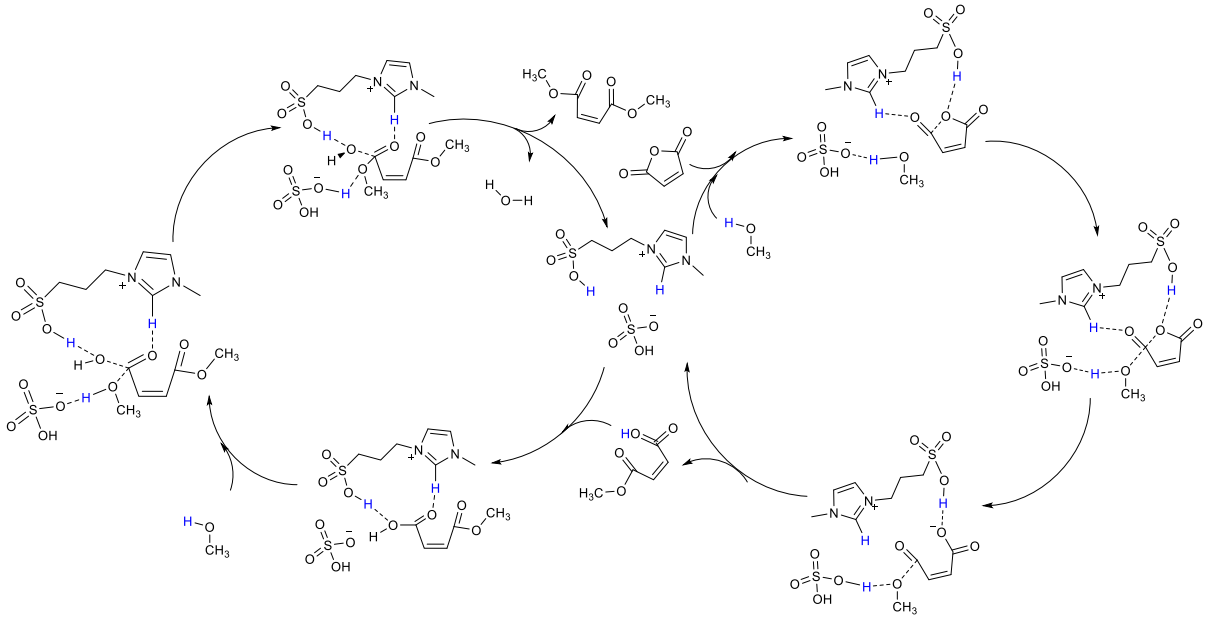

Scheme 1- 6 Proposed mechanisms for the first esterification (right) and the second esterification (left) of MA with methanol using ILs as catalyst [97]

1.2.4 Conclusions

This part has briefly introduced ionic liquids (ILs) and its properties as well as applications in polymer systems. The advantages of ILs are related to their thermal stability and the numerous combinations of anions and cations as well as the fact that they could be as green solvents and catalysts. In addition, thanks to the numerous pairs of anions and cations, the resulting physical and chemical properties of polymer/ILs blends could be tuned from a proper selection of the ion pairs.

1.3 Foaming processing under $scCO_2$

Given the various advantages of supercritical carbon dioxide ($scCO_2$) as 'solvent' medium [98–101], *i.e. i)* being environmentally friendly, non-toxic, non-flammable, and low cost; *ii)* low critical temperature and critical pressure [102] ($T_{critical}$=31.1 ºC and $P_{critical}$=7.37 MPa) (see Figure 1-20), *i.e.* simple equipment suitable for industrialization; *iii)* weak molecular polarity, *i.e.* able to dissolve non-polar or less polar polymers; *iv)* high diffusion rate and high production efficiency; *v)* high solubility in most polymers, considered as an ideal green foaming agent.

The basic principle of $scCO_2$ polymer foams is to dissolve them into the polymer

at high pressure and temperature to form a polymer/CO_2 homogeneous saturated system. Then, by releasing pressure or increasing temperature, phase separation occurs and triggers the generation as well as the growth of bubble nuclei of the foam [103–115]. The details are described in the latter section.

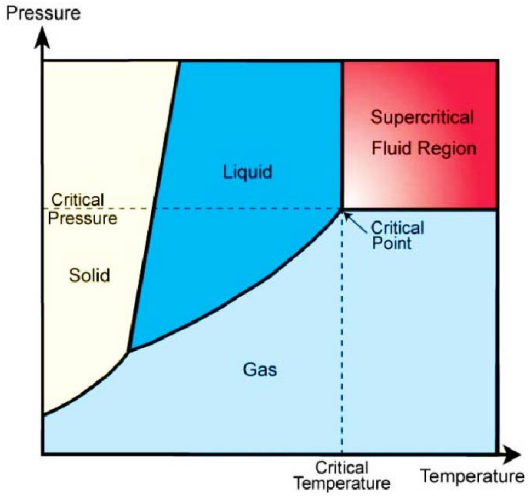

Figure 1- 20 Phase diagram of supercritical carbon dioxide Pressure-Temperature

1.3.1 Procedure of polymer foaming

The basic procedure for preparing polymer foams using $scCO_2$ is shown in Figure 1-21. It goes through four steps including nucleation, growth, cooling, and shaping [107,116]. First, $scCO_2$ is injected into the polymer matrix, the polymer/gas blend is then thoroughly mixed to reach saturation. After a suitable saturation time, the $scCO_2$ dissolves and diffuses rapidly within the matrix, as well as enters the polymer substrate to form a homogeneous polymer/gas system after equilibrium. Then, by rapidly increasing the temperature or decreasing the pressure, a large thermodynamic instability is created inducing the nucleation of vesicles in the polymer substrate. In addition, the gas dissolves rapidly and diffuses into the bubble nuclei. The bubble pores grow gradually and the morphology of pores merge/break depending on the gas concentration. Finally, as the temperature further decreases, the cell structure is gradually defined. The process of vesicle growth is also usually accompanied by vesicle consolidation or vesicle collapse (not shown in Figure 1-21), depending on the foaming conditions and the nature of the polymer [103].

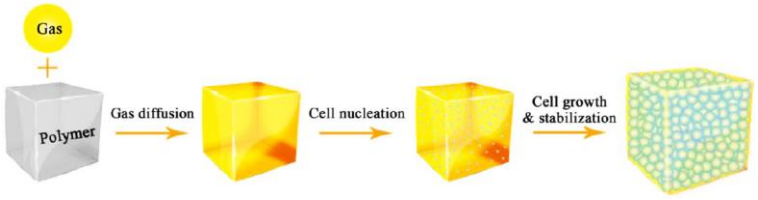

Figure 1- 21 Schematic of polymer foaming process [107,116]

1.3.1.1 Cell nucleation

During microcellular foaming, the formation of pore structures may occur due to fluctuations in pressure and temperature within the homogenous polymer/gas mixture. In order to create pores in the polymer melt, sufficient energy must be consumed to overpass break the free energy barrier, which could be gained from a sudden temperature rise or a sudden pressure drop. Therefore, in the process of supercritical CO_2 microcellular foaming, the nucleation of bubbles is a crucial step. It not only affects the growth of bubbles, but also plays a critical factor in the evolution of the bubble structure. At the beginning of the 20th century, Gibbs proposed the classical nucleation theory. Later, Suh and Colton *et al* [117,118] improved and developed a nucleation theory applicable to polymer foams. Nucleation theories can be divided into three main categories: homogeneous nucleation, heterogeneous nucleation, and mixed homogeneous-heterogeneous nucleation.

Homogeneous nucleation

When gas molecules are dissolved in a polymer/gas homogeneous system and in the absence of any other nucleating agents or impurities, these ones clump together to form a stable second phase, *i.e.* bubbles. This phenomenon is known as homogeneous nucleation (see Figure 1-22). In this process, each gas molecule acts as a nucleation point. Homogeneous nucleation theoretically leads to a final product with the greatest nucleation density and the smallest bubble size. At the same time, the absence of a second phase requires more super-saturation during supercritical fluid microporous foaming, generating more energy to overcome the "energy barrier". Thus, more stable nucleation barriers. Based on the classical nucleation theory, Suh and Colton *et al* [117,118] studied the homogeneous nucleation of vesicles during

microcellular foaming and proposed equations to describe the homogeneous nucleation rate as well as free energy barrier of vesicles.

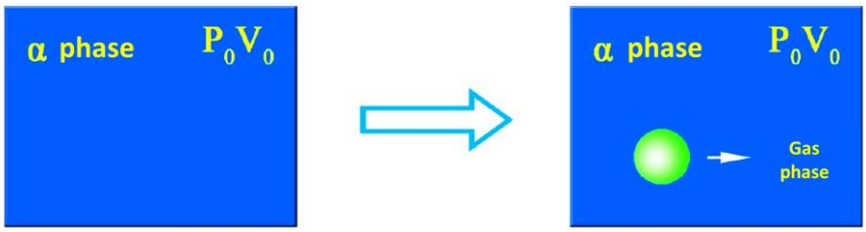

Figure 1- 22 Process of homogeneous nucleation

In general, the formation of bubble holes during homogeneous nucleation requires sufficient energy to overcome the free energy barrier of the substrate itself. If the energy generated is lower than that of the free energy barrier, the bubble holes will not form. The energy needed to overcome the barrier for the formation of bubbles is commonly referred to as the Gibbs' free energy, also known as the activation energy ($\Delta G^*_{hom} = \frac{16\,\pi\sigma^3}{3\Delta P^2}$). It could be defined by differentiating ∂G/∂r=0 from Equation 1-1 calculating the work required to form a standard circular bubble of radius size r in the following:

$$G = 4\pi r^2\sigma - \frac{4}{3}\pi r^3\Delta P \qquad \text{Equation 1- 1 [117,119,120]}$$

where σ is the surface energy of cells and ΔP represents the difference between the internal pressure of the gas and the surrounding pressure which is used to estimate the immersion pressure.

In the homogeneous nucleation system, the Gibbs' free energy ΔG^*_{hom} decreases as the immersion pressure ΔP increases, *i.e.* the energy required to form bubble nuclei becomes smaller, therefore increasing the number of bubble nuclei. In addition, the dissolution of gas into the polymer reduces the surface tension of the polymer, the Gibbs' free energy ΔG^*_{hom} also decreases, *i.e.* the energy required to form bubble nuclei becomes smaller, thus increasing the nucleation rate (The reason for this is given by the following Equation 1-2)

Based on the Boltzmann' coefficient, the equation for the homogeneous nucleation rate can be derived:

Nucleation rate: $N = f_0 c_0 exp\left(-\frac{\Delta G^*_{hom}}{kT}\right)$ Equation 1- 2 [117,119,120]

where, f_0 being the frequency factor of gas molecules entering the nucleus of a bubble ($1 \cdot s^{-1}$); c_0 being the concentration of the gas in a homogeneous nucleation system or the concentration of the nucleating agent in a heterogeneous nucleation system ($1 \cdot m^{-3}$); while ΔG^*_{hom} (J) and k being Gibbs free energy of nucleation and Boltzmann constant (1.38×10^{-23} $J \cdot K^{-1}$) respectively; T the foaming temperature (°C).

Heterogeneous nucleation

Heterogeneous nucleation refers to the presence of a second phase (e.g. nucleating agent, talc, nano-silica, clay, other polymers, etc. [103,117,121–124]) in the system. It plays a crucial role in the nucleation barrier and produces nucleation sites at the interface as well as promotes heterogeneous process, leading to a lower nucleation energy barrier, as well as an increased nucleation rate and pore density (see Figure 1-23).

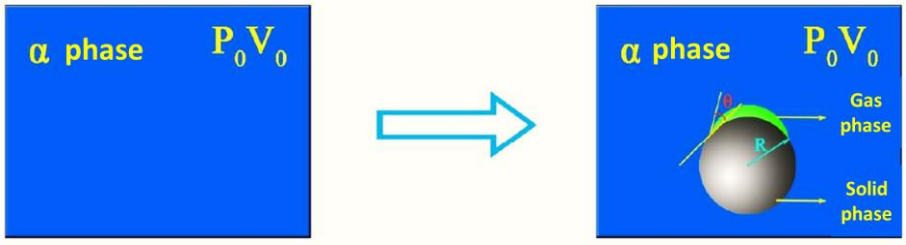

Figure 1- 23 Process of heterogeneous nucleation

Based on the theory of heterogeneous nucleation, the Gibbs' free energy required for heterogeneous nucleation can be deduced, ΔG^*_{het}:

$$\Delta G^*_{het} = \frac{16\,\pi\sigma^3}{3\Delta P^2} S(\theta^*)$$ Equation 1- 3 [116]

where $S(\theta^*) = \frac{1}{4}(2 + cos\theta)(1 - cos\theta)^2$ Equation 1- 4

The $S(\theta^*)$ value in Equation 1-4 is always lower than 1, which means the Gibbs' free energy required for heterogeneous nucleation is always less than that for homogeneous nucleation. Compared to homogeneous nucleation, heterogeneous nucleation requires less energy to break the free energy barrier within the matrix, thus increasing the efficiency of vesicle nucleation and the density of vesicles.

Heterogeneous nucleation rate (N_1) could be expressed as:

$$N_1 = f_1 c_1 exp\left(-\frac{\Delta G_{het}^*}{kT}\right) \qquad \text{Equation 1- 5 [116]}$$

where f_1 ($1 \cdot s^{-1}$) is the frequency factor of gas molecules participating in nucleation; while c_1 ($1 \cdot m^{-3}$) represents the solubility of heterophase nucleation sites; ΔG_{het}^* (J) is the energy barrier required for heterogeneous nucleation; T (°C) and k ($J \cdot K^{-1}$) are the absolute temperature and Boltzmann' coefficient respectively.

From the classical nucleation theory, it can be obtained that a faster unloading rate is required to improve the vesicle nucleation ability of polymers. At the same time, the vesicle nucleation ability of the heterogeneous nucleation system with an additional nucleating agent (the second phase) is stronger than that of the homogeneous nucleation system. However, classical nucleation theory has some limitations, for example, it does not take into account the effect of melt flow rate and shear stress on vesicle nucleation when the molten polymer is in a shear flow field [125]. For this reason, later researchers have proposed some new nucleation theories based on the classical nucleation theory, among which shear nucleation theory, interface nucleation theory, and hot spot nucleation theory [126–128].

Heterogeneous-homogeneous mixed-phase nucleation

On the other hand, the homogeneous and heterogeneous nucleation are not mutually exclusive, and bubble nucleation could also be a mixed heterogeneous-homogeneous nucleation in microcellular foam nucleation [116]. Heterogeneous nucleation tends to occur prior to homogeneous nucleation due to the lower activation energy required to overcome former nucleation than that of the latter one. It is known from the afore mentioned bubble nucleation theory that when gas molecules diffuse into the bubble nucleus of heterogeneous nucleation and then grow into bubbles, the solubility of the gas molecules in solution decreases, resulting in a reduction in the number of nuclei generated. The nucleation rate for homogeneous nucleation can be rewritten as Equation 1-6 [116]:

$$N^* = f_0(C_0 - N_1 t n_b) exp\left(-\frac{\Delta G_{hom}^*}{kT}\right) \qquad \text{Equation 1- 6}$$

where t and n_b represent timing from the time of the first heterogeneous nucleation and the number of gas molecules in the nucleus of a gas bubble, respectively.

1.3.1.2 Vesicular growth

As previously reported, the bubble growth process is caused by a thermodynamic imbalance in the homogeneous system through a sudden rise in temperature or drop in pressure. Then precipitation of bubble nuclei is resulted. It continues to grow as the surrounding gas diffuses into the nuclei. In the growth process, the growth of vesicles is mainly influenced by the viscosity, diffusion coefficient, gas solubility, number of bubble nuclei, etc. For the growth of vesicles after the formation of bubble nuclei, it is mainly through the continuous diffusion of gas into the cell nuclei. Therefore, gas diffusion control is very important. The key to controlling gas diffusion lies in regulating the concentration of gas in the polymer/gas homogeneous system. The solubility of the gas within the homogeneous system is tightly related to the external pressure and temperature, but also to the viscosity and surface tension of the polymer matrix itself.

1.3.2 Effect of viscosity

During the foaming process, the viscosity plays a key role for the final foamed materials. In fact, due to the low melting strength of the polymer, the cell walls of the separating cells are not strong enough to withstand the extension force. Several small cells may collapse into one large cell. Many strategies have been conducted to process outstanding polymer foams, particularly designing ionomers thanks to its easy operation. Mori *et al* [129] has reported the cell growth and coalescence of cell during foaming process is strongly related to the ionic crosslinked structure depending on the degree of the neutralization (see Figure 1-24). Li *et al* [130] has obtained one significantly improved foam by preparing a series of polyprolylene (PP) ionomers (see Figure 1-25). According to their work, the amine-modified PP ionomers showed the best foamability due to the combined effected of rheological properties and the underlying favourable interactions with physical agents (carbon dioxide).

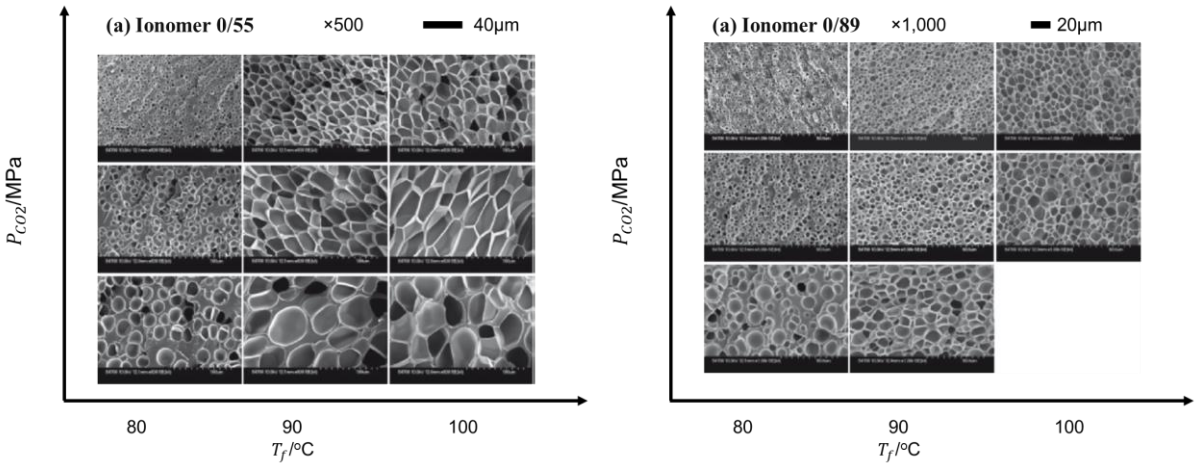

Figure 1- 24 Typical morphologies observed by FE-SEM of the fracture surfaces of (a) polyethylene-based ionomer 0/55 and (b) ionomer 0/89 foamed as a function of temperature and pressure [129]

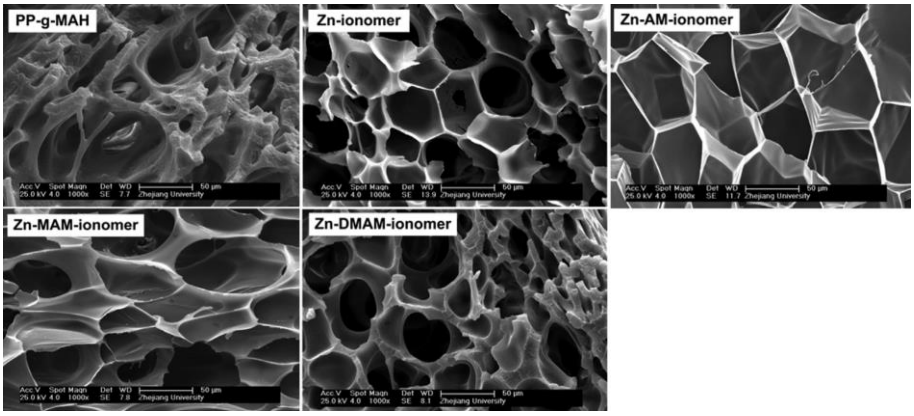

Figure 1- 25 Cell morphology of PP-g-MAH and PP-based ionomers foamed at 157°C and 24 MPa under $scCO_2$ [130]

On the other side, using chain extender is the other effective way to improve the rheological properties. Corre *et al* [131] achieved a significant improvement in melt viscosity and elasticity through the use of an epoxy additive. According to their study, the increase of the melt strength is due to this chain extension process (see Scheme 1-7) which was confirmed by rheology. At the same time, the increased melt viscoelasticity due to the chain extender not only favours the nucleation process over the cell growth but also leads to a denser structure (see Figure 1-26).

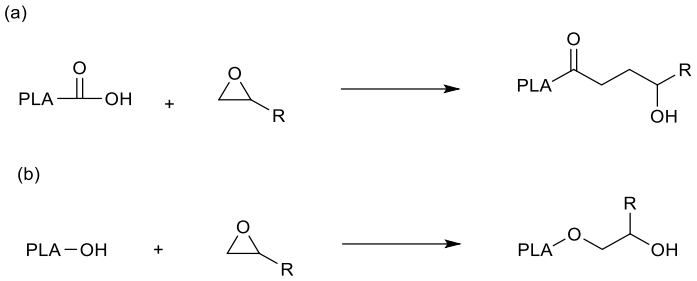

Scheme 1- 7 Reactional mechanisms possible between epoxy groups and carboxyl or hydroxyl end groups of PLA chains [131]

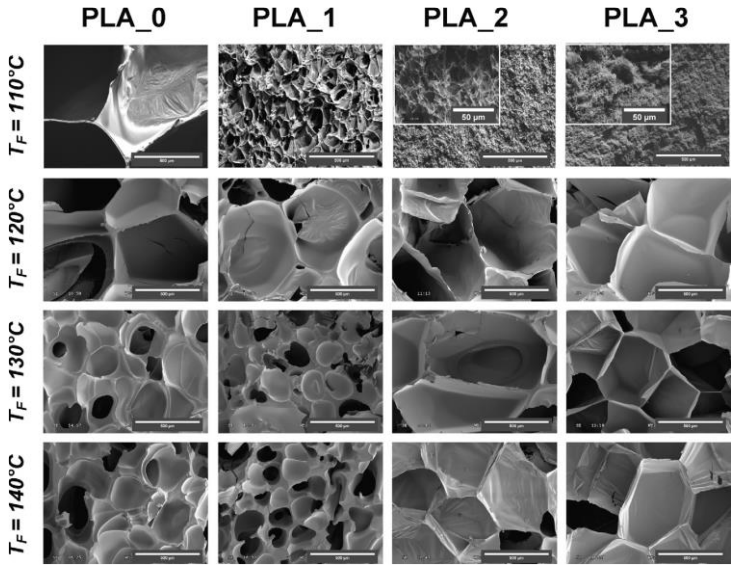

Figure 1- 26 SEM micrographs of foams from neat and chain extended PLAs as a function of foaming temperatures (110, 120, 130 and 140 °C) and foaming pressures (7.6, 7.8, 8.2 and 8.4 MPa) (1, 2, 3phr content of chain extender) [131]

1.3.3 Conclusions

This part has briefly introduced foaming procedure, as well as the effect of viscosity on the resulting foams. The advantages of supercritical carbon dioxide ($scCO_2$) related to its high solubility in most of the polymers, its low critical temperature and pressure as well as its environmental friendliness. $scCO_2$ could be considered as an ideal green-blowing agent. Numerous researchers have poured into plenty of attention into foaming analysis, and they divide the procedure into four steps including nucleation, growth, cooling, and shaping. In terms of nucleation rate, due to the less free energy barrier carried in heterogeneous system and the presence of the nucleation agents, it exhibits

a high rate than that of homogeneous nucleation. In general, heterogeneous nucleation and mixed homogeneous-heterogeneous nucleation are very popular. According to this route, the gas concentration control is strongly associated with the growth of nuclei foamed, while the viscosity and surface tension of the polymer substrate could influence the final morphology of cells.

1.4 Conclusions and Objectives

1.4.1 Conclusions

Ionomer is regarded as macromolecular materials containing ionic/ionizable groups in the range of 1-15 molar%, and prepared by the cooperation of metal salts and polymers possessing ionized units. The presence of polar (polar groups on polymer backbone and added ions) and non-polar (mainly in polymer chains) components contributes to the compatibility with both polar and non-polar substances. Combined with the presence of multiple interactions within ionomers, including ion-ion interactions, ion pair-ion pair interactions, ion-dipole interactions, metal complexation interactions, hydrogen bonding interactions, and hydrophobic interactions, ionomers have received plenty of attention in both academic and industry fields. On the other side, ionic liquids are salts in the liquid state with a melting temperature lower than 100 ^{o}C composing of crowded anions/cations combinations. Their low vapor pressure and high thermal stability as well as special compositions make them widely used in polymers. Particularly, they could act as the raw materials and participate in the polymerizations and chain extension process. In addition, the lightweight materials market is moving in the industry towards the development of polymeric nanocomposite foams to improve the compressive properties, mechanical strength, and dimensional stability of unmodified foams. Researchers have considered the supercritical carbon dioxide as the green physical agent to foam thanks to its environmental friendliness.

1.4.2 Objectives of the following look

As discussed in previous text, ionic liquids as innovative additives have been reported to improve the viscoelastic properties of polymer. Their specific properties as

well as the physical-chemical interactions with polymers could be customized through changing cation or anion natures [132–135]. Therefore, ILs are very promising components for numerous applications in polymer systems. Considering the special ionic character of ILs, this work plans to design a new generation of ionomer (denoted as LIonomers) processed from the thermoplastic polymers (for example: polypropylene). Different investigations need to be done about:

i) the interactions between maleic anhydride grafted PP (as this polymer will be related as thermoplastic matrix) and the tunability of IL cation and anion on the strength of the generated interactions;

ii) the effect of ILs combinations on the physical properties of neat polymer matrix;

iii) the role of introduced ILs on the nanostructuration and their location;

iv) the perspective application of such LIonomers on lightweight foams processed under supercritical carbon dioxide.

References

[1] Kirkmeyer B P, Weiss R A, Winey K I. Spherical and vesicular ionic aggregates in Zn-neutralized sulfonated polystyrene ionomers[J]. Journal of Polymer Science Part B: Polymer Physics, 2001, 39(5): 477-483.

[2] Zhang L, Brostowitz N R, Cavicchi K A, et al. Perspective: ionomer research and applications[J]. Macromolecular Reaction Engineering, 2014, 8(2): 81-99.

[3] Eisenberg A. Structure and viscoelastic properties of ion-containing polymers in the solid state[M]. Macromolecular Chemistry–11. Elsevier, 1977: 171-175.

[4] Capek I. Nature and properties of ionomer assemblies. II[J]. Advances in Colloid and Interface Science, 2005, 118(1-3): 73-112.

[5] Ambrose M. Halogenated polyethylene[M]. US, 1946.

[6] Brown H P, Gibbs C F. Carboxylic elastomers[J]. Rubber Chemistry & Technology, 1955, 47(5).

[7] Brown H P. Crosslinking reactions of carboxylic elastomers[J]. Rubber Chemistry and Technology, 1963, 36(4): 931-962.

[8] Brown H P. Carboxylic elastomers[J]. Rubber Chemistry and Technology, 1957, 30(5): 1347-1386.

[9] Macknight W J, Earnest T R. The structure and properties of ionomers[J]. Journal of Polymer Science: Macromolecular Reviews, 1981, 16(1).

[10] Bonotto S, Bonner E F. Effect of ion valency on the bulk physical properties of salts of ethylene-acrylic acid copolymers[J]. Macromolecules, 1968, 1(6): 510-515.

[11] Longworth R, Vaughan D J. Physical structure of ionomers[J]. Nature, 1968, 218(5136): 85-87.

[12] Eisenberg A. Clustering of ions in organic polymers. A theoretical approach[J]. Macromolecules, 1970, 3(2): 147-154.

[13] Marx C L, Caulfield D F, Cooper S L. Morphology of ionomers[J]. Macromolecules, 1973, 6(3): 344-353.

[14] MacKnight W J, Taggart W P, Stein R S. A model for the structure of ionomers[J]. Journal of Polymer Science: Polymer Symposia, 1974, 45: 113-128.

[15] Roche E J, Stein R S, Russell T P, et al. Small-angle x-ray scattering study of ionomer deformation[J]. Journal of Polymer Science: Polymer Physics Edition, 1980, 18(7): 1497-1512.
[16] Forsman W C. Effect of segment-segment association on chain dimensions[J]. Macromolecules, 1982, 15(4): 1032-1040.
[17] Yarusso D J, Cooper S L. Microstructure of ionomers: interpretation of small-angle x-ray scattering data[J]. Macromolecules, 1983, 16(12): 1871-1880.
[18] Yarusso D J, Cooper S L. Analysis of SAXS data from ionomer systems[J]. Polymer, 1985, 26(3): 371-378.
[19] Ding Y S, Hubbard S R, Hodgson K O, et al. Anomalous small-angle X-ray scattering from a sulfonated polystyrene ionomer[J]. Macromolecules, 1988, 21(6): 1698-1703.
[20] Dreyfus B. Model for the clustering of multiplets in ionomers[J]. Macromolecules, 1985, 18(2): 284-292.
[21] Datye V K, Taylor P L, Hopfinger A J. Simple model for clustering and ionic transport in ionomer membranes[J]. Macromolecules, 1984, 17(9): 1704-1708.
[22] Eisenberg A, Hird B, Moore R B. A new multiplet-cluster model for the morphology of random ionomers[J]. Macromolecules, 1990, 23(18): 4098-4107.
[23] Register R A, Foucart M, Jerome R, et al. Structure-property relationships in elastomeric carboxy-telechelic polyisoprene ionomers neutralized with divalent cations[J]. Macromolecules, 1988, 21(4): 1009-1015.
[24] Lu X, Steckle Jr W P, Hsiao B, et al. Thermally induced microstructure transitions in a block copolymer ionomer[J]. Macromolecules, 1995, 28(8): 2831-2839.
[25] Jiang M, Liu W, Wu C, et al. Complexation of SEBS-based ionomers with pyridine-unit-containing copolymers in solution and bulk[J]. Polymer, 1997, 38(2): 405-412.
[26] Laurer J H, Winey K I. Direct Imaging of Ionic Aggregates in Zn-Neutralized Poly (ethylene-co-methacrylic acid) Copolymers[J]. Macromolecules, 1998, 31: 9106-9108.
[27] Yan W, Zhang X, Zhu Y, et al. Synthesis and characterization of self-crosslinkable zinc polyacrylate latices at room temperature[J]. Iranian Polymer Journal, 2012, 21(9): 631-639.
[28] GHOSH S K, De P P, Khastgir D, et al. Sodium and zinc ionomers of sulfonated maleated EPDM rubber[J]. Polymer-Plastics Technology and Engineering, 2000, 39(1):

47-59.

[29] Pregi E, Kun D, Wacha A, et al. The role of ionic clusters in the determination of the properties of partially neutralized ethylene-acrylic acid ionomers[J]. European Polymer Journal, 2021, 142: 110110.

[30] Gao Y, Choudhury N R, Dutta N K. Effects of neutralization on the structure and properties of an ionomer[J]. Journal of Applied Polymer Science, 2012, 124(4): 2908-2918.

[31] Sampath J, Hall L M. Impact of ion content and electric field on mechanical properties of coarse-grained ionomers[J]. The Journal of Chemical Physics, 2018, 149(16): 163313.

[32] Fujiyama M, Kondou M, Ayama K, et al. Rheological properties of ionically and covalently crosslinked polypropylene‐type thermoplastic elastomers[J]. Journal of Applied Polymer Science, 2002, 85(4): 762-773.

[33] Rousseaux D D, Drooghaag X, Sclavons M, et al. Polypropylene ionic thermoplastic elastomers: Synthesis and properties[J]. Polymer degradation and stability, 2010, 95(3): 363-368.

[34] Wang B, Zhang L, Zhao J, et al. Synthesis and properties of two kinds of CPVC carboxylated ionic copolymers[J]. Iranian Polymer Journal (English), 2008, 17(8): 625-633.

[35] Natansohn A, Murali R, Eisenberg A. How to blend ionomers[J]. Chemtech, 1990, 20(7): 418-424.

[36] Sinthavathavorn W, Nithitanakul M, Grady B P, et al. Melt rheology of low-density polyethylene/polyamide 6 using ionomer as a compatibilizer[J]. Polymer Bulletin, 2008, 61(3): 331-340.

[37] Granado A, Eguiazabal J I, Nazábal J. Compatibilization of PP/PAE blends by means of the addition of an ionomer[J]. Polymer Engineering & Science, 2010, 50(8): 1512-1519.

[38] Charoenpongpool S, Nithitanakul M, Grady B P. Melt-neutralization of maleic anhydride grafted on high-density polyethylene compatibilizer for polyamide-6/high-density polyethylene blend: effect of neutralization level on compatibility of the blend[J]. Polymer bulletin, 2013, 70(1): 293-309.

[39] Thankappan Ramesan M, Lee D. S. The effect of block copolymer and its ionomer

on the crystallization behaviour of poly(ethylene terephthalate)[J]. Iranian Polymer Journal, 2008, 17(4).

[40] Wu T, Yang G. Synthesis and characterization of monomer‐casting polyamide 6/polymethacrylic ionomer blends[J]. Journal of Applied Polymer Science, 2009, 111(6): 2970-2979.

[41] Zhu J, Zhou Y. Effects of ionomer films on secondary alkaline zinc electrodes[J].Journal of Power Sources: Vol. 73. 1998: 266-270.

[42] Kim C H, Lee K H, Kim W S, et al. Ion conductivities and interfacial characteristics of the plasticized polymer electrolytes based on poly (methyl methacrylate-co-Li maleate)[J]. Journal of Power Sources, 2001, 94(2): 163-168.

[43] Van Der Zwaag S. Self-healing materials: an alternative approach to 20 centuries of material science[M]. Self healing materials. Delft: Springer, 2007

[44] Varley R. Ionomers as self healing polymers[M]. Self healing materials. Springer, 2007: 95-114.

[45] Kalista S J. Self-healing ionomers[J]. Self-Healing Materials, 2009.

[46] Kalista S J, Pflug J R, Varley R J. Effect of ionic content on ballistic self-healing in EMAA copolymers and ionomers[J]. Polymer Chemistry, 2013, 4(18): 4910-4926.

[47] Ratti R. Ionic liquids: synthesis and applications in catalysis[J]. Advances in Chemistry, 2014, 2014.

[48] Liu J fu, Chi Y guang, Jiang G bin, et al. Ionic liquid-based liquid-phase microextraction, a new sample enrichment procedure for liquid chromatography[J]. Journal of Chromatography A, 2004, 1026(1-2): 143-147.

[49] Hurley F H, Wier J. Electrodeposition of aluminum[M]. US, 1948.

[50] Graenacher C. Cellulose solution[M]. US, 1934.

[51] Hasan M, Kozhevnikov I V, Siddiqui M R H, et al. Gold compounds as ionic liquids. synthesis, structures, and thermal properties of N, N ‘-dialkylimidazolium tetrachloroaurate salts[J]. Inorganic Chemistry, 1999, 38(25): 5637-5641.

[52] Chum H L, Koch V R, Miller L L, et al. Electrochemical scrutiny of organometallic iron complexes and hexamethylbenzene in a room temperature molten salt[J]. Journal of the American Chemical Society, 1975, 97(11): 3264-3265.

[53] Wilkes J S, Zaworotko M J. Air and water stable 1-ethyl-3-methylimidazolium based ionic liquids[J]. Journal of the Chemical Society, Chemical Communications,

1992(13): 965-967.

[54] Marciniak A. The solubility parameters of ionic liquids[J]. International Journal of Molecular Sciences, 2010, 11(5): 1973-1990.

[55] Hapiot P, Lagrost C. Electrochemical reactivity in room-temperature ionic liquids[J]. Chemical Reviews, 2008, 108(7): 2238-2264.

[56] Plechkova N V, Seddon K R. Applications of ionic liquids in the chemical industry[J]. Chemical Society Reviews, 2008, 37(1): 123-150.

[57] Fraser K J, Macfarlane D R. Phosphonium-based ionic liquids: An overview[J]. Australian Journal of Chemistry, 2009, 62(34): 309-321.

[58] Lu J, Yan F, Texter J. Advanced applications of ionic liquids in polymer science[J]. Progress in Polymer Science, 2009, 34(5): 431-448.

[59] Awad W H, Gilman J W, Nyden M, et al. Thermal degradation studies of alkyl-imidazolium salts and their application in nanocomposites[J]. Thermochimica Acta, 2004, 409(1): 3-11.

[60] Ngo H L, LeCompte K, Hargens L, et al. Thermal properties of imidazolium ionic liquids[J]. Thermochimica Acta, 2000, 357: 97-102.

[61] Earle M J, Seddon K R. Ionic liquids. Green solvents for the future[J]. Pure and Applied Chemistry, 2000, 72(7): 1391-1398.

[62] Bates E D, Mayton R D, Ntai I, et al. CO_2 capture by a task-specific ionic liquid[J]. Journal of the American Chemical Society, 2002, 124(6): 926-927.

[63] Gardas R L, Costa H F, Freire M G, et al. Densities and derived thermodynamic properties of imidazolium-, pyridinium-, pyrrolidinium-, and piperidinium-based ionic liquids[J]. Journal of Chemical & Engineering Data, 2008, 53(3): 805-811.

[64] Nakajima H, Ohno H. Preparation of thermally stable polymer electrolytes from imidazolium-type ionic liquid derivatives[J]. Polymer, 2005, 46(25): 11499-11504.

[65] Zhu S, Wu Y, Chen Q, et al. Dissolution of cellulose with ionic liquids and its application: a mini-review[J]. Green Chemistry, 2006, 8(4): 325-327.

[66] Lagrost C, Hapiot P, Vaultier M. The influence of room-temperature ionic liquids on the stereoselectivity and kinetics of the electrochemical pinacol coupling of acetophenone[J]. Green Chemistry, 2005, 7(6): 468-474.

[67] Xing C, Zhao L, You J, et al. Impact of ionic liquid-modified multiwalled carbon nanotubes on the crystallization behavior of poly (vinylidene fluoride)[J]. The Journal of Physical Chemistry B, 2012, 116(28): 8312-8320.

[68] Xing C, Guan J, Chen Z, et al. Novel multifunctional nanofibers based on thermoplastic polyurethane and ionic liquid: towards antibacterial, anti-electrostatic and hydrophilic nonwovens by electrospinning[J]. Nanotechnology, 2015, 26(10): 105704.

[69] Li D, Pang Z, Wang Q, et al. Fabrication and characterization of polyamide6-room temperature ionic liquid (PA6-RTIL) composite nanofibers by electrospinning[J]. Fibers and Polymers, 2013, 14(10): 1614-1619.

[70] Kubisa P. Ionic liquids in the synthesis and modification of polymers[J]. Journal of Polymer Science Part A: Polymer Chemistry, 2005, 43(20): 4675-4683.

[71] Scott M P, Rahman M, Brazel C S. Application of ionic liquids as low-volatility plasticizers for PMMA[J]. European Polymer Journal, 2003, 39(10): 1947-1953.

[72] Ye H, Huang J, Xu J J, et al. Li ion conducting polymer gel electrolytes based on ionic liquid/PVDF-HFP blends[J]. Journal of the Electrochemical Society, 2007, 154(11): A1048-A1057.

[73] Nguyen T K L. New generation of epoxy networks based on ionic liquids: From structuration to final properties[D]. Université de Lyon, 2016.

[74] Kubisa P. Ionic liquids as solvents for polymerization processes—Progress and challenges[J]. Progress in Polymer Science, 2009, 34(12): 1333-1347.

[75] Vygodskii Y S, Lozinskaya E I, Shaplov A S, et al. Implementation of ionic liquids as activating media for polycondensation processes[J]. Polymer, 2004, 45(15): 5031-5045.

[76] Strehmel V, Laschewsky A, Wetzel H, et al. Free radical polymerization of n-butyl methacrylate in ionic liquids[J]. Macromolecules, 2006, 39(3): 923-930.

[77] Soares B G, Livi S, Duchet-Rumeau J, et al. Synthesis and characterization of epoxy/MCDEA networks modified with imidazolium - based ionic liquids[J]. Macromolecular Materials and Engineering, 2011, 296(9): 826-834.

[78] Livi S, Silva A A, Thimont Y, et al. Nanostructured thermosets from ionic liquid building block–epoxy prepolymer mixtures[J]. RSC Advances, 2014, 4(53): 28099-28106.

[79] Nguyen T K L, Livi S, Pruvost S, et al. Ionic liquids as reactive additives for the preparation and modification of epoxy networks[J]. Journal of Polymer Science Part A: Polymer Chemistry, 2014, 52: 3463-3471.

[80] Livi S, Gérard J F, Duchet-Rumeau J. Ionic liquids: Structuration agents in a fluorinated matrix[J]. Chemical Communications, 2011, 47(12): 3589-3591.

[81] Livi S, Duchet-Rumeau J, Gérard J F. Nanostructuration of ionic liquids in fluorinated matrix: Influence on the mechanical properties[J]. Polymer, 2011, 52(7): 1523-1531.

[82] Jing Y. Phosphonium ionic liquids: versatile nanostructuration and interfacial agents for poly(vinylidene fluoride-chlorotrifluoroethylene)[D]. Université de Lyon, 2016.

[83] Jing Y, Pruvost S, Livi S, et al. Understanding of versatile and tunable nanostructuration of ionic liquids on fluorinated copolymer[J]. Macromolecules, 2015, 48(13): 4581-4590.

[84] Livi S, Bugatti V, Soares B G, et al. Structuration of ionic liquids in a poly (butylene-adipate-co-terephthalate) matrix: Its influence on the water vapour permeability and mechanical properties[J]. Green Chemistry, 2014, 16(8): 3758-3762.

[85] Soares B G, Livi S, Duchet-Rumeau J, et al. Preparation of epoxy/MCDEA networks modified with ionic liquids[J]. Polymer, 2012, 53(1): 60-66.

[86] Soares B G, Silva A A, Pereira J, et al. Preparation of epoxy/Jeffamine networks modified with phosphonium based ionic liquids[J]. Macromolecular Materials and Engineering, 2015, 300(3): 312-319.

[87] Soares B G, Silva A A, Livi S, et al. New Epoxy/Jeffamine networks modified with ionic liquids[J]. Journal of Applied Polymer Science, 2014, 131(3).

[88] Lins L C, Livi S, Duchet-Rumeau J, et al. Phosphonium ionic liquids as new compatibilizing agents of biopolymer blends composed of poly (butylene-adipate-co-terephtalate)/poly (lactic acid)(PBAT/PLA)[J]. RSC Advances, 2015, 5(73): 59082-59092.

[89] Shamsuri A A, Md. Jamil S N A. Compatibilization effect of ionic liquid-based surfactants on physicochemical properties of PBS/rice starch blends: An initial study[J]. Materials, 2020, 13(8): 1885.

[90] Yousfi M, Livi S, Duchet-Rumeau J. Ionic liquids: A new way for the compatibilization of thermoplastic blends[J]. Chemical Engineering Journal, 2014, 255: 513-524.

[91] Zuo H, Chen X, Ding Y, et al. Novel Designed PEG-DICATIONIC IMIDAZOLIUM-BASED Ionic Liquids as Effective Plasticizers for Sustainable Polylactide[J]. Chinese Journal

of Chemistry, 2021, 39(8): 2234-2240.
[92] Asnawi A, Hamsan M H, Aziz S B, et al. Impregnation of [Emim] Br ionic liquid as plasticizer in biopolymer electrolytes for EDLC application[J]. Electrochimica Acta, 2021, 375: 137923.
[93] Kowalczyk K, Spychaj T. Ionic liquids as convenient latent hardeners of epoxy resins[J]. Polimery, 2003(T. 48, nr 11-12): 833-835.
[94] Ham Y, Kim S, Shin Y, et al. A comparison of some imidazoles in the curing of epoxy resin[J]. Journal of Industrial and Engineering Chemistry, 2010, 16: 556-559.
[95] Nguyen T K L, Livi S, Soares B G, et al. Ionic liquids: A New Route for the Design of Epoxy Networks[J]. ACS Sustainable Chemistry & Engineering, 2016, 4(2): 481-490.
[96] Silva A A, Livi S, Netto D B, et al. New epoxy systems based on ionic liquid[J]. Polymer, 2013, 54(8): 2123-2129.
[97] Liu Y, Chen S, An R, et al. Development of a correlation equation between the diesterification of maleic anhydride and the acidic ionic liquids nature[J]. Green Chemical Engineering, 2023, 4(1): 57-63.
[98] Arora K A, Lesser A J, McCarthy T J. Synthesis, characterization, and expansion of poly (tetrafluoroethylene-co-hexafluoropropylene)/polystyrene blends processed in supercritical carbon dioxide[J]. Macromolecules, 1999, 32(8): 2562-2568.
[99] Watkins J J, McCarthy T J. Polymerization in supercritical fluid-swollen polymers: a new route to polymer blends[J]. Macromolecules, 1994, 27(17): 4845-4847.
[100] Kung E, Lesser A J, McCarthy T J. Morphology and mechanical performance of polystyrene/polyethylene composites prepared in supercritical carbon dioxide[J]. Macromolecules, 1998, 31(13): 4160-4169.
[101] Kumar V, Suh N P. A process for making microcellular thermoplastic parts[J]. Polymer Engineering & Science, 1990, 30(20): 1323-1329.
[102] Nalawade S P, Picchioni F, Janssen L. Supercritical carbon dioxide as a green solvent for processing polymer melts: Processing aspects and applications[J]. Progress in Polymer Science, 2006, 31(1): 19-43.
[103] Jin W, Xingguo C, Mingjun Y, et al. An investigation on the microcellular structure of polystyrene/LCP blends prepared by using supercritical carbon dioxide[J]. Polymer, 2001, 42(19): 8265-8275.
[104] Matuana L M, Park C B, Balatinecz J J. Structures and mechanical properties of microcellular foamed polyvinyl chloride[J]. Cellular polymers, 1998, 17(1): 1-16.

[105] Park C B, Behravesh A H, Venter R D. Low density microcellular foam processing in extrusion using CO_2[J]. Polymer Engineering & Science, 1998, 38(11): 1812-1823.

[106] Rodeheaver B A, Colton J S. Open-celled microcellular thermoplastic foam[J]. Polymer Engineering & Science, 2001, 41(3): 380-400.

[107] Reverchon E, Cardea S. Production of controlled polymeric foams by supercritical CO_2[J]. The Journal of Supercritical Fluids, 2007, 40(1): 144-152.

[108] Xu Z M, Jiang X L, Liu T, et al. Foaming of polypropylene with supercritical carbon dioxide[J]. The Journal of Supercritical Fluids, 2007, 41(2): 299-310.

[109] Lee K N, Suh Y J, Lee H J, et al. Preparation of microcellular SAN foam using supercritical CO_2[J]. Polymer (korea), 1999, 23(2): 181-188.

[110] Mills N J, Zhu H X. The high strain compression of closed-cell polymer foams[J]. Journal of the Mechanics and Physics of Solids, 1999, 47(3): 669-695.

[111]Liang M T, Wang C M. Production of engineering plastics foams by supercritical CO_2[J]. Industrial & engineering chemistry research, 2000, 39(12): 4622-4626.

[112] Suh K W, Park C P, Maurer M J, et al. Lightweight cellular plastics[J]. Advanced Materials, 2000, 12(23): 1779-1789.

[113] Cooper A I. Recent developments in materials synthesis and processing using supercritical CO_2[J]. Advanced Materials, 2001, 13(14): 1111-1114.

[114] Krause B, Sijbesma H J P, Münüklü P, et al. Bicontinuous nanoporous polymers by carbon dioxide foaming[J]. Macromolecules, 2001, 34(25): 8792-8801.

[115] Okamoto M, Nam P H, Maiti P, et al. A house of cards structure in polypropylene/clay nanocomposites under elongational flow[J]. Nano letters, 2001, 1(6): 295-298.

[116] Colton J S, Suh N P. Nucleation of microcellular foam: Theory and practice[J]. Polymer Engineering & Science, 1987, 27(7): 500-503.

[117] Colton J S, Suh N. The nucleation of microcellular thermoplastic foam with additives: Part I: Theoretical considerations[J]. Polymer Engineering & Science, 1987, 27(7): 485-492.

[118] Youn J R, Suh N P. Processing of microcellular polyester composites[J]. Polymer composites, 1985, 6(3): 175-180.

[119] Colton J S, Suh N P. The nucleation of microcellular thermoplastic foam with

additives: Part II: Experimental results and discussion[J]. Polymer Engineering & Science, 1987, 27(7): 493-499.

[120] Han J H, Dae Han C. Bubble nucleation in polymeric liquids. II. Theoretical considerations[J]. Journal of Polymer Science Part B: Polymer Physics, 1990, 28(5): 743-761.

[121] Lee L J, Zeng C, Cao X, et al. Polymer nanocomposite foams[J]. Composites Science and Technology, 2005, 65(15-16): 2344-2363.

[122] Chandra A, Gong S, Yuan M, et al. Microstructure and crystallography in microcellular injection-molded polyamide-6 nanocomposite and neat resin[J]. Polymer Engineering & Science, 2005, 45(1): 52-61.

[123] Zeng C, Han X, Lee L J, et al. Polymer–clay nanocomposite foams prepared using carbon dioxide[J]. Advanced Materials, 2003, 15(20): 1743-1747.

[124] Di Y, Iannace S, Maio E D, et al. Poly (lactic acid)/organoclay nanocomposites: thermal, rheological properties and foam processing[J]. Journal of Polymer Science Part B: Polymer Physics, 2005, 43(6): 689-698.

[125] Leung S N, Wong A, Wang L C, et al. Mechanism of extensional stress-induced cell formation in polymeric foaming processes with the presence of nucleating agents[J]. The Journal of Supercritical Fluids, 2012, 63: 187-198.

[126] Matuana L M, Park C B, Balatinecz J J. Cell morphology and property relationships of microcellular foamed pvc/wood - fiber composites[J]. Polymer Engineering & Science, 1998, 38(11): 1862-1872.

[127] Blyler Jr L L, Kwei T K. Flow behavior of polyethylene melts containing dissolved gases[J]. Journal of Polymer Science Part C: Polymer Symposia, 1971, 35: 165-176.

[128] Guo M C, Peng Y C. Study of shear nucleation theory in continuous microcellular foam extrusion[J]. Polymer Testing, 2003, 22(6): 705-709.

[129] Mori T, Hayashi H, Okamoto M, et al. Foam processing of polyethylene ionomers with supercritical CO_2[J]. Composites Part A: Applied Science and Manufacturing, 2009, 40(11): 1708-1716.

[130] Li Y, Yao Z, Chen Z hua, et al. High melt strength polypropylene by ionic modification: Preparation, rheological properties and foaming behaviors[J]. Polymer, 2015, 70: 207-214.

[131] Corre Y M, Maazouz A, Duchet J, et al. Batch foaming of chain extended PLA with supercritical CO_2: Influence of the rheological properties and the process parameters on the cellular structure[J]. The Journal of Supercritical Fluids, 2011, 58(1): 177-188.

[132] Livi S, Duchet-Rumeau J, Pham T N, et al. A comparative study on different ionic liquids used as surfactants: Effect on thermal and mechanical properties of high-density polyethylene nanocomposites[J]. Journal of Colloid and Interface Science, 2010, 349(1): 424-433.

[133] Chen Y, Zhang Y, Ke F, et al. Solubility of neutral and charged polymers in ionic liquids studied by laser light scattering[J]. Polymer, 2011, 52(2): 481-488.

[134] Hajipour A R, Rafiee F. Recent progress in ionic liquids and their applications in organic synthesis[J]. Organic Preparations and Procedures International, 2015, 47(4): 249-308.

[135] Yue C, Fang D, Liu L, et al. Synthesis and application of task-specific ionic liquids used as catalysts and/or solvents in organic unit reactions[J]. Journal of Molecular Liquids, 2011, 163(3): 99-121.

Chapter 2: LIonomers-new generation of ionomers: by combining PPgMA and different ionic liquids

Table of Contents

Chapter 2: LIonomers-new generation of ionomers: by combining PPgMA and different ionic liquids

2.1 Effect of phosphonium based ionic liquids on the structuration and physical properties of LIonomers

2.1.1 Introduction

Ionomers are considered as materials based on macromolecules containing one type of ionic/ionizable groups that are composed of the acid anions and metal salts [1–4]. These materials display a multi-scale structuration: the ion-pairs, formed between acids anions and metal salts, usually assemble to form multiplet structures involved themselves in ionic clusters [5]. Not only the generated ionic networks through the ion pair interactions between metal cations and acid anions but also aggregated ionic domains can create confined regions where the mobility of polymer chains is restricted [6]. According to the literature, various types of morphologies and physical properties can be obtained coming from the same initial polymer chemistry [7,8]. The formation of nano- and microstructures through the clustering of ion-pairs in a low dielectric constant medium is both well-documented and theoretically predictable [6]. These generated restrained motions improve the thermo-mechanical and rheological properties [9–13]. Many metal salts have been added into different polymers (like poly (lactic acid), polypropylene grafted maleic anhydride) to prepare ionomers with significant improvement of the physical properties. For example, thanks to the ionic crosslinkings between the carboxylate groups from maleic anhydride hydrolysis and metal cations, nine different polypropylene-ionomers were obtained by cooperating various metal compounds including aluminium stearate (AlSt), magnesium stearate (MgSt), calcium stearate (CaSt), zinc stearate (ZnSt), potassium stearate (KSt), sodium stearate (NaSt), magnesium hydroxide (MH), zinc oxide (ZnO), and zinc sulfide (ZnS) [14]. According to this study, the viscosity measured at low shear rate of these cross-linked ionomers followed the arrangement according to the following order, *i.e.*

ionomers processed with AlSt > MgSt > ZnSt > NaSt > KSt > MH > ZnO > ZnS > neat substrate. The highest ionic charge of the Al^{3+}-salts leads to the greatest viscosity, revealing the strongest interactions since each Al^{3+} could interact with three anions. At the same time, due to the steric effects of metal ions, the mechanical properties vary with the metal nature, *i.e.* sodium and zinc acetate could enhance the mechanical properties of ethylene-acrylic acid copolymers, while the Al^{3+}-salts decrease them [15] This literature reported the impacted microstructure and comprehensive properties due to three parameters, *i.e.* the nature of the counter anion, the steric hindrance of the cation as well as the contents of metal salts.

More recently, ionic liquids （ILs）have been widely described as promising components of polymer matrix according to their intrinsic features and their ionic characters [16–23]. Thanks to their special combinations, the multitude of cation/anion combination could promote the interactions with polar groups. As a consequence, they are considered as interfacial agents in polymer blends or organic-inorganic hybrids [24,25]. In addition, they may act as reactant participating in the opening of the epoxide rings for further designing new IL-epoxy networks [26,27], or activating maleic anhydride groups for esterification reactions [28]. In 2023, they are applied for the first time to design LIonomer, *i.e*. a new generation of thermoplastic ionomers, whose physical behaviours could be tailored from the management of interactions intensity within ILs/thermoplastic polymer blends from various ionic pairs of ionic liquids [29]. In this paper, new ionic crosslinked has been obtained due to the basicity and nucleophilicity of the counter anions as well as the original electrostatic interactions of ILs cation/anion pair. Imidazolium ILs acting together achieve an outstanding equilibrium between stiffness and stretchiness of the resulting ionomers. Here, phosphonium-based ionic liquids (PhILs) are found to be promising additives due to their outstanding properties, such as thermal stability [30], no acidic proton avoiding the generation of carbine, and fire-resistance ability [31]. Four phosphonium based cations combined with different anions, chloride *vs.* acetate *vs.* phosphinate *vs.* phosphate anions have been

considered (Scheme 2-1). In addition to the parameters controlling the location and rearrangement of PhILs in the bulk of the polymer matrix or defining the nanostructuration and their consequence of LIonomers considered in the literature [29]. The objectives of this paper are *i)* analyse the strength of ionic interactions between polymer polar groups and PhILs in relation with steric hindrance due to the conformation of PhILs; *ii)* assess how these PhILs affect the viscoelastic and thermal-mechanical behaviours as well as the crystallization processes.

2.1.2. Experimental section

2.1.2.1 Materials

Two types of thermoplastic polymers were considered as matrices, *i.e.* continuous medium. The first one, named PPgMA, is produced by Arkema (OREVAC® CA 100) with 1 wt.% MA (maleic anhydride) content and the second one, named PPgMA8, supplied from Sigma-Aldrich with 8-10 wt.% MA content. Three PhILs: tetradecyl (trihexyl) phosphonium-bis-(2,4,4-trimethylpentyl) phosphinate (P^+TMP), tributyl (ethyl) phosphonium diethyl phosphate (P^+DEP) and trihexyl (tetradecyl) phosphonium chloride (P^+Cl), were produced by Cytec industries B. V. Their chemical structures shown (Scheme 2-1) consider the same phosphonium cation with a varying alkyl chain surrounding and a different anion. Sodium acetate and silver nitrate were purchased from Sigma Aldrich.

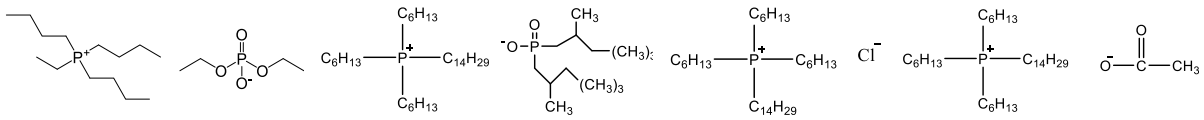

P^+DEP P^+TMP P^+Cl P^+Ac

Scheme 2- 1 Cation-anion combination of PhILs

2.1.2.2 Samples preparation and characterizations

Synthesis of P+Ac ionic liquid

According to the literature and the order to consider the same phosphonium cation [32], one new PhIL, *i.e.* trihexyl (tetradecyl) phosphonium acetate (P^+Ac), was

successfully synthesized following this procedure 5.7g of P^+Cl, 1.5g sodium acetate, and 20g H_2O have been fed into a closed round bottom flask at 55°C and stirred for 1.5h. Repeated removal of the inorganic phase and alternate washing with deionised water until that no Cl^- was detectable in aqueous silver nitrate. The final product was collected after removing volatile compounds by drying under vacuum. Figure 2-2 describes the detailed procedure. NMR and IR [32–34] spectroscopies have been employed to confirm the resulting chemical.

^{13}C NMR (δ/ppm; C_6D_5Cl): 13.57, 13.71, 19.50, 19.97, 21.98, 22.26, 22.55, 31.05, 174.58. ^{31}P NMR (δ/ppm; C_6D_5Cl): 33.45. IR ν_{max} (KBr disc)/cm^{-1}: 2955, 2923, 2854, 1568, 1466, 1111, 1044, 1412, 720.

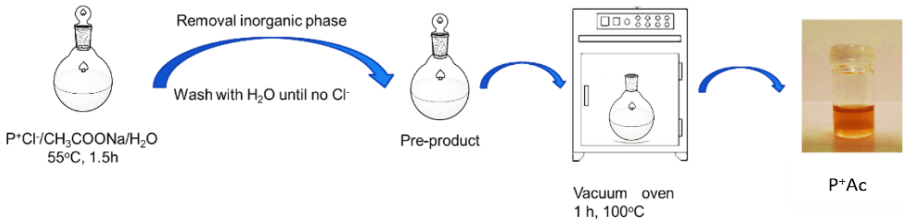

Figure 2- 1 Schematic preparation procedure of P^+Ac

Preparation of LIonomers and characterizations

The polymer matrices, *i.e.* MA-grafted PP, were dried at 70 °C for 12 hours. The PhILs were blended with these polymers into a DSM micro extruder at 180 °C for 5 min and injected at 30 °C as tutting (Scheme 2-2). Thus, different LIonomers conformations, *i.e.* combining different cation/anion couple pair, MA and/or IL contents were prepared (Table 2-1).

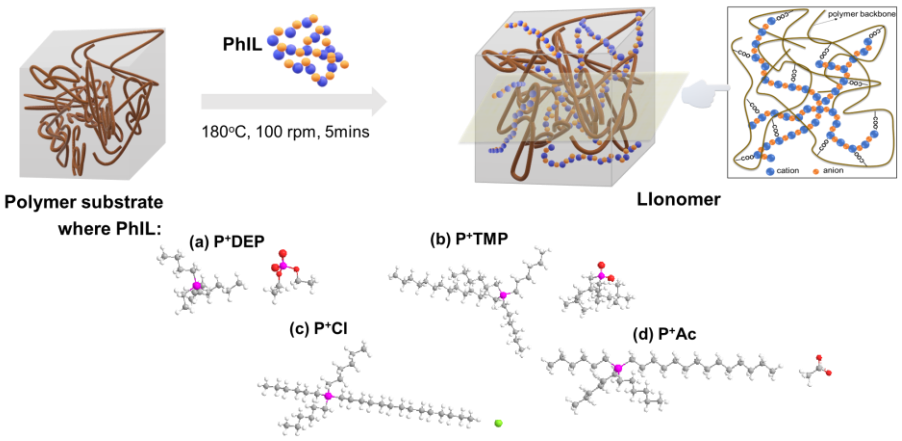

Scheme 2- 2 The schematic diagram of the processing process

Table 2- 1 PPgMA/IL blends considered in this study

Polymer matrix	PPgMA1	PPgMA8	10wt% PhILs	Abbreviations
PPgMA	100 wt%	0 wt%	P^+TMP	L-P^+TMP-10
			P^+Cl	L-P^+Cl-10
			P^+DEP	L-P^+DEP-10
			P^+Ac	L-P^+Ac-10
Blends-1	90 wt%	10 wt%	P^+TMP	LB1-P^+TMP-10
			P^+Cl	LB1-P^+Cl-10
			P^+DEP	LB1-P^+DEP-10
			P^+Ac	LB1-P^+Ac-10

The interactions between PPgMA and PhILs were characterized by NMR spectroscopy. ^1H and ^{31}P NMR spectra of all LIonomers processed based on PPgMA8 and PhILs were recorded using a Bruker Avance III 400 MHz spectrometer operating at 373K. Samples are dissolved in C_6D_5Cl. The chemical shifts (δ) are expressed in ppm relative to the internal reference of solvent for ^1H nuclei.

The Fourier-Transform Infrared (FTIR) spectroscopy (using a Thermo Scientific Nicolet iS10 spectrometer) in transmission mode (128 scans) was used.

The rheological and dynamic mechanical analysis (DMA) were performed using a ARES-G2 rheometer (SN#4010-0255, TA Instrument). The rheological behaviour was

recorded at 180°C for a parallel plate geometry (d=25mm) under N_2 atmosphere. Dynamic mechanical curves were recorded in the -80/100 °C temperature range with a heating rate of 3 K·min^{-1}.

The morphology of the neat PPgMA and LIonomers was characterized by transmission electron microscope (TEM, Phillips CM 120) operating at an accelerating voltage of 120 kV. Specimens were prepared by ultramicrotomy and collected on a carbon film-coated cooper grid.

Melting and crystallization processes were recorded by using Differential Scanning Calorimetry (DSC, Q10 TA Instrument) after erasing the thermal history of the samples by heating and furthering cooling rates at different thermal rates (5, 10, and 20 K·min^{-1}) under N_2 flow. The crystallization temperatures (T_c, °C) were characterised during a first cooling circle and Crystallinity rate (X_c) was calculated by Equation 2-1 using enthalpy change from the 2rd heating scan.

$$X_c = \frac{\Delta H_f}{(1-\varphi)\Delta {H_f}^0} \quad \text{Equation 2- 1}$$

where ΔH_f^0 is 209J/g, *i.e.* corresponding to the melting enthalpy of 100% crystallized polymer [35]. ΔH_f the melting enthalpy of the analyzed sample, and φ the mass fraction of introduced PhILs.

Jeziorny's [36] non-isothermal crystallization model was considered to analyze the crystallization process:

$$\ln[-\ln(1-X_t)] = \mathrm{nlnt} + \ln Z_t \quad \text{Equation 2- 2}$$

$$X_T = \frac{\int_{T_0}^{T_c}(\frac{dH_c}{dT})/dT}{\int_{T_0}^{T_\infty}(\frac{dH_c}{dT})/dT} \quad \text{Equation 2- 3}$$

$$t = \frac{T_0 - T}{\varphi} \quad \text{Equation 2- 4}$$

where X_t is the relative crystallinity at a given crystallization time t; n and Z_t correspond to Avrami' exponent and crystallization kinetic constant, respectively. Their values can be obtained by plotting the $\ln[-\ln(1-X_t)]$ as a function of lnt. X_T is related to crystallinity rate with the change of temperature, T_0 and T_∞ being the onset

and the end of crystallization temperature. T is the temperature for a given crystallization time t, while φ is the cooling rate.

The crystallization half-time, denoted $t_{1/2}$, could be determined from Equation 2-5:

$$t_{1/2} = (\frac{ln2}{Z_t})^{1/n} \quad \text{Equation 2- 5}$$

The crystalline lattice was analysed by Wide Angle X-Ray Diffraction (WAXD) using a Bruker D8-Advance diffractometer operating at room temperature (2θ=10-45° using Cu Kα radiation-λ=0.15406 nm). The diffractograms were further analysed using Origin 2018 software considering Gauss' fitting function. The crystal size was calculated according to the Scherrer's equation:

$$D = \frac{K\lambda}{(\beta - s)cos(\theta)} \quad \text{Equation 2- 6}$$

where D is the crystal size; K is the crystalline shape parameter (≈0.89); λ equals to 0.15406 nm-the Cu Kα wavelength; β is the diffraction peak half-height width; s is the instrument factor calibration (0.05°); θ is the diffraction angle.

Uniaxial tensile tests were carried using an Instron mechine operating at room temperature for a crosshead speed of 50 mm·min^{-1}. Each tensile test was repeated at least three times.

2.1.3 Results and discussion

2.1.3.1 Interaction between PhILs and polymer matrix

In agreement with the literature [29], interactions must take place in LIonomers, *i.e.* between carboxylate groups issued from maleic anhydrides groups of PPgMA backbone and cation of phosphonium cations of the ILs. The NMR spectroscopy was used to evidence IL-polymer chain interactions, from the comparing neat IL spectra and the ones of the LIonomers as shown in Figures 2-2 and 2-3, respectively. First, let's consider P^+DEP and its LIonomer. The change of the chemical shifts in ^{31}P NMR spectra from 34.64 ppm into 34.99 ppm of P^+DEP cation and from -0.38 ppm into -0.95

ppm of counter anion [37] (see Figure 2-2a) reveals that the electron of P^+DEP anion attacks and participates into the opening of MA ring, resulting in the circle opening and then ionic-ionic interactions between generated COO^- and P^+DEP cation [28]. Therefore, the rearrangement of P^+DEP anion/cation pairs are achieved. More specifically, the positive shielding effect induced by the interaction between polar groups in matrix (C=O as shown in Scheme 2-3) causes the enhanced electron cloud density of phosphorus atom in P^+DEP anion. Meanwhile, the ionic-ionic interactions between P^+DEP cation and generated COO^- of polymer matrix lead to shifting of the resonance of the anion phosphorus to lower field because of the strong electronegativity of oxygen. Consequently, other P^+DEP anion/cation pairs may self-assemble into 'ionic-branched chains' from the polar species of the grafted PP chains which play the role of a head and the original electrostatic interactions between anions and cations (see Scheme 2-3).

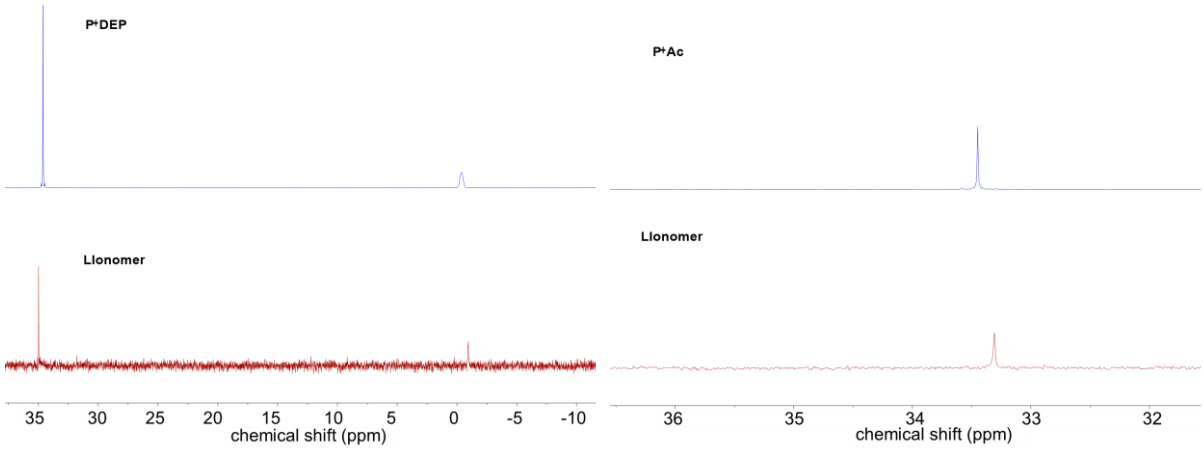

a b

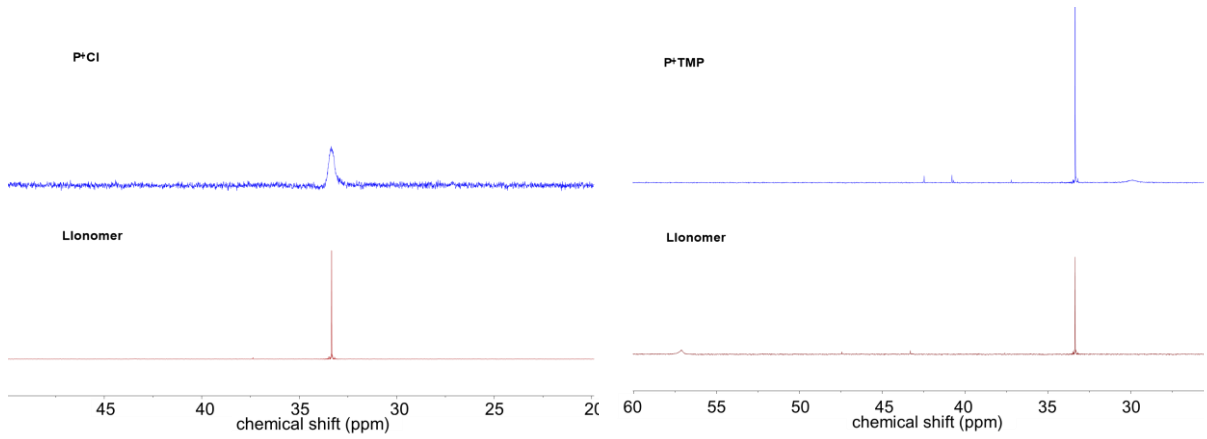

c d

Figure 2- 2 The ^{31}P NMR spectra (400 MHz; C_6D_5Cl solvent) of P^+DEP, P^+Ac, P^+Cl, P^+TMP and their LIonomers (10 wt.%)

Such a self-assembling of PhILs into 'ionic-branched chains' could also be observed by introducing P^+Ac, P^+TMP, or P^+Cl into a MA-grafted-PP matrix. Nevertheless, some differences are present according to the differences of the interaction intensities due to various steric hindrance, *i.e*. the PhILs conformation. As for the LIonomer based on P^+Ac, the electron cloud density of phosphorus is increased leading to the ^{31}P shifting from 33.45 into 33.31 ppm (Figure 2-2b), since the free electron of COO^- migrates into the P^+Ac cation. However, such change on ^{31}P cation becomes unobvious by comparing P^+TMP and P^+Cl to the corresponding LIonomer, from 33.36 ppm in former cation [38,39] to 33.37 ppm in corresponding LIonomer, from 33.35 [33] to 33.34 ppm in later pair. Such change may be attributed to the hindered conformations and low activity of anion of PhILs. While ^1H NMR also evidences the interactions between PP chains and the cation of P^+TMP or P^+Cl. In fact, a shift could be observed (from 2.57 ppm for P^+TMP cation position #1 to 2.33 ppm for the LIonomer Figure 2-3a and from 2.88 ppm for P^+Cl cation position #1 to 2.58 ppm for LIonomer Figure 2-3b). On the other side, the ^{31}P of P^+TMP anion shifts from 40.79 to 43.30 ppm as it is influenced by the connected polar groups.

In summary, the presence of maleic anhydride groups along the PP chains could activate interactions for the four PhILs considered in this study [28]. The strength of such

generated interactions is strongly dependent on the cation/anion combination (*i.e.* steric hindrance). In present, these confirmed interactions and the generated 'ionic-branched chains' morphology must affect the macroscopic behaviour both in the solid and molten states of the resulting materials.

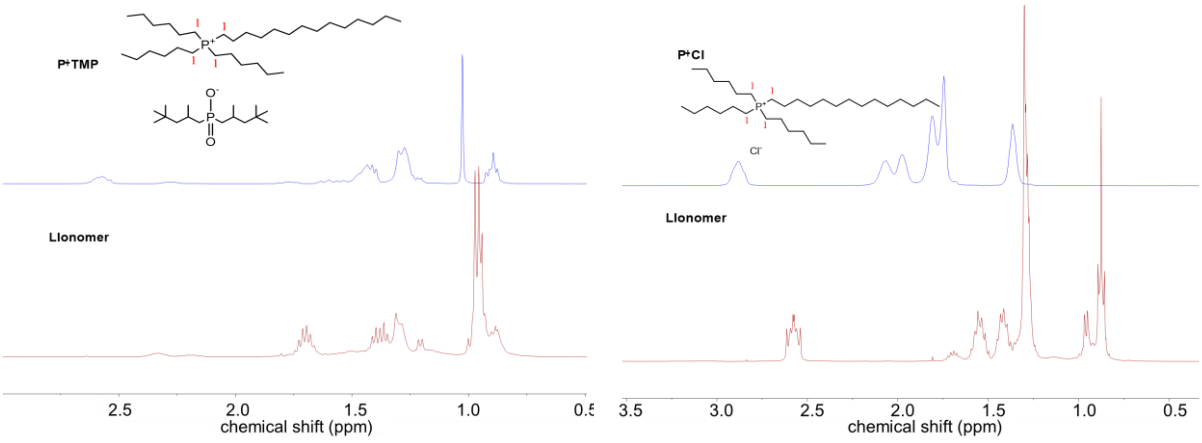

a b

Figure 2- 3 ^{1}H NMR spectra (400 MHz; C6D5Cl solvent) of P^{+}TMP, P^{+}Cl and corresponding LIonomers (10 wt.%)

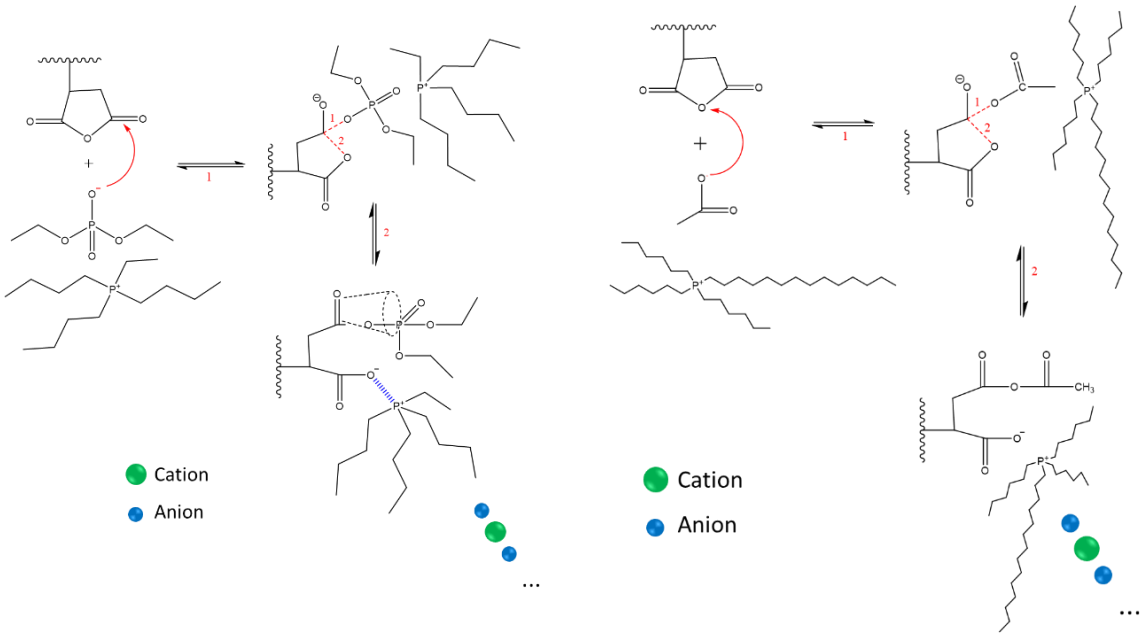

a b

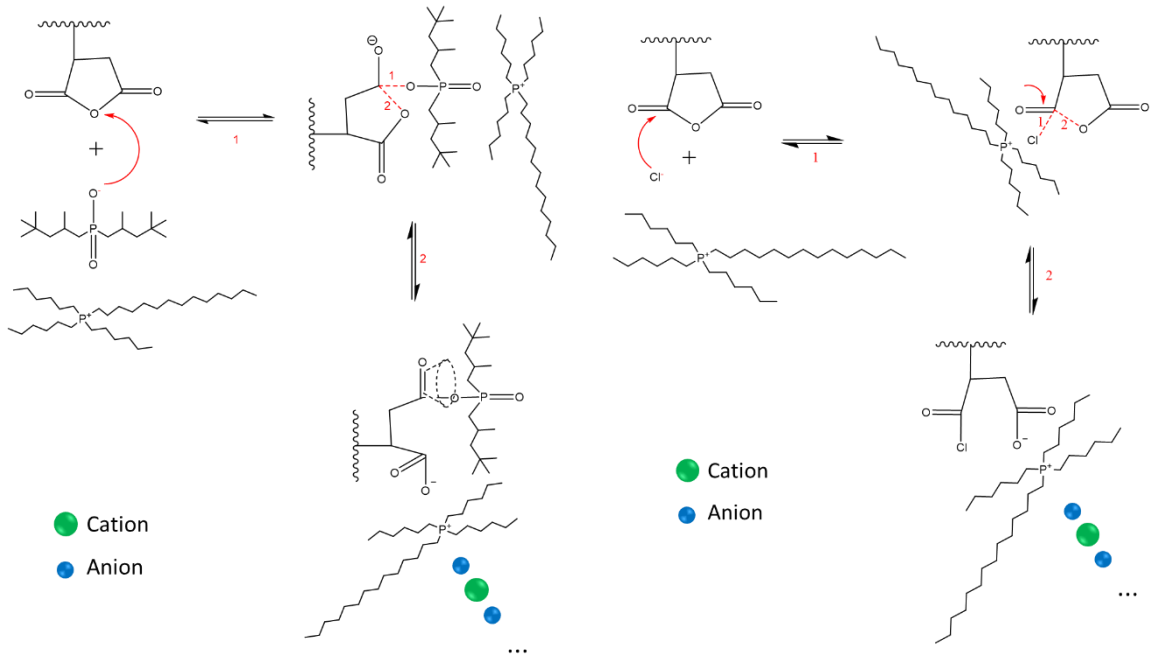

c d

Scheme 2- 3 Proposed reaction mechanism for the synthesis of LIonomers considered in this study (based on: P^+DEP: a; P^+Ac: b; P^+TMP: c; P^+Cl: d)

2.1.3.2 The effect of PhILs on rheological properties: Interaction strength

The molten state behavior of LIonomers appears to be very different to neat PPgMA due to the existence of ion-ion/ion-dipolar interactions, as previously described. In fact, all LIonomers display a more pronounced shear thinning behavior compared to neat PPgMA as shown in Figure 2-4. This effect is more pronounced for LIonomers processed with the addition of P^+DEP. Owing to the low viscosity of PhILs at high temperature (few mPa·s), only the COO^-/IL combined with IL/IL interactions could lead to the generation of inter-chains connecting nanostructures as reported for ionomers [6,21,30]. Such ionic branching nanophases lead to a reduction of the chain mobility, resulting in an increase of the melt viscosity [1,10,40–42]. Viscosity values dependence with the nature of the ionic liquid follows the same trend in both matrices, PPgMA and the Blends-1. Thus, the interaction strength can be tuned from the anion and cation steric hindrance. The P^+DEP cation/anion pair is the less sterically hindered one allowing it to establish strong interactions with the COO^- groups. The other cations are

more sterically hindered which leads to decrease the interactions with carboxylate groups. Meanwhile, all these changes indicate that the generated ionic interactions can stand at temperatures up to 180ºC.

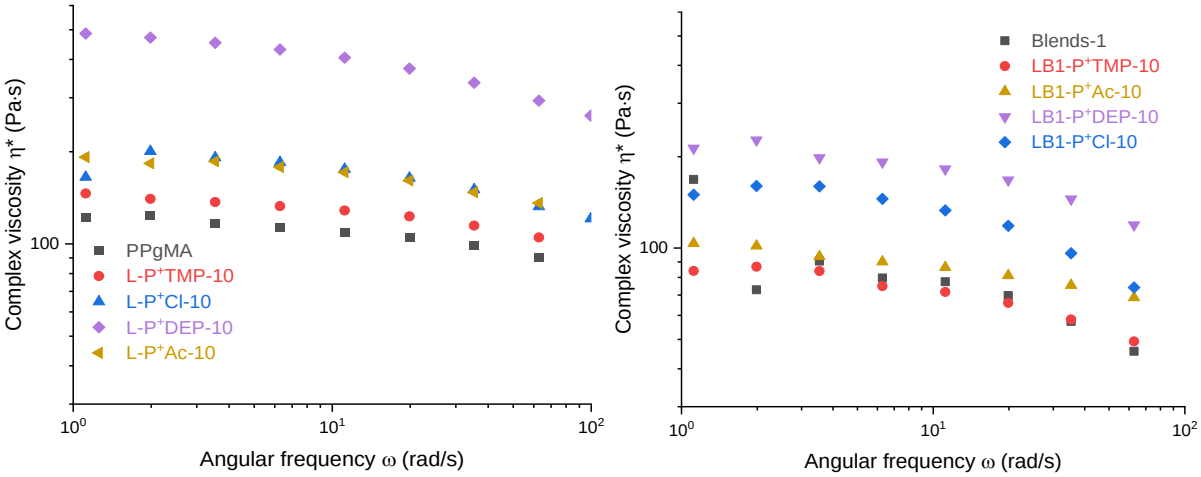

Figure 2- 4 Viscosity of polymer matrix and LIonomers with different kinds or PhILs content at 180 ºC

The rheological behavior of LIonomers tends more towards gel-like behavior compared to the neat polymer due to *i)* the ionic interactions generated between PhILs and polymer chains acting as crosslinkings restraining segmental motions [29,43]; *ii)* the gel-like structure induced by introducing PhILs [21,44]; *iii)* the presence of ionic domains within LIonomers (Figure 2-5) [1,10,40–42,45]. On the other hand, the increase of MA content in the matrix causes a decrease of the viscosity (L-P$^+$DEP-10 > LB1-P$^+$DEP-10). Due to the fact that more MA groups are available to generate more interactions while shortening the length of 'ionic branched chains' made from cation-anion pairs association [43]. Less crosslinking points and/or clusters lead to the decrease of the viscosity of blends.

2.1.3.3 Microstructure characterization: location of PhILs

Transmission electron microscopy (TEM) is an efficient tool to evidence a potential phase separation of IL ion pairs within the polypropylene matrix. The morphologies of polymer/P$^+$DEP blends (Figure 2-5) were considered thanks to the strongest interaction strength evidenced previously. Considering the expected morphologies of

LIonomers, these granular “bean-spots” features could be attributed to a phase-separation and the association of ILs [29]. Nevertheless, the state of the ionic liquid in the final LIonomers results from the equilibrium of its interactions between the carboxylates onto the grafted-PP matrix and the ones between IL pairs. The size of the IL-rich phase is dependent on the host matrix. With 1 wt.% MA content, IL-rich phases are many and of a sub-micro size (Figure 2-5b). As a more grafted PPgMA is considered, bigger IL-rich phases are formed (Figure 2-5c). This coarse morphology is in agreement with the reduction of viscosity of the corresponding LIonomers previously reported

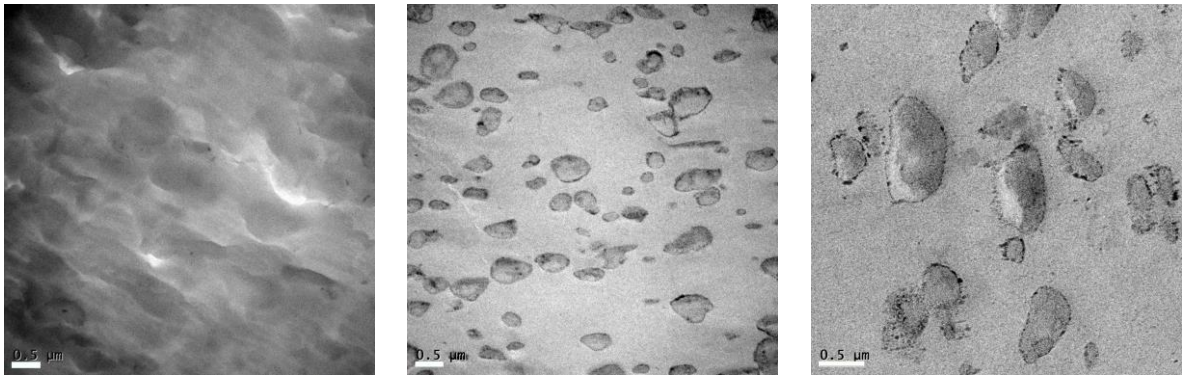

a b c

Figure 2- 5 TEM microscopies of a: PPgMA, b: L-DEP-10, and c: LB1-DEP-10 (scale bar: 0.5µm)

Studying the molecular relaxation behaviour contributes to the understanding of the structuration of the neat PPgMA as well as the resulting LIonomers. Figure 2-6 and Table 2-2 report the parameters from solid state mechanical spectroscopy (DMA). Considering the polypropylene morphology, the rigid amorphous fraction (denoted as RAF) displays one relaxation value since the associated polymer chains are attached close to crystalline fraction and therefore hold reduced segmental movement [46–48]. While the chains in mobile amorphous fraction (denoted as MAF) exhibit higher segmental mobility. As a consequence, the two relaxations at 5 and 80 °C (at 1Hz) could be attributed to the mobile amorphous fraction and rigid amorphous fraction, respectively. The sub-Tg relaxation, denoted β relaxation, belongs to the local

segmental motions of methyl and methylene (T_β) [49]. The slight changes of T_β for the different LIonomers demonstrate that the PhILs do not affect the local segmental motions. Similarly, T_α (MAF) of LIonomers associated to the glass transition temperature remain the same.

On the other side, the increased $T_{\alpha'}$, associated with RAF large amplitude motions, of the LIonomers compared to the one of the neat PP polymer and confirms the location of the PhILs close to crystalline lamellae [29]. In fact, the alkyl chains of the phosphonium cation may promote the miscibility with PPgMA. This effect is particularly pronounced for the LIonomer processed with 10 wt.% P^+DEP that displays the strongest COO^-/phosphate ionic interactions owing. Only chloride anion does not modify $T_{\alpha'}$ (associated to RAF). Consequently, one can concluded that this anion is only localized in MAF. Increasing MA content leads not only to fewer ionic regions (Figure 2-6b *vs.* 2-6c) but to ionic-branched chains leading to reduce $T_{\alpha'}$ (RAF). Such a decrease is consistent with the conclusions from the analyses of the rheological behaviours.

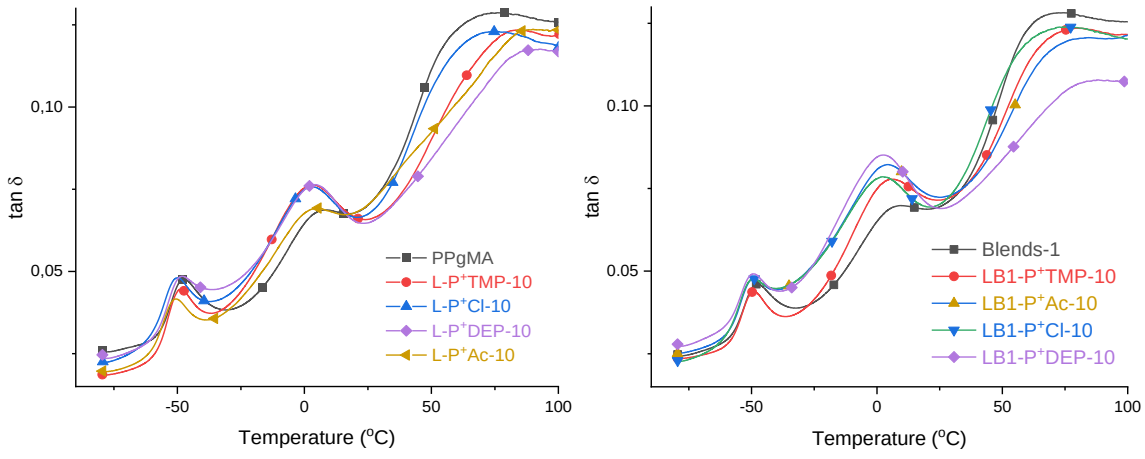

Figure 2- 6 Loss factor (tan δ) *vs.* temperature for polymer matrix and LIonomers at 1 Hz

Table 2- 2 Temperatures at the maximum of tan δ at 1 Hz of the β, α, and α' relaxations of neat PPgMA and associated LIonomers

Samples	T_β (°C)	T_α (MAF, °C)	$T_{\alpha'}$ (RAF, °C)
PPgMA	-47	7	76
L-P$^+$TMP-10	-49	3	85
L-P$^+$Cl-10	-49	3	76
L-P$^+$DEP-10	-47	5	93
L-P$^+$Ac-10	-51	5	88
Blends-1	-47	10	74
LB1-P$^+$TMP-10	-49	7	80
LB1-P$^+$Cl-10	-50	2	74
LB1-P$^+$DEP-10	-49	3	88
LB1-P$^+$Ac-10	-49	5	84

2.1.3.4 Effect of PhILs on crystallization of PPgMA

In thermoplastic (PVDF)/IL blends, some PhILs could migrate into RAF between crystalline layers influencing the crystallization ability of polymer chains [24]. In this study, LIonomers show very limited changes on their final X_c and T_c as shown in Table 2- 3. Such phenomenon could be associated with the location of PhILs. The effect of PhILs on the crystallization process has been highlighted by means of Jeziorny's non-isothermal crystallization kinetics model [36] (data reported in Figure S2-1 and S2-2, and Table S2-1). The $t_{1/2}$ value expresses the crystallization rate [50]. Adding PhILs doesn't change $t_{1/2}$. It implies that the ionic interactions and generated "ionic-branched chains" within LIonomers do not restrain the regular folding of polymer chains into crystalline regions during crystallization step. One the other side, in addition to increasing ionic liquid content [29], the delayed crystallization process could be also obtained by increasing the carboxylate groups content, *i.e.* $t_{1/2}$ value increases from 0.76 min in L-P$^+$DEP-10 to 0.83 min in LB1-P$^+$DEP-10, 0.65 min in L-P$^+$TMP-10 and L-

P⁺Ac-10 to 0.71 min in LB1-P⁺TMP-10 and LB1-P⁺Ac-10.

Table 2- 3 Crystallization parameters of PPgMA and related LIonomers measured by DSC (5 K·min^{-1})

Materials	$t_{1/2}$ (min)	T_c (°C)	X_c (°C)
PPgMA	0.77	116	34
L-P⁺TMP-10	0.65	115	35
L-P⁺Cl-10	0.78	116	37
L-P⁺Ac-10	0.65	115	34
L-P⁺DEP-10	0.76	116	35
Blends-1	0.74	116	36
LB1-P⁺TMP-10	0.71	115	35
LB1-P⁺Cl-10	0.74	116	34
LB1-P⁺Ac-10	0.71	116	35
LB1-P⁺DEP-10	0.83	116	35

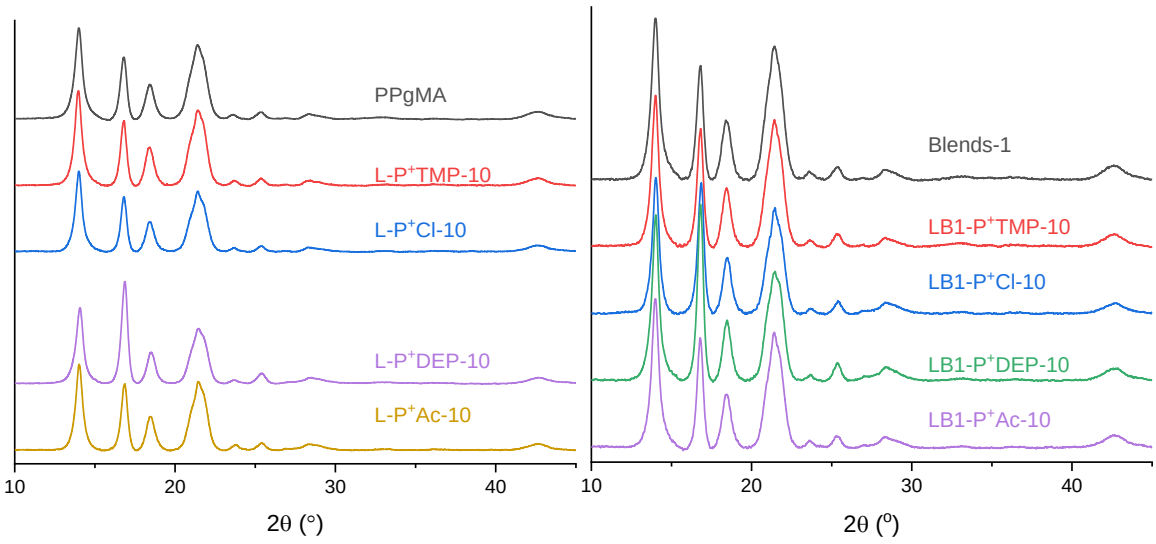

Figure 2- 7 WAXD diffraction patterns of maleic anhydride-grafted PP and related LIonomers

Table 2- 4 Average crystalline lamellae thickness of PP polymer matrices and related LIonomers based on various PhILs

	$D_{[110]}$ (nm)	$D_{[040]}$ (nm)	$D_{[130]}$ (nm)	Average size
PPgMA	12.7	18.2	12.8	12.7
L-P^+TMP-10	13.5	18.7	13.2	12.9
L-P^+Cl-10	14.3	19.2	13.3	13.3
L-P^+DEP-10	13.6	18.3	13.8	12.4
L-P^+Ac-10	14.5	18.0	13.4	12.3
Blends-1	12.3	17.7	12.7	12.1
LB1-P^+TMP-10	13.7	17.9	13.4	12.0
LB1-P^+Cl-10	15.0	18.0	13.1	13.2
LB1-P^+DEP-10	13.7	19.5	13.7	14.9
LB1-P^+Ac-10	13.3	19.2	12.9	12.5

On the DSC melting traces of PPgMA and related LIonomers, two melting peaks are evidenced at low heating rate, *i.e* at 158 and 165°C (Figure S2-1). The high value of melting temperature (165 °C) is attributed to the stable crystalline phase (α-form) whereas the other one belongs to low crystal density phase (for example β, γ, etc.) [51,52]. However, WAXD analyses show that PPgMA crystallizes mainly under the α type crystalline form [53] (see Figure 2-7 and Table 2-4). The presence of PhILs seems not to change α-phase into other types (such as β-form) due to the relative low interaction strength [29] and the effect on average crystal size (calculated based on their α-form crystalline size) of PPgMA remains unclear. Therefore, it can be concluded that the ionic liquid did not 'enter' into the crystal lamellaes to influence the crystallization process [24]. On the other hand, the addition of PhILs to PPgMA has a pronounced effect on the average crystalline size of LIonomers based on PP grafted with a higher MA content. The crystalline lamellaes become thicker for a higher concentration of maleic anhydride groups (for example 14.9 nm in LB1-P^+DEP-10 > 12.4 nm in L-P^+DEP-10). It demonstrates the promoted growth of thicker crystalline lamellaes

thanks to the more dispersed ions. At the same time, the increased crystal size seems to be another evidence of the location of PhILs within LIonomers.

2.1.3.5 Effect of PhILs on mechanical properties of LIonomers

The mechanical characteristics are reported in Figure 2-8 and Table 2-5. These ones can be analysed according to the nature of the PhILs. The strongest ionic interactions between DEP anion and PPgMA with carboxylates as grafted species along the PP chains are favoured due to the lowest steric hindrance for this IL which leads to the highest modulus for both PPgMA (492 and 448 MPa as L-P$^+$DEP-10 and LB1-P$^+$DEP-10 were considered, respectively). The increase of the number of polar groups along PP chains able to generate short these “ionic branched chains” from (micro) phase separation phenomenon has also a large response on mechanical properties of LIonomers. Except for LIonomers processed using P$^+$Ac, the modulus increases [54–56]. The mechanical properties are comparable to the ones reported for polymer/ILs blends [16,22,24,29,57,58]. The location of ILs in the RAF [24], *i.e.* in the confined regions between lamellar crystallites and/or as a "spider web" morphology [16] results in a significant increase of strain at break (200%). This ability to sustain large deformations is related to the location of PhILs and to the interactions between PhILs and polar groups of grafted PP (as shown by NMR and rheology). In summary, owing to the generated interactions and the structuration of the PhILs within PPgMA matrix which can be tuned by the nature of PhILs, *i.e.* the nature of the anion and cation, the mechanical behaviour of LIonomers can be also tailored.

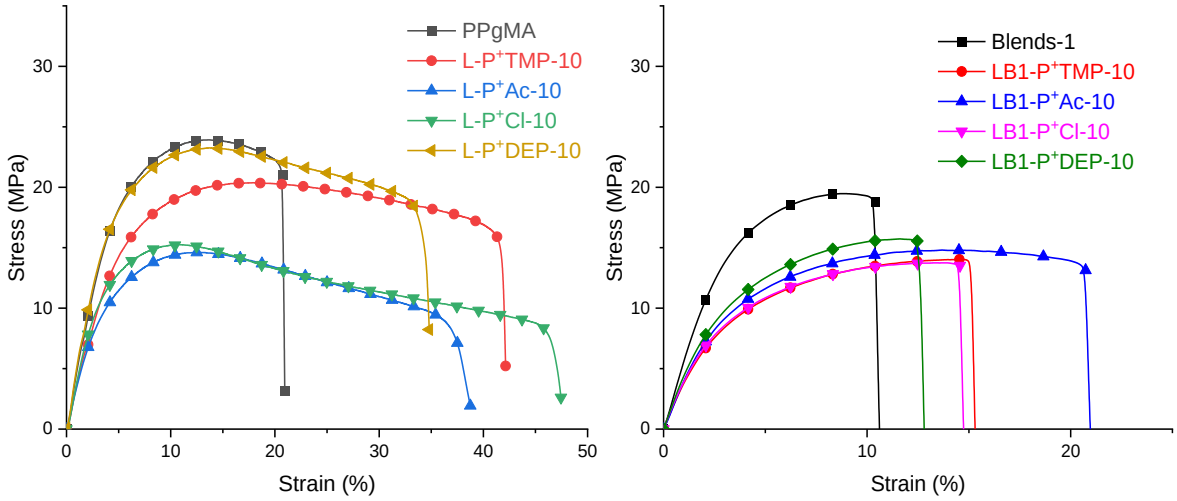

Figure 2- 8 Stress-strain curves of polymer matrix (PPgMA) and its LIonomers

Table 2- 5 Mechanical characteristics of polymer matrix (PPgMA) and LIonomers at room temperature

Samples	Young's modulus (MPa)	Strain break (%)
PPgMA	456±18	24±6
L-P$^+$TMP-10	392±3	39±1
L-P$^+$Cl-10	434±12	50±8
L-P$^+$DEP-10	492±12	35±5
L-P$^+$Ac-10	377±15	37±4
Blends-1	534±18	12±1
LB1-P$^+$TMP-10	403±28	17±3
LB1-P$^+$Cl-10	407±4	19±4
LB1-P$^+$DEP-10	448±11	17±3
LB1-P$^+$Ac-10	427±32	21±4

2.1.4. Conclusions

In this section, LIonomers based on phosphonium ILs and maleic anhydride grafted polypropylene (PPgMA) have been successfully designed. Four phosphonium-based ionic liquids (PhILs) were considered, including tetradecyl (trihexyl) phosphonium bis (2,4,4-trimethylpentyl) phosphinate (P$^+$TMP), tributyl (ethyl)

phosphonium diethyl phosphate (P^+DEP), trihexyl (tetradecyl) phosphonium chloride (P^+Cl), and trihexyl (tetradecyl) phosphonium acetate (P^+Ac). Due to the various chemical nature of the cation/anion combinations as well as the steric hindrance of PhILs and the MA content in the matrix, the interactions between PhILs and polar groups of polymer matrix within LIonomers can be tuned. The resulting morphologies of PhIL/PPgMA blends can be based on long or short “ionic-branched chains” considering the polar groups of PP polymer as the “connecting sites” and cations/anions pairs of PhILs as percolating components. Such morphologies have a significant effect on the physical properties of the resulting polymer materials such as viscosity in the molten state, crystallization process, and mechanical properties. The analysis of segmental motions indicates that the PhILs prefer being localized in the surroundings of MA groups to interact. The generation of “ionic-branched chains” as well as ionic clusters contribute to increase the relaxation temperature of rigid amorphous fraction ($T_{\alpha'}$(RAF)). In addition, LIonomers processed with P^+DEP display the highest increase of stiffness and viscosity because of the strongest interactions between P^+DEP and polar units of PP matrix. On the other side, the incorporation of P^+TMP, P^+Ac and P^+Cl induce a plasticizing effect which can be explained by the steric hindrance of the phosphonium cation. Owing to these outstanding features, these new blends may have the ability to be stretched and could be used to produce lightweight materials such as foams and will be the subject of future studies.

2.1.5 References

[1] Li Y, Yao Z, Chen Z hua, et al. High melt strength polypropylene by ionic modification: Preparation, rheological properties and foaming behaviors[J]. Polymer, 2015, 70: 207-214.

[2] Rainglet B, Chalamet Y, Bounor-Legaré V, et al. Polypropylene foams under CO_2 batch conditions: From formulation and rheological modelling to cell-growth simulation[J]. Polymer, 2021, 218: 123496.

[3] Zhang L, Brostowitz N R, Cavicchi K A, et al. Perspective: Ionomer research and applications[J]. Macromolecular Reaction Engineering, 2014, 8(2): 81-99.

[4] Kirkmeyer B P, Weiss R A, Winey K I. Spherical and vesicular ionic aggregates in Zn-neutralized sulfonated polystyrene ionomers[J]. Journal of Polymer Science Part B: Polymer Physics, 2001, 39(5): 477-483.

[5] Nyrkova I A, Khokhlov A R, Doi M. Microdomains in block copolymers and multiplets in ionomers: parallels in behavior[J]. Macromolecules, 1993, 26(14): 3601-3610.

[6] Eisenberg A, Hird B, Moore R B. A new multiplet-cluster model for the morphology of random ionomers[J]. Macromolecules, 1990, 23(18): 4098-4107.

[7] Capek I. Nature and properties of ionomer assemblies. II[J]. Advances in Colloid and Interface Science, 2005, 118(1-3): 73-112.

[8] Bazuin C G, Eisenberg A. Modification of polymer properties through ion incorporation[J]. Industrial & Engineering Chemistry Product Research and Development, 1981, 20(2): 271-286.

[9] Ma Y, Yang G, Xie L. Morphology, nonisothermal crystallization behavior and mechanical properties of polypropylene modified by ionomers[J]. Journal of Macromolecular Science, Part B, 2014, 53(12): 1829-1845.

[10] Aitken B S, Buitrago C F, Heffley J D, et al. Precision ionomers: synthesis and thermal/mechanical characterization[J]. Macromolecules, 2012, 45(2): 681-687.

[11] Qiao X, Weiss R A. Nonlinear rheology of lightly sulfonated polystyrene ionomers[J]. Macromolecules, 2013, 46(6): 2417-2424.

[12] Ling G H, Wang Y, Weiss R A. Linear viscoelastic and uniaxial extensional rheology of alkali metal neutralized sulfonated oligostyrene ionomer melts[J]. Macromolecules, 2012, 45(1): 481-490.

[13] Weiss R A, Zhao H. Rheological behavior of oligomeric ionomers[J]. Journal of Rheology, 2009, 53(1): 191-213.

[14] Fujiyama M, Kondou M, Ayama K, et al. Rheological properties of ionically and covalently crosslinked polypropylene-type thermoplastic elastomers[J]. Journal of Applied Polymer Science, 2002, 85(4): 762-773.

[15] Gao Y, Choudhury N R, Dutta N K. Effects of neutralization on the structure and properties of an ionomer[J]. Journal of Applied Polymer Science, 2012, 124(4): 2908-2918.

[16] Livi S, Duchet-Rumeau J, Gérard J F. Nanostructuration of ionic liquids in fluorinated matrix: Influence on the mechanical properties[J]. Polymer, 2011, 52(7): 1523-1531.

[17] Chen Y, Zhang Y, Ke F, et al. Solubility of neutral and charged polymers in ionic liquids studied by laser light scattering[J]. Polymer, 2011, 52(2): 481-488.

[18] Hajipour A R, Rafiee F. Recent progress in ionic liquids and their applications in organic synthesis[J]. Organic Preparations and Procedures International, 2015, 47(4): 249-308.

[19] Yue C, Fang D, Liu L, et al. Synthesis and application of task-specific ionic liquids used as catalysts and/or solvents in organic unit reactions[J]. Journal of Molecular Liquids, 2011, 163(3): 99-121.

[20] Livi S, Duchet-Rumeau J, Pham T N, et al. A comparative study on different ionic liquids used as surfactants: Effect on thermal and mechanical properties of high-density polyethylene nanocomposites[J]. Journal of Colloid and Interface Science, 2010, 349(1): 424-433.

[21] Yousfi M, Livi S, Duchet-Rumeau J. Ionic liquids: A new way for the compatibilization of thermoplastic blends[J]. Chemical Engineering Journal, 2014, 255: 513-524.

[22] Livi S, Bugatti V, Soares B G, et al. Structuration of ionic liquids in a poly (butylene-adipate-co-terephthalate) matrix: Its influence on the water vapour permeability and mechanical properties[J]. Green Chemistry, 2014, 16(8): 3758-3762.

[23] Livi S, Duchet-Rumeau J, Gérard J F, et al. Polymers and ionic Liquids: A successful wedding[J]. Macromolecular Chemistry and Physics, 2015, 216(4): 359-368.

[24] Yang J, Pruvost S, Livi S, et al. Understanding of versatile and tunable

nanostructuration of ionic liquids on fluorinated copolymer[J]. Macromolecules, 2015, 48(13): 4581-4590.

[25] Lins L C, Livi S, Duchet-Rumeau J, et al. Phosphonium ionic liquids as new compatibilizing agents of biopolymer blends composed of poly (butylene-adipate-co-terephtalate)/poly (lactic acid)(PBAT/PLA)[J]. RSC Advances, 2015, 5(73): 59082-59092.

[26] Nguyen T K L, Livi S, Pruvost S, et al. Ionic liquids as reactive additives for the preparation and modification of epoxy networks[J]. Journal of Polymer Science Part A: Polymer Chemistry, 2014: 52: 3463-3471.

[27] Nguyen T K L, Livi S, Soares B G, et al. Ionic liquids: A New Route for the Design of Epoxy Networks[J]. ACS Sustainable Chemistry & Engineering, 2016, 4(2): 481-490.

[28] Liu Y, Chen S, An R, et al. Development of a correlation equation between the diesterification of maleic anhydride and the acidic ionic liquids nature[J]. Green Chemical Engineering, 2023, 4(1): 57-63.

[29] Hou L, Livi S, Gérard J F, et al. LIonomers - New generation of ionomer: Understanding of their interaction and structuration as a function of the tunability of cation and anion[J]. Polymers, 2023, 15(2): 370.

[30] Ullah Z, Bustam M A, Man Z, et al. Phosphonium-based ionic liquids and their application in separation of dye from aqueous solution[J]. ARPN Journal of Engineering and Applied Sciences, 2016, 11: 1653-1659.

[31] Atefi F, Garcia M T, Singer R D, et al. Phosphonium ionic liquids: design, synthesis and evaluation of biodegradability[J]. Green Chemistry, 2009, 11(10): 1595-1604.

[32] Cieniecka-Rosłonkiewicz A, Pernak J, Kubis-Feder J, et al. Synthesis, anti-microbial activities and anti-electrostatic properties of phosphonium-based ionic liquids[J]. Green Chemistry, 2005, 7(12): 855-862.

[33] Cholico-Gonzalez D, Avila-Rodriguez M, Cote G, et al. Chemical properties of trihexyl (tetradecyl) phosphonium chloride and bis (2, 4, 4-trimethylpentyl) phosphinic acid mixtures: Interaction study by FT-IR and NMR spectroscopies[J]. Journal of Molecular Liquids, 2013, 187: 165-170.

[34] Li Y, Hu J, Fu M, et al. Investigation of intermolecular interactions of mixed extractants of quaternary phosphonium or ammonium chlorides and bis(2,4,4-ethylhexyl)phosphoric acid for metal separation[J]. RSC Advances, 2016, 6(62):

56772-56779.

[35] Clark E J, Hoffman J D. Regime III crystallization in polypropylene[J]. Macromolecules, 1984, 17(4): 878-885.

[36] Jeziorny A. Parameters characterizing the kinetics of the non-isothermal crystallization of poly(ethylene terephthalate) determined by DSC[J]. Polymer, 1978, 19(10): 1142-1144.

[37] Taylor S A. New biocatalysts: myoglobin in phosphonium ionic liquids: Master of Science, Thesis[D]. Department of Chemistry, Simon Fraser University, 2008.

[38] Marták J, Schlosser Š. Density, viscosity, and structure of equilibrium solvent phases in butyric acid extraction by phosphonium ionic liquid[J]. Journal of Chemical & Engineering Data, 2017, 62(10): 3025-3035.

[39] Dhiman S, Gupta B. Recovery of pure germanium oxide from Zener diodes using a recyclable ionic liquid Cyphos IL 104[J]. Journal of Environmental Management, 2020, 276: 111218.

[40] Weiss R A, Yu W C. Viscoelastic behavior of very lightly sulfonated polystyrene ionomers[J]. Macromolecules, 2007, 40(10): 3640-3643.

[41] Page K A, Park J K, Moore R B, et al. Direct analysis of the ion-hopping process associated with the α-relaxation in perfluorosulfonate ionomers using quasielastic neutron scattering[J]. Macromolecules, 2009, 42(7): 2729-2736.

[42] Castagna A M, Wang W, Winey K I, et al. Influence of cation type on structure and dynamics in sulfonated polystyrene ionomers[J]. Macromolecules, 2011, 44(13): 5420-5426.

[43] Hou L, Gérard J F, Livi S, et al. Understanding and compressive investigation between conventional and the next generation of ionomers: Zn-Ionomer versus LIonomers[J]. ACS Applied Polymer Materials, 2023(in press).

[44] Liu H, Xie T, Ou Y, et al. Dynamic rheological properties of polypropylene/polyamide-6 blends modified with a maleated thermoplastic elastomer[J]. Polymer Journal, 2004, 36(9): 754-760.

[45] Tierney N K, Register R A. The role of excess acid groups in the dynamics of ethylene−methacrylic acid ionomer melts[J]. Macromolecules, 2002, 35(16): 6284-6290.

[46] Ma Q, Georgiev G, Cebe P. Constraints in semi-crystalline polymers: Using quasi-

isothermal analysis to investigate the mechanisms of formation and loss of the rigid amorphous fraction[J]. Polymer, 2011, 52(20): 4562-4570.

[47] Arnoult M, Dargent E, Mano J F. Mobile amorphous phase fragility in semi-crystalline polymers: Comparison of PET and PLLA[J]. Polymer, 2007, 48(4): 1012-1019.

[48] Wang L, Wang Y nan, Huang Z gang, et al. Heat resistance, crystallization behavior, and mechanical properties of polylactide/nucleating agent composites[J]. Materials & Design (1980-2015), 2015, 66: 7-15.

[49] Bajsić E G, Šmit I, Leskovac M. Blends of thermoplastic polyurethane and polypropylene. I. Mechanical and phase behavior[J]. Journal of Applied Polymer Science, 2007, 104(6): 3980-3985.

[50] Yu J, He J. Crystallization kinetics of maleic anhydride grafted polypropylene ionomers[J]. Polymer, 2000, 41(3): 891-898.

[51] Yang G, Li X, Chen J, et al. Crystallization behavior of isotactic polypropylene induced by competition action of β nucleating agent and high pressure[J]. Colloid and Polymer Science, 2012, 290(6): 531-540.

[52] Varga J. β-modification of isotactic polypropylene: Preparation, structure, processing, properties, and application[J]. Journal of Macromolecular Science, Part B, 2002, 41(4-6): 1121-1171.

[53] Clark E S. Unit cell information on some important polymers[M]. Physical Properties of Polymers Handbook. Springer, 2007: 619-624.

[54] Lee H, Yamaguchi K, Nagaishi T, et al. Enhancement of mechanical properties of polymeric nanofibers by controlling crystallization behavior using a simple freezing/thawing process[J]. RSC Advances, 2017, 7(69): 43994-44000.

[55] Li J, Zhu Z, Li T, et al. Quantification of the Young's modulus for polypropylene: Influence of initial crystallinity and service temperature[J]. Journal of Applied Polymer Science, 2020, 137(16): 48581.

[56] Sanders B, Cant E, Amel H, et al. The effect of physical aging and degradation on the re-use of polyamide 12 in powder bed fusion[J]. Polymers, 2022, 14: 2682.

[57] Chaves Lins L, Livi S, Maréchal M, et al. Structural dependence of cations and anions to building the polar phase of PVDF[J]. European Polymer Journal, 2018, 107: 236-248.

[58] Scott M P, Rahman M, Brazel C S. Application of ionic liquids as low-volatility plasticizers for PMMA[J]. European Polymer Journal, 2003, 39(10): 1947-1953.

2.1.6 Supporting Information

1.DSC thermograms of polymer matrix and Lionomers

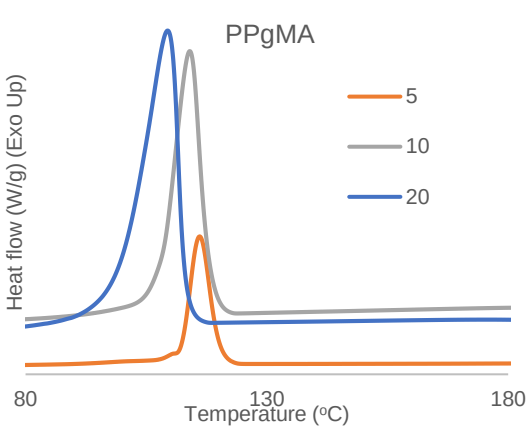

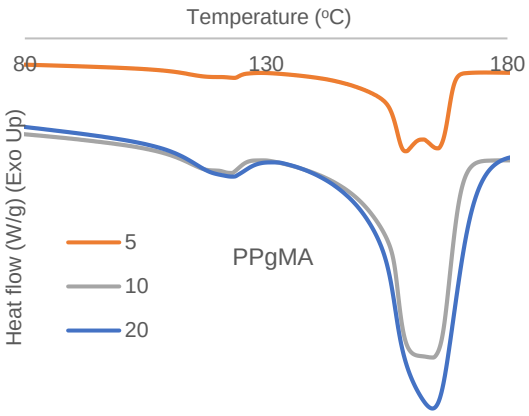

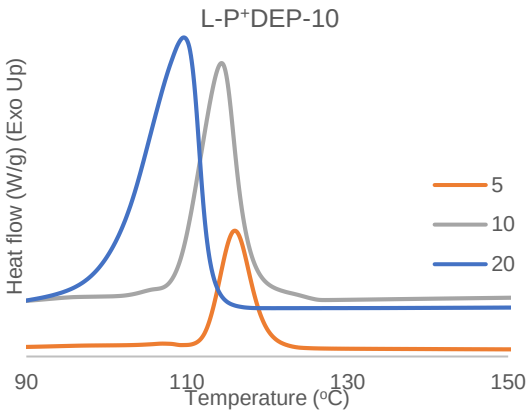

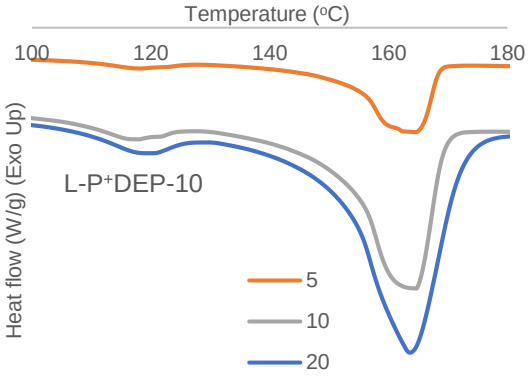

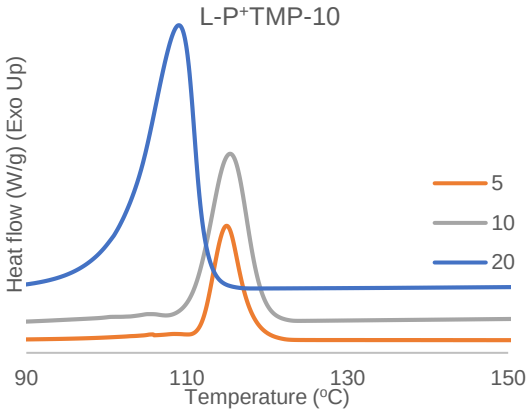

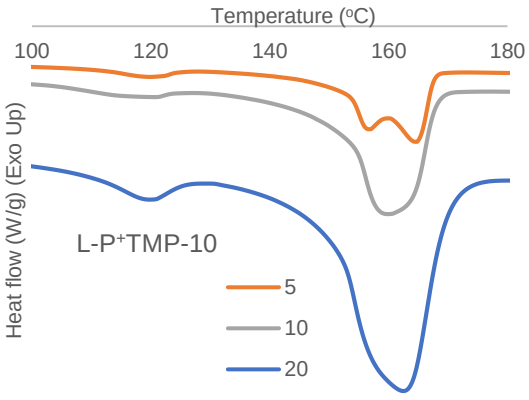

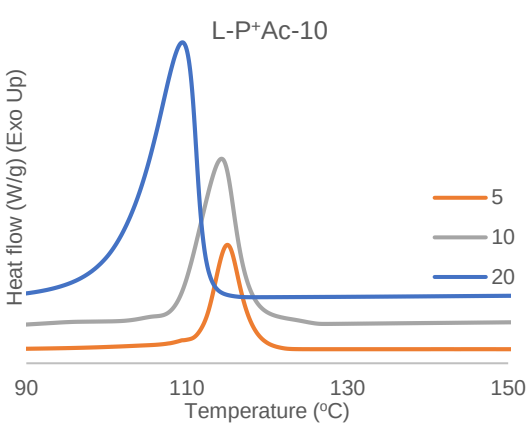

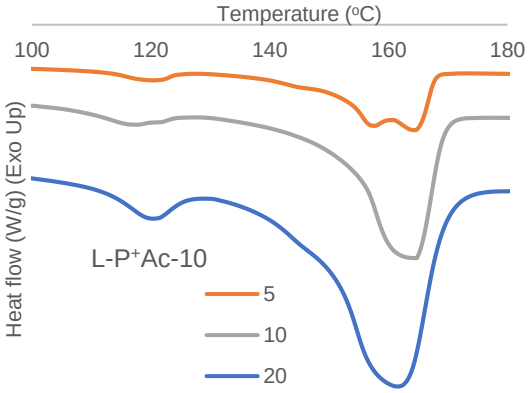

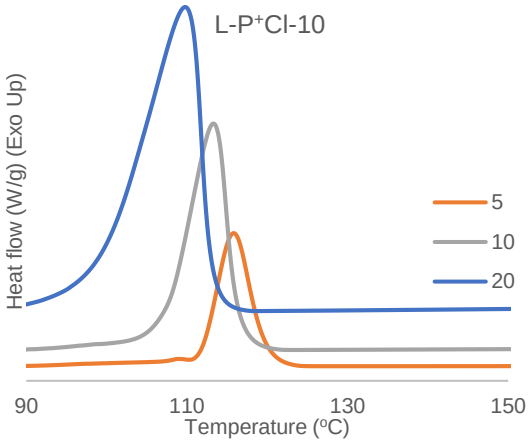

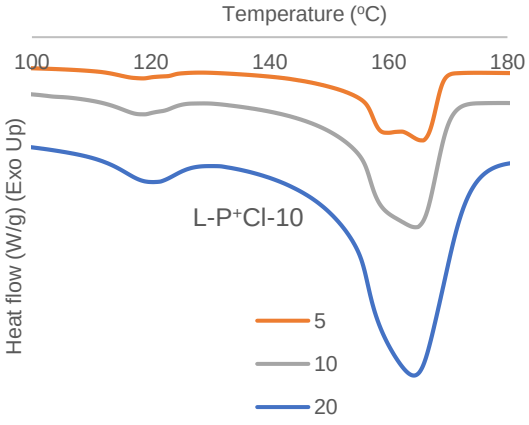

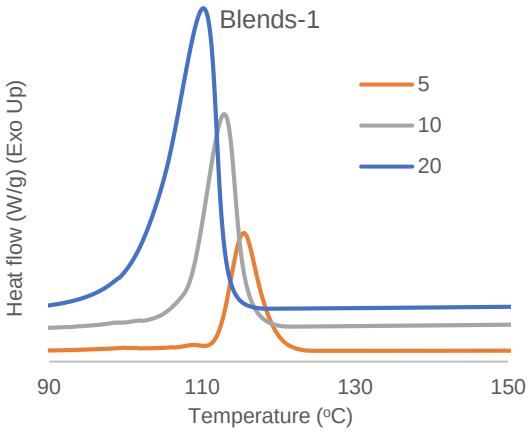

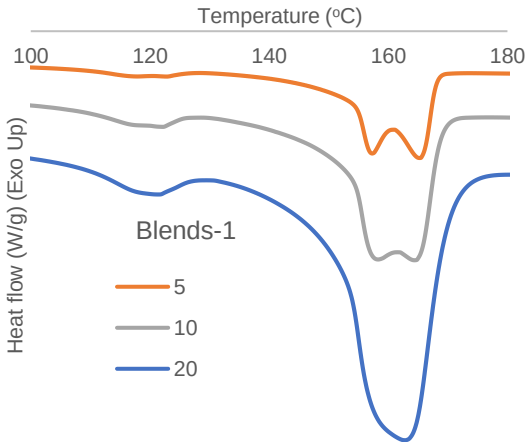

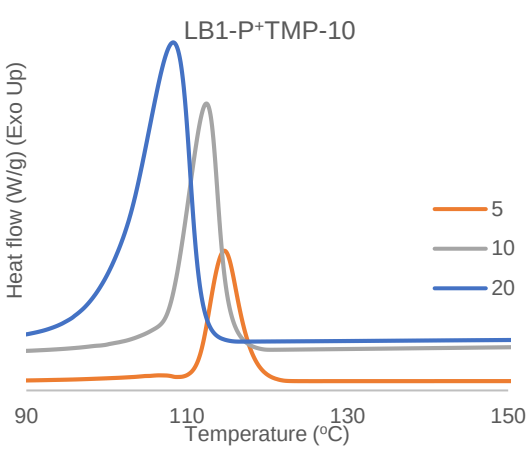

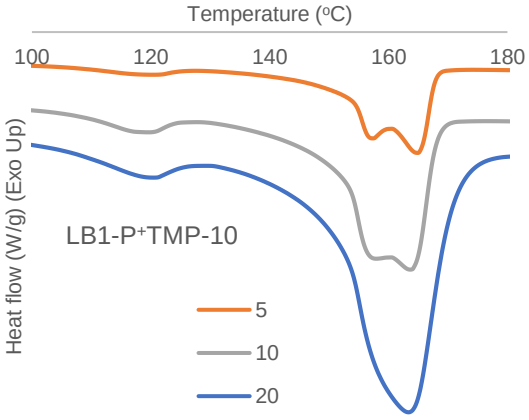

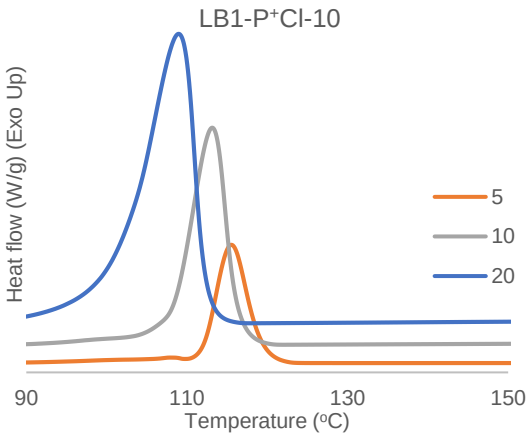

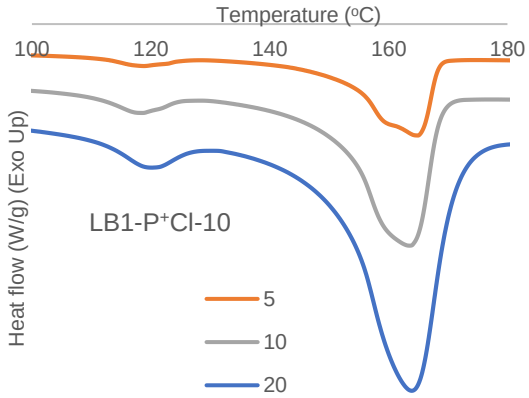

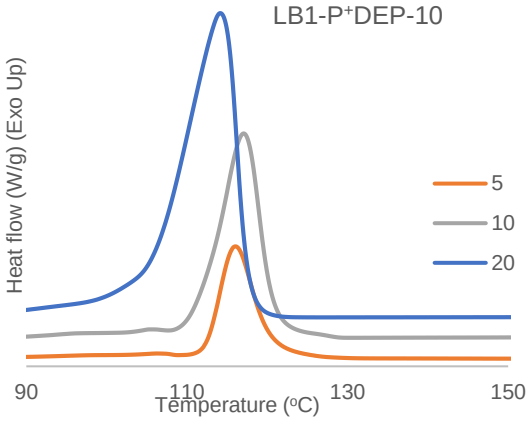

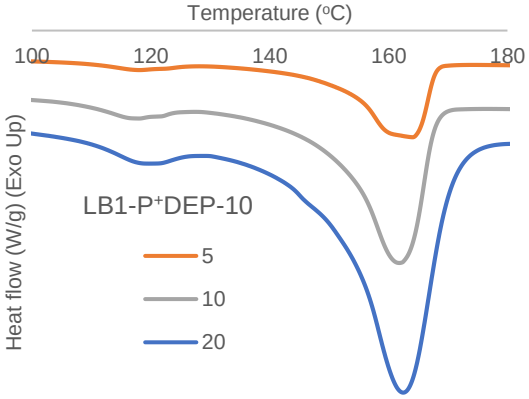

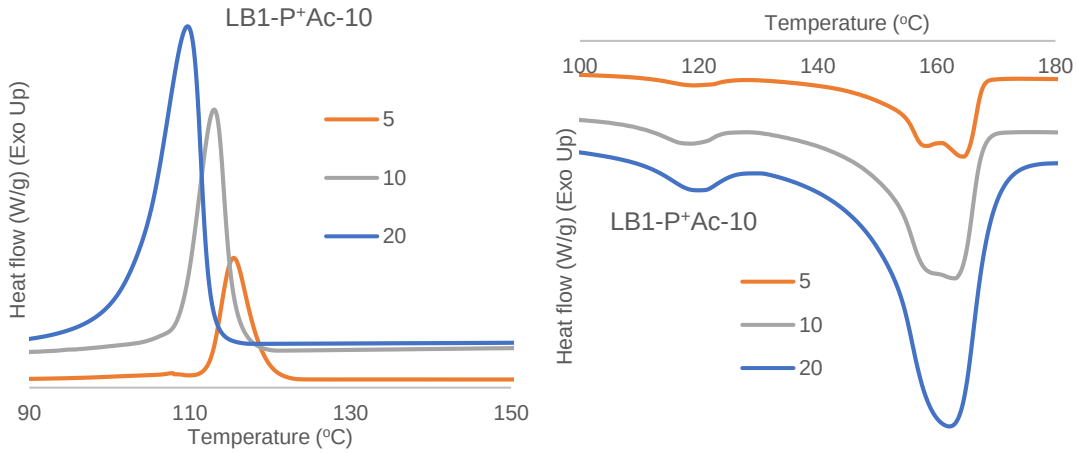

Figure S2- 1 The melting and crystallization curves of matrix and LIonomers with various ionic liquid content (2 and 10 wt.%) at different heating and cooling rates (5, 10, and 20 $K \cdot min^{-1}$) under nitrogen atmosphere.

2. The $ln[-ln(1-X_t)]$ vs lnt .plots according to Jeziorny's Non-isothermal crystallization model

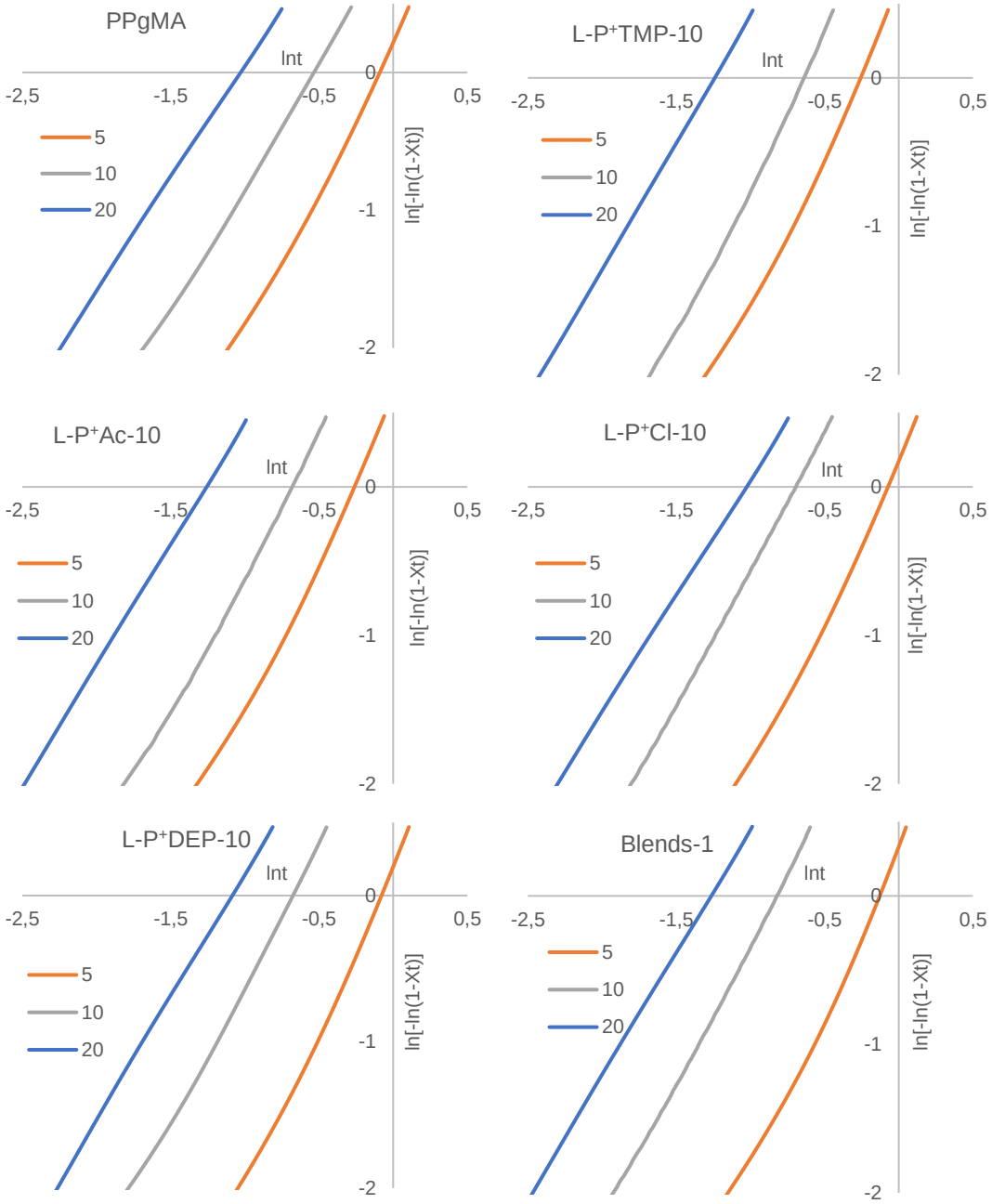

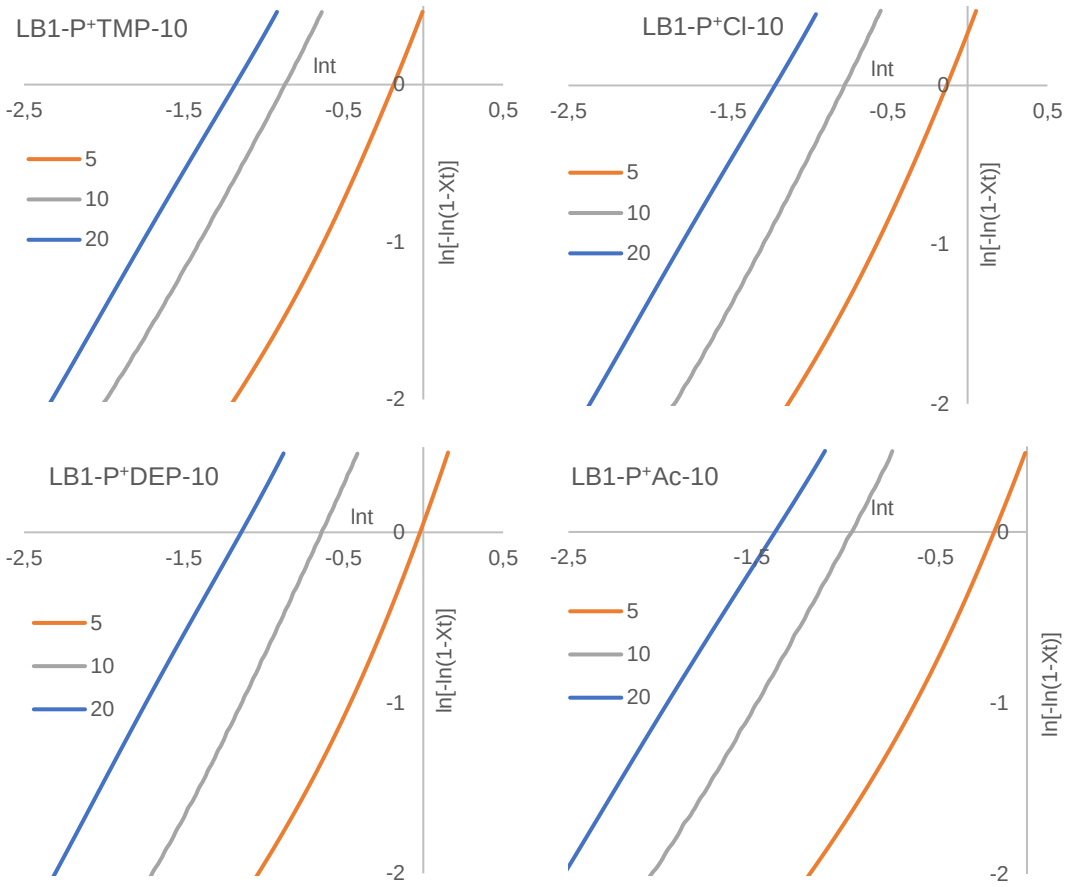

Figure S2- 2 The ln[-ln(1-Xt)] vs Int plots of all produced materials based on Jeziorny's theory

3. The details of non-isothermal crystallization process from Jeziorny's theory

Table S2- 1 The non-isothermal crystallization parameters of materials in this study

Samples	φ	$t_{1/2}$(min)	n	Z_t	T_m(°C)	T_c(°C)	X_c(%)
PPgMA	5	0.77	2.01	1.17	159.0/165.6	116.1	34.1
	10	0.47	1.78	2.68	164.2	114.1	35.5
	20	0.28	1.65	5.55	164.5	109.5	31.6
L-P$^+$TMP-10	5	0.65	1.96	1.59	156.8/164.6	115.0	35.4
	10	0.44	1.92	3.39	159.8	115.4	36.2
	20	0.23	1.70	8.26	162.5	109.0	33.3
L-P$^+$Cl-10	5	0.78	2.00	1.13	160.0/165.7	115.8	36.5
	10	0.41	1.82	3.52	164.6	113.3	36.5
	20	0.28	1.57	5.03	164.3	109.8	34.3
L-P$^+$DEP-10	5	0.76	2.06	1.22	164.5	116.0	35.1
	10	0.41	1.81	3.54	164.7	114.3	34.0
	20	0.27	1.65	6.16	163.7	109.6	32.1
L-P$^+$Ac-10	5	0.65	1.94	1.61	157.7/164.5	115.1	34.2
	10	0.42	1.80	3.36	161.7	116.7	36.7
	20	0.23	1.63	7.81	161.7	109.5	32.6
Blends-1	5	0.74	1.96	1.25	157.3/165.3	115.5	35.6
	10	0.36	1.83	4.45	158.3/164.5	113.0	35.7
	20	0.23	1.66	8.16	162.9	110.2	33.6
LB1-P$^+$TMP-10	5	0.71	2.05	1.42	157.3/164.9	114.7	35.2
	10	0.34	1.80	4.72	158.0/163.7	112.4	37.2
	20	0.25	1.74	7.81	163.4	108.3	33.4
LB1-P$^+$Cl-10	5	0.74	2.06	1.27	164.9	115.5	34.3
	10	0.38	1.90	4.28	163.6	113.1	35.7
	20	0.24	1.72	8.03	164	109.0	32.4
LB1-P$^+$DEP-10	5	0.83	2.03	1.01	164.1	116.1	35.1
	10	0.44	1.91	3.34	161.9	117.1	37.1
	20	0.26	1.71	7.08	162.5	114.1	33.7
LB1-P$^+$Ac-10	5	0.71	2.03	1.38	158.5/164.6	115.5	35.2
	10	0.32	1.86	5.89	163.1	113.0	36.5
	20	0.20	1.73	10.86	162.4	109.7	33.3

Note: φ: cooling rate (K·min^{-1}), T_m: melting temperature (°C), T_c: crystallization temperature (°C) and X_c:

crystallinity rate (%).

2.2 LIonomers-New Generation of Ionomer: Understanding of their Interaction and Structuration as a function of the tunability of Cation and Anion

Note: The content presented in this section was published in Polymers: https://doi.org/10.3390/polym15020370.

2.2.1 Introduction

In the past decades, large attention has been poured into the study of ionomers. Ionomers are polymers containing up to 15 molar% of ionic groups that are frequently carboxylic, phosphoric, or sulfonic acid anions neutralized by metal salts, *i.e.* zinc, sodium or potassium cations [1, 2]. These materials display a multi-scale structuration: the ion-pairs formed between acids anions and metal salts, usually assemble to form multiple states and participate in ionic clusters. Such ionic structuration leads to a restricted motion of polymer chains [3, 4]. Consequently, a significant improvement of molten and solid state properties are realized thanks to the physical crosslinking points generated via ionic interactions [5-11]. This effect is strongly related to the ionic multiplets generated as a segregated phase as for polyurethanes [12]. The rheological behaviour (as for sulfonated poly-styrene [10] as well as the final crystalline state could be strongly affected by the existence of ion-pairs interactions. This effect is also demonstrated for the glass transition and melt elasticity of PLA-based ionomers [13, 14]. According to the same approach, ionomers have been processed from different polymers such as polybutadiene-co acrylic acid or ethylene methacrylic acid copolymers neutralized by zinc cations. Using maleic anhydride grafted polypropylene (PPgMA) as precursor to design ionomers neutralized by zinc acetate leads to an increase of the molten strength due to the generation of branched chain structures [15, 16]. Ionomer-like materials could be also used as efficient compatibilizers in non-miscible PP/PE blends [17, 18]. For maleic anhydride-grafted polymers, zinc acetate and sodium hydrogen carbonate are usually considered. In fact, carboxylic functions generated from the hydration of the

anhydride are known to interact with the corresponding cat-ions. The establishment of interactions between grafted polyolefin chains and salts can be successfully realized via twin-screw extrusion. Such modification is demonstrated to be efficient for improving the elongation at break and impact properties. On another hand, owing to the advantages of Ionic Liquids (ILs) such as thermal stability, non-flammability, and low saturated vapour pressure, they have been used as surfactants [19], plasticizers [20], compatibilizers [21], and structuring agents [22]. For example, 1-butyl-3-methyl imidazolium chloride could act as plasticizer and compatibilizer of starch/zinc blends, leading to smaller zinc aggregates [23]. Trihexyltetradecylphosphonium bis(trifluoromethylsulfonyl) imide and trihexyltetradecylphosphonium bis 2,4,4-(trimethylpentyl) phosphinate could serve as compatibilizers for thermoplastic blends (PP/PA6) [21]. In this study, ILs located at PP/PA interface behave as interfacial agents, resulting in the depressed size of dispersed phase and a decrease of the PP/PA interfacial tension. In fact, ionic liquids are promising components according to their intrinsic features and their ionic characters [19, 24-26] which could promote interactions with polar groups.

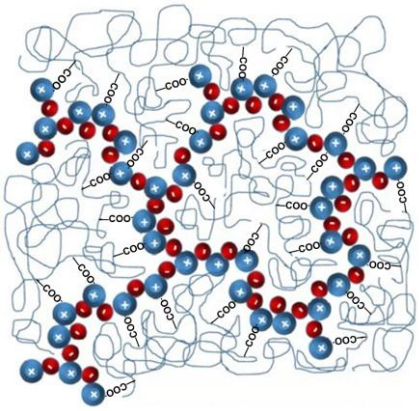

Figure 2- 9 Targeted nano/microstructure of LIonomers

Thus, a new generation of polypropylene-based ionomer is proposed for the first time in this study. New types of ionomers designed from Ionic Liquids (ILs) and maleic anhydride grafted polypropylene (denoted as LIonomers) have been considered. An ionic interaction continuum must be generated from the interactions COO^- from PPgMA

with the cation and the anion pairs of ILs. The microstructure shown in Figure 2-9 describes the targeted assembling of ionic liquid pairs leading to a percolated ionic species network within the grafted polyolefin matrix. This novel approach offers the way to tune the final LIonomers behaviour by using different types of ILs. In this work, a phosphonium-based ionic liquid (PhIL), *i.e.* tributyl (ethyl)phosphonium diethyl phosphate (P^+DEP) and two imidazolium-based ionic liquids (ImILs), *i.e.* 1-ethyl-3-methylimidazolium diethyl phosphate (EMIM DEP) and 1-ethyl-3-methylimidazolium acetate (EMIM Ac) have been considered to investigate the role of cation, phosphonium vs imidazolium and the role of anion, acetate vs diethyl phosphate. This section proposes to explore how *i)* ILs generate ionic-ionic/dipole interactions with PPgMA; *ii)* ionic-ionic/dipole interactions influence the PPgMA crystallization process and morphologies as well as consequently mechanical properties.

2.2.2 Experimental Section

2.2.2.1 Materials

OREVAC® CA 100 from Arkema, was considered as PPgMA (1 wt.% MA). Ionic liquids supplied from TCI (Scheme 2-4) were selected according to the nature of the cation (combined with the same anion), *i.e.* tributyl (ethyl) phosphonium diethyl phosphate (P^+DEP) *vs* 1-ethyl-3-methylimidazolium diethyl phosphate (EMIM DEP). The nature of the anion was also considered by comparing the same cation, *i.e.* 1-ethyl-3-methylimidazolium acetate (EMIM Ac) *vs* 1-ethyl-3-methylimidazolium diethyl phosphate (EMIM DEP).

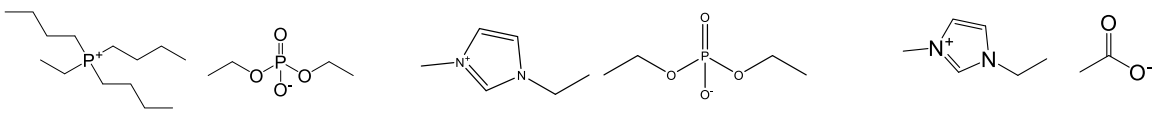

P^+DEP EMIM DEP EMIM Ac

Scheme 2- 4 Structure of the ionic liquids considered in this study

2.2.2.2 Material preparation and characterizations

The PPgMA was dried at 70 °C for 12 hours. The PPgMA/IL mixtures (2 and

10wt%) were blended into a DSM micro extruder at 180 °C for 5 min and injected at 30 °C. Three different LIonomer types, *i.e.* depending on the nature of the (cation/anion) pair and of IL content were prepared (Table 2-6) according to Scheme 2-5.

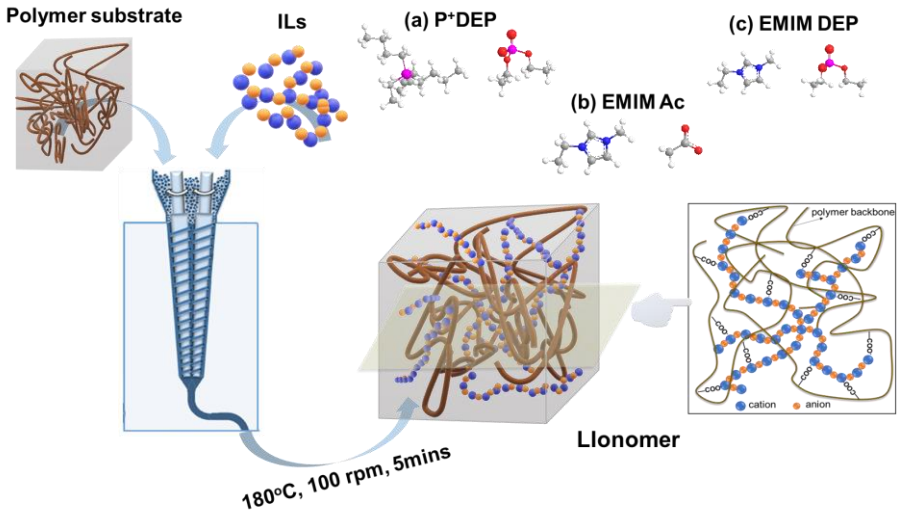

Scheme 2- 5 Processing diagram of LIonomers in this section

Table 2- 6 PPgMA/IL blends considered in this present

Polymer	IL	IL content (wt.%)	Abbreviation
PPgMA	P^+DEP	2	L-P^+DEP-2
	P^+DEP	10	L-P^+DEP-10
	EMIM DEP	2	L-EMIM DEP-2
	EMIM DEP	10	L-EMIM DEP-10
	EMIM Ac	2	L-EMIM Ac-2
	EMIM Ac	10	L-EMIM Ac-10

The morphology of samples was carried out by transmission electron microscope (TEM, Phillips CM 120) at an accelerating voltage of 120kV. To characterize PPgMA and LIonomer, they are cut using ultramicrotomy firstly and collected on a carbon film-coated cooper grid.

The chemical interactions between PPgMA and ILs were characterized by NMR spectroscopy. ^{1}H and ^{31}P NMR spectra of ionic liquids and LIonomers processed on PPgMA8 (8wt.% MA) were recorded using a Bruker Avance III 400 MHz at 373K. All

materials were dissolved in chlorobenzene-D5 (C_6D_5Cl). The chemical shifts (δ) are expressed in ppm relative to the internal reference C_6D_5Cl for ^1H nuclei.

The rheological and dynamic mechanical analysis (DMA) were performed using a ARES-G2 rheometer (ARES-G2 SN#4010-0255, TA Instrument). The rheological behavior was recorded at 180 °C using parallel plate geometry (d=25mm) under N_2 atmosphere. Dynamic mechanical curves were recorded in the -80/100 °C temperature range with a heating rate of 3 K·min^{-1}.

Melting and crystallization curves were recorded by Differential Scanning Calorimetry (DSC, Q10 TA Instrument) after erasing the thermal history under 5, 10, and 20 K·min^{-1} heating and cooling rates. The crystallinity, X_c, was defined:

$$X_c = \frac{\Delta H_f}{(1-m)\Delta H_f{}^0} \quad \text{Equation 2- 7}$$

where ΔH_f^0 is 209 J/g, *i.e.* corresponding to the melting enthalpy of 100% crystallized polymer [27], ΔH_f being the melting enthalpy of the analyzed sample. Jeziorny's [28] non-isothermal crystallization model was employed to analyse the crystallization process:

$$ln[-ln(1-X_t)] = nlnt + lnZ_t \quad \text{Equation 2- 8}$$

$$X_T = \frac{\int_{T_0}^{T_c}(\frac{dH_c}{dT})/dT}{\int_{T_0}^{T_\infty}(\frac{dH_c}{dT})/dT} \quad \text{Equation 2- 9}$$

$$t = \frac{T_0 - T}{\varphi} \quad \text{Equation 2- 10}$$

where X_t is the relative crystallinity at crystallization time t; n, and Z_t correspond to Avrami' exponent and crystallization kinetic constant, respectively. Their values can be obtained by plotting $\ln[-\ln(1-X_t)]$ as a function of $\ln t$. X_T is related to the crystallinity with the change of temperature, T_0 and T_∞ being the onset and the end of crystallization temperature; T is the temperature for a given crystallization time t, while φ is the cooling rate.

The crystallization half-time ($t_{1/2}$) could be determined from:

$$t_{1/2} = (\frac{ln2}{Z_t})^{1/n}$$ Equation 2- 11

The crystalline phase of the samples was analyzed by Wide Angle X-Ray Diffraction (WAXD, Bruker D8-Advance diffractometer) at room temperature (2θ=10-45° using Cu Kα radiation-λ=0.15406 nm). The diffractograms were further analyzed using Origin 2018 software considering Gauss' fitting function. The crystal size was calculated according to the Scherrer's equation:

$$D = \frac{K\lambda}{(\beta - s)cos(\theta)}$$ Equation 2- 12

where D is the crystal size, K the crystalline shape parameter (≈0.89), β the measured sample diffraction peak half-height width, s the instrument factor calibration (0.05o), and θ the diffraction angle.

The crystalline morphology of PPgMA and LIonomers materials was observed by polarizing optical microscopy (POM). Materials were heated at 200 °C and remained for 3 minutes to eliminate the thermal history. Their crystal growth was observed after cooling at 120 °C with a cooling rate of 50 K·min^{-1}.

The strain-stress curves were recorded using an Instron tensile machine at room temperature operating at a strain speed of 50 mm·min^{-1}. Each sample has been repeated at least three times.

2.2.3 Results and discussion

2.2.3.1 LIonomer morphology

Transmission electron microscopy (TEM) is an efficient tool to study the phase separation of IL ion pairs within the polymer matrix (Figure 2-10). Owing to the expected morphologies of LIonomers, these granular "bean spots" could be attributed to phase-separated and associated ILs. IL-based aggregates can be also confirmed by EDX analyses as shown in Figure S2-3 of Supporting Information (spectrum 1 of L-EMIM DEP-10: C: 85.19 wt%, N: 2.51 wt%, O: 10.94 wt%, P: 1.36 wt%; spectrum 1 of polymer matrix within L-P$^+$DEP-10: C: 96.89 wt%, O: 3.11 wt%; spectrum 1 of L-

P^+DEP-10: C: 94.35 wt%, O: 4.7 wt%, P: 0.96 wt%; spectrum 1 of L-EMIM Ac-10: C: 90.11 wt%, N: 1.92 wt%, O: 7.97 wt%). From comparison between L-P^+DEP-10 (Figure 2-10c) and L-EMIM DEP-10 (Figure 2-10b), the previous one displays large ionic clusters, while the second one exhibits a multiscale structure based on not only large ionic liquid particles but also ionic multiplets (black spots) due to associated cation-anion pairs. These multiplets and particles dual microstructure are more pronounced in L-EMIM Ac-10 (Figure 2-10d), and numerous multiplets are observed compared to L-EMIM DEP-10 (Figure 2-10b). These various types of sub-structures of prepared LIonomers are strongly dependent on the ion pair nature of the ILs. In fact, it is possible to predict theoretically the aggregation of ion pairs or multiplet structures in a low dielectric medium. Both are influenced by polar-polar interactions that are responsible for the differences in size. The resulting morphology of the ionic liquid interactions is related to the equilibrium of interactions between the grafted-PP matrix and ILs. In fact, the size of the IL-rich phase could be tailored from nanoscale to microscale by a proper selection of the cation/anion combinations [29].

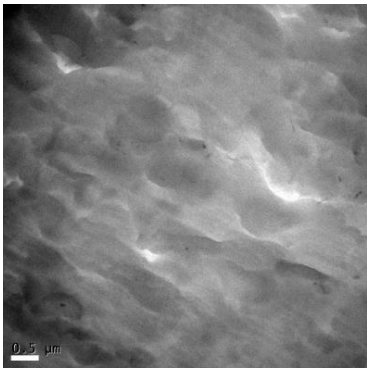

PPgMA (a)

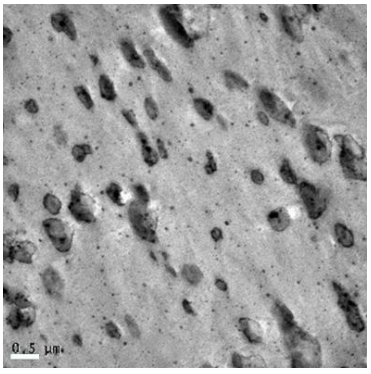

L-EMIM DEP-10 (b)

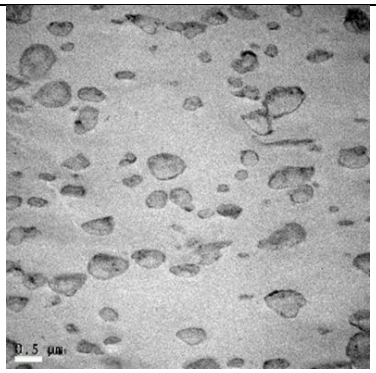

L-P^{+}DEP-10 (c)

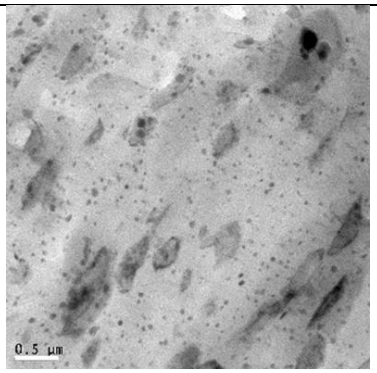

L-EMIM Ac-10 (d)

Figure 2- 10 Transmission Electron Microscopy (TEM) images of PPgMA and related LIonomers containing 10 wt% of IL (scale bar: 0.5µm)

2.2.3.2 PPgMA-ILs interactions

^{1}H and ^{31}P NMR spectroscopy were recorded to detect IL-polymer chain interactions from the comparison between neat IL spectra and the ones from corresponding LIonomer as shown in Figures 2-11 and 2-12, respectively. In the case of EMIM Ac and the corresponding LIonomers, ^{1}H NMR spectra reveal a shift of the protons on the cation (positions #6, #2, and #3 of EMIM Ac), from 10.85, 8.49, and 8.64 ppm [30, 31] to higher fields, *i.e.* 10.09, 8.09, and 8.01 ppm. Such shifts could be attributed to the enhancement of electronic cloud density because of the ionic-ionic interactions between the cation and polymer matrix (Scheme 2-6a). Thus, ***a*** the COO^{-} group, *i.e*. the counter anion of the IL is positioned near the maleic anhydride group, then ***b*** the counter anion participates in the opening of maleic anhydride leading to the formation of a new structure “ionic-branched chains” via the electrostatic interaction among cation/anion in EMIM Ac. In addition, the hydrogens in positions #2 and #3 of terminal cation may be positively shielded by C=O in the matrix. Besides, the hydrogen moving from 1.94 into 2.07 ppm at position #7 confirms the capture of the hydrogen carried by the imidazolium cation, thus inducing the generation of acetic anhydride group.

In addition to the enhanced electronic cloud density at positions #2 and #3 (from 8.22 and 8.36 ppm of neat EMIM DEP [32, 33] into 7.25 and 7.30 ppm of its LIonomer)

as a result of the positive shielding effect of C=O in matrix (Scheme 2-6b), the electronic cloud density at position #6 decreases due to the strong electronic absorption capacity of oxygen in COO^- in matrix, thus its hydrogen shifts from 10.54 to 10.76 ppm. In fact, the same phenomenon is also observed with imidazolium IL combined with acetate or phosphate counter anions. In terms of the phosphonium IL combined with phosphate counter anion, the phosphorous compound of the anion displays a movement into low field (from 0.18 in EMIM DEP to 0.57 ppm in LIonomer) because of the effect of connected C=O group in matrix. In addition, the e-cloud density of phosphorus in P^+DEP anion increases (^{31}P NMR from -0.38 ppm into -0.95 ppm) since it lies in the positive shielded area induced by connected C=O (Scheme 2-6c), while the strong electronegativity of oxygen in generated COO^- of matrix results in the migration in ^{31}P NMR from 34.64 ppm into 34.99 ppm.

In summary, one may obtain that ***a*** all introduced ILs (EMIM Ac, EMIM DEP and P^+DEP) can interact ionically with polar units in matrix; ***b*** the interaction structures between ILs and matrix varies with the change of anion/cation combinations; ***c*** the exceed ILs arrange as one ionic-branched chains using the generated COO^- group in PPgMA as the “head” and the cation/anion as the component via their original electrostatic interaction, such different interactions may connect the various dispersion of ILs in PPgMA and bring about some improvements into the overall performance (like molten viscosity, crystallization behavior, etc.).

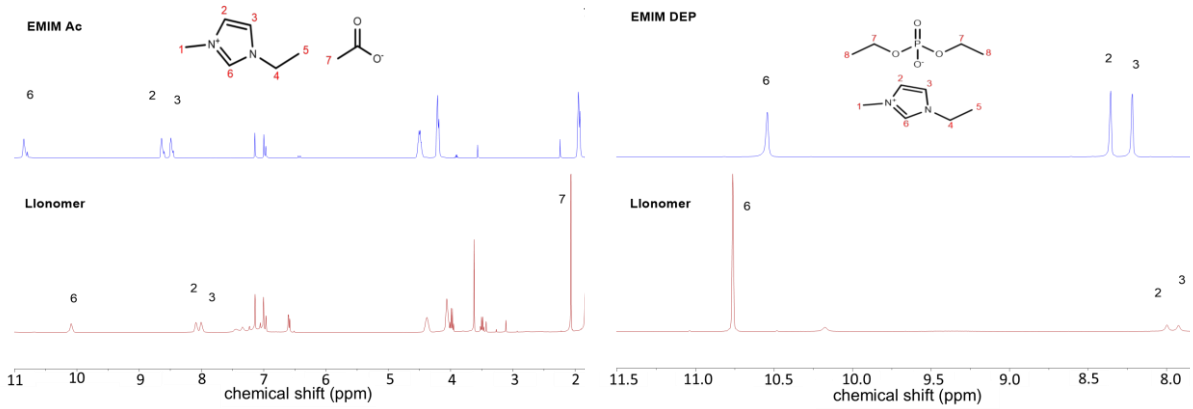

Figure 2- 11 ^{1}H NMR spectra (400 MHz; C_6D_5Cl solvent) of ILs and related LIonomers

(10 wt.% IL)

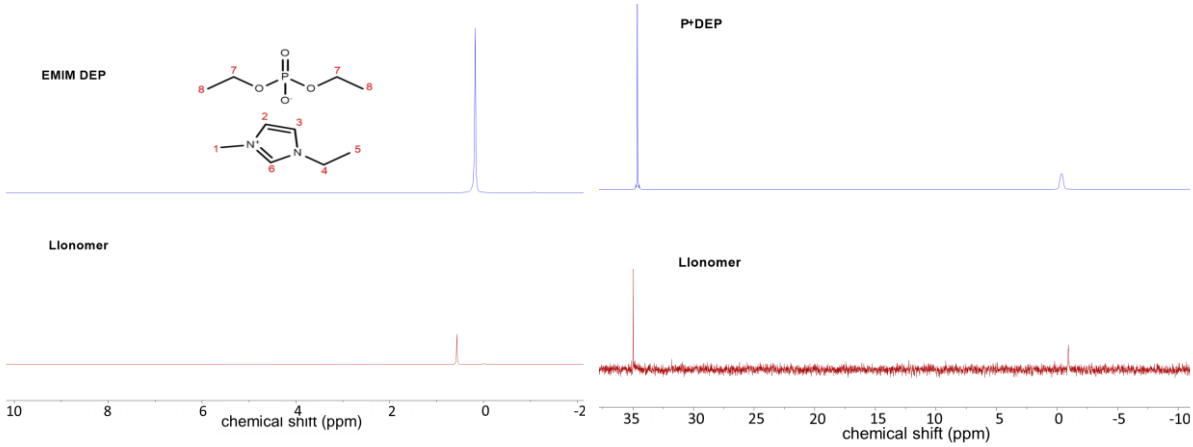

Figure 2- 12 ^{31}P NMR spectra (400 MHz; C_6D_5Cl solvent) of neat ILs and LIonomers (10 wt.% IL)

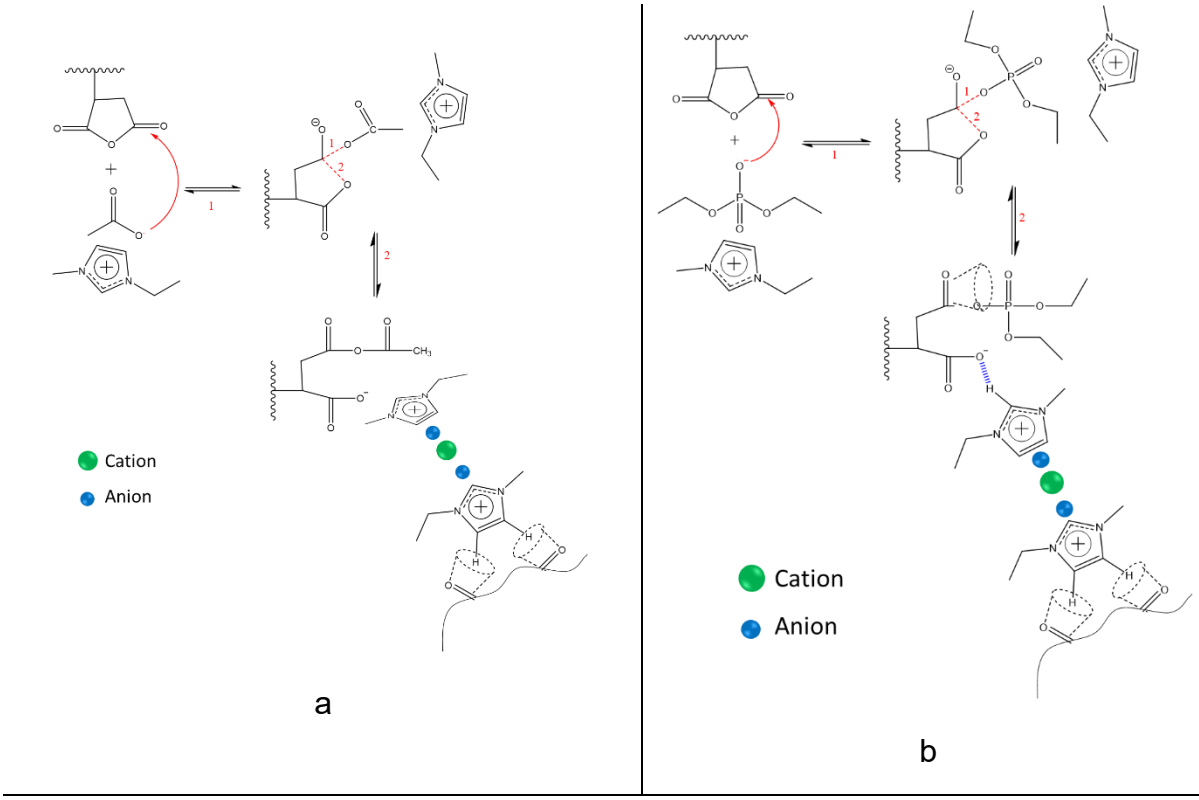

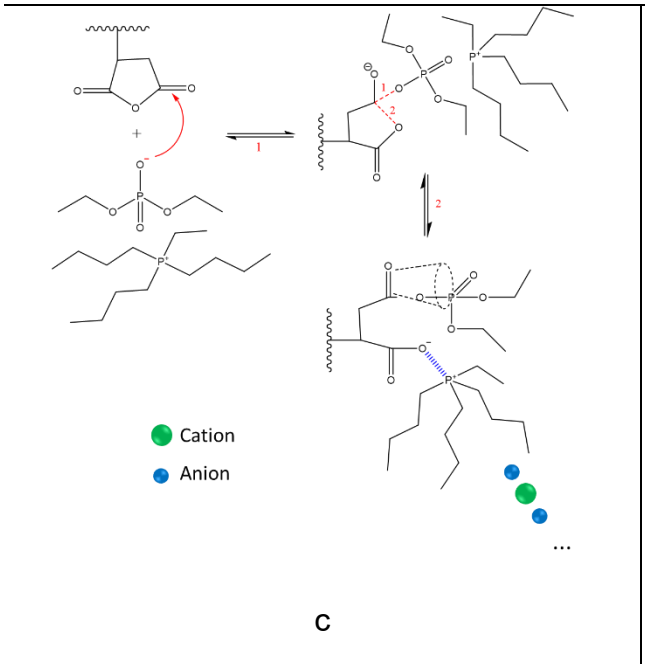

Scheme 2- 6 Various types of interactions which could be established between ionic liquid pairs and PPgMA within the different LIonomers materials considered in this section (based on: EMIM Ac: a; EMIM DEP: b; P^+DEP: c)

2.2.3.3 Effect of ILs on rheological properties: Strength of interactions

The molten state behavior of LIonomers has been greatly changed compared to the neat PPgMA one due to the existence of the ion-ion/ion-dipolar interactions described previously. All LIonomers display a strong shear thinning behavior compared to neat PPgMA as shown in Figure 2-13. This effect is more pronounced for L-EMMI Ac-10. Owing to the low viscosity of ILs (few mPa·s) [21], only the COO^-/IL combined with IL/IL interactions could induce inter-chains connecting nanostructures as reported in ionomers [3]. Such ionic branching nanophases lead to a reduction of the chain mobility, resulting in a large increase of the melt viscosity [8, 16, 34-36]. For each LIonomers, the complex η^* value increases with the ILs content, as more ionic interchain connections are formed. Such viscosity values dependence with the nature of the ionic liquid and its content could be easily explained according to the previously reported interactions. In fact, the viscosity value of LIonomer processed with EMIM Ac is the highest one because the ionic interactions between imidazolium cation and

carboxylic acid is the strongest one (three positions could create ionic-ionic interactions with carboxylic group as shown in Scheme 2-6a). Additionally, the acetate anion is also highly polar and could be strongly associated with cation. These cation-anion pairs could also self-assemble to form multiplets and lead to this double scale structuration observed by TEM. For the LIonomer with 10wt% EMIM DEP, a double structuration is observed with not only ionic liquid-rich particles but also ionic multiplets. Compared with LIonomers prepared with EMIM Ac, less fine phase separation is obtained due to ionic-ionic (1 position) and dipolar-ionic (2 positions) interactions (Scheme 2-6b) generated to a lesser extent. The numerous multiplets act as branching agents, leading to increase the viscosity. The morphology as well as the strength of the interaction explain the ranking of viscosity values. Thus, clusters-based morphology, *i.e.* without larger multiplet structures, combined with the low intensity interactions established between the phosphonium cation and the carboxylate anion explain the lowest viscosity of LIonomers prepared with the phosphonium cation. Besides, the sequence of corresponding solid density, *i.e.* 0.909 g·cm^{-3} of PPgMA < 0.910 g·cm^{-3} of L-P^{+}DEP-10 < 0.915 g·cm^{-3} of L-EMIM DEP-10 < 0.917 g·cm^{-3} of L-EMIM Ac-10 at around 20 °C could reveal the generation of ionic network within LIonomers, which could also reflect the interaction strength and is consistent with the resulted ranking of viscosity values.

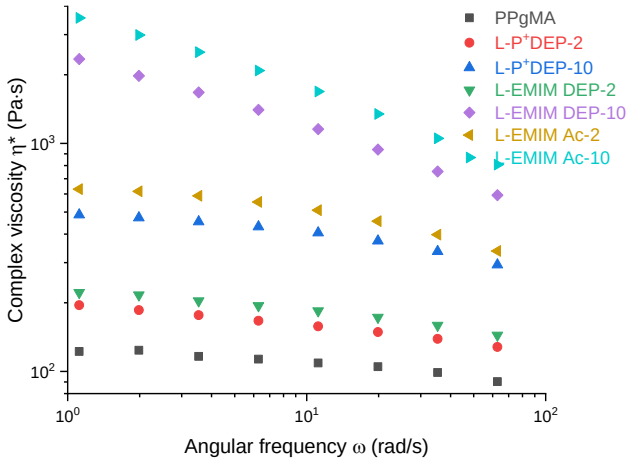

Figure 2- 13 Complex viscosity of neat PPgMA and LIonomers as a function of the dynamic angular frequency at 180 °C

2.2.3.4 Microstructure of LIonomers

Semi-crystalline polymers are considered as the heterogeneous medium including crystalline fraction (CF), rigid amorphous fraction (RAF), and mobile amorphous fraction (MAF) [37]. Ordered crystalline chains constitute the CF phase, which is surrounded by macromolecular chains in the amorphous state [37, 38]. Close to the CF lamellas, the neighboring polymer chains in amorphous state-denoted as tie molecules-undergo strong confinement effects and the reduction of segmental motions. As a consequence, this reduced molecular mobility of this confined amorphous phase may result in its own glass transition temperature, different from the glass transition of chains in MAF. The amorphous fraction close to the crystalline fraction is denoted as RAF. Identifying the location of ILs in the final LIonomers materials could help understanding the structuration mechanisms and their effect on the overall performance of LIonomers. The solid state Dynamic Mechanical Analyses reveal two relaxations of the amorphous, *i.e.* the ones of the MAF and RAF regions. Figure 2-14 and Table 2-7 indicate the temperature of the α and α' relaxations related of the MAF and RAF fractions respectively, as well as the one of the β secondary relaxation (at -47°C) of PPgMA. Such a relaxation corresponds to T_β local segmental motions [39]. As various types of IL are combined with PPgMA, the temperature of this β relaxation supports the fact that ionic interactions don't affect the local segmental motions of PPgMA. Similarly, T_α (MAF) of LIonomers associated to the glassy transition temperature remain the same as neat PPgMA one.

But the effect of P^+DEP on the α' relaxation (RAF) is more pronounced (93°C of LIonomer L-P^+DEP-10), which involves the mobility of the confined chains close to the crystalline lamellae [22, 40, 41]. The same trend could be also observed from L-P^+DEP-2 but to a lesser extent since the ionic liquid content is lower. This effect may be attributed to the preferential localization of these ILs in the RAF phase. The chemical structure of ILs could explain their influence on the relaxation spectra of LIonomers. The strong interactions between ionic liquids and polar group within EMIM Acetate-

based LIonomers highlighted by NMR and rheology account for the corresponding higher $T_{\alpha'}$ value than that of EMIM DEP-based LIonomers. While for L-P$^+$DEP-10, the alkyl chains of the phosphonium cation could promote the miscibility with PPgMA.

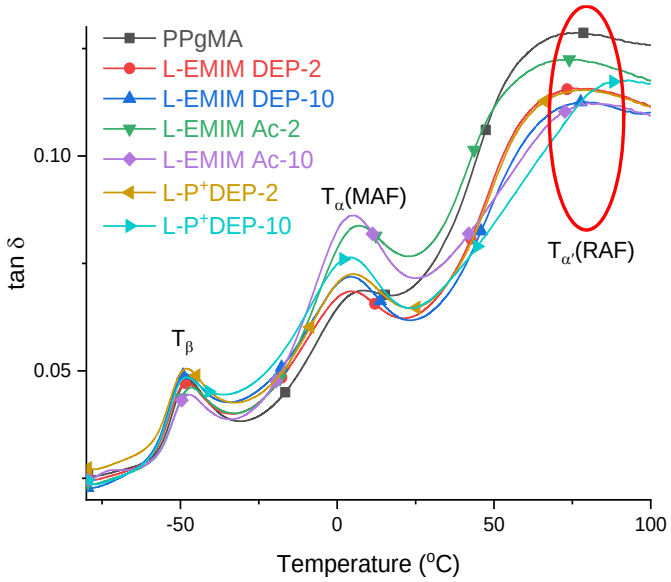

Figure 2- 14 Loss factor (tan δ) vs. temperature for LIonomers at 1 Hz

Table 2- 7 Temperatures at the maximum of tan δ at 1 Hz of the β, α and α' relaxations of neat PPgMA and associated LIonomers.

Materials	T_β (°C)	T_α (MAF, °C)	$T_{\alpha'}$ (RAF, °C)
PPgMA	-47	7	76
L-P$^+$DEP-2	-47	5	79
L-P$^+$DEP-10	-47	5	93
L-EMIM DEP-2	-47	5	74
L-EMIM DEP-10	-48	5	78
L-EMIM Ac-2	-47	7	78
L-EMIM Ac-10	-47	6	80

2.2.3.5 Effect of ILs on crystallization of PPgMA

Role of ILs in the crystallization process

Some works have already reported the influence of ILs on crystallization of semi-crystalline thermoplastics. For example, it was shown that phosphonium-based ILs

could reduce the crystallinity (X_c) and crystallization temperature (T_c) of P(VDF-CTFE) [22, 40]. In this work dedicated to maleic anhydride polypropylene/IL blends, no significant change of X_c could be observed (see Table 2-8 from Figure S2-4 and Table S2-2). This phenomenon is related to the location and distribution of ILs within LIonomers. It agrees with the previous conclusions on the fact that PPgMA and ionic liquids exist as separated phases. The ion-ion and ion-dipole interactions occur at the interface between phases. On another hand, the temperature of crystallization of PPgMA, T_c, increases with the addition of a small amount of P$^+$DEP or EMIM DEP, *i.e.* ILs having a phosphate anion, and retrieve almost the value of neat PPgMA with 10 wt.% of IL. The addition of EMIM Ac has no influence on T_c whatever its content.

DSC analyses of non-isothermal crystallization kinetics as well as observations by polarized optical microscopy (POM) can be used to detect the overall or partial crystallization process of PPgMA and LIonomers. The $\ln[-\ln(1-X_t)]$ vs. $\ln t$ plots according to Jeziorny's non-isothermal crystallization model are shown in Figure S2-5 and Table S2-2. The value of $t_{1/2}$ (half-time crystallization) represents the time consumed to half crystallize, *i.e.* a longer time indicates a slower crystallization rate. As mentioned previously for the other parameters, $t_{1/2}$ slightly depends on *i)* the nature of ion-ion and dipole-ion interactions within LIonomers that could delay the process of regular chain folding to generate the crystalline fraction, since the chain motions to change the configuration are restricted by nearby ILs involved in the interactions [22, 40] ($t_{1/2}$: 0.86min of L-EMIM DEP-10 *vs.* 0.77min of PPgMA); *ii)* the IL content, since high IL content may induce more interactions, followed by a greater impact on the crystallization process ($t_{1/2}$: 0.74min of L-P$^+$DEP-2 *vs* 0.76min of L-P$^+$DEP-10; 0.72min of L-EMIM DEP-2 *vs* 0.86min of L-EMIM DEP-10); *iii)* the intensity of interactions could inhibit the movement of chain segment with some different extent, *i.e.* the restriction of chain motion caused by ion-ion interactions is stronger than that due to dipole-ion interactions. As a consequence, it results in a slower crystallization

rate (L-EMIM DEP-10 *vs*. L-P$^+$DEP-10); *iv)* the miscibility of DEP anion in PPgMA promotes the crystallization process at low content.

In addition to the impact of the existing interactions within LIonomers on the crystallization process, IL itself may also influence the nucleation process. From the comparison of pure PPgMA matrix and LIonomers processed with 10 wt.% IL (at 5 K·min^{-1}, Table 2-8), L-EMIM Ac-10 crystallizes fasterly than all other systems. Because EMIM Ac could restrict the generation of nuclei (as shown in POM images a *vs* d, a' *vs* d' Figure 2-15) and cause a larger volume for the growth of the generated spherulites.

Table 2- 8 The T_c, $t_{1/2}$, and X_c values measured by DSC (heating and cooling rates: 5 K·min^{-1})

Materials	X_c, (%)	T_c, (°C)	$t_{1/2}$ (min)
PPgMA	34.1	116.1	0.77
L-P$^+$DEP-2	37.6	126.8	0.74
L-P$^+$DEP-10	35.1	116.0	0.76
L-EMIM DEP-2	36.8	124.6	0.72
L-EMIM DEP-10	35.3	118.0	0.86
L-EMIM Ac-2	34.2	118.8	0.77
L-EMIM Ac-10	36.9	118.5	0.72

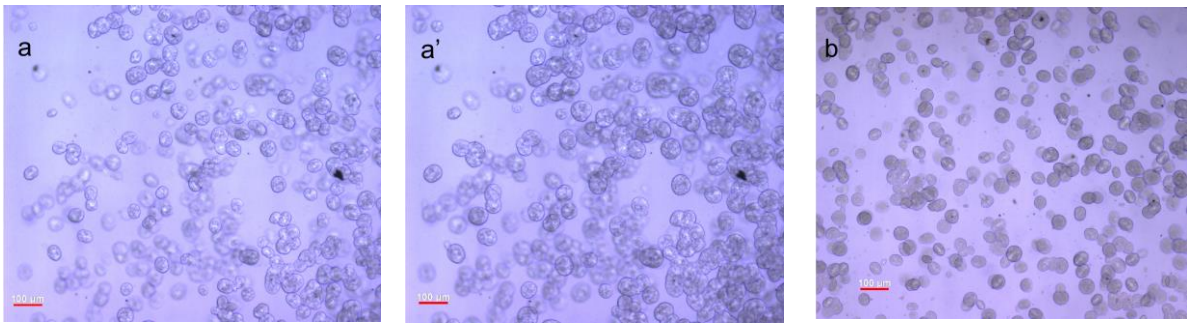

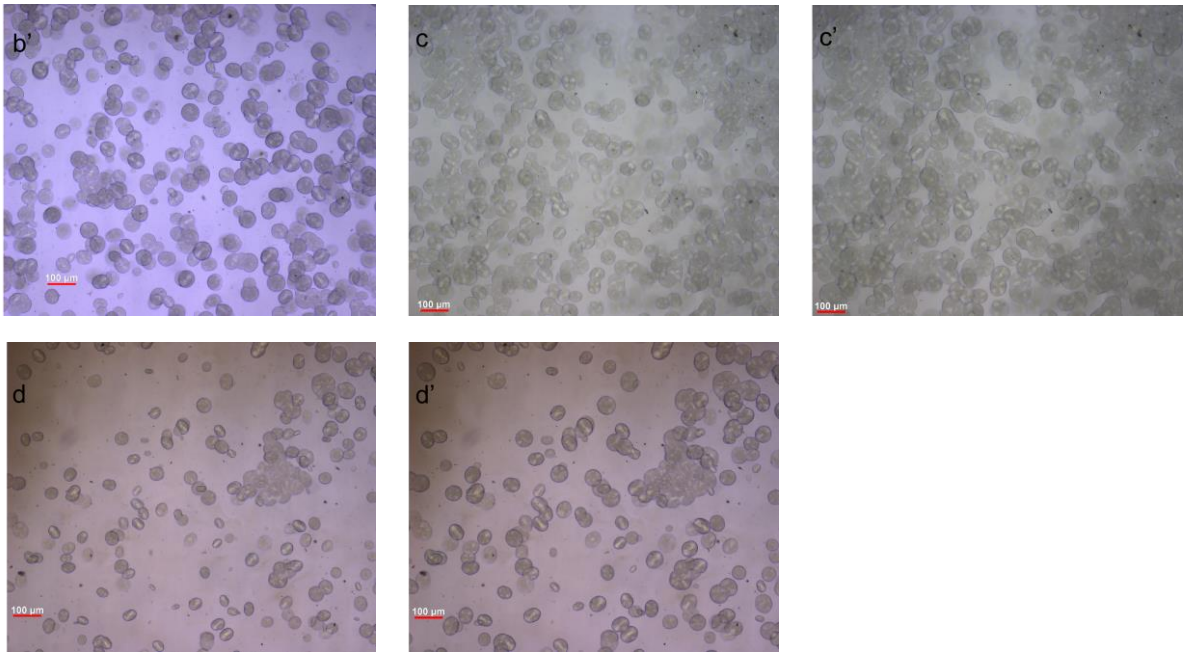

Figure 2- 15 POM microscopies of PPgMA and LIonomers as a function of annealing time at 120 °C (scale bar: 100µm): PPgMA (a) 80s, (a') 100s; L-P$^+$DEP-10 (b) 80s, (b') 100s; L-EMIM DEP-10 (c) 70s, (c') 90s; L-EMIM Ac-10 (d) 100s, (d') 120s

Effect on crystalline phase

As shown in Figure 2-16, the PPgMA crystallizes according to the syndiotactic monoclinic system, mainly in α type crystalline form characterized by the Bragg diffraction peaks at 2θ ≈ 14.0° [110], 16.8° [040], 18.4° [130], 25.3° [060&150], 28.5° [220], and 42.6° [212]. A very weak diffraction peak belonging to (002) plane of the syndiotactic monoclinic [42] can also be detected at 23.6°. γ-form diffraction peak is not observed in the XRD profile (21.4° [α111&γ202]) because it is very difficult to distinguish γ-form from α-form diffraction peaks. γ-form cannot be present in this case, as the generation of this form requires specific crystallization conditions such as high pressure [43]. In LIonomers, most of diffraction peaks of PPgMA are not modified, but a new peak at 2θ ≈ 16.0° belonging to β (300) could be observed when 10 wt.% of EMIM DEP and EMIM Ac ILs are considered. The relative content of β-phase can be calculated from:

$$K = \frac{I_{300}}{I_{300}+I_{110}+I_{040}+I_{130}} \qquad \text{Equation 2- 13}$$

where I_{300}, I_{110}, I_{040}, and I_{130} are the intensities of the corresponding monoclinic phase diffraction reflections at 2θ ≈ 16.0, 14.0, 16.8, and 18.4 respectively [44].

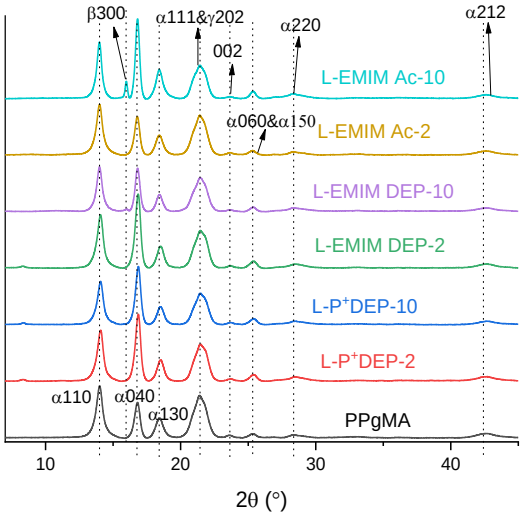

Figure 2- 16 XRD diffraction patterns of PPgMA and its LIonomers based on various ILs at different IL contents

The generation of β-phase in LIonomers based on EMIM DEP and EMIM Ac is related to the existence of stronger ion-ion and ion-dipole interactions with PPgMA than ones generated with P^+DEP. These interactions within L-EMIM DEP-10 and L-EMIM Ac-10 restrain the folding and rearrangement of polymers chains into ordered conformation, resulting in the β-phase which is less stable crystalline form than the α-form. On the other side, LIonomer based on 10 wt.% EMIM Ac exhibits larger β-form area than one obtained with the addition of 10 wt.% EMIM DEP (9.6% *vs* 3.2%; see Table 2-9). As these two ILs hold the same cation ($EMIM^+$), the extent-of-influence of these ILs on crystallinity morphology is associated with their interaction patterns (in NMR analysis) and the size of the anion (acetate *vs.* phosphate). More ion-ion positions contribute EMIM Ac to reinforce interactions, while the bigger and less interactive anion makes EMIM DEP less prone to promote strong interaction. The strongest ion-ion and ion-dipole interactions within LIonomers can be correlated to their rheological behavior.

Table 2- 9 XRD analyses of the PPgMA and its related LIonomers

	$D_{[110]}$ (nm)	$D_{[040]}$ (nm)	$D_{[130]}$ (nm)	$D_{[300]}$ (nm)	K (%)	Average size (Å)[a]
PPgMA	12.7	18.2	12.8	-	-	12.7
L-P^+DEP-2	13.5	18.2	14.1	-	-	12.3
L-P^+DEP-10	13.6	18.3	13.8	-	-	12.4
L-EMIM DEP-2	13.3	18.0	13.7	-	-	12.5
L-EMIM DEP-10	8.9	21.0	15.8	72.4	3.2	13.1
L-EMIM Ac-2	13.0	18.6	13.0	-	-	12.6
L-EMIM Ac-10	17.4	24.3	13.0	51.2	9.6	14.0

where D is the crystallite size, [a]these values are calculated based on their α-crystalline form size

2.2.3.6 Effect of ILs on mechanical behaviour of LIonomers

Owing to the generated interactions and the structuration of the ILs within PPgMA matrix which can be tuned by the nature of ILs, *i.e.* the type of the anion and cation, the mechanical behavior of LIonomers can be also tailored. At low content of ILs, the Young's modulus significantly increases whatever the nature of the ionic liquid, as shown in Figure 2-17 and Table 2-10. With the addition of a large amount of ILs, the modulus decreases significantly due to the presence of large separated IL-rich phases that act as defects except for L-EMIM Ac-10. In the latter case, strong ion-dipole interactions have been confirmed and the specific mechanical behavior of this LIonomer agrees with rheology results. On the other side, the strain at break increases dramatically for LIonomers based on imidazolium cation unlike phosphonium cation. Based on the DSC and WAXD results, especially crystallinity rates and morphisms, the generation of β-phase caused by strong ion-ion/dipole-ion interactions and multiscale morphologies, *i.e.* ILs as clusters and separated phase, can explain the difference of strain at break observed from the various types of LIonomers. The addition of EMIM Ac (even at low content, *i.e.* 2 wt.%) leads to the enhancement of

both Young's modulus and strain at break. The imidazolium cation plays a key role in the reinforcement of the mechanical properties. This cation leads to strong interactions with PPgMA that governs the macroscopic behavior of the corresponding LIonomers. The interactions based on phosphate anion are not sufficient to reinforce the mechanical behavior of the related LIonomers. The interactions are even stronger with the imidazolium cation and further when imidazolium is combined with acetate anion as more ion-ion interaction positions.

In summary, it is worth to noting that the introduced ionic liquids in grafted polypropylene don't behave as plasticizers, *i.e.* leading to decrease the Young's modulus and increase the strain at break as reported in the literature [22, 40]. The mechanical behavior can be tailored to the nature of the cation and anion of the ionic liquid. For LIonomers, the slightly enhanced crystallinity rate contributes partly to the increase of stiffness while the multiscale distribution of ILs within the PPgMA matrix, *i.e. as* ionic multiplets and IL-separated phase, as well as strong ion-ion/dipole-ion interactions are the major contributors to the mechanical property of LIonomers.

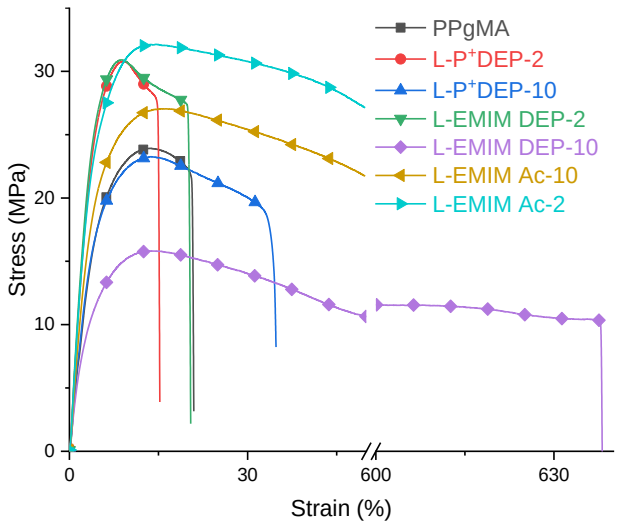

Figure 2- 17 Stress-strain curves from tensile tests for of PPgMA and related LIonomers

Table 2- 10 Mechanical properties of PPgMA and related LIonomers (from tensile tests performed at room temperature)

Samples	Young's modulus (MPa)	Strain at break (%)	Yield stress (MPa)
PPgMA	456±18	24±6	24±1
L-P$^+$DEP-2	705±4	14±3	30±1
L-P$^+$DEP-10	492±12	35±5	24±1
L-EMIM DEP-2	803±10	23±2	31±1
L-EMIM DEP-10	431±11	655±20	16±1
L-EMIM Ac-2	756±9	65±4	31±3
L-EMIM Ac-10	609±12	550±34	28±1

2.2.4 Conclusions

From the combination of the maleic anhydride-grafted polypropylene (PPgMA) and three different ionic liquids, tributyl (ethyl)phosphonium diethyl phosphate (named P$^+$DEP), 1-ethyl-3-methylimidazolium diethyl phosphate (named EMIM DEP), and 1-ethyl-3-methylimidazolium acetate (named EMIM Ac), LIonomers, *i.e.* a new generation of ionomers, have been successfully synthesized. This section reveals that the presence of grafted maleic anhydride on the polypropylene backbone as the "head group" combined with ionic liquid pairs could lead to the formation of new nanostructures via the generation of ionic and polar interactions. Different morphologies can be designed, *i.e.* from a phase separation resulting in a single-(nano) scale structuration composed of distribution of ionic clusters when LIonomers regarding phosphonium-based ILs, to a multi-scale structure combining ionic clusters but also IL-rich separated phase as for imidazolium cation-based ILs. The smaller size of the separated IL-rich phases is prone to establish the stronger ILs/polymer interactions. The imidazolium cation combined with the acetate anion appears as the most relevant IL to optimize the interactions with maleic anhydride group grafted onto the polypropylene backbone. The physical properties both in the molten and solid

states appear to be strongly influenced by these interactions. In fact, the increase of the complex viscosity highlights the existence of IL/polymer interactions and the ability in such a case to form an ionic network. In relation with their morphology, crystallinity, and the existence of percolated ionic phase, LIonomers display both improved Young's modulus and ability to sustain large strains before break. Therefore, these LIonomers are very promising for processing functional materials such as foams or melt blown membranes.

2.2.5 References

[1] Zhang L, Brostowitz N R, Cavicchi K A, et al. Perspective: Ionomer research and applications [J]. Macromolecular Reaction Engineering, 2014, 8(2): 81-99.

[2] Kirkmeyer B P, Weiss R A, Winey K I. Spherical and vesicular ionic aggregates in Zn-neutralized sulfonated polystyrene ionomers [J]. Journal of Polymer Science Part B: Polymer Physics, 2001, 39(5): 477-483.

[3] Eisenberg A, Hird B, Moore R. A new multiplet-cluster model for the morphology of random ionomers [J]. Macromolecules, 1990, 23(18): 4098-4107.

[4] Datta S, De P, De S. Blends of ionomers [J]. Journal of Applied Polymer Science, 1996, 61(10): 1839-1846.

[5] Longworth R, Vaughan D J. Physical structure of ionomers [J]. Nature, 1968, 218(5136): 85-87.

[6] Kim J-S, Yoshikawa K, Eisenberg A. Molecular weight dependence of the viscoelastic properties of polystyrene-based ionomers [J]. Macromolecules, 1994, 27(22): 6347-6357.

[7] Dalmas F, Leroy E. New insights into ionic aggregate morphology in Zn-neutralized sulfonated polystyrene ionomers by transmission electron tomography [J]. Macromolecules, 2011, 44(20): 8093-8099.

[8] Aitken B S, Buitrago C F, Heffley J D, et al. Precision ionomers: synthesis and thermal/mechanical characterization [J]. Macromolecules, 2012, 45(2): 681-687.

[9] Weiss R, Zhao H. Rheological behavior of oligomeric ionomers [J]. Journal of Rheology, 2009, 53(1): 191-213.

[10] Qiao X, Weiss R. Nonlinear rheology of lightly sulfonated polystyrene ionomers [J]. Macromolecules, 2013, 46(6): 2417-2424.

[11] Ling G H, Wang Y, Weiss R. Linear viscoelastic and uniaxial extensional rheology of alkali metal neutralized sulfonated oligostyrene ionomer melts [J]. Macromolecules, 2012, 45(1): 481-490.

[12] Rapone I, Taresco V, Lisio V D, et al. Silver-and Zinc-Decorated Polyurethane Ionomers with Tunable Hard/Soft Phase Segregation [J]. International Journal of Molecular Sciences, 2021, 22(11): 6134.

[13] Ro A J, Huang S J, Weiss R. Synthesis and properties of random poly (lactic acid)-based ionomers [J]. Polymer, 2009, 50(5): 1134-1143.

[14] Ro A J. Synthesis and properties of poly(lactic acid) ionomers [D]. University of Connecticut, 2008.

[15] Wu M-H, Wang C-C, Chen C-Y. Preparation of high melt strength polypropylene by

addition of an ionically modified polypropylene [J]. Polymer, 2020, 202(122743.
[16] Li Y, Yao Z, Chen Z-H, et al. High melt strength polypropylene by ionic modification: Preparation, rheological properties and foaming behaviors [J]. Polymer, 2015, 70: 207-214.
[17] Colbeaux A, Fenouillot F, Gerard J F, et al. Compatibilization of a polyolefin blend through covalent and ionic coupling of grafted polypropylene and polyethylene. II. Morphology [J]. Journal of Applied Polymer Science, 2004, 93(5): 2237-2244.
[18] Colbeaux A, Fenouillot F, Gérard J F, et al. Compatibilization of a polyolefin blend through covalent and ionic coupling of grafted polypropylene and polyethylene. I. Rheological, thermal, and mechanical properties [J]. Journal of Applied Polymer Science, 2005, 95(2): 312-320.
[19] Livi S, Duchet-Rumeau J, Pham T-N, et al. A comparative study on different ionic liquids used as surfactants: Effect on thermal and mechanical properties of high-density polyethylene nanocomposites [J]. Journal of Colloid and Interface Science, 2010, 349(1): 424-433.
[20] Rahman M, Brazel C S. Ionic liquids: New generation stable plasticizers for poly (vinyl chloride) [J]. Polymer Degradation and Stability, 2006, 91(12): 3371-3382.
[21] Yousfi M, Livi S, Duchet-Rumeau J. Ionic liquids: A new way for the compatibilization of thermoplastic blends [J]. Chemical Engineering Journal, 2014, 255: 513-524.
[22] Yang J, Pruvost S B, Livi S B, et al. Understanding of versatile and tunable nanostructuration of ionic liquids on fluorinated copolymer [J]. Macromolecules, 2015, 48(13): 4581-4590.
[23] Leroy E, Jacquet P, Coativy G, et al. Compatibilization of starch–zein melt processed blends by an ionic liquid used as plasticizer [J]. Carbohydrate Polymers, 2012, 89(3): 955-963.
[24] Chen Y, Zhang Y, Ke F, et al. Solubility of neutral and charged polymers in ionic liquids studied by laser light scattering [J]. Polymer, 2011, 52(2): 481-488.
[25] Hajipour A R, Rafiee F. Recent progress in ionic liquids and their applications in organic synthesis [J]. Organic Preparations and Procedures International, 2015, 47(4): 249-308.
[26] Yue C, Fang D, Liu L, et al. Synthesis and application of task-specific ionic liquids used as catalysts and/or solvents in organic unit reactions [J]. Journal of Molecular Liquids, 2011, 163(3): 99-121.
[27] Clark E J, Hoffman J D. Regime III crystallization in polypropylene [J]. Macromolecules, 1984, 17(4): 878-885.
[28] Jeziorny A. Parameters characterizing the kinetics of the non-isothermal crystallization of poly (ethylene terephthalate) determined by DSC [J]. Polymer, 1978, 19(10): 1142-1144.
[29] Livi S, Duchet-Rumeau J, Gérard J-F. Nanostructuration of ionic liquids in fluorinated matrix: influence on the mechanical properties [J]. Polymer, 2011, 52(7): 1523-1531.
[30] Dibble D C, Li C, Sun L, et al. A facile method for the recovery of ionic liquid and lignin

from biomass pretreatment [J]. Green Chemistry, 2011, 13(11): 3255-3264.
[31] Clough M T, Geyer K, Hunt P A, et al. Thermal decomposition of carboxylate ionic liquids: trends and mechanisms [J]. Physical Chemistry Chemical Physics, 2013, 15(47): 20480-20495.
[32] Dubey S, Bharmoria P, Gehlot P S, et al. 1-Ethyl-3-methylimidazolium diethylphosphate based extraction of bioplastic “Polyhydroxyalkanoates” from bacteria: green and sustainable approach [J]. ACS Sustainable Chemistry & Engineering, 2018, 6(1): 766-773.
[33] Binks F C, Cavalli G, Henningsen M, et al. Examining the influence of anion nucleophilicity on the polymerisation initiation mechanism of phenyl glycidyl ether [J]. Polymers, 2019, 11(4): 657.
[34] Weiss R, Yu W-C. Viscoelastic behavior of very lightly sulfonated polystyrene ionomers [J]. Macromolecules, 2007, 40(10): 3640-3643.
[35] Page K A, Park J K, Moore R B, et al. Direct analysis of the ion-hopping process associated with the α-relaxation in perfluorosulfonate ionomers using quasielastic neutron scattering [J]. Macromolecules, 2009, 42(7): 2729-2736.
[36] Castagna A M, Wang W, Winey K I, et al. Influence of cation type on structure and dynamics in sulfonated polystyrene ionomers [J]. Macromolecules, 2011, 44(13): 5420-5426.
[37] Ma Q, Georgiev G, Cebe P. Constraints in semicrystalline polymers: Using quasi-isothermal analysis to investigate the mechanisms of formation and loss of the rigid amorphous fraction [J]. Polymer, 2011, 52(20): 4562-4570.
[38] Arnoult M, Dargent E, Mano J. Mobile amorphous phase fragility in semi-crystalline polymers: Comparison of PET and PLLA [J]. Polymer, 2007, 48(4): 1012-1019.
[39] Bajsić E G, Šmit I, Leskovac M. Blends of thermoplastic polyurethane and polypropylene. I. Mechanical and phase behavior [J]. Journal of Applied Polymer Science, 2007, 104(6): 3980-3985.
[40] Xing C, Zhao M, Zhao L, et al. Ionic liquid modified poly (vinylidene fluoride): crystalline structures, miscibility, and physical properties [J]. Polymer Chemistry, 2013, 4(24): 5726-5734.
[41] Mijovic J, Sy J-W, Kwei T. Reorientational dynamics of dipoles in poly (vinylidene fluoride)/poly (methyl methacrylate)(PVDF/PMMA) blends by dielectric spectroscopy [J]. Macromolecules, 1997, 30(10): 3042-3050.
[42] Clark E S. Unit cell information on some important polymers [M]. Physical Properties of Polymers Handbook. Springer. 2007: 619-624.
[43] Yang G, Li X, Chen J, et al. Crystallization behavior of isotactic polypropylene induced by competition action of β nucleating agent and high pressure [J]. Colloid and Polymer Science, 2012, 290(6): 531-540.
[44] Zipper P, Janosi A, Wrentschur E. Scanning X-ray scattering of mouldings from

semicrystalline polymers [J]. Journal de Physique IV, 1993, 3(C8): C8-33-C8-36.

2.2.6 Supporting Information

1. Elemental Analysis Spectra (EDX-TEM)

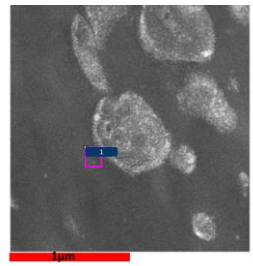
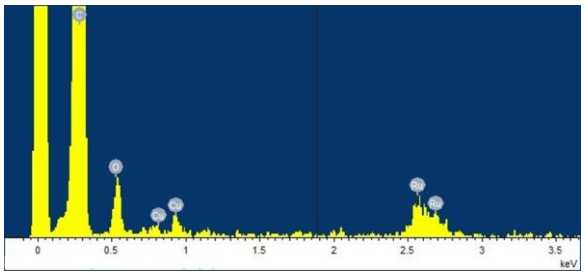
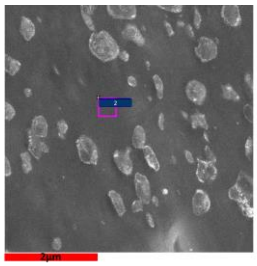
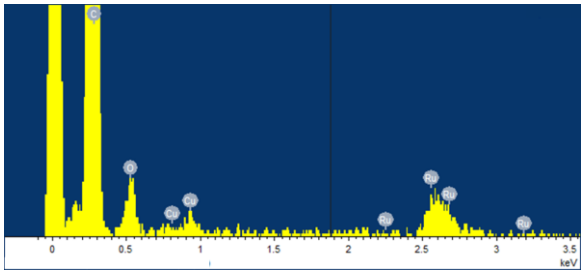

Polymer matrix within L-P⁺DEP-10

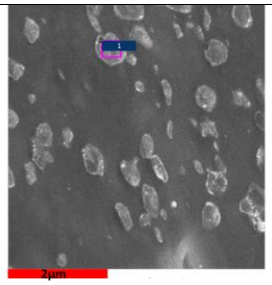
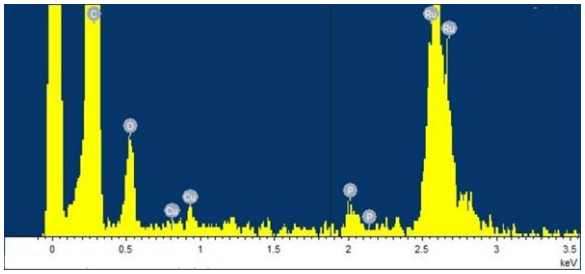
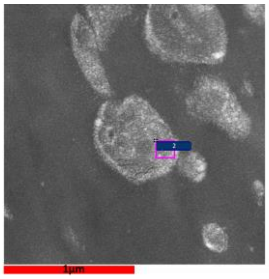
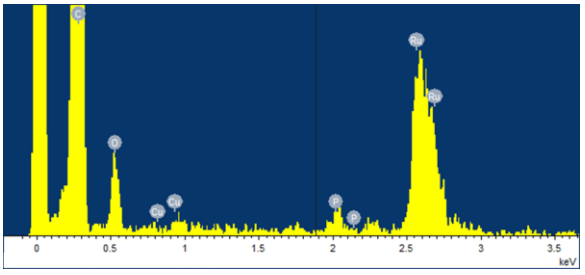

L-P⁺DEP-10

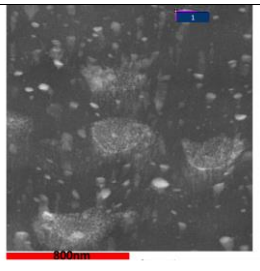
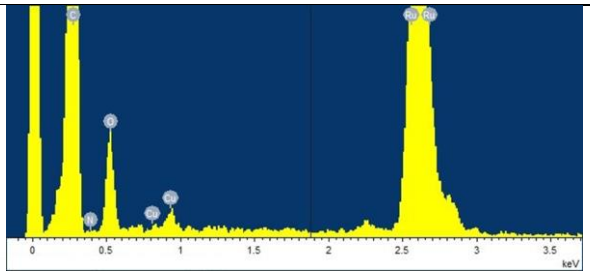

L-EMIM Ac-10

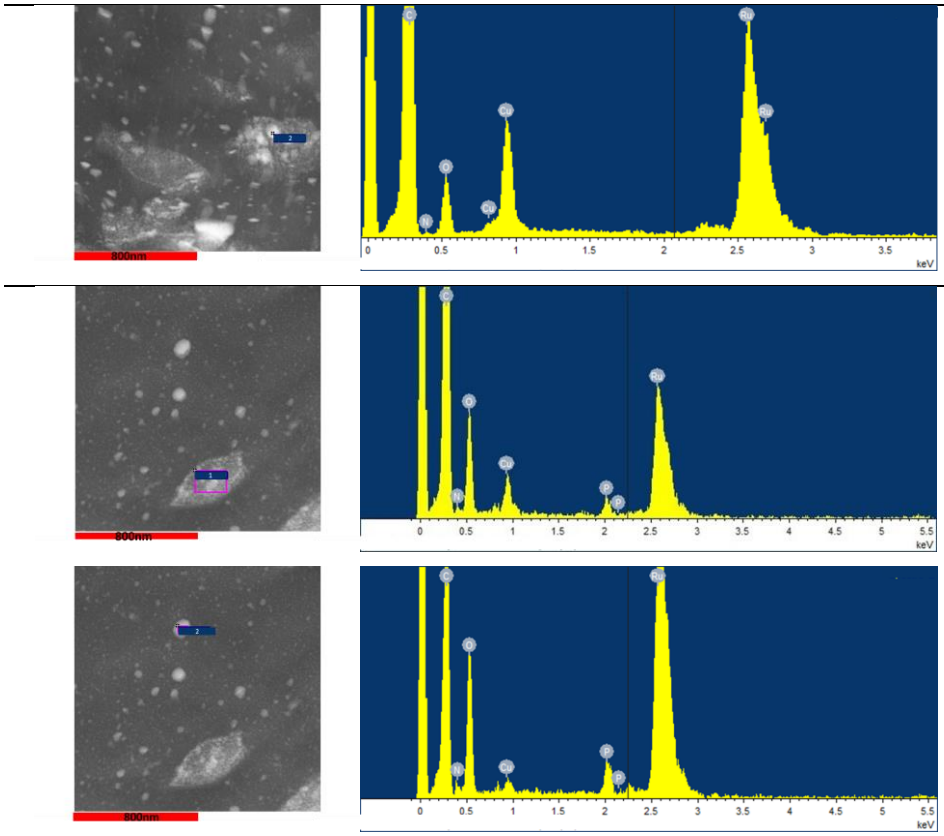

L-EMIM DEP-10

Figure S2- 3 Elemental analysis spectra (EDX) of LIonomers performed on fractured surfaces observed by TEM

2. DSC thermograms of PPgMA and related LIonomers

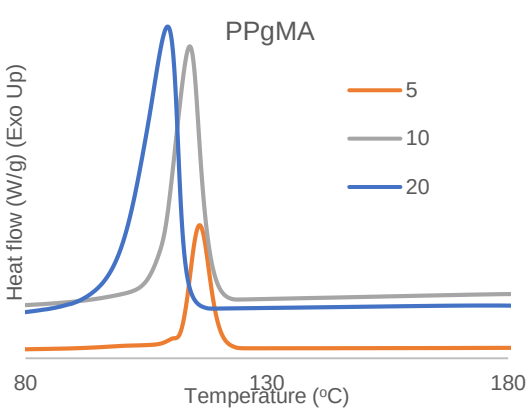

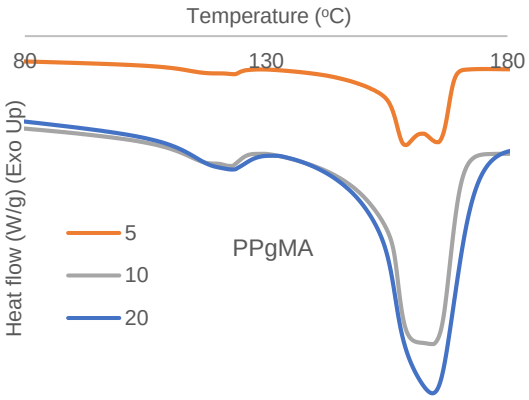

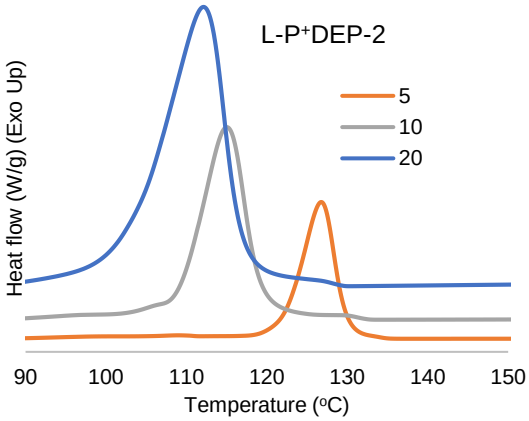

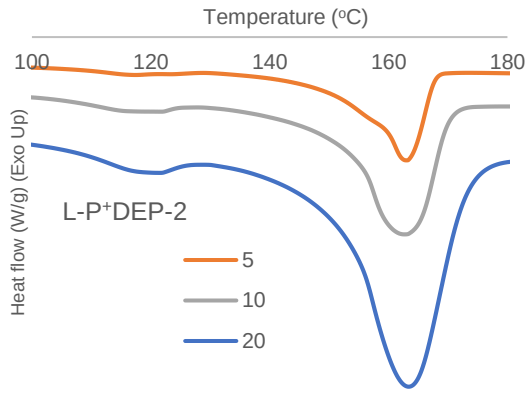

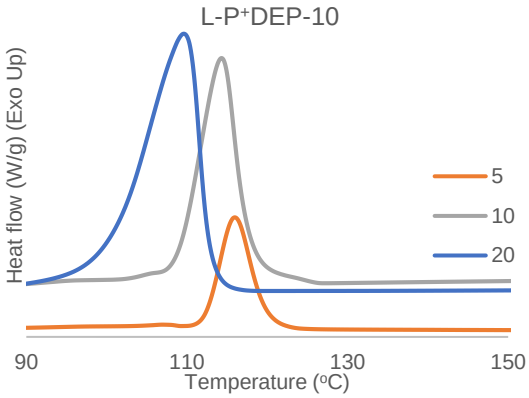

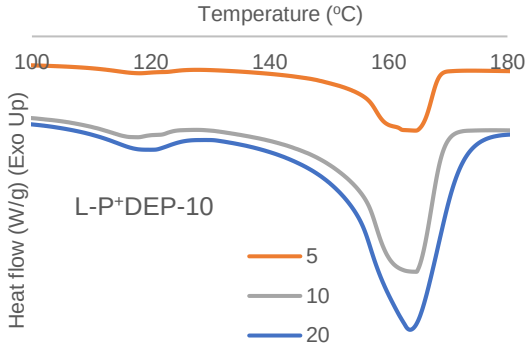

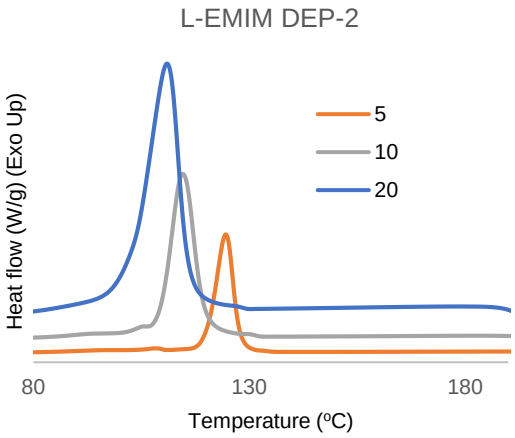

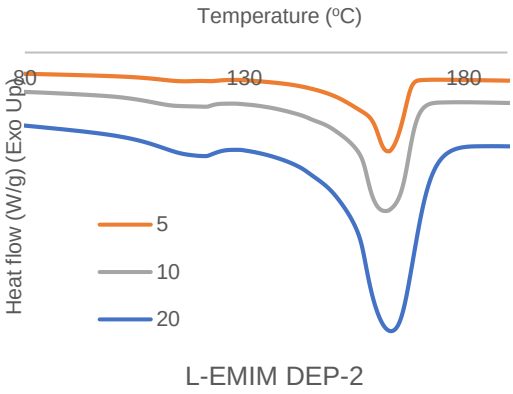

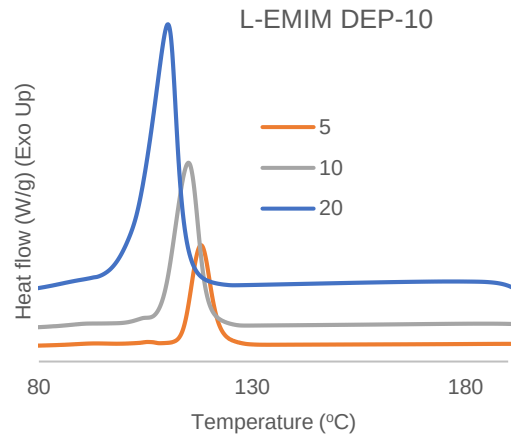

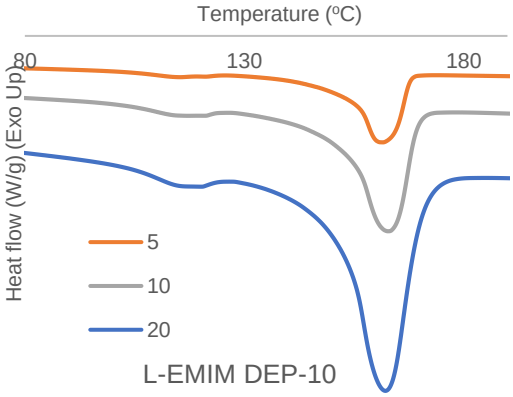

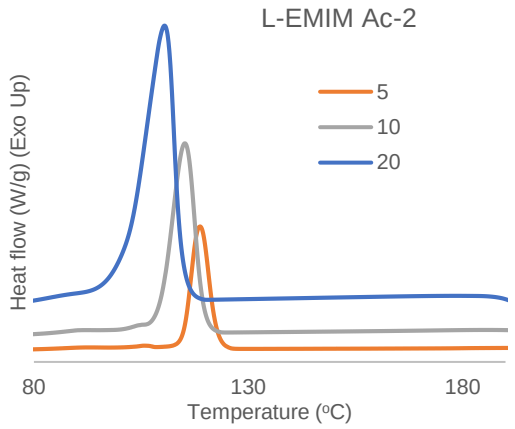

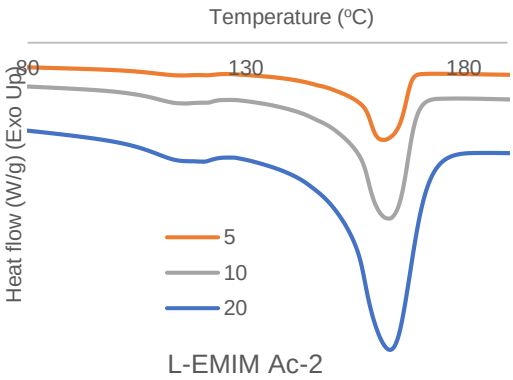

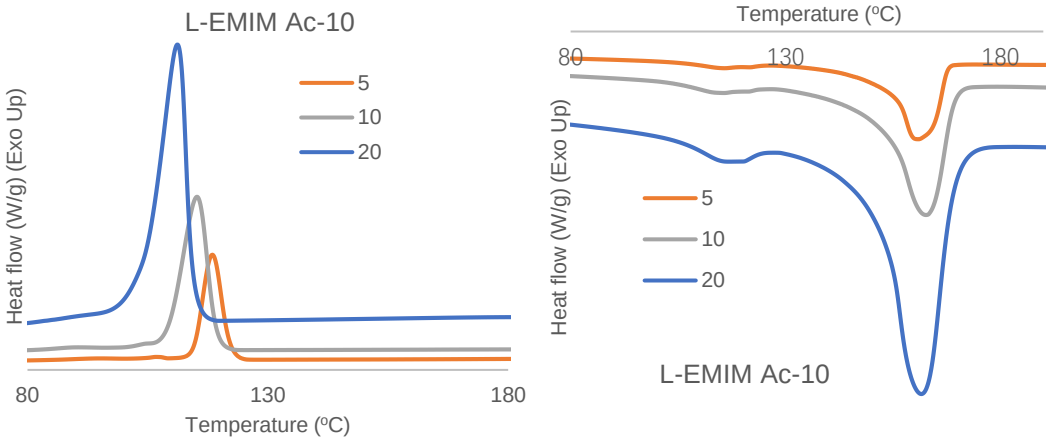

Figure S2- 4 DSC traces of PPgMA and related LIonomers prepared with various ionic liquids (2 and 10 wt.%). Melting and crystallization phenomenon was observed for different heating and cooling rates (5, 10, and 20 $K \cdot min^{-1}$) under nitrogen atmosphere.

3. $ln[-ln(1-X_t)]$ vs. $ln\ t$ plots according to Jeziorny's non-isothermal crystallization model

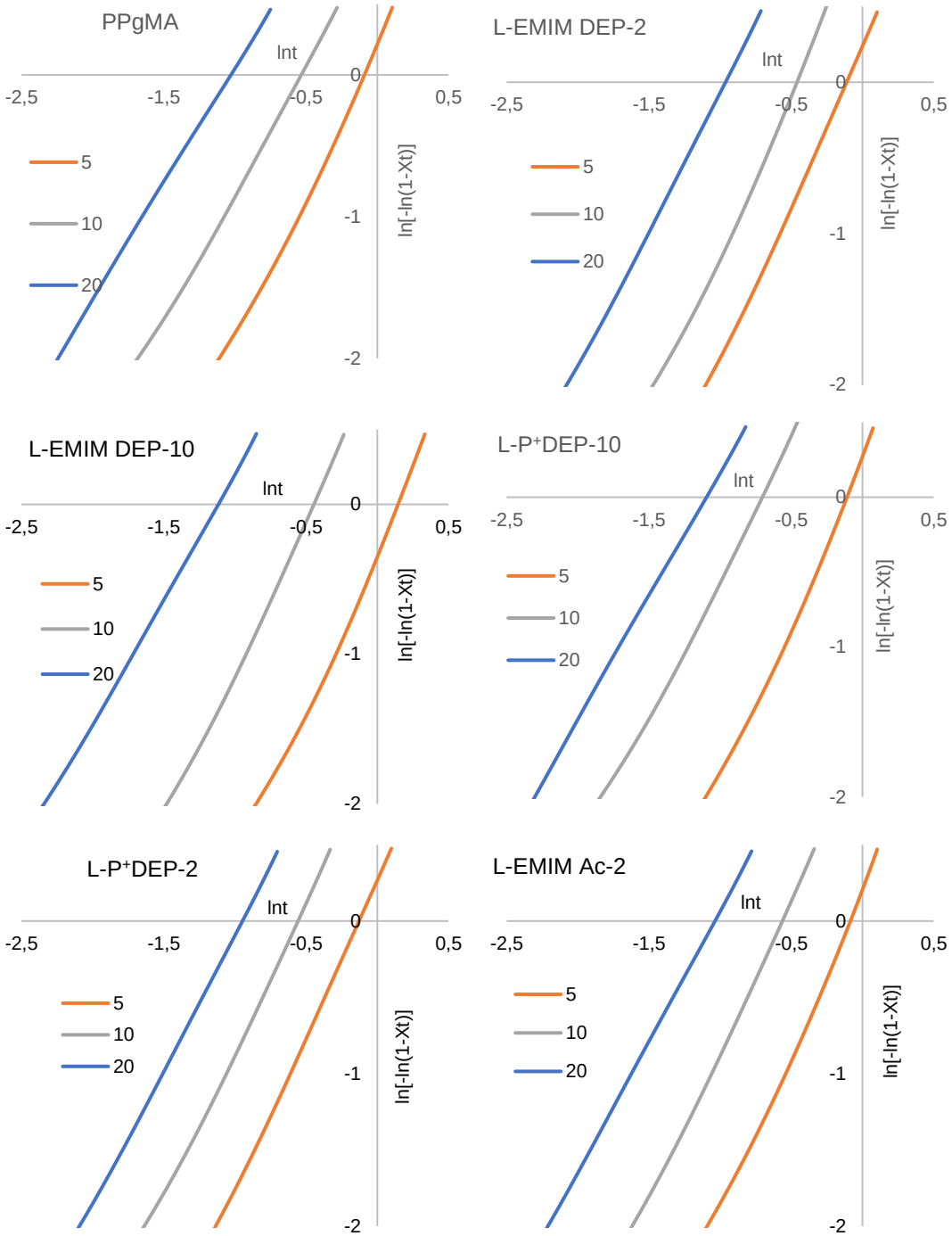

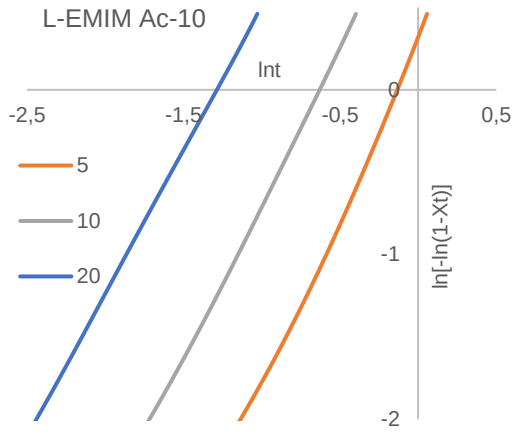

Figure S2- 5 $ln[-ln(1-X_t)]$ vs. $ln\,t$ plots according to Jeziorny's crystallization model for neat PPgMA and related LIonomers based on various ionic liquids (2 and 10 wt.%) for different cooling rates (5, 10, and 20 $K{\cdot}min^{-1}$)

4. Detailed parameters of non-isothermal crystallization process in accordance with Jeziorny's model

Table S2- 2 Parameters of non-isothermal crystallization process based on Jeziorny's model

Samples	Φ	$t_{1/2}$ (min)	n	Z_t	T_m (°C)	T_c (°C)	X_c (%)
PPgMA	5	0.77	2.01	1.17	159.0/165.6	116.1	34.1
	10	0.47	1.78	2.68	164.2	114.1	35.5
	20	0.28	1.65	5.55	164.5	109.5	31.6
L-P$^+$DEP-2	5	0.74	2.01	1.28	163.0	126.8	37.6
	10	0.48	1.88	2.81	162.8	115.0	34.7
	20	0.32	1.76	5.29	163.4	112.2	33.6
L-P$^+$DEP-10	5	0.76	2.06	1.22	164.5	116.0	35.1
	10	0.41	1.81	3.54	164.7	114.3	34.0
	20	0.27	1.65	6.16	163.7	109.6	32.1
L-EMIM DEP-2	5	0.72	1.98	1.33	162.9	124.6	36.8
	10	0.50	1.94	2.65	162.3	114.6	34.3
	20	0.31	1.81	5.66	163.4	111.0	33.2
L-EMIM DEP-10	5	0.87	2.04	0.92	161.6	118.0	35.3
	10	0.49	1.85	2.56	162.9	115.1	34.0
	20	0.28	1.69	5.98	162.2	110.2	33.4
L-EMIM Ac-2	5	0.77	2.03	1.16	161.9	118.8	34.2
	10	0.47	1.92	2.92	162.9	115.2	33.7
	20	0.29	1.71	5.90	163.2	110.5	34.6
L-EMIM Ac-10	5	0.72	2.30	0.84	161.0	118.5	36.9
	10	0.44	1.86	3.20	162.8	115.3	35.8
	20	0.22	1.73	9.35	161.7	111.2	35.0

Note: φ: cooling rate (K·min^{-1}), T_m: melting temperature (°C), T_c: crystallization temperature (°C) and X_c: crystallinity (%).

Chapter 3: 2.0 Generation of ionomers based on PPgMA-LIonomers: by introducing functional imidazolium-based ionic liquids, and the comparison with traditional Zn-Ionomer

Table of Contents

Chapter 3: 2.0 Generation of ionomers based on PPgMA-LIonomers : by introducing functional imidazolium-based ionic liquids and the comparison with traditional Zn-Ionomer

3.1 Designing and understanding of LIonomers-2.0 generation ionomer: the effect of generated ionic-branched chains consisting of cation/anion pairs of ionic liquids

3.1.1 Introduction

As we all know, designing of ionomers is one efficient pathway to improve the crystallization process, molten strength and thermal-mechanical properties of polymer [1–5]. Such materials are regarded as one macromolecules that include ionic or ionisable groups consisting of metal salts cations and acidic anions [6,7]. Of course such system possesses ionic multiplets and/or ionic networks that create the limited zones of polymer chains and restrict the motion of polymer chains through the ion-pair interactions between acidic anions in matrix and metal cations [8]. Then, one large, continuous and flowability-restrained area is formed by overlapping multiples and ionic networks [1]. Together with the generated physical cross-linked networks composed of multiplets and/or clusters, next the polymer chains exhibit greater resistance and any change of chain segment becomes more difficult, resulting in some modifications in overall properties [1–5]. Researchers have introduced various metal salts (such as Zn^{2+}, Na^{+}, Ca^{2+}) into different polymers and obtained superior improvement. The presence of the apparent cross-linked structure could not only improve the thermal stability but also enhance the glass transition temperature (T_g) of Zn-ionomer based on polyacrylate latexes [9]. While the strong intermolecular dipole-dipole interactions can bring about great modification on molten strength [10]. Thanks to the presence of inter-chain ionic interactions and generation of nano-separated structure induced by the

ionic aggregates within the products, Zn-ionomer has several times higher melt viscosity compared to polypropylene grafted maleic anhydride [11]. Ion-enriched fragments can spontaneously build inter- and intra-molecular ionic aggregates in poly (butylene succinate) (PBS), which function as physical cross-linking points to improve the crystallization efficiency and compound viscosity of PBS matrices [12]. The degradation temperature and T_g of Zn-ionomer (as for waterborne polyurethane) are enhanced compared to its virgin polymer due to the strong interaction within composites, such interaction also leads to an increase in Young's modulus and fracture strain [13]. To sum up, the intermolecular and intramolecular ion-pair combinations are the main factors defining the solid and molten properties of ionomers [14].

On the other hand, ionic liquids (ILs) as one novel compound composed of cation and anion offer promising new approaches for the design of new (multi) functional objects and materials. Thanks to their special combinations, they can be adapted in polar or non-polar polymer-based materials. ILs may act as the interfacial agents to improve the compatibility between polymer blends [15] and organic-inorganic hybrids [16]. They could also participate in the anionic polymerization [17,18] and organic synthesis [19–21] as reactive functional additives. In addition, its excellent thermal stability makes it possible to use in high temperature conditions [22,23]. More recently, some non-reactive phosphonium- and imidazolium-based ionic liquids are considered as the effective additives to design the new generation of ionomers, as well as tailor the properties [24]. Because the ionic interactions with polymer backbone within LIonomers could be adjusted by changing the cation/anion pairs of ionic liquid, resulting in the desired performance. This work is dedicated to the processing of new structural foams made from LIonomers by mixing PPgMA and one functional imidazolium-based ionic liquid, *i.e.* 1-aminoethyl-3-methylimidazolium Bromide ([AEMIM] Br) (Scheme 3-1). Considering the structure of PPgMA and [AEMIM] Br, ionic interactions must take place within PPgMA/[AEMIM] Br blends, leading to the "liquid-like" branch networks (Figure 3-1) when introducing high content of [AEMIM] Br and paving the ability to foam. We attempt to explore what parameter plays a key role in

the location of [AEMIM] Br and nanostructuration as well as crystallization behavior within LIonomers. Also by planning various molar ratio of [AEMIM] Br/MA and different MA contents, the effect on shear rheological behavior due to the number of chemical reactive points and the length of “liquid-like branches” is investigated. Besides, we attempt to explore what plays a dominant role in the location of [AEMIM] Br and nanostructuration.

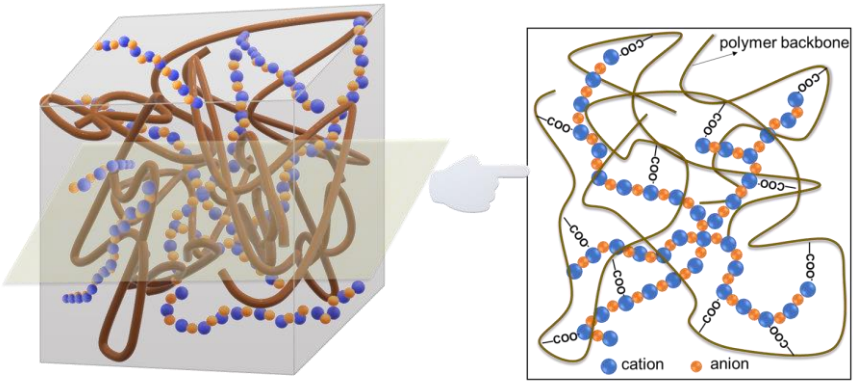

Figure 3- 1 Proposed microstructure of LIonomers

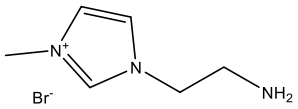

Scheme 3- 1 Molecular structure of 1-aminoethyl-3-methylimidazolium Bromide ([AEMIM] Br)

3.1.2 Experimental Section

3.1.2.1 Materials

PPgMA1 and PPgMA8 are received from Arkema (OREVAC® CA) and Sigma-Aldrich, with the MA content of 1 wt.% and 8-10 wt.%, respectively. 1-aminoethyl-3-methylimidazolium Bromide ([AEMIM] Br) is provided by Chemfish Tokyo CO.,LTD.

3.1.2.2 Samples preparation and characterizations

The blends of polymer matrix and [AEMIM] Br have been fed into micro extruder at 180 °C and stirred for 5 minutes. Then the products are collected after syringe them

into moulds at room temperature, the details of all samples are shown in Table 3-1.

Table 3- 1 The formula of LIonomers in this present

Polymer matrix	PPgMA1 (wt%)	PPgMA8 (wt%)	[AEMIM] Br (wt.%)	Abbreviations	$mol_{[AEMIM]Br}/mol_{MA}$
PPgMA	100	0	2	L-2-1	1
			10	L-10-5	5
Blends-1	90	10		LB1-10-3	3
Blends-2	70	30	15	LB2-15-3	3

The Fourier-transform infrared spectroscopy (FTIR, Nicolet iS10) in attenuated total reflectance (ATR) mode (128 scans) has been used to characterize the chemical structure of all samples.

The rheological and dynamic mechanical measurements have been conducted in the platform of ARES-G2 rheometer (ARES-G2 SN#4010-0255, TA Instrument). The former one is detected at 180 °C applying parallel plate geometry (d = 25mm) under nitrogen protection, while the curves of dynamic mechanical analysis (DMA) are plotted at the temperature range of -80 °C/100 °C with one heating rate 3 °C·min^{-1}.

Transmission electron microscope (TEM, Phillips CM 120) is measured to view the dispersed [AEMIM] Br within LIonomers at an accelerating voltage of 120 kV. To achieve the morphology of samples, they are cut using ultramicrotomy firstly and collected on a carbon film-coated cooper grid.

The DSC (Q10 TA Instrument, New Castle, DE, USA) is preformed to record the thermal property. After erase thermal history by heating samples into 200 °C and remained for 3 mins, cooling/heating/cooling cycles are recorded with different cooling rate 5/10/20 °C·min^{-1}. The crystallization temperature peak (T_c, °C) is obtained from the first cooling run and crystallinity (X_c, %) is calculated by Equation 3- 1 using enthalpy change from the 2rd heating.

$$X_c = \frac{\Delta H_f}{(1-\varphi)\Delta H_f{}^0} \quad \text{Equation 3- 1}$$

where H_f^0 being the melting enthalpy 100 % crystallization of polymer (209J/g for PP [25]), ΔH_f being detected by DSC, and φ being the mass fraction of introduced ILs.

The non-isothermal crystallization kinetics of polymer matrix and LIonomers are investigated using Jeziorny's theory [26]:

$$ln[-ln(1-X_t)] = nlnt + lnZ_t \quad \text{Equation 3- 2}$$

where X_t being the relative crystallinity at crystallization time t and can be defined by Equation 3- 3 and 3-4, n being the Avrami exponent involving the mechanisms of crystal nucleation and growth, while Z_t being the crystallization kinetic constant concerning nucleation and growth rate parameters. The value of n and $\ln Z_t$ can be gained via plotting the line $\ln[-\ln(1-X_t)]$ versus $\ln t$.

$$X_T = \frac{\int_{T_0}^{T_c}(\frac{dH_c}{dT})/dT}{\int_{T_0}^{T_\infty}(\frac{dH_c}{dT})/dT} \quad \text{Equation 3- 3}$$

where X_T being the relative crystallinity with the change of temperature, T_0 and T_∞ being the onset and end of crystallization temperature respectively.

$$t = \frac{T_0 - T}{\varphi} \quad \text{Equation 3- 4}$$

where T being the temperature at crystallization time t, φ is the cooling rate.

Based on Jeziorny's theory, the crystallization half-time ($t_{1/2}$) is calculated by Equation 3- 5:

$$t_{1/2} = (\frac{ln2}{Z_t})^{1/n} \quad \text{Equation 3- 5}$$

Wide angle X-Ray scattering diffraction (WAXD) has been used to investigate the crystal phase of polymer matrix and LIonomers, which is measured on the Bruker D8-Advance diffractometer (USA) platform at room temperature and performed in the scattering range 2θ=10-45° using Cu Kα radiation (λ=0.15406 nm) at 40 kV and 40 mA. Their diffraction diagrams are further analysed by Origin 2018 software using Gauss fitting function, then the crystal size at different scattering angle was calculated based on Scherrer's equation:

$$D = \frac{K\lambda}{(\beta - s)cos(\theta)} \quad \text{Equation 3- 6}$$

where D being the crystal size; K being the crystalline shape parameter (≈0.89); λ equals to 0.15406 nm, the Cu Kα wavelength; β being the measured sample diffraction peak half-height width; s being the instrument factor calibration (0.05°), and θ being the diffraction angle.

Uniaxial tensile tests are performed under Instron platform at room temperature at crosshead speed of 50 mm·min^{-1}, and each test had been repeated at least three times.

3.1.3 Results and discussion

3.1.3.1 Interaction between [AEMIM] Br and polymer matrix

ATR-FTIR has been performed to detect the chemical structure of polymer substrate and LIonomers (see Figure 3-2). As for the pure [AEMIM] Br, the peak at 1668 cm^{-1} is attributed to -NH_2 bending mode, while the bands at 1563 and 1168 cm^{-1} are due to imidazole ring stretching vibration and the ring in-plane asymmetric stretching of imidazolium ring [27–31]. The peaks at 1780 and 1712 cm^{-1} of polymer substrate spectra belong to the asymmetric $\nu_{C=O}$ vibrations of the MA group and $\nu_{C=O}$ of carboxylic group. Then these two peaks disappear because of the addition of [AEMIM] Br, implying the adequate chemical reactions. At the same time, the presence of two peaks at 1773 and 1701 cm^{-1} in PPgMA/[AEMIM] Br blends assign to asymmetrical stretching and symmetrical stretching $\nu_{C=O}$ respectively [31–33], and it interprets the generation of the imide structure via cyclization of the acid and amide (Scheme 3-2).

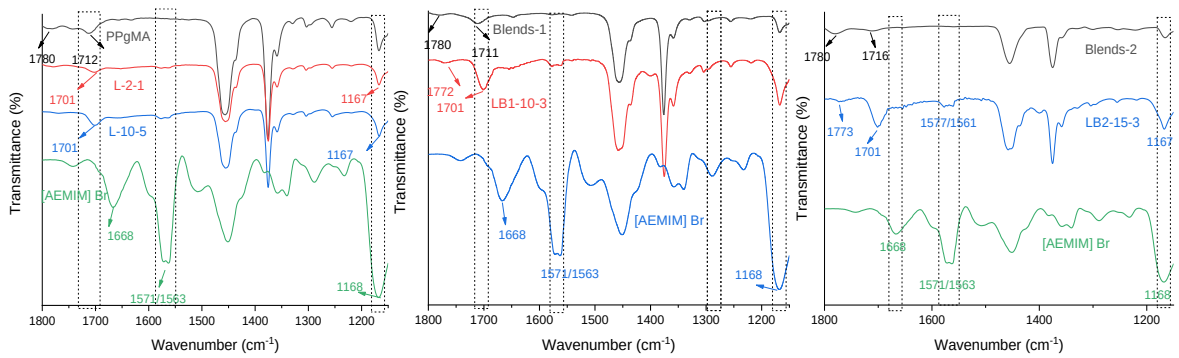

Figure 3- 2 ATR-FTIR spectra of matrix, [AEMIM] Br and LIonomers

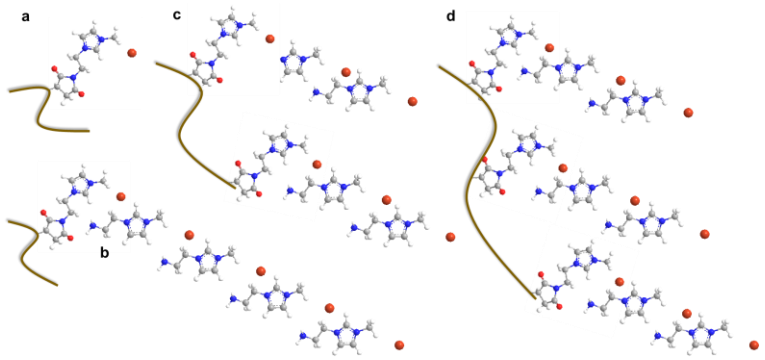

Scheme 3- 2 Formed "liquid-like branches" within LIonomers (a: L-2-1; b: L-10-5; c: LB1-10-3, d: LB2-15-3, the number and length of "liquid-like branches" are based on the molar ratio of [AEMIM] Br/MA)

3.1.3.2 The effect of [AEMIM] Br on rheological properties

Figure 3-3 indicates the dynamic viscosity as a function of angular frequency at 180 °C. All samples show shear thinning behavior at the whole detected angular frequency, and the addition of [AEMIM] Br leads to a significant increase in viscosity. At operating temperature, ILs exhibits very low viscosity (few mPa·s), thus it can't contribute to the reinforced viscosity of LIonomers alone [15], therefore the strengthened viscosity should be attributed exclusively to the ionic-network within LIonomer (Figure 3-1). As for the LIonomer L-2-1, ***a*** the formation of imide structure and ***b*** the cation-anion interaction among reacted $[EMIM]^+$ and corresponding Br^- anion take the responsible for the increased viscosity, by four times with the comparison of neat PPgMA. Then more addition of [AEMIM] Br (L-10-5) results in the considerable enhancement of viscosity, enhanced by 84 times. Because the excess [AEMIM] Br (partial after complete reaction with MA group to form the imide group) could generate one novel "liquid-like branches" (see Scheme 3-2 and Figure 3-1), leading to *i)* more crosslinking points among long "liquid-like branches" themselves and/or between long "liquid-like branches" and polymer chains, *ii)* the additional ionic-ionic interactions among nearby ionic liquids. Such self-assembly arrangements of [AEMIM] Br are created using generated imide group as the "head" and the cation/anion pairs composing [AEMIM] Br as the component via their initial ionic-ionic interactions. These

ionic-networks contribute to the reinforcement of viscosity. In addition, the nanostructuration morphology (TEM illustration in Figure 3-3) may also contribute to the improved molten viscosity [11]. Similar change trend in viscosity could be observed from LIonomers containing higher MA content, *e.g*. increased by 91 times in LB2-15-3, increased by 79 times in LB1-10-3 *vs* Blends-1.

On the other hand, with one given [AEMIM] Br content (10 wt.%), more addition of MA content produces a decrease of the dynamic viscosity from around 10^4 Pa·s of L-10-5 to around 9100 Pa·s of LB1-10-3. The increase of MA content provides more anchoring site on polymer backbone reducing the length of "liquid-like branches" (Scheme 3-2b *vs.* 3c). It highlights the critical role of the length of formed "liquid-like branches" on melting strength. In addition, considering the same length of generated "liquid-like branches" (LB1-10-3 *vs.* LB2-15-3), increasing the number of such branches (Scheme 3-2c *vs.* 3d) could also promote the shear viscosity at low frequency (see Figure 3-3).

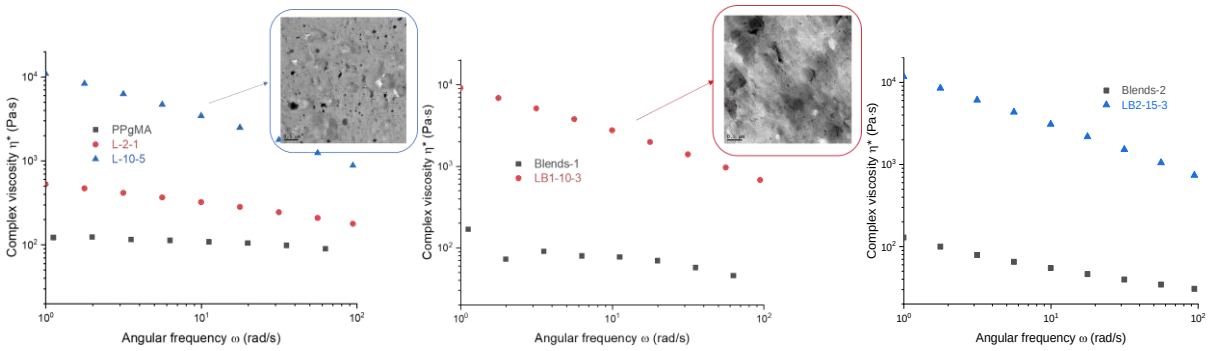

Figure 3- 3 Dynamic viscosity of matrix and LIonomers at 180 °C

3.1.3.3 Microstructure Characterization: Location Determination of [AEMIM] Br

The study of relaxation behavior is one very efficiency method to confine the location of introduced [AEMIM] Br, and insight the microstructure to interpret structuring mechanism. In this present, the dynamic mechanical analysis (DMA) has been carried out to detect the modification of relaxation temperature in amorphous region (see Figure 3-4 and Table 3-2).

On the spectra of all samples, three relaxation peaks are shown-one is located at

-47 °C due to the motions of small-chain groups in polymer, methyl and methylene groups [34]. A shift of this peak is not observed when IL is added to polymer which means the absence of ILs in this region. Most of the cooperating [AEMIM] Br must be located in the region close to the MA unit because of their reactivity and ionic interactions towards these groups. In addition, two peaks located at around 7 and 80 °C are assigned to the relaxation of mobile amorphous fraction (T_α (MAF)) and rigid amorphous fraction ($T_{\alpha'}$, (RAF)) respectively. The chains in mobile amorphous fraction display great mobility on a long range especially when the melting temperature is overpassed [35,36]. On the other side, the rigid amorphous fraction means the amorphous part confined between crystallites which are called tie chains and have a low mobility [35–37]. As a consequence, the RAF fraction displays the higher relaxation temperature, different from the glass transition temperature of materials. No significant alterations in T_α (MAF) are observed herein after the addition of [AEMIM] Br, whereas $T_{\alpha'}$ (RAF) change considerably. The measured $T_{\alpha'}$ (RAF) on LIonomer in comparison with 76 °C in PPgMA *vs.* 81 °C in L-2-1 *vs.* 83 °C in L-10-5, 74 °C in Blends-1 *vs.* 85 °C in LB1-10-3 indicate the formation of ionic aggregates in this area. They may act as the crosslinking points to restrain the motions of chain segments and any change of polymer chains. The “liquid-like branches” made from the resulting imide group as the "head" and the cation/anion pairs of [AEMIM] Br as the component within the LIonomers promote the reduced mobility as described previously. Consequently, the enhanced value of $T_{\alpha'}$ (RAF) is due to the effect of generated ionic networks.

On the other side, when chemical reactive sites increase (LIonomers based on Blends-2), the increase of $T_{\alpha'}$ (RAF) is not observed anymore. The $T_{\alpha'}$ (RAF) is reduced (from 78 to 69 °C) due to the higher amount of MA involving free volume affecting the balance of ionic interactor and increase $T_{\alpha'}$ (RAF). It suggests the low amount of [AEMIM] Br and/or the absence of ionic domains in RAF, as well as the presence of ionic enriched regions in MAF (4 °C in Blends-2 *vs.* 8 °C in LB2-15-3). Therefore, one may conclude the generation of long “liquid-like branches” (for example: L-10-5 see Scheme 3-2b) makes great contribution to the formation of ionic networks

due to the interactions among neighboring cation/anion pairs of “liquid-like branches” and/or the entanglement points between polymer chains and “liquid-like branches”, bringing about the improved relaxation behaviour.

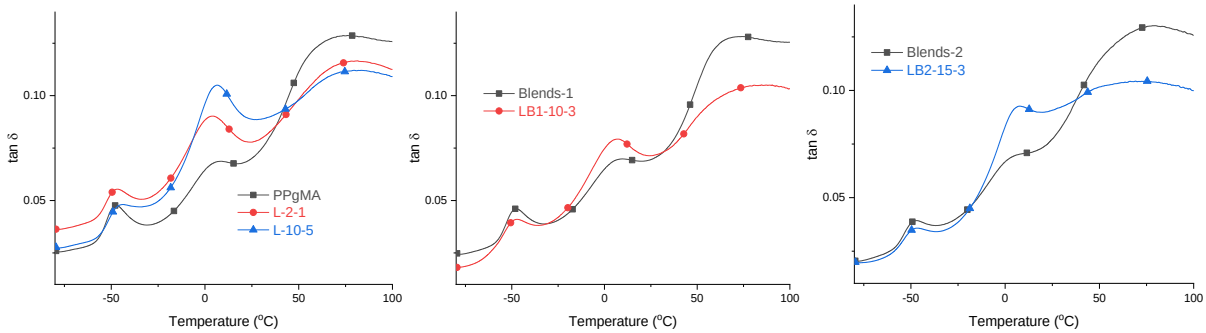

Figure 3- 4 Dynamic mechanical loss tangent (tan δ) vs temperature for all samples at 1Hz

Table 3- 2 Relaxation peak temperature values of all samples, β, α and α’ relaxations

Samples	T_β (°C)	T_α (MAF, °C)	$T_{\alpha'}$ (RAF, °C)
PPgMA	-47	7	76
L-2-1	-47	5	81
L-10-5	-44	6	83
Blends-1	-47	10	74
LB1-10-3	-47	8	85
Blends-2	-47	4	78
LB2-15-3	-46	8	69

3.1.3.4 Effect of introduced [AEMIM] Br on crystallization process

The DSC thermograms of polymers and LIonomers are reported in Figure S3-1. After erasing the thermal history, two melting peaks can be visualized on polymer matrix (PPgMA, Blends-1 and 2) highlighting the presence of two crystalline phases, while the only one melting peak of LIonomers indicates the transformation of crystalline phase because of the cooperative effect of [AEMIM] Br.

Table 3- 3 The T_c, X_c, and $t_{1/2}$ values of all samples at 5 °C·min^{-1}

Samples	$t_{1/2}$ (min)	T_c (°C)	X_c (%)
PPgMA	0.77	116.1	34.1
L-2-1	0.64	122.7	36.4
L-10-5	0.89	124.2	34.2
Blends-1	0.74	115.5	35.6
LB1-10-3	0.84	124.6	34.1
Blends-2	0.66	117.7	33.7
LB2-15-3	0.87	120.8	32.2

The crystallization half-time ($t_{1/2}$) originated from Jeziorny's non-isothermal crystallization kinetics [26] (see Figure S3-2) and crystallization temperature (T_c), crystallinity (X_c) values under 5 °C·min^{-1} (see Table S3-1) are collected in Table 3-3. The crystallization temperature of LIonomers is higher in comparison with corresponding matrix alone due to the addition of [AEMIM] Br. It means that ILs has a nucleating effect on PPgMA. The $t_{1/2}$ value is also a useful index to evaluate different crystallization rate, *i.e.* high $t_{1/2}$ value implies long time of crystallization and slow crystallization rate. For the same [AEMIM] Br content (10 wt%, L-10-5 *vs.* LB1-10-3), the $t_{1/2}$ decreases with the increase of MA content: 0.89 min in L-10-5 > 0.84 min in LB1-10-3. By increasing MA groups, more interactions between COO^- and cation are generated (imide groups by Scheme 3-2b *vs.* 3c) and this introduction continuum, *i.e.* decreasing the length of "liquid-like" branch, does not inhibit the crystallization. Rather, this structuration promotes the crystallization. On the other side, with one given MA content, the increase of [AEMIM] Br content, *i.e.* increasing the length of "liquid-like branches" (Scheme 3-2a *vs.* 3b), delays the crystallization process. It is revealed by the increased $t_{1/2}$ value: 0.64 min in L-2-1 to 0.89 min L-10-5. Such delayed crystallization process could be explained by *i)* the change of configuration is restrained by nearby [AEMIM] Br due to their interactions, restricting the folding

rearrangement of the polymer chains [38]; *ii)* the generated long "liquid-like branches" due to high ILs content (Scheme 3-2a *vs.* 3b) may create more crosslinking points with polymer chains, limiting the motions of polymer chains into ordered ones; *iii)* long "liquid-like branches" (Scheme 3-2b) may produce extra inter-chain crosslinking points among them, generating additional resistance for any change of chain segment.

3.1.3.5 Effect of introduced [AEMIM] Br on crystalline phase

Figure 3-5 and Table 3-4 collect the WAXD and crystal size of all samples. The monoclinal α-phase [39] at Bragg reflections 2θ ≈ 14.0° [α110], 16.8° [040], 18.4° [130], 25.3° [060&150], 28.5° [220] and 42.6° [212] and the syndiotactic monoclinic crystalline [40] at 2θ ≈ 23.6° (002) are identified on PPgMA matrix. In addition, the β-crystalline form is generated due to the addition of [AEMIM] Br, which is defined by Equation 3- 7 and collected in Table 3-4. The LB1-10-3 exhibits the larger β-form crystal (58.4 nm) and fraction (11.2%) than that of L-10-5 (51.6 nm, 9.3%). It's known that the β-phase crystalline form is not as stable as α-form, thus its presence which gives a proof of the strong impact on crystalline phase caused by [AEMIM] Br.

$$K = \frac{I_{300}}{I_{300}+I_{110}+I_{040}+I_{130}} \quad \text{Equation 3- 7 [41]}$$

where K represents the relative amount of β phase, while I_{300}, I_{110}, I_{040} and I_{130} are the intensities of the corresponding diffraction reflections at 2θ ≈ 16.0°, 14.0°, 16.8° and 18.4°.

It was reported that some ImILs could behave as the nucleating agent leading to a significant increase in nuclei number [42]. In their study, the formed nuclei grow in a multi-layered structure, greatly reducing the spherulite size to no measurable dimension. In this work, bigger crystals are obtained by the comparison of LIonomers with its corresponding matrix. Because the added [AEMIM] Br may act as a nucleating inhibitor to some extent, allowing the matrix to provide more place for these generated nuclei growing into larger crystals. This proposition is evidenced by the reduced value of the nuclei factor (N, by Equation 3-8) of LIonomers compared to one of corresponding polymer matrix, as shown in Table 3-4. In addition, the V value (average

crystallization rate) calculated from Equation 3-9 verifies the order of $t_{1/2}$ value obtained from the non-isothermal crystallization process. The LIonomer possessing the longest (L-10-5 see Scheme 3-2b) and shortest (L-2-1 see Scheme 3-2a) "liquid-like branches" exhibit the slowest (16.33 nm·min^{-1}) and fastest (23.2 nm·min^{-1}) crystallization rate respectively, consistent with the largest (0.89 min) and smallest (0.64 min) $t_{1/2}$ value correspondingly.

$$N = \frac{X_c}{A} \times 100 \qquad \text{Equation 3- 8}$$

$$V = \frac{A}{t_{1/2}} \qquad \text{Equation 3- 9}$$

where the value of N and V (nm·min^{-1}) represent the nuclei factor and the average crystallization rate in each sample, while X_c, $t_{1/2}$ and A are obtained from DSC at 5 K·min^{-1} and WAXD respectively.

Note: these two equations are created for the first time to describe the influence on nuclei and crystallization speed by combining the crystallization half-time ($t_{1/2}$), crystallinity (X_c) and average spherulite size (A) according to three hypothesises that *i)* the area of tested sample is regarded as 1; *ii)* all crystals hold the same efficiency in changing conformation of polymer chains; *iii)* all spherulites end up being the same size.

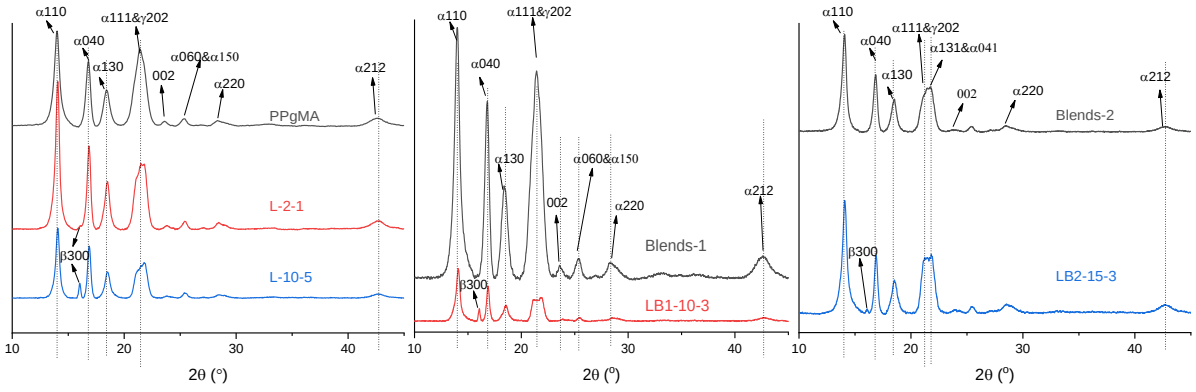

Figure 3- 5 WAXD curves of polymer matrix and LIonomers

To sum up, the [AEMIM] Br and MA content could affect the crystallization process, since they are very related to the generated ionic networks within LIonomers. High

molar ratio, *i.e.* long “liquid-like” branch, inhibits the crystallization. Considering the LB1-10-3 *vs.* LB2-15-3 containing constant “liquid-like” branch (see Scheme 3-2c *vs.* 2d), the change of $t_{1/2}$, T_c and X_c interprets the retarded crystallization process due to the most reactive sites between the polymer backbone and [AEMIM] Br cation within latter case. Moreover, unlike the role of phosphonium-based ionic liquids in the literature [38], the addition of [AEMIM] Br doesn’t reduce the crystal size (see Table 3-4) and weak the macroscopic mechanical property (see the strain-stress curves in Figure S3-3), *i.e.* the Young’s modulus of PPgMA is reinforced from 456 MPa into 819 MPa and 690 MPa by the incorporation 2 and 10 wt.% [AEMIM] Br respectively, and modulus as well as yield stress increase by more than 50% and 30% respectively by introducing 10 wt.% [AEMIM] Br into Blends-1 matrix.

Table 3- 4 The crystalline form and crystal size of all samples

Samples	$D_{[110]}$	$D_{[040]}$	$D_{[130]}$	$D_{[300]}$	K (%)	Average size[a]	N	V ($nm \cdot min^{-1}$)
PPgMA	12.7	18.2	12.8	-	-	12.7	2.70	16.43
L-2-0.97	17.3	22.1	15.2	-	-	14.9	2.45	23.20
L-10-5.34	18.8	26.3	14.5	51.6	9.3	14.5	2.35	16.33
Blends-1	12.3	17.7	12.7	-	-	12.1	2.94	16.38
LB1-10-3.15	16.1	27.9	13.2	58.4	11.2	14.7	2.30	17.49
Blends-2	15.4	21.1	14.8	-	-	13.4	2.51	20.32
LB2-10-1.72	14.1	26.6	12.4	52.5	9.4	14.6	2.13	17.78
LB2-15-2.74	26.2	25.5	13.6	-	-	15.3	2.11	17.54

D being the crystal size, [a]the value is calculated crystalline size except β-form.

3.1.4 Conclusions

In this article, the LIonomer as the 2.0 generation of ionomer has been designed and adjusted by changing the MA contents and 1-aminoethyl-3-methylimidazolium Bromide ([AEMIM] Br) concentration. ATR-FTIR demonstrates the generation of imide groups in the PPgMA/[AEMIM] Br mixture and the alignment of new "liquid-like branches" using the formed imide units as "heads" and the cation/anion combination

through its initial interactions as components. Rheological property confirms the effect of these added [AEMIM] Br, and concludes that four factors could impact the melting strength considerably, *i.e.* ***a*** the number of chemical reaction points (the MA content), ***b*** the length of "liquid-like branches", ***c*** the ionic-ionic interactions among long "liquid-like branches" and/or crosslinking points between "liquid-like branches" and polymer chains, ***d*** generated ionic enriched zones. It concludes that the long "liquid-like branches" result in significant improvement for melting viscosity, up to 10^4 Pa·s in L-10-5 (increased by 84 times L-10-5 *vs.* PPgMA). On the other hand, with one constant [AEMIM] Br content the decreased length of the "liquid-like branches" leads to the reduce of melting viscosity, by from 1.1×10^4 Pa·s (L-10-5) into 9.2×10^3 Pa·s (LB1-10-3). With one same length of “ionic branched” chains, more interacting points (LB1-10-3 *vs.* LB2-15-3) between ionic liquids and polymer backbone also contributes to the improvement of molten viscosity. Besides, the introduced [AEMIM] Br-10 could act as the nucleating inhibitor to some extent. Either the long ionic branched chains or more chemical reactive points could bring some disadvantages to the nuclei and crystallization rate, whereas improve the mechanical properties. Furthermore, these added AEMIM] Br prefer to lie in the area close to MA units, and the region (RAF or MAF) of generated ionic clusters depends greatly on the MA content. Such understanding of the effect on molten strength, crystallization performance, phase structure and microstructure in this study could realize the application of lightweight materials in the future.

3.1.5 References

[1] Ma Y, Yang G, Xie L. Morphology, nonisothermal crystallization behavior and mechanical properties of polypropylene modified by ionomers[J]. Journal of Macromolecular Science, Part B, 2014, 53(12): 1829-1845.

[2] Aitken B S, Buitrago C F, Heffley J D, et al. Precision ionomers: Synthesis and thermal/mechanical characterization[J]. Macromolecules, 2012, 45(2): 681-687.

[3] Qiao X, Weiss R A. Nonlinear rheology of lightly sulfonated polystyrene ionomers[J]. Macromolecules, 2013, 46(6): 2417-2424.

[4] Ling G H, Wang Y, Weiss R A. Linear viscoelastic and uniaxial extensional rheology of alkali metal neutralized sulfonated oligostyrene ionomer melts[J]. Macromolecules, 2012, 45(1): 481-490.

[5] Weiss R A, Zhao H. Rheological behavior of oligomeric ionomers[J]. Journal of Rheology, 2009, 53(1): 191-213.

[6] Zhang L, Brostowitz N R, Cavicchi K A, et al. Perspective: Ionomer research and applications[J]. Macromolecular Reaction Engineering, 2014, 8(2): 81-99.

[7] Kirkmeyer B P, Weiss R A, Winey K I. Spherical and vesicular ionic aggregates in Zn-neutralized sulfonated polystyrene ionomers[J]. Journal of Polymer Science Part B: Polymer Physics, 2001, 39(5): 477-483.

[8] Eisenberg A, Hird B, Moore R B. A new multiplet-cluster model for the morphology of random ionomers[J]. Macromolecules, 1990, 23(18): 4098-4107.

[9] Yan W, Zhang X, Zhu Y, et al. Synthesis and characterization of self-crosslinkable zinc polyacrylate latices at room temperature[J]. Iranian Polymer Journal, 2012, 21(9): 631-639.

[10] Ro A J, Huang S J, Weiss R A. Synthesis and properties of random poly (lactic acid)-based ionomers[J]. Polymer, 2009, 50(5): 1134-1143.

[11] Li Y, Yao Z, Chen Z hua, et al. High melt strength polypropylene by ionic modification: Preparation, rheological properties and foaming behaviors[J]. Polymer, 2015, 70: 207-214.

[12] Wu F, Xie S Y, Chen J H, et al. Regulating the crystallizing and rheological behaviors of poly (butylene succinate) by incorporating novel macromolecular ionomers[J]. Journal of Applied Polymer Science, 2018, 135(24): 45545.

[13] Soares R R, Carone C, Einloft S, et al. Synthesis and characterization of waterborne polyurethane/ZnO composites[J]. Polymer Bulletin, 2014, 71(4): 829-838.

[14] Han S I, Im S S, Kim D K. Dynamic mechanical and melt rheological properties of sulfonated poly (butylene succinate) ionomers[J]. Polymer, 2003, 44(23): 7165-7173.

[15] Yousfi M, Livi S, Duchet-Rumeau J. Ionic liquids: A new way for the compatibilization of thermoplastic blends[J]. Chemical Engineering Journal, 2014, 255: 513-524.

[16] Xing C, Zhao L, You J, et al. Impact of ionic liquid-modified multiwalled carbon nanotubes on the crystallization behavior of poly (vinylidene fluoride)[J]. The Journal of Physical Chemistry B, 2012, 116(28): 8312-8320.

[17] Maka H, Spychaj T, Pilawka R. Epoxy resin/ionic liquid systems: the influence of imidazolium cation size and anion type on reactivity and thermomechanical properties[J]. Industrial & Engineering Chemistry Research, 2012, 51(14): 5197-5206.

[18] Silva A A, Livi S, Netto D B, et al. New epoxy systems based on ionic liquid[J]. Polymer, 2013, 54(8): 2123-2129.

[19] Zhu S, Wu Y, Chen Q, et al. Dissolution of cellulose with ionic liquids and its application: a mini-review[J]. Green Chemistry, 2006, 8(4): 325-327.

[20] Lagrost C, Hapiot P, Vaultier M. The influence of room-temperature ionic liquids on the stereoselectivity and kinetics of the electrochemical pinacol coupling of acetophenone[J]. Green Chemistry, 2005, 7(6): 468-474.

[21] Nakajima H, Ohno H. Preparation of thermally stable polymer electrolytes from imidazolium-type ionic liquid derivatives[J]. Polymer, 2005, 46(25): 11499-11504.

[22] Ngo H L, LeCompte K, Hargens L, et al. Thermal properties of imidazolium ionic liquids[J]. Thermochimica Acta, 2000, 357: 97-102.

[23] Tsunashima K, Sugiya M. Physical and electrochemical properties of room temperature ionic liquids based on quaternary phosphonium cations[J].

Electrochemistry, 2007, 75(9): 734-736.

[24] Hou L, Livi S, Gérard J F, et al. LIonomers-New Generation of Ionomer: Understanding of Their Interaction and Structuration as a Function of the Tunability of Cation and Anion[J]. Polymers, 2023, 15(2): 370.

[25] Clark E J, Hoffman J D. Regime III crystallization in polypropylene[J]. Macromolecules, 1984, 17(4): 878-885.

[26] Jeziorny A. Parameters characterizing the kinetics of the non-isothermal crystallization of poly (ethylene terephthalate) determined by DSC[J]. Polymer, 1978, 19(10): 1142-1144.

[27] Zhou X, Jing G, Liu F, et al. Mechanism and kinetics of CO_2 absorption into an aqueous solution of a triamino-functionalized ionic liquid[J]. Energy & Fuels, 2017, 31(2): 1793-1802.

[28] Cai Y, Peng Y, Song G. Amino-functionalized ionic liquid as an efficient and recyclable catalyst for Knoevenagel reactions in water[J]. Catalysis Letters, 2006, 109(1): 61-64.

[29] Xiang W, Shen C, Lu Z, et al. CO_2 cycloaddition over ionic liquid immobilized hybrid zeolitic imidazolate frameworks: Effect of Lewis acid/base sites[J]. Chemical Engineering Science, 2021, 233: 116429.

[30] Li Y, Zhang Q, Xie X, et al. Enhanced electromagnetic wave absorption properties of ionic liquid doped graphene[J]. Journal of Materials Science: Materials in Electronics, 2020, 31(16): 13273-13283.

[31] Zhou X, Zhang Y, Huang Z, et al. Ionic liquids modified graphene oxide composites: a high efficient adsorbent for phthalates from aqueous solution[J]. Scientific Reports, 2016, 6(1): 1-10.

[32] Létoffé A, Hoppe S, Lainé R, et al. Resilience improvement of an isotactic polypropylene-g-maleic anhydride by crosslinking using polyether triamine agents[J]. Polymer, 2019, 179: 121655.

[33] Suckow M, Zschoche S, Heinrich G, et al. New reactive poly (ionic liquid) s synthesized by polymer analogous conversion of maleic anhydride containing

polymers[J]. Polymer, 2016, 96: 20-25.

[34] Bajsić E G, Šmit I, Leskovac M. Blends of thermoplastic polyurethane and polypropylene. I. Mechanical and phase behavior[J]. Journal of Applied Polymer Science, 2007, 104(6): 3980-3985.

[35] Ma Q, Georgiev G, Cebe P. Constraints in semicrystalline polymers: Using quasi-isothermal analysis to investigate the mechanisms of formation and loss of the rigid amorphous fraction[J]. Polymer, 2011, 52(20): 4562-4570.

[36] Arnoult M, Dargent E, Mano J F. Mobile amorphous phase fragility in semi-crystalline polymers: Comparison of PET and PLLA[J]. Polymer, 2007, 48(4): 1012-1019.

[37] Wang L, Wang Y nan, Huang Z gang, et al. Heat resistance, crystallization behavior, and mechanical properties of polylactide/nucleating agent composites[J]. Materials & Design (1980-2015), 2015, 66: 7-15.

[38] Yang J, Pruvost S, Livi S, et al. Understanding of versatile and tunable nanostructuration of ionic liquids on fluorinated copolymer[J]. Macromolecules, 2015, 48(13): 4581-4590.

[39] Qiao X, Zhang Y, Zhang Y. Maleic anhydride grafted polypropylene as a coupling agent for polypropylene composites filled with ink-eliminated waste paper sludge flour[J]. Journal of Applied Polymer Science, 2004, 91(4): 2320-2325.

[40] Clark E S. Unit cell information on some important polymers[M]. Physical Properties of Polymers Handbook. Springer, 2007: 619-624.

[41] Zipper P, Janosi A, Wrentschur E. Scanning X-ray scattering of mouldings from semicrystalline polymers[J]. Journal de Physique IV, 1993, 3(C8): C8-33-C8-36.

[42] He L, Sun J, Wang X, et al. Facile and effective promotion of β crystalline phase in poly (vinylidene fluoride) via the incorporation of imidazolium ionic liquids[J]. Polymer International, 2013, 62(4): 638-646.

3.1.6 Supporting Information

1. DSC thermograms of all polymer matrix and LIonomers

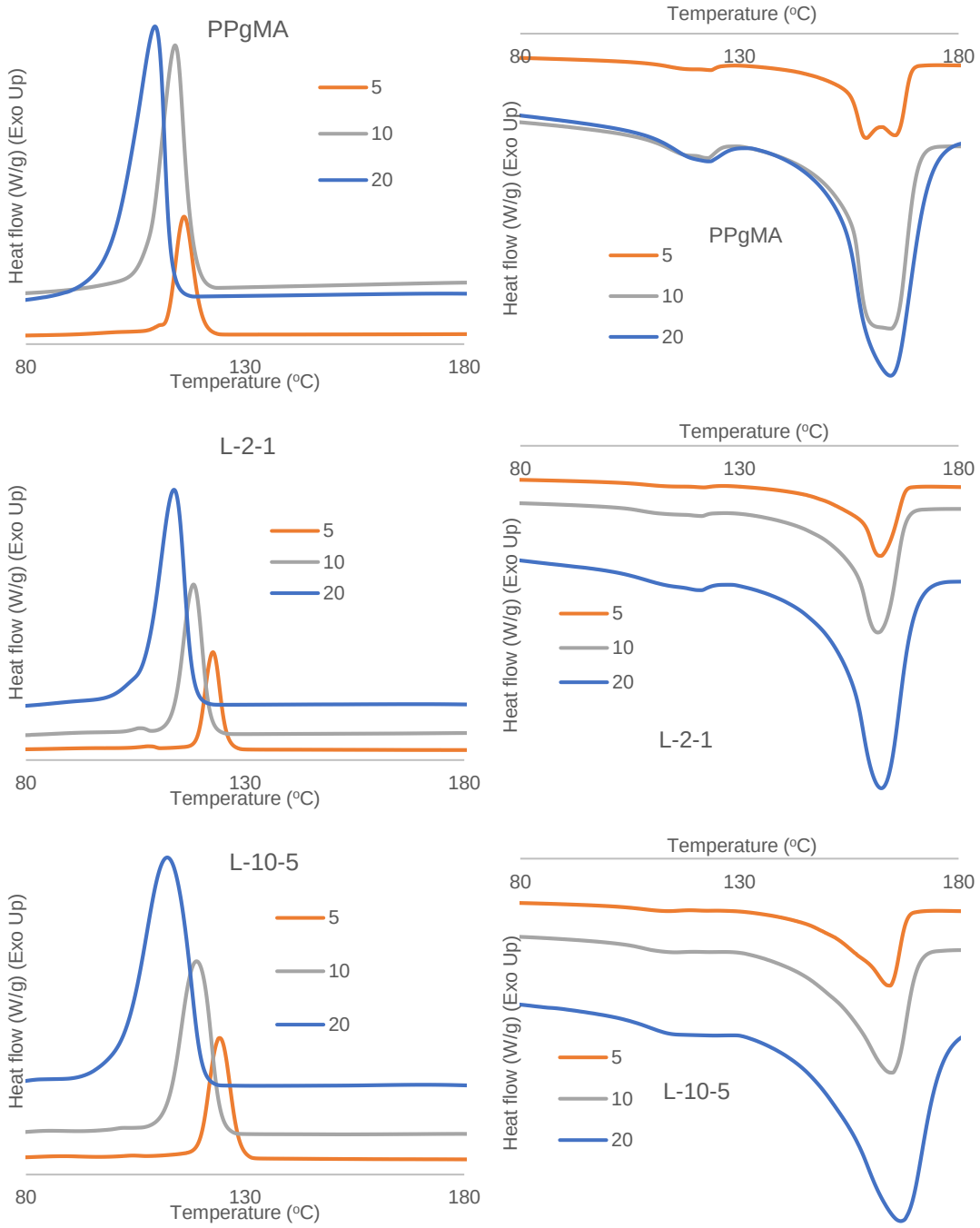

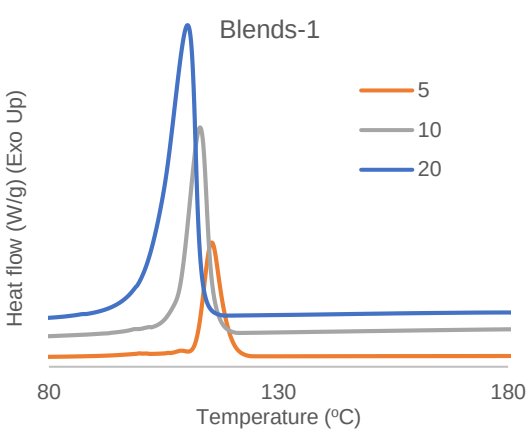

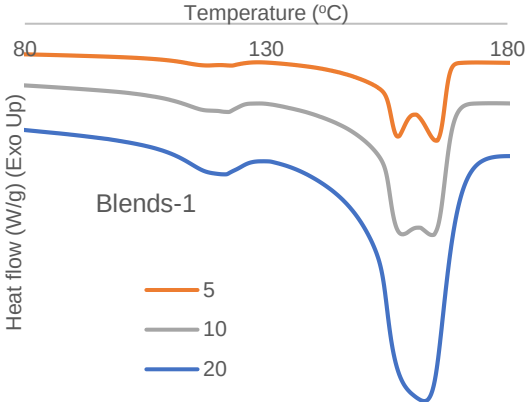

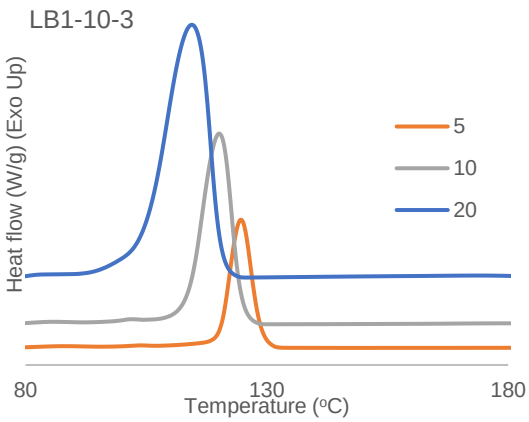

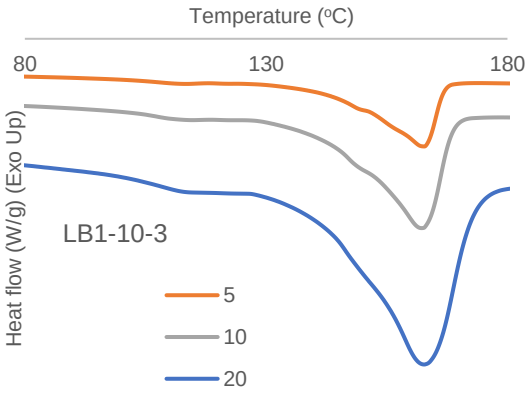

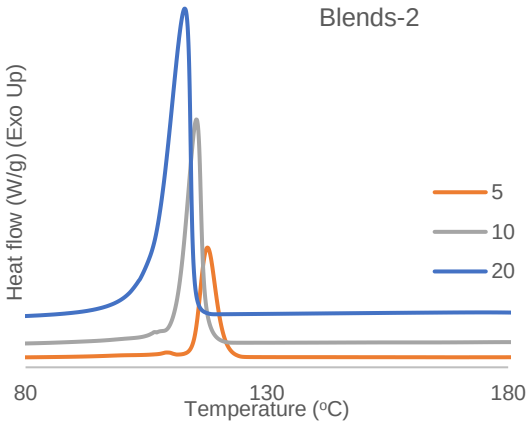

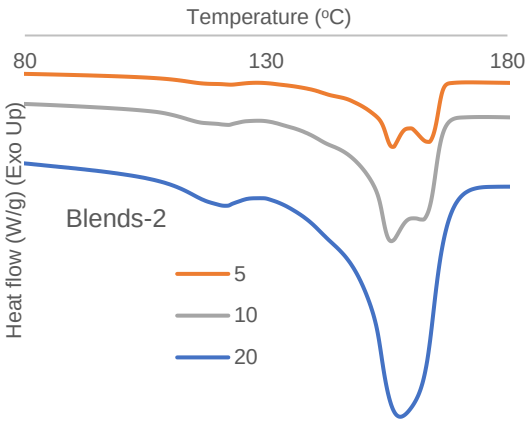

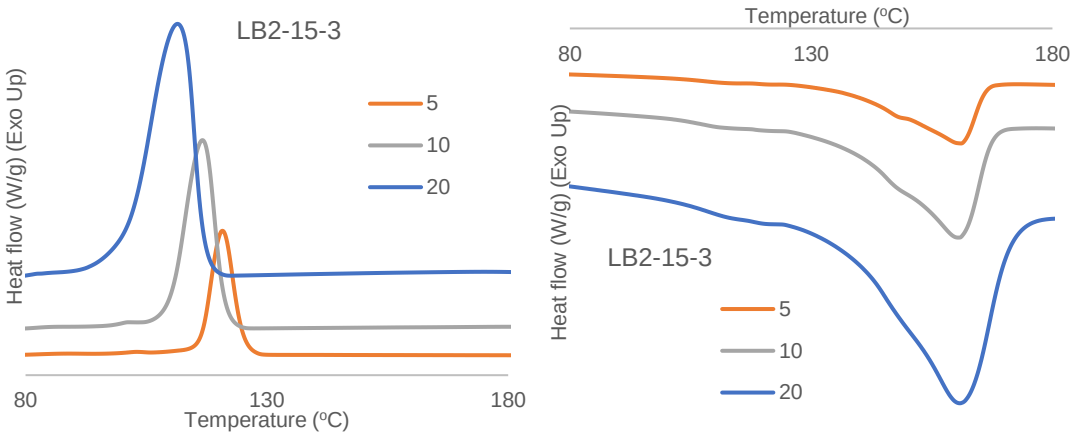

Figure S3- 1 The DSC curves at first cooling and second heating run of all samples

2. The $ln[-ln(1-Xt)]$ vs lnt plots according to Jeziorny's non-isothermal crystallization model

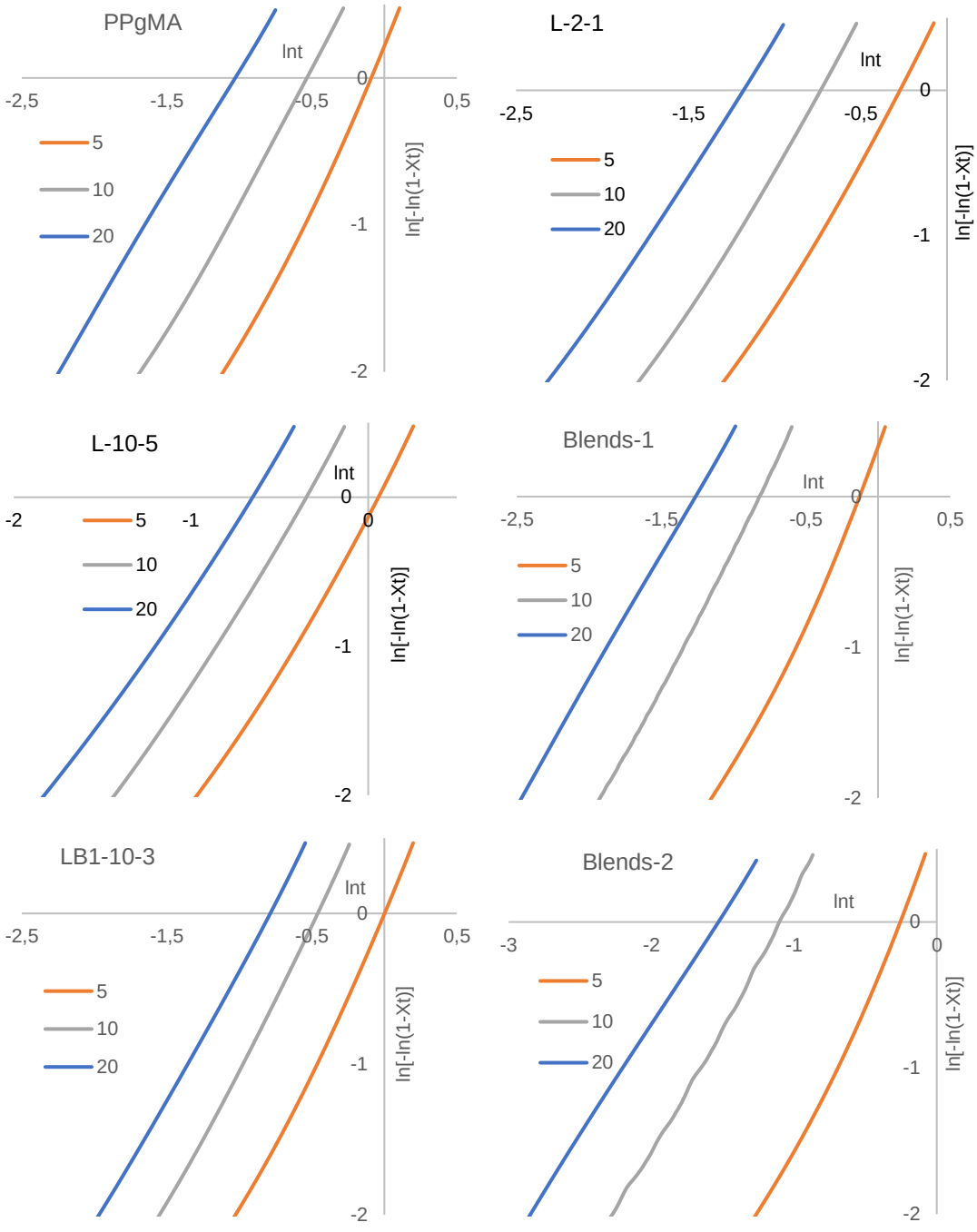

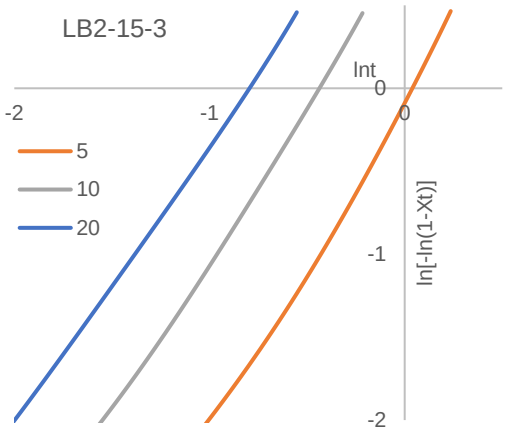

Figure S3- 2 The curves of $ln[-ln(1-Xt)]$ vs lnt obtained from Jeziorny's model

3. The parameters of non-isothermal crystallization process based on Jeziorny's theory

Table S3- 1 The parameters of non-isothermal crystallization process based on Jeziorny's theory

Samples	Φ (K·min^{-1})	$t_{1/2}$ (min)	n	Z_t	T_m (°C)	T_c (°C)	X_c (%)
PPgMA	5	0.77	2.01	1.17	159.0/165.6	116.1	34.1
	10	0.48	1.78	2.68	164.2	114.1	35.5
	20	0.28	1.65	5.55	164.5	109.5	31.6
L-2-1	5	0.64	2.00	1.70	162.2	122.7	36.4
	10	0.40	1.91	4.05	161.7	118.2	35.2
	20	0.25	1.78	8.15	162.5	113.8	34.4
L-10-5	5	0.89	2.01	0.88	164.4	124.2	34.2
	10	0.58	1.86	1.94	164.8	118.9	34.2
	20	0.42	1.74	3.10	166.9	112.3	32.8
Blends-1	5	0.74	1.96	1.25	157.3/165.3	115.5	35.6
	10	0.36	1.83	4.45	158.3/164.5	113.0	35.7
	20	0.23	1.66	8.16	162.9	110.2	33.6
LB1-10-3	5	0.84	2.00	0.98	162.8	124.6	34.1
	10	0.52	1.87	2.34	162.3	120.1	33.8
	20	0.37	1.72	3.86	162.8	114.4	32.4
Blends-2	5	0.66	2.03	1.62	156.2/163.8	117.7	33.7
	10	0.27	1.72	6.60	156.0/162.5	115.4	33.3
	20	0.17	1.52	10.34	158.0	113.1	32.5
LB2-15-3	5	0.87	1.96	0.91	161.1	120.8	32.2
	10	0.53	1.91	2.31	160.5	116.7	30.6
	20	0.36	1.68	3.82	160.9	111.4	29.2

Note: φ: cooling rate (K.min^{-1}), T_m: melting temperature (°C), T_c: crystallization temperature (°C) and X_c: crystallinity (%).

4. Mechanical tests results

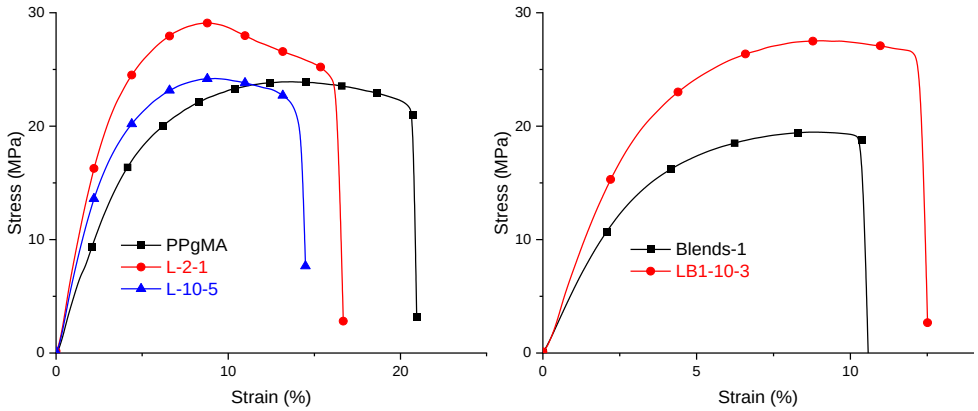

Figure S3- 3 The mechanical results at room temperature

3.2 Understanding and Compressive Investigation between Conventional and the next generation of Ionomers: Zn-Ionomer versus LIonomers

3.2.1 Introduction

Ionomers are defined as macromolecules owning one type of ionic/ionisable groups combined with appropriate counter ions. The polymer chains usually carry acid anions (such as carboxylic, phosphonate, and sulfonic acids) [1,2] with less than 15 mol. % of ionic groups. The counter ions usually consist of metal cations such as Al^{3+}, Zn^{2+} or Na^{+} which are introduced from the corresponding salts. Within ionomers, the existing ion-pair interactions act as crosslinks between chain segments (Figure 3-6a [1,2]). A significant restriction of polymer chain dynamics is thus induced [3,4]. Consequently, the overlap of restricted regions produces large, continuous, mobility-constrained areas containing microphase-separated clusters [5]. Therefore, physically and ionically crosslinked polymers are formed [6–11] influencing the crystallinity rate [12]. Such ionic type of structuration of matter may also bring about other modifications in solid and molten states. The reduced segmental motions are related to the generation of ionic multiplets, *i.e.* ionic clusters, due to the metal coordination of Ag^{+} or Zn^{2+} [13]. Except for the trend for the glass transition to increase with the interaction strength of the ion pairs within PLA-based ionomers, the strong polar interactions also lead to an enhancement of the melt elasticity and viscosity [14,15]. On another hand, the viscosity in molten state and mechanical properties of sulfonated polystyrene are strongly modified thanks to the presence of ionic clusters [16]. In fact, the medium could even behave as a solid due to the presence of ionic aggregates-based within Zn-neutralized sulfonated polystyrene-based ionomer [7]. Similar changes of physical properties were also observed for polypropylene-based ionomers [5]. In fact, their viscosity and elasticity in molten state of PP ionomers based on zinc acetate, ammonia, methylamine, or dimethylamine could be significantly improved compared to neat maleic anhydride-grafted polypropylene (PPgMA) [17]. According to this study, the melt strength has been

improved even in comparison to commercial products because of the formation of branched-chain structures [18]. On the other hand, ionic liquids (ILs) are attractive compounds due to their outstanding anion-cation combinations, and some desired physic-chemical properties could be customized by changing the nature of the cation or the anion [19–22]. The dispersion of ILs in polymer could allow to design a structuration at nanoscale and tailor the overall physical properties of the resulting materials. For example, 1-butyl-3-methylimidazolium hexafluorophosphate can be completely miscible with PVDF under negative interaction parameter (-2.84 calculated by the revised Nishi–Wang equation) [23]. According to this study, in addition to the modifications on stretchability, the PVDF/IL blends illustrate outstanding antistatic behaviours thanks to the ionic conductivity of the ionic liquid itself. In addition, ionic liquids may reinforce the fracture behaviour by influencing the spherulitic morphologies [24] since mechanical performance is very related with the spherulitic morphologies, or act as the plasticizer weakening the mechanical property of polymer backbone [25,26].

In this present paper, using PPgMA as basic component and introducing various ionic liquids, a new generation of ionic polyolefin polymers, denoted as LIonomers, are designed with tailored physical properties according to *i)* the functional group, *i.e.* 1-aminoethyl-3-methylimidazolium bromide ([AEMIM] Br) *vs.* 1-ethyl-3-methylimidazolium diethyl phosphate (EMIM DEP), and *ii)* the IL content, *i.e.* 2 *vs.* 10 wt.%. Within the polypropylene matrix, large and continuous ionic structures must exist from the interactions of the COO^- groups of the PPgMA and the ImIL ion-pairs. Figure 3-6b represents the expected nano/microstructures generated from the ionic species. Such self-assembly behaviours have been realized recently [27]. Herein, in addition to introduce the tuneability of ionic liquids (the presence of functionated-amino group), the performances of the resulting PPgMA/ImIL blends are then compared to the conventional Zn-PP ionomer processed from the addition of Zn acetate to PPgMA. The conclusions should be helpful to conclude the effect of the generated ionic microstructures of different LIonomers and conventional ionomers. In this study, we aim to explore *i)* the effect of different interactions within PPgMA/ILs belnds, *i.e.*

covalent bond *vs.* polar/ionic-ionic interactions according to the ILs nature, on the solid-molten properties; *ii)* what is the various influence of ImIL and Zn^{2+} on the crystallization process, the crystalline morphism, and consequently on mechanical performances.

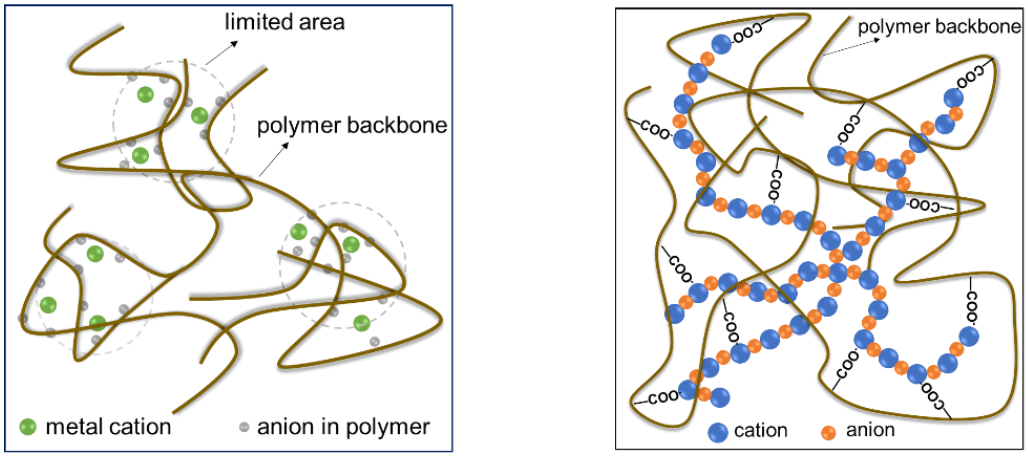

a b

Figure 3- 6 Schematic of (a) ionomer microstructure; and (b) targeted diagram of PPgMA/ImIL blends

3.2.2 Experimental Section

3.2.2.1 Materials

PPgMA was supplied from Arkema (1 wt.%, OREVAC® CA 100). Two imidazolium-based ionic liquids (ImILs) supplied from TCI and Chemfish Tokyo CO., LTD (Table 3-5) were chosen to investigate the role of amino group making ILs reactive towards PPgMA, *i.e.* 1-aminoethyl-3-methylimidazolium bromide ([AEMIM] Br) *vs.* non-reactive ILs (1-ethyl-3-methylimidazolium diethyl phosphate (EMIM DEP). Zinc acetate was produced by Sigma-Aldrich.

Table 3- 5 Structure of used ImILs

Cation	Anion	Designation
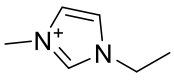	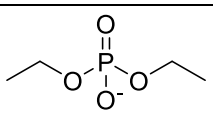	EMIM DEP
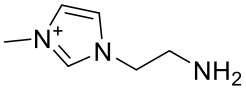	Br^-	[AEMIM] Br

3.3.2.2 Samples preparation and Instruments

Before extrusion, PPgMA pellets were dried at 70°C for 12 hours to remove the water uptake. The pre-mixture of PPgMA and various additives (ImIL and Zn^{2+} Ac) were prepared using a 15g-capacity DSM micro-extruder (Midi 2000 Heerlen, NL) with co-rotating screws (length-to-diameter (L/D) ratio: 18). The blends were processed at 180°C for 5 min under a 100 rpm speed and injected in a 10 cm^3 mould at 30°C to obtain disk or dumbbell-shaped specimens. Scheme 3-3 indicates the detailed preparation diagram, and Table 3-6 describes the polymer/IL mixtures in function of the additive nature (ImIL and Zn^{2+} Ac), and of their content (2 and 10 wt.%).

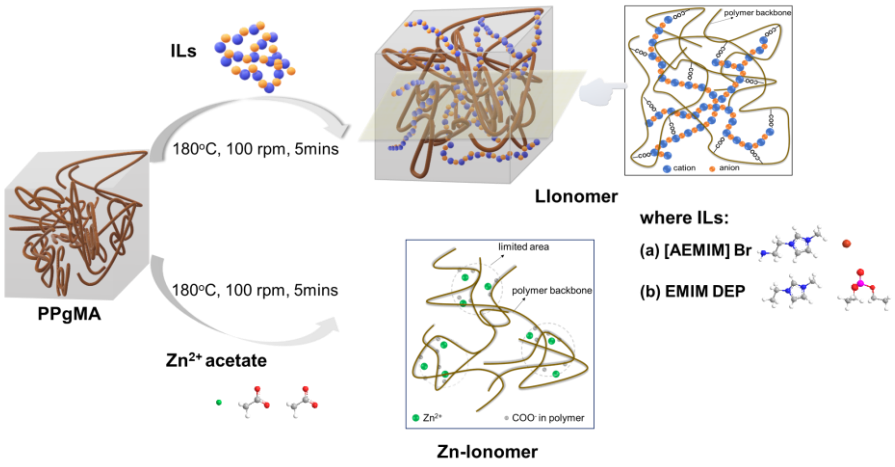

Scheme 3- 3 Preparation diagram of LIonomers and Zn-Ionomer

Table 3- 6 Details of LIonomers and Zn-Ionomers in this study

Polymer matrix	Additive	Content (wt.%)	Abbreviations
PPgMA	EMIM DEP	2	L-EMIM DEP-2
		10	L-EMIM DEP-10
	[AEMIM] Br	2	L-[AEMIM] Br-2
		10	L-[AEMIM] Br-10
	Zinc Acetate	2	Zn-Ionomer-2
		10	Zn-Ionomer-10

The dispersion of additives (ImILs and Zn^{2+}Ac) within PPgMA is determined by

transmission electron microscope (TEM, Phillips CM 120) at an accelerating voltage of 120kV. The samples were obtained as thin layers using an ultramicrotome equipped with a diamond knife. Then, the ultrathin polymer layers were set on the TEM grids (Carbon Film-Copper, 300 mesh, EMS) and analyzed.

The Nuclear Magnetic Resonance (Bruker Avance III 400 MHz) and Fourier-Transform Infrared spectroscopies (FT-IR, Nicolet iS10) are measured together to characterize the nature of the established interactions (ionic-ionic/polar or covalent bonding) within PPgMA blends. ^{1}H and ^{31}P NMR spectra of ionic liquids and LIonomers processed on PPgMA8 (8wt.% MA) were recorded using a Bruker Avance III 400 MHz at 373K. All materials were dissolved in chlorobenzene-D5 (C_6D_5Cl). The chemical shifts (δ) are expressed in ppm relative to the internal reference C_6D_5Cl for ^{1}H nuclei. At room temperature, the ionic liquids and corresponding LIonomers were characterized by FT-IR (Nicolet iS10) under attenuated total reflection (ATR) mode.

The rheology property and the relaxation behaviour were measured on the platform ARES-G2 rheometer (SN#4010-0255, TA Instrument, New Castle, DE, USA). The complex viscosity as a function of shear frequency were plotted at 180°C under the protection of nitrogen atmosphere. The geometry herein is parallel plate with a diameter 25 mm. The curves of loss tangent (tan δ) vs temperature were recorded by 3°C·min^{-1} with a temperature range -80/100°C.

Uniaxial extensional measurement is conducted using a second-generation Sentimental Extensional rheometer universal testing platform (SER-G2) detachable fixture (Xpansion Instruments LLC) mounted on the DHR-G2 rheometer. Experiments are run at constant elongational rates ranging from 1 to 10 s^{-1}.

Differential scanning calorimetry (DSC) (Q10 TA Instrument) is carried out to record the thermal property at 5, 10, and 20 K.min^{-1}. The crystallinity (X_c) is defined by Equation 3- 10:

$$X_c = \frac{\Delta H_f}{(1-m)\Delta {H_f}^0} \quad \text{Equation 3- 10}$$

where H_f^0 being 209J/g [25] corresponding to the melting enthalpy of 100%

crystallized polymer, ΔH_f being the melting enthalpy of samples and measured by DSC, and m being the mass fraction of ImIL. While Jeziorny's [26] non-isothermal crystallization model is employed to explore the crystallization procedure:

$$\ln[-\ln(1-X_t)] = \mathrm{nlnt} + \ln Z_t \quad \text{Equation 3- 11}$$

$$X_T = \frac{\int_{T_0}^{T_c}(\frac{dH_c}{dT})/dT}{\int_{T_0}^{T_\infty}(\frac{dH_c}{dT})/dT} \quad \text{Equation 3- 12}$$

$$\mathrm{t} = \frac{T_0 - T}{\varphi} \quad \text{Equation 3- 13}$$

where X_t being the relative crystallinity at crystallization time t; n and Z_t correspond to Avrami exponent and crystallization kinetic constant respectively, and their value can be obtained by plotting the line $\ln[-\ln(1-X_t)]$ *vs* lnt; X_T being related to crystallinity with the change of temperature, T_0 and T_∞ being the onset and the end of crystallization temperature; T being the temperature at crystallization time t, and φ the cooling rate.

The crystallization half-time ($t_{1/2}$) is defined by Equation 3- 14:

$$t_{1/2} = (\frac{ln2}{Z_t})^{1/n} \quad \text{Equation 3- 14}$$

The density (p) of samples is defined via drainage method following ASTM D792 (by Equation 3- 15):

$$p = \frac{a}{a+b-c} \times p_w \quad \text{Equation 3- 15}$$

where p_w is the density of water at the testing temperature, a is the apparent mass of specimen in air without the sinker, while b is the apparent mass of completely immersed sinker (if used), c is apparent mass of specimen and sinker (if used) totally immersed in water.

Wide Angle X-Ray diffraction (WAXD) using a Bruker D8-Advance diffractometer (45° using Cu Kα radiation: λ=0.15406 nm) is carried out to explore the crystalline phase with 2θ from 10°. The diffractograms are further analysed using the Origin 2018 software considering a Gaussian fitting, and the crystallite dimensions are defined according to Scherrer's equation:

$$D = \frac{K\lambda}{(\beta - s)cos(\theta)}$$ Equation 3- 16

where D is the crystal size; K the crystalline shape parameter (≈0.89); λ being 0.15406 nm, the Cu Kα wavelength; β being the measured sample diffraction peak half-height width; s being the instrument factor calibration (0.05°), and θ being the diffraction angle.

Strain-stress curves were obtained using an Instron testing machine at room temperature with a speed of 50 mm·min^{-1}, and each sample has been tested at least three times.

3.2.3 Results and discussion

3.2.3.1 LIonomer morphology

As previously mentioned, the dispersion of additives within LIonomers blends is investigated by Transmission Electron Microscopy (TEM) (Figure 3-7). Considering the difference of PPgMA and its blends morphologies (Figure 3a and Figure 3b-d), the granular “bean-spots” correspond to additive-rich phases and the surrounding continuous medium to PPgMA. This assignment is confirmed by elemental analysis under microscope e-beam (EDX) [27]. The EDX spectrum 1 of image S3-4a (LIonomer processed with 10 wt.% EMIM DEP) leads to the following elemental composition: C: 85.19 wt.%, N: 2.51 wt.%, O: 10.94 wt.%, and P: 1.36 wt.% (see Figure S3-4 of the Supporting Information). From the comparison between polymer blends with 10 wt% EMIM DEP (Figure 3-7b) and 10 wt% Zn^{2+} Ac (Figure 3-7d), the previous one displays a dual scale structure, i.e. ionic liquid multiplets (black spots) as well as ImIL-separated dispersed spherical particles of a larger size, while the second one exhibits ionic domains because of the nature of associated EMIM DEP and Zn^{2+} Ac. On another hand, by using amine-functionalized IL ([AEMIM] Br), the generated morphology is totally different due to the reactivity of this amino functionalized IL and the maleic anhydride groups carried by the PP chains. This reactivity enhances the compatibility with the PPgMA matrix and a nanoscale structuration is thus generated.

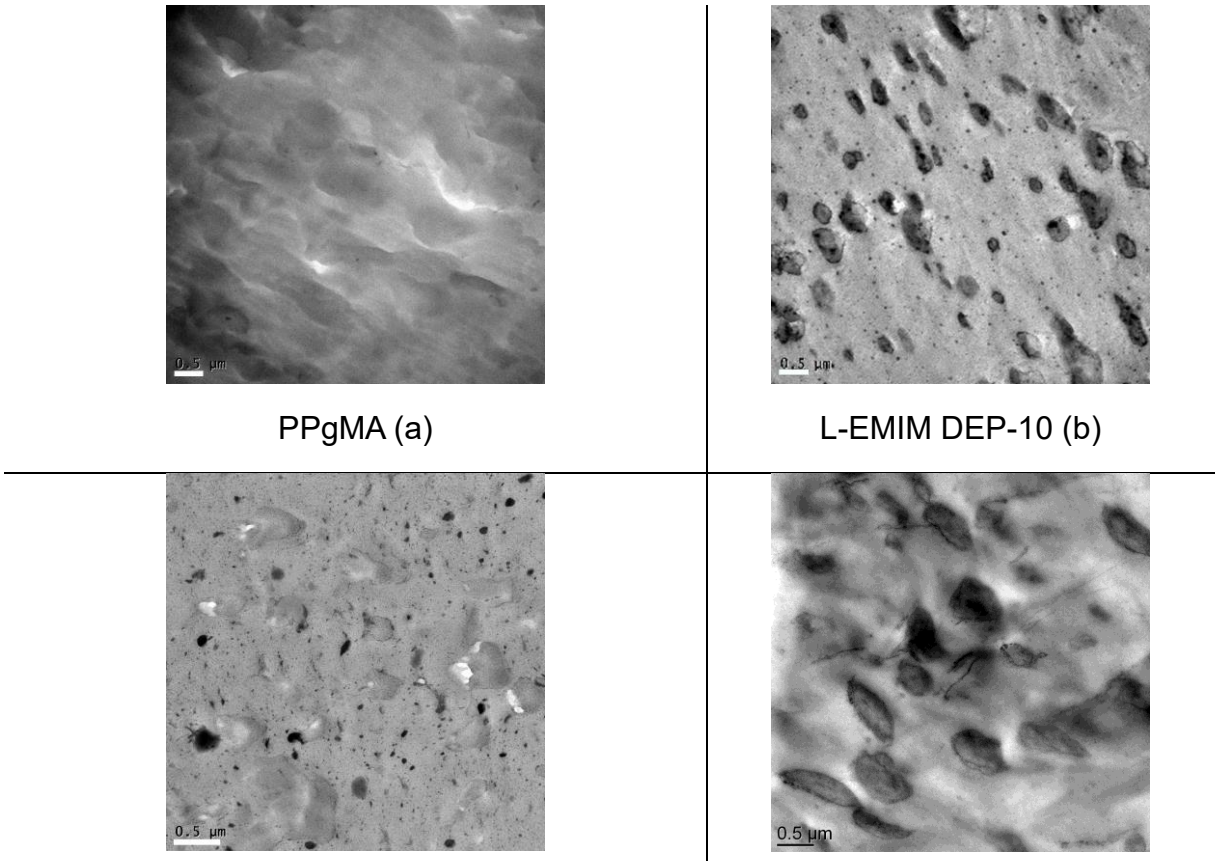

PPgMA (a) | L-EMIM DEP-10 (b)

L-[AEMIM] Br-10 (c) | Zn-Ionomer-10 (d)

Figure 3- 7 TEM micrographs of PPgMA and its blends prepared with 10 wt.% of the different additives (ImILs and Zn^{2+} Ac) (scale bar: 0.5µm)

As expected, a double scale structuration of the ILs is observed for non-reactive ILs, since the generated interactions take place between the cation ($EMIM^+$) and COO^- of PPgMA [27], and in terms of traditional ionomer, the observations are only of ionic clusters (Figure 3-7d). In fact, the resulting morphology either aggregation or multi-structured depends on dipole-dipole interactions [27 ,30]. While the resulting dispersion state of the amino-functionalized ionic liquid is governed by the balance of the interactions between the COO^- groups (from PPgMA) and the cation reactivity, *i.e.* the formation of amide and imide bonds from the reaction of maleic anhydride and the IL amine groups [31]. Therefore, from such reactive IL-based Lionomer, a nanoscale structuration is observed. As reported in the literature [25], size distribution varying from the nano- to micro-scale of ILs could be designed by selecting appropriate cation/anion

combinations.

3.2.3.2 Characteristic structures of modified PPgMA

NMR and ATR-FTIR spectroscopies are the powerful methods to identify the nature of the established interactions between PPgMA and added ionic salts (ImIL or Zn^{2+} Ac). The ^{1}H NMR spectra of EMIM DEP and the corresponding LIonomer are reported in Figure 3-8a. According to previous literature [27], the enhanced electronic cloud density in positions #2 and #3 could be gained by comparing of EMIM DEP with its LIonomer because of the effect of neighbouring C=O of the grafted PP matrix (Scheme 3-4a). Consequently, these two hydrogens in neat EMIM DEP shift from 8.22 and 8.36 ppm [32,33] into 7.25 and 7.30 ppm in its LIonomer, respectively (Figure 3-8a). Additionally, the hydrogen in position #6 shifts from 10.54 to 10.76 ppm from the reduced electronic cloud density. This phenomenon is due to the strong electronic absorption capacity of oxygen in generating COO^{-} from the PPgMA. Meanwhile, the C=O group carried by the PP chain leads to a shift of the phosphorous compound of the anion to low field, *i.e.* from 0.18 ppm into 0.57 ppm (Figure 3-8b).

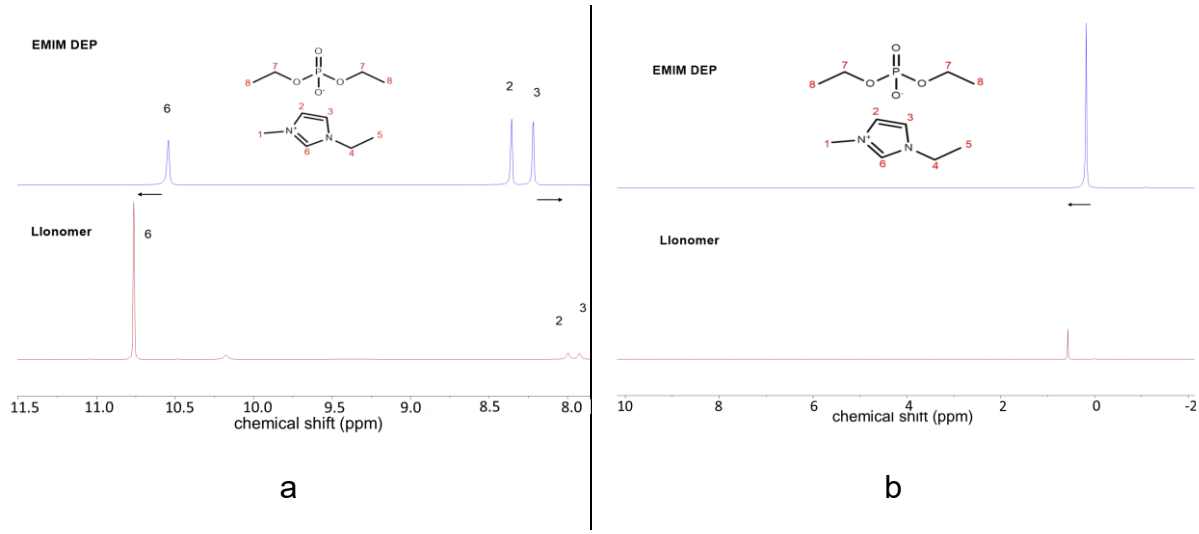

Figure 3- 8 ^{1}H (a) and ^{31}P NMR (b) spectra (400 MHz; C_6D_5Cl) of EMIM DEP ionic liquid and its corresponding LIonomer (10 wt.%)

Figure 3-9 shows the ATR-FTIR spectra of [AEMIM] Br ionic liquid and its corresponding LIonomers, as well as Zn-Ionomers. The spectrum of the neat [AEMIM] Br (Figure 3-9a) evidences the $-NH_2$ bending peak at 1,668 cm^{-1} and the one of the

imidazolium ring at 1,765 and 1,168 cm^{-1}.[34–38]. As the [AEMIM] Br ionic liquid is introduced into PPgMA, the asymmetric $\nu_{C=O}$ vibration of the MA group at 1,780 cm^{-1} and $\nu_{C=O}$ of carboxylic group at 1,712 cm^{-1} disappear. At the same time, a new peak at 1,701 cm^{-1} for the LIonomer is observed. This one could be assigned to an imide group which is formed via cyclization of the acid and amide [38–40]. Such phenomenon reveals the reactivity of the $[AEMIM]^+$ ionic liquid as shown in Scheme 3-4b. With respect to Zn-Ionomers (Figure 3-9b), two absorbance peaks in the 1,500-1,600 cm^{-1} regions are attributed to carboxylate stretching vibration because of the generation of ionic bonds with Zn cations [17,41] (see Scheme 3-4c).

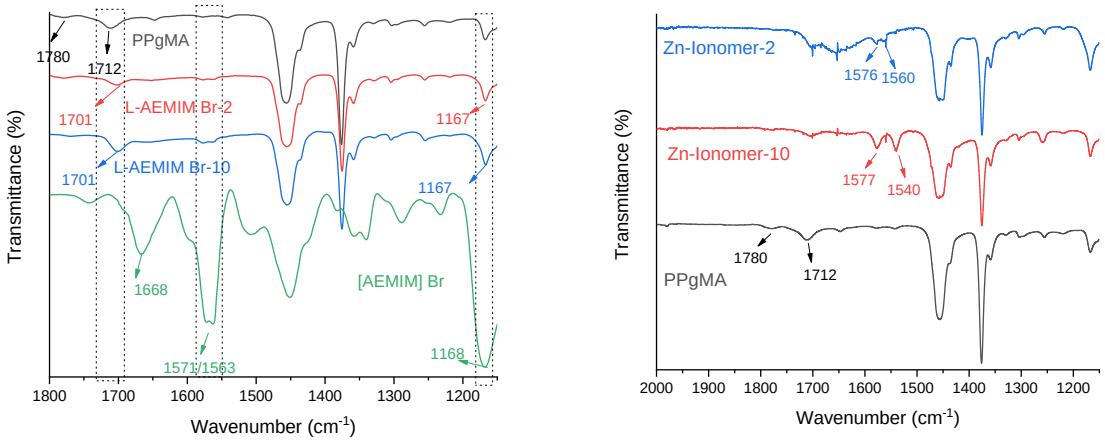

Figure 3- 9 ATR-FTIR spectra of LIonomers processed with [AEMIM] Br (a) and Zn-Ionomers (b)

To sum up, all of these three additives (EMIM DEP, [AEMIM] Br and $Zn^{2+}Ac$) can interact with polar groups carried by the PPgMA chains. Nevertheless, these ionic interactions vary with the presence of the functional amino group, *i.e.* [AEMIM] Br *vs.* EMIM DEP, and the nature of the additives, *i.e.* ImILs *vs.* $Zn^{2+}Ac$. Such difference in the nature of the interactions between the ionic liquid and the PP chains according to the different cation/anion combinations could explain the various types of morphologies of the LIonomers as shown previously. Meanwhile, whatever the cation/anion combination of ImILs, the targeted microstructure (see Figure 3-6b) can be achieved, *i.e.* the use of generating COO^- groups on the polypropylene chains or formed imide

group as the connecting points and cation/anion pairs of ImIL as the ionic phase via their inherent electrostatic interactions. As reported latter, the different generated interactions in the Zn-Ionomer and the designed LIonomers could also influence the viscosity in the molten state, *i.e.* at high temperature, and on the mechanical properties as the morphologies of the blends, *i.e.* the dispersion states of the ILs and the crystallization rate and morphism are different.

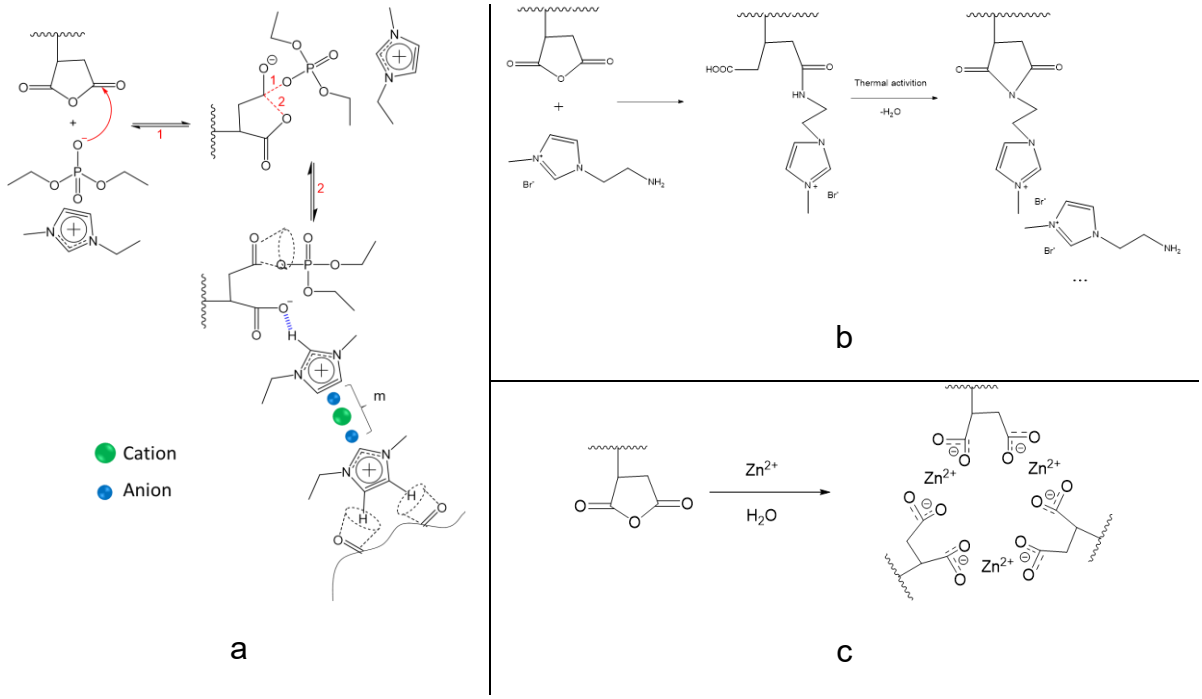

Scheme 3- 4 Various natures of interactions existing in the different polymer blends (based on: a: EMIM DEP; b: [AEMIM] Br and c: $Zn^{2+}Ac$; m=1, 2, 3⋯)

3.2.3.3 Effect of ImIL and Zn^{2+} on rheological behaviour: Interaction Strength

The viscosity of the different materials in the molten state could be employed to investigate the effect of incorporated ions, *i.e.* ImILs *vs.* Zn^{2+} within LIonomers and Zn-Ionomers (Figure 3-10a). A considerable enhancement on complex viscosity (η^*) is observed when comparing LIonomers or Zn-Ionomers with neat PPgMA. The viscosity depends on the interaction modes (*i.e.* ionic-ionic/polar interactions or chemical bonds). η^* increase could be tailored from the selection of the ionic group. Such increase can be explained by the existence of more interaction sites, *i.e.* reduction of the segmental dynamics induced from COO^-/IL cation and IL cation/anion pairs [3] especially for high

ImIL or Zn^{2+} contents. Either interactions or inter-chains as well as generated ionic networks within PPgMA blends can not only act as crosslinking points (resulting in the enhanced density of the samples at room temperature 0.940 g·cm^{-3} of L-[AEMIM] Br-10 > 0.937 g·cm^{-3} of Zn-Ionomer-10 > 0.917 g·cm^{-3} of L-EMIM Ac-10 > 0.915 g·cm^{-3} of L-EMIM DEP-10 > 0.909 g·cm^{-3} of PPgMA), but also create more barrier preventing the motions of chain segment of polymer matrix in large-scale, resulting in increased viscosity value [8,16,17,43,44]. In addition, the dynamic viscosity, η^*, values show the following sequence for 10 wt.% of ionic additive: L-[AEMIM] Br-10 and Zn-Ionomer-10 > L-EMIM DEP-10. For blends based on ImILs, none of the ImILs can lead to an increase of the η^* value solely due to the low viscosity of ILs at high temperature [44]. Therefore, the ranking of the η^* values of LIonomers reveals the strength of the interactions established between polar groups of PPgMA and the cation of the various ImILs. As discussed previously, such magnitudes must be associated with the corresponding patterns of the interactions. The dynamic viscosity, η^*, of the LIonomers based on [AEMIM] Br IL (2 or 10 wt.%) display one higher value due to the formation of the chemical bonds (imide group) between carboxylic acid and the amine from [AEMIM] Br. These bonds are much stronger than ion-ion or dipole-ion interactions established within EMIM DEP-based blends. As a result, the resulting ionic network from reactive ILs is greater than that from non-reactive EMIM DEP. This claim is proved by the presence of stress hardening phenomenon in L-[EMIM] Br-10 (see Figure S3-10b), *i.e.* a direct manifestation of the network microstructure in the blend, whose existence and interaction confine the flexibility of the polymer chains and strengthen the system elasticity [18]. As for LIonomers based on 10 wt.% of EMIM DEP, these cation-anion pairs self-assemble to form and give this dual morphology observed by TEM. However, coarser phase separation is obtained than LIonomers based on 10 wt.% of [AEMIM] Br. This phenomenon may be due to a lower level of generated ion-ion and dipole-ion interactions [27]. The numerous multiplets acting as crosslinkings limit the segmental motions of polymer chains and contribute to the increase in the viscosity. The viscosity

of the LIonomers is thus the result of the effect of the morphology, *i.e.* the dispersion state of the ionic liquids combined with the one of the interaction strengths.

Concerning the conventional ionomers, each Zn^{2+} cation is able to interact with two carboxylates (Scheme 3-4c). Thus, the blends containing Zn^{2+} Ac exhibit very close viscosity profile to that of the LIonomer processed with [AEMIM] Br (especially at low frequency).

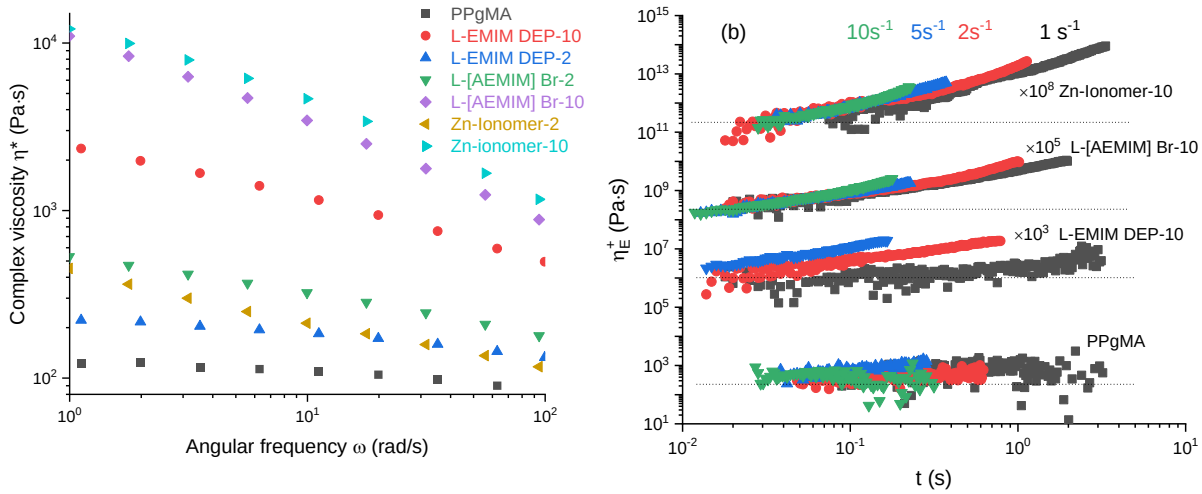

a b

Figure 3- 10 Viscosity as a function of the dynamic angular frequency at 180°C of PPgMA, LIonomers based on $EMIM^+$ and $[AEMIM]^+$ ionic liquids and Zn-ionomers (a); the measured tensile stress growth coefficients (η_E^+) of the at rates of 1, 2, 5, $10s^{-1}$ (b)

3.2.3.4 Microstructure of PPgMA blends: Location of ImIL and Zn^{2+}

Depending on the polymer chain conformations and the changes in molecular dynamics without or with ionic species, the crystalline microstructure of the LIonomers and Zn-Ionomer could be also modified. The semi-crystalline polymer could be seen as composed of three fractions: crystalline fraction (CF), rigid amorphous fraction (RAF), and mobile amorphous fraction (MAF) [45]. The chains in CF fraction undergo the largest restrictions in their segmental motions. This region is surrounded by macromolecular chains in an amorphous state [45,46]. These chains, denoted as tie molecules, imply strong intermolecular interactions preventing segmental movements [45–47]. As a result, this confined fraction (denoted as RAF) shows more limited

molecular mobility than amorphous phase one and displays its own relaxation temperature, distinct from the one of the chains of the MAF fraction (T_a). In this study, to know where ImILs and Zn^{2+} are located within PPgMA can help understand the structuring mechanism and how it influences the overall behaviours of the corresponding blends. The dynamics of amorphous segmental relaxation as a function of temperature is analysed to recognize the MAF and RAF relaxations of the amorphous phase, as shown in Figure 3-11 and Table 3-7.

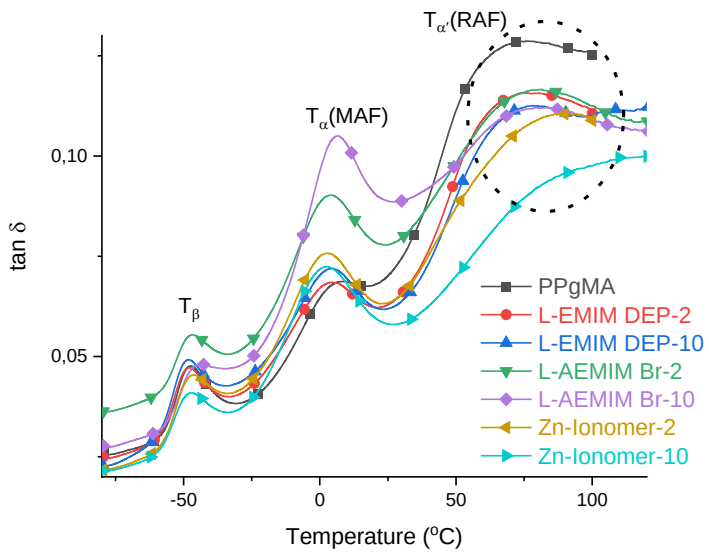

Figure 3- 11 Evolution of loss tangent (tan δ) vs temperature measured by DMA at 1Hz

Table 3- 7 Temperature associated to β, α and α' relaxations measured from DMA

Samples	T_β (°C)	T_α (MAF, °C)	$T_{\alpha'}$ (RAF, °C)
PPgMA	-47	7	76
L-EMIM DEP-2	-47	5	74
L-EMIM DEP-10	-48	5	78
L-[AEMIM] Br-2	-47	5	81
L-[AEMIM] Br-10	-44	6	83
Zn-Ionomer-2	-46	3	87
Zn-Ionomer-10	-47	3	>120

The molecular relaxation peak at -47 °C corresponds to the secondary relaxation mode, β, corresponding to local molecular motions (methyl and methylene) [48]. The constancy of T_β is the evidence that ImILs and Zn^{2+} prefer to be near the opened maleic anhydride groups owing to the interactions described before. The T_α (MAF) of LIonomers keeps almost the same value as that of neat PPgMA, while one of Zn-Ionomers decreases. Such a decrease may be associated with the predominant distribution of Zn^{2+} in RAF, leading to the maximum $T_{\alpha'}$ (RAF) value [23,49,26], *i.e.* 87 °C in Zn-Ionomer-2 and higher than 120 °C in Zn-Ionomer-10. The highest $T_{\alpha'}$ (RAF) value observed with the addition of Zn^{2+} Ac may be attributed to the interactions between Zn^{2+} and generated COO^- [26], since each Zn^{2+} interacts with two COO^- groups. Such a result is consistent with the previously reported viscosity ranking. The increase of $T_{\alpha'}$ (RAF) is also observed when incorporating ImILs. The different natures of ImIL pairs lead to the differences of LIonomers α'-relaxation. The reactivity of the amine groups of the [AEMIM] Br with the anhydride groups carried by the PP leads to both the stronger bonds (formation of imides as shown in Scheme 3-4b) and to the higher $T_{\alpha'}$ (RAF) value among LIonomers (see Table 3-7). Because the interaction strength between ionic and polar groups within LIonomers is responsible for the $T_{\alpha'}$ (RAF) value [27]. In addition to the ionic additives' nature (ImIL or Zn^{2+}), the changes of $T_{\alpha'}$ (RAF) are also associated with their weight content. Such changes are in agreement with the strength of the generated interactions and the rheological behaviours.

3.2.3.5 Role of ImIL and Zn^{2+} on crystallization

Effect on crystallization process

As reported previously for P(VDF-CTFE)/IL blends, some phosphonium-based ionic liquids (PhILs) could be located between crystalline lamellas leading to the depression of crystallinity rate (X_c) and crystallization temperature (T_c) [23,26]. According to these authors, these PhILs could act as barriers for the regular chain folding and the dipolar interactions with P(VDF-CTFE). In this present work, such a trend cannot be observed by incorporating either ImIL or Zn^{2+} Ac (see Table 3-8 values collected from

Figures S3-5 and S3-6). The difference between the PVDF/IL and PP/IL blends could be explained by the different positions and distribution of ionic additives. TEM micrographs reveal that a microphase separation of PPgMA and additives (ImILs and Zn^{2+} Ac). As a consequence, the interactions take place only at the interfacial boundaries (in amorphous region).

Table 3- 8 The T_c, $t_{1/2}$, and X_c values measured from DSC traces at 5 °C·min^{-1}

Materials	X_c, (%)	T_c, (°C)	$t_{1/2}$ (min)
PPgMA	34.1	116.1	0.77
L-EMIM DEP-2	36.8	124.6	0.72
L-EMIM DEP-10	35.3	118.0	0.86
L-[AEMIM] Br-2	36.4	122.7	0.64
L-[AEMIM] Br-10	34.2	124.2	0.89
Zn-Ionomer-2	35.8	120.2	0.67
Zn-Ionomer-10	38.9	128.9	0.76

In order to analyse the effect of ImIL and Zn^{2+} species on the crystallization process, the analysis of the non-isothermal crystallization kinetics according to Jeziorny's is employed (see Figure S3-7, Table S3-2). The $t_{1/2}$ value (crystallization half-time) quantifies the rate of crystallisation, *i.e.* a low value reflects a fast crystallisation rate. As reported in the literature [27], some ImILs (for example, 1-ethyl-3-methylimidazolium acetate) itself may act as the nucleation inhibitors leading to the depression of $t_{1/2}$ with increasing IL content. Because such effect restrains the nucleation process and thus a bigger volume is provided for the growth of these formed nuclei, resulting in a higher re-organization rate (revealed by decreased $t_{1/2}$ value). Considering the ImIL or Zn^{2+} content herein, $t_{1/2}$ value increases for a higher content of ions, since more ionic and inter-chains interactions within could induce even more mobility constraints to the segmental dynamics [23,26]. In addition, the effect on crystallization behaviour is dependent on the nature of the interactions and

morphologies, *i.e.* distribution state of the ionic liquid. Consequently, the $t_{1/2}$ value of the L-[AEMIM] Br -10 is the highest.

Effect on crystalline phase

PPgMA and its blends display predominantly α-monoclinic crystalline form (see Figure 3-12) according to the presence of the following Bragg reflections on the WAXD patterns at 2θ ≈ 14.0° [α110], 16.8° [040], 18.4° [130], 25.3° [060&150], 28.5° [220], and 42.6° [212]. A distinct reflection at 2θ ≈ 23.6° which is assigned to the syndiotactic monoclinic (002) plane [50] is evidenced. The individual γ-form peak is not identified by WAXD at 2θ ≈ 21.4° [α111&γ202]). Such a crystalline phase could appear under some specific crystallization conditions such as high pressure [51]. From the comparison of PPgMA spectra with its blends, no significant changes on diffraction reflections are observed, except for the additional peaks at 2θ=11.7° (200 plane) as well as 35.7° (101 plane) for Zn^{2+} Ac-based blends [52] and at 2θ ≈ 16.0° corresponding β (300) for ImIL-based blends. The contents of β phase can be calculated from Equation 3-17 [53] and are reported in Table 3-9.

$$K = \frac{I_{300}}{I_{300}+I_{110}+I_{040}+I_{130}} \qquad \text{Equation 3- 17}$$

where I_{300}, I_{110}, ,I_{040} and I_{130} being the intensities of 2θ ≈ 16.0, 14.0, 16.8 and 18.4° respectively.

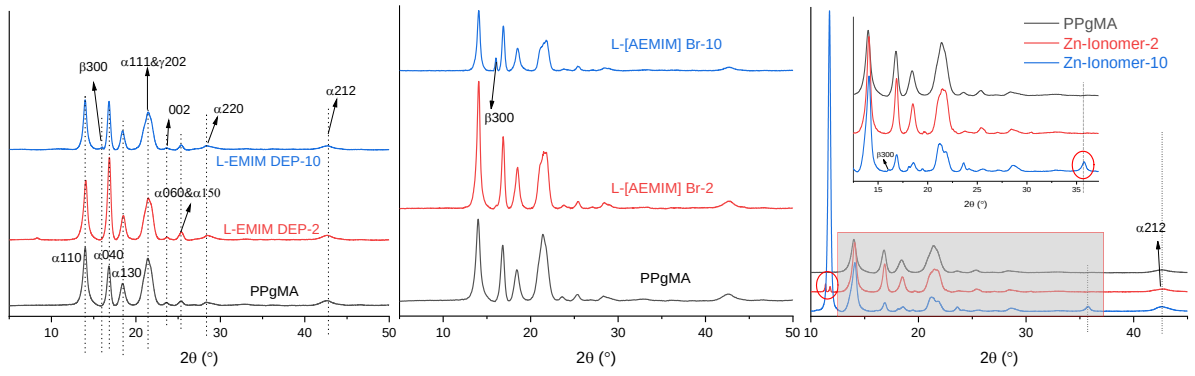

Figure 3- 12 WAXD diffractions of PPgMA and its blends with various additives

The generation of β-crystalline phase is associated with the distribution patterns of ionic additives as well as the interaction strength between the COO^- and the cations

of the ImILs within LIonomers [27]. These formation of such interactions within LIonomers strongly influence the chain dynamics. From the comparison of L-EMIM DEP-10 and L-[AEMIM] Br -10, the weak interactions within LIonomers processed with EMIM DEP account for its lower β-form content (3.2 % in L-EMIM DEP-10), instead of 9.3 % in L-[AEMIM] Br-10. In addition to the transformation of crystalline phase due to ImIL within LIonomer, the incorporation of Zn^{2+} Ac induces the thicker crystals.

Table 3- 9 WAXD analyses of the PPgMA and its related blends

	$D_{[110]}$ (nm)	$D_{[040]}$ (nm)	$D_{[130]}$ (nm)	$D_{[300]}$ (nm)	K (%)	Average size[a]
PPgMA	12.7	18.2	12.8	-	-	12.7
L-EMIM DEP-2	13.3	18.0	13.7	-	-	12.5
L-EMIM DEP-10	8.9	21.0	15.8	72.4	3.2	13.1
L-[AEMIM] Br-2	17.3	22.1	15.2	-	-	14.9
L-[AEMIM] Br-10	18.8	26.3	14.5	51.6	9.3	14.5
Zn-Ionomer-2	29.5	22.0	16.7	-	-	15.1
Zn-Ionomer-10	14.0	25.0	15.5	-	-	15.7

where D being the crystallite size, [a]being calculated according to α-crystalline size

3.2.3.6 Effect on mechanical property

It was demonstrated that the generated interactions and the structuration can be tailored by incorporating different additives (ImILs and Zn^{2+}), therefore the strain stress behaviour should be also designed differently (see Figure 3-13). Incorporating a low content (2 wt.%) of ImIL (whatever its nature) or Zn^{2+} leads to a significant increase of Young's modulus. Among them, LIonomers based on 2 wt.% [AEMIM] Br display the highest moduli due to the strongest bonding via the generation of imide groups. The modulus of LIonomers declines extremely at high content of ImIL (from 803 MPa in L-EMIM DEP-2 to 431 MPa in L-EMIM DEP-10), except for with [AEMIM] Br. Such depression could be related to the corresponding morphologies (see TEM images). In fact, the large separated ImIL-rich phases in L-EMIM DEP-10 contribute to decrease

the material stiffness [27]. On another hand, the strong interactions and fine distribution for [AEMIM] Br-based LIonomers lead to the highest moduli. In addition, the modulus ranking of these two types of LIonomers is in agreement with the conclusions issued from rheology analysis and relaxation behaviors, especially for high content of ImIL. In addition, the ability of the materials to sustain large deformations is considerably improved, *i.e.* the strain at break increases from 23 % in L-EMIM DEP-2 to 655 % in L-EMIM DEP-10 (see Table 3-10). Considering the conclusions done on the crystallization behaviour, such an enhanced toughness relies on the generation of crystalline β-form and the dual morphology of the PPgMA /ImILs blends. As a consequence, the nature and strength of interactions between COO^- groups and imidazolium cations are critical not only to tailor the morphologies but also to manage the macroscopic physical behavior of the corresponding LIonomers. Nevertheless, the addition of [AEMIM] Br or Zn^{2+} Ac leads to more brittle materials, *i.e.* strain at break is reduced from 25 % for PPgMA *vs.* 15 % and 10 % in blends with [AEMIM] Br and Zn^{2+} Ac, respectively. For blends with [AEMIM] Br, the five-membered ring is responsible for such phenomenon, while the interaction of each Zn^{2+} with two generated COO^- of PPgMA contributes not only to brittleness but also a continuous increase of the modulus, from 719 MPa in Zn-Ionomer-2 to 878 MPa in Zn-Ionomer-10.

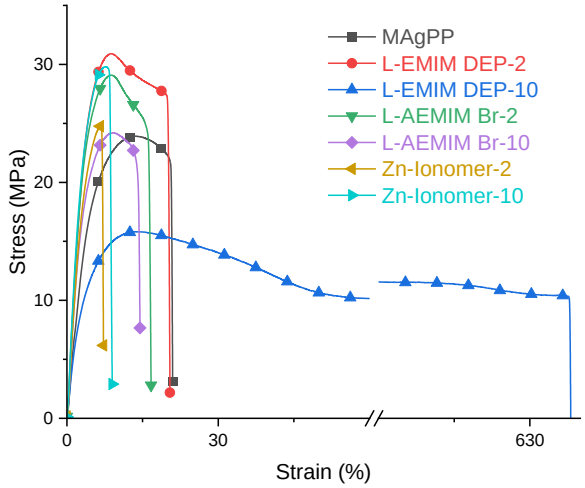

Figure 3- 13 Evolution of mechanical behavior from tensile test of PPgMA and its related blends

As a conclusion, neither ImILs nor Zn^{2+} Ac play a role of plasticizer leading to a significant decrease of modulus and an enhanced strain at break as reported in other papers [23,26]. The mechanical behaviour is associated with the generated interactions and their morphologies in corresponding blends. In addition to the increased crystallinity, the strong interactions within blends govern the Young's modulus value, while the generation of β-phase crystalline and dual morphologies (including ionic multiplets and ionic-separated phase) contribute to the stretchability.

Table 3- 10 Mechanical data of PPgMA and its related blends

Samples	Young's modulus (MPa)	Strain at break (%)
PPgMA	456±18	24±6
L-EMIM DEP-2	803±10	23±2
L-EMIM DEP-10	431±11	655±20
L-[AEMIM] Br-2	819±15	15±3
L-[AEMIM] Br-10	690±7	14±1
Zn-Ionomer-2	719±5	9±1
Zn-Ionomer-10	878±29	7±2

3.2.4 Conclusions

In this study, LIonomers as a new generation of ionomers are synthesised by combining maleic anhydride-grafted polypropylene (PPgMA) and imidazolium-based ionic liquids (ImILs), *i.e.* 1-ethyl-3-methylimidazolium diethyl phosphate (EMIM DEP), and 1-aminoethyl-3-methylimidazolium bromide ([AEMIM] Br). Their performances could be tailored by changing the cation/anion pairs of ImIL and be further compared to that of the traditional Zn-Ionomers. NMR and FTIR spectroscopies prove that the interactions (ion-ion, dipole-ion, and chemical bonding) between ImILs and polar groups of PPgMA vary with the nature of ImILs. The various interaction strengths and patterns govern the distribution of ImIL within corresponding LIonomers. As a consequence, the morphology of LIonomers processed with [AEMIM] Br which is reactive according to the presence of an amine group, displays it's a specific behavior

due to the generation of imide bonds. On another hand, the LIonomer based on EMIM DEP shows multiscale distributions, *i.e.* ionic multiplets and ImIL-separated phase. On the other side, the value of complex viscosity in the molten state signs the strength of interactions within LIonomers and the ability to generate continuous ionic-network. The Zn-Ionomer shows a similar value to that of LIonomers based on [AEMIM] Br. Moreover, all ionic additives are likely to lie in the amorphous phase, particularly in the rigid amorphous fraction (RAF) resulting in significantly promoted relaxation value. In addition to the effect of cation-anion pairs on crystallization process, the β-phase crystalline is also produced. Besides, in relation with the microstructure and the crystallinity, an excellent compromise of stiffness and toughness is observed. In a conclusion, these LIonomers are very prospective for processing highly functional materials, such as foams or melt-blown films in which stretching ability is required.

3.2.5 References

[1] Zhang L, Brostowitz N R, Cavicchi K A, et al. Perspective: Ionomer research and applications[J]. Macromolecular Reaction Engineering, 2014, 8(2): 81-99.

[2] Kirkmeyer B P, Weiss R A, Winey K I. Spherical and vesicular ionic aggregates in Zn-neutralized sulfonated polystyrene ionomers[J]. Journal of Polymer Science Part B: Polymer Physics, 2001, 39(5): 477-483.

[3] Eisenberg A, Hird B, Moore R B. A new multiplet-cluster model for the morphology of random ionomers[J]. Macromolecules, 1990, 23(18): 4098-4107.

[4] Datta S, De P P, De S K. Blends of ionomers[J]. Journal of Applied Polymer Science, 1996, 61(10): 1839-1846.

[5] Ma Y, Yang G, Xie L. Morphology, nonisothermal crystallization behavior and mechanical properties of polypropylene modified by ionomers[J]. Journal of Macromolecular Science, Part B, 2014, 53(12): 1829-1845.

[6] Kim J S, Yoshikawa K, Eisenberg A. Molecular weight dependence of the viscoelastic properties of polystyrene-based ionomers[J]. Macromolecules, 1994, 27(22): 6347-6357.

[7] Dalmas F, Leroy E. New insights into ionic aggregate morphology in Zn-neutralized sulfonated polystyrene ionomers by transmission electron tomography[J]. Macromolecules, 2011, 44(20): 8093-8099.

[8] Aitken B S, Buitrago C F, Heffley J D, et al. Precision ionomers: synthesis and thermal/mechanical characterization[J]. Macromolecules, 2012, 45(2): 681-687.

[9] Weiss R A, Zhao H. Rheological behavior of oligomeric ionomers[J]. Journal of Rheology, 2009, 53(1): 191-213.

[10] Qiao X, Weiss R A. Nonlinear rheology of lightly sulfonated polystyrene ionomers[J]. Macromolecules, 2013, 46(6): 2417-2424.

[11] Ling G H, Wang Y, Weiss R A. Linear viscoelastic and uniaxial extensional rheology of alkali metal neutralized sulfonated oligostyrene ionomer melts[J]. Macromolecules, 2012, 45(1): 481-490.

[12] Longworth R, Vaughan D J. Physical structure of ionomers[J]. Nature, 1968, 218(5136): 85-87.

[13] Rapone I, Taresco V, Lisio V D, et al. Silver-and Zinc-Decorated Polyurethane Ionomers with Tunable Hard/Soft Phase Segregation[J]. International Journal of Molecular Sciences, 2021, 22(11): 6134.

[14] Ro A J, Huang S J, Weiss R A. Synthesis and properties of random poly (lactic acid)-based ionomers[J]. Polymer, 2009, 50(5): 1134-1143.

[15] Ro A J. Synthesis and properties of poly(lactic acid) ionomers[D]. University of Connecticut, 2008.

[16] Weiss R A, Yu W C. Viscoelastic behavior of very lightly sulfonated polystyrene ionomers[J]. Macromolecules, 2007, 40(10): 3640-3643.

[17] Li Y, Yao Z, Chen Z hua, et al. High melt strength polypropylene by ionic modification: Preparation, rheological properties and foaming behaviors[J]. Polymer, 2015, 70: 207-214.

[18] Rainglet B, Chalamet Y, Bounor-Legaré V, et al. Polypropylene foams under CO2 batch conditions: From formulation and rheological modeling to cell-growth simulation[J]. Polymer, 2021, 218: 123496.

[19] Chen Y, Zhang Y, Ke F, et al. Solubility of neutral and charged polymers in ionic liquids studied by laser light scattering[J]. Polymer, 2011, 52(2): 481-488.

[20] Hajipour A R, Rafiee F. Recent progress in ionic liquids and their applications in organic synthesis[J]. Organic Preparations and Procedures International, 2015, 47(4): 249-308.

[21] Yue C, Fang D, Liu L, et al. Synthesis and application of task-specific ionic liquids used as catalysts and/or solvents in organic unit reactions[J]. Journal of Molecular Liquids, 2011, 163(3): 99-121.

[22] Livi S, Duchet-Rumeau J, Pham T N, et al. A comparative study on different ionic liquids used as surfactants: Effect on thermal and mechanical properties of high-density polyethylene nanocomposites[J]. Journal of Colloid and Interface Science, 2010, 349(1): 424-433.

[23] Xing C, Zhao M, Zhao L, et al. Ionic liquid modified poly (vinylidene fluoride): crystalline structures, miscibility, and physical properties[J]. Polymer Chemistry, 2013, 4(24): 5726-5734.

[24] Chaves Lins L, Livi S, Maréchal M, et al. Structural dependence of cations and anions to building the polar phase of PVDF[J]. European Polymer Journal, 2018, 107: 236-248.

[25] Livi S, Duchet-Rumeau J, Gérard J F. Nanostructuration of ionic liquids in fluorinated matrix: Influence on the mechanical properties[J]. Polymer, 2011, 52(7): 1523-1531.

[26] Yang J, Pruvost S, Livi S, et al. Understanding of versatile and tunable nanostructuration of ionic liquids on fluorinated copolymer[J]. Macromolecules, 2015, 48(13): 4581-4590.

[27] Hou L, Livi S, Gérard J F, et al. LIonomers-New Generation of Ionomer: Understanding of Their Interaction and Structuration as a Function of the Tunability of Cation and Anion[J]. Polymers, 2023, 15(2): 370.

[28] Clark E J, Hoffman J D. Regime III crystallization in polypropylene[J]. Macromolecules, 1984, 17(4): 878-885.

[29] Jeziorny A. Parameters characterizing the kinetics of the non-isothermal crystallization of poly (ethylene terephthalate) determined by DSC[J]. Polymer, 1978, 19(10): 1142-1144.

[30] Khokhlov A R, Dormidontova E E. Self-organization in ion-containing polymer systems[J]. Physics-Uspekhi, 1997, 40(2): 109.

[31] Colbeaux A, Fenouillot F, David L, et al. Multifunctional covalent and ionic coupling agents of maleic anhydride modified polyethylene[J]. Journal of Applied Polymer Science, 2007, 105(5): 2605-2610.

[32] Dubey S, Bharmoria P, Gehlot P S, et al. 1-Ethyl-3-methylimidazolium diethylphosphate based extraction of bioplastic “Polyhydroxyalkanoates” from bacteria: green and sustainable approach[J]. ACS Sustainable Chemistry & Engineering, 2018, 6(1): 766-773.

[33] Binks F C, Cavalli G, Henningsen M, et al. Examining the influence of anion nucleophilicity on the polymerisation initiation mechanism of phenyl glycidyl ether[J]. Polymers, 2019, 11(4): 657.

[34] Zhou X, Jing G, Liu F, et al. Mechanism and kinetics of CO_2 absorption into an aqueous solution of a triamino-functionalized ionic liquid[J]. Energy & Fuels, 2017, 31(2): 1793-1802.

[35] Cai Y, Peng Y, Song G. Amino-functionalized ionic liquid as an efficient and recyclable catalyst for Knoevenagel reactions in water[J]. Catalysis Letters, 2006, 109(1): 61-64.

[36] Xiang W, Shen C, Lu Z, et al. CO_2 cycloaddition over ionic liquid immobilized hybrid zeolitic imidazolate frameworks: Effect of Lewis acid/base sites[J]. Chemical Engineering Science, 2021, 233: 116429.

[37] Li Y, Zhang Q, Xie X, et al. Enhanced electromagnetic wave absorption properties of ionic liquid doped graphene[J]. Journal of Materials Science: Materials in Electronics, 2020, 31(16): 13273-13283.

[38] Zhou X, Zhang Y, Huang Z, et al. Ionic liquids modified graphene oxide composites: a high efficient adsorbent for phthalates from aqueous solution[J]. Scientific Reports, 2016, 6(1): 1-10.

[39] Létoffé A, Hoppe S, Lainé R, et al. Resilience improvement of an isotactic polypropylene-g-maleic anhydride by crosslinking using polyether triamine agents[J]. Polymer, 2019, 179: 121655.

[40] Suckow M, Zschoche S, Heinrich G, et al. New reactive poly (ionic liquid) s synthesized by polymer analogous conversion of maleic anhydride containing polymers[J]. Polymer, 2016, 96: 20-25.

[41] Choi S S, Kwon H M, Kim Y, et al. Characterization of maleic anhydride-grafted ethylene–propylene–diene terpolymer (MAH-g-EPDM) based thermoplastic elastomers by formation of zinc ionomer[J]. Journal of Industrial and Engineering Chemistry, 2013, 19(6): 1990-1995.

[42] Page K A, Park J K, Moore R B, et al. Direct analysis of the ion-hopping process

associated with the α-relaxation in perfluorosulfonate ionomers using quasielastic neutron scattering[J]. Macromolecules, 2009, 42(7): 2729-2736.

[43] Castagna A M, Wang W, Winey K I, et al. Influence of cation type on structure and dynamics in sulfonated polystyrene ionomers[J]. Macromolecules, 2011, 44(13): 5420-5426.

[44] Yousfi M, Livi S, Duchet-Rumeau J. Ionic liquids: A new way for the compatibilization of thermoplastic blends[J]. Chemical Engineering Journal, 2014, 255: 513-524.

[45] Ma Q, Georgiev G, Cebe P. Constraints in semicrystalline polymers: Using quasi-isothermal analysis to investigate the mechanisms of formation and loss of the rigid amorphous fraction[J]. Polymer, 2011, 52(20): 4562-4570.

[46] Arnoult M, Dargent E, Mano J F. Mobile amorphous phase fragility in semi-crystalline polymers: Comparison of PET and PLLA[J]. Polymer, 2007, 48(4): 1012-1019.

[47] Wang L, Wang Y nan, Huang Z gang, et al. Heat resistance, crystallization behavior, and mechanical properties of polylactide/nucleating agent composites[J]. Materials & Design (1980-2015), 2015, 66: 7-15.

[48] Bajsić E G, Šmit I, Leskovac M. Blends of thermoplastic polyurethane and polypropylene. I. Mechanical and phase behavior[J]. Journal of Applied Polymer Science, 2007, 104(6): 3980-3985.

[49] Mijovic J, Sy J W, Kwei T K. Reorientational dynamics of dipoles in poly (vinylidene fluoride)/poly (methyl methacrylate)(PVDF/PMMA) blends by dielectric spectroscopy[J]. Macromolecules, 1997, 30(10): 3042-3050.

[50] Clark E S. Unit cell information on some important polymers[M]. Physical Properties of Polymers Handbook. Springer, 2007: 619-624.

[51] Yang G, Li X, Chen J, et al. Crystallization behavior of isotactic polypropylene induced by competition action of β nucleating agent and high pressure[J]. Colloid and Polymer Science, 2012, 290(6): 531-540.

[52] Sreekanth M, Ghosh S, Mehta S K, et al. Investigation of the growth mechanism

of the formation of ZnO nanorods by thermal decomposition of zinc acetate and their field emission properties[J]. CrystEngComm, 2017, 19(16): 2264-2270.

[53] Zipper P, Janosi A, Wrentschur E. Scanning X-ray scattering of mouldings from semicrystalline polymers[J]. Journal de Physique IV, 1993, 3(C8): C8-33-C8-36.

3.2.6 Supporting Information

1. Elemental Analysis Spectrum

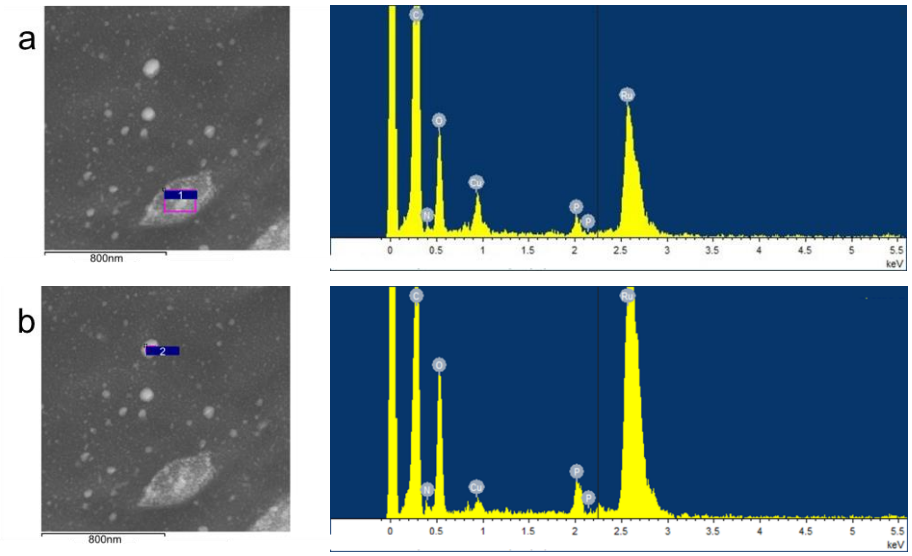

L-EMIM DEP-10

Figure S3- 4 The Elemental Analysis Spectrum of LIonomers

2. DSC thermograms of all polymer matrix and blends

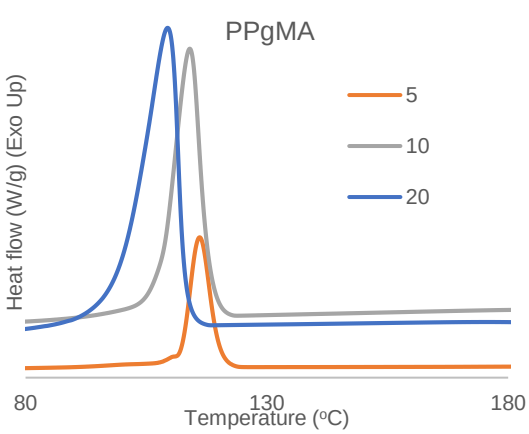

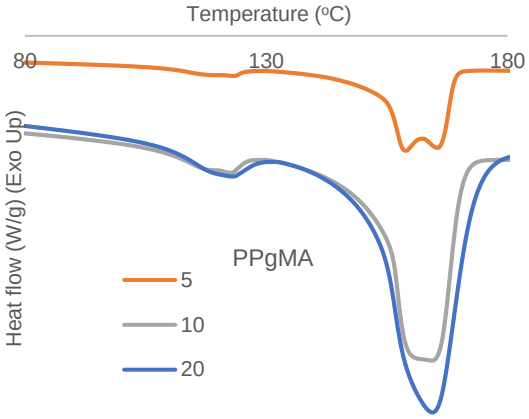

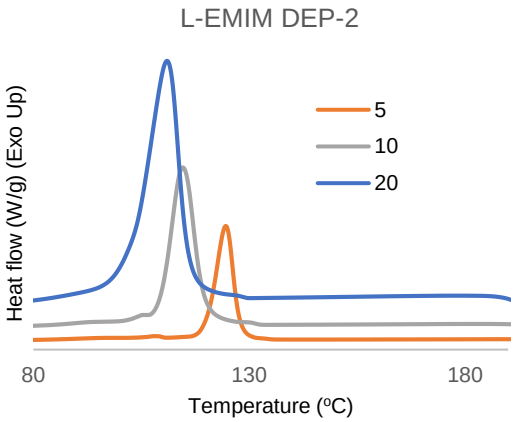

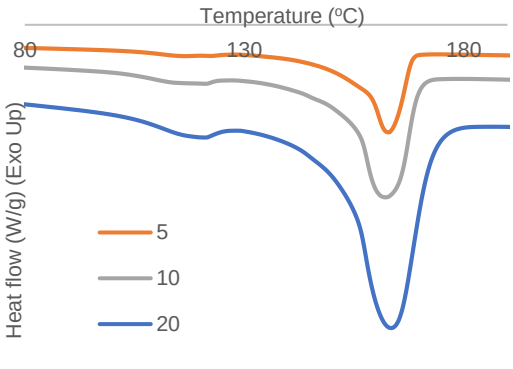

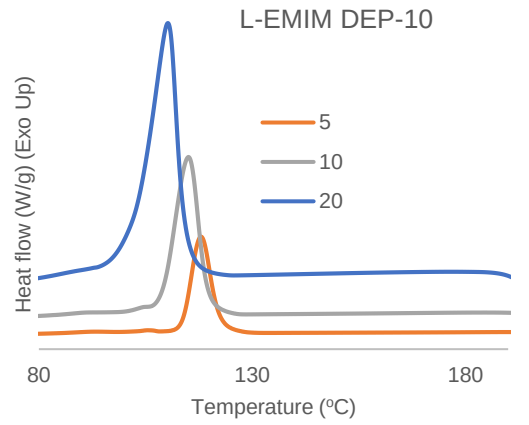

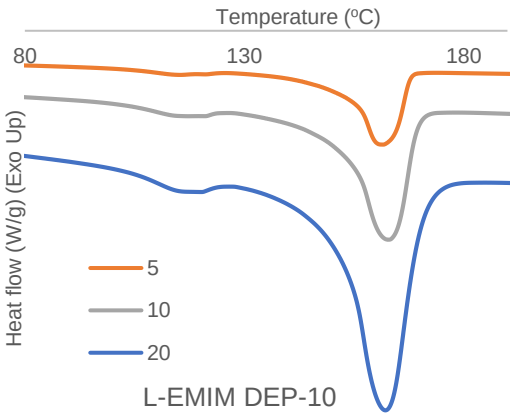

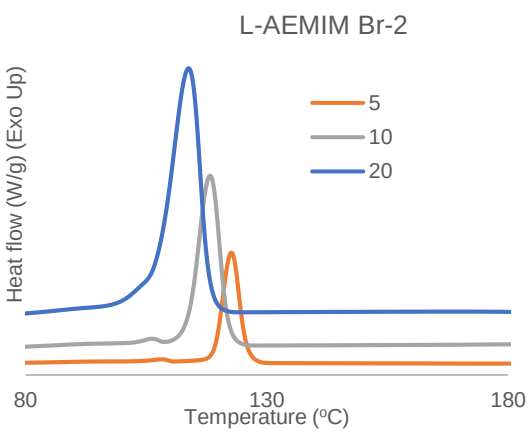

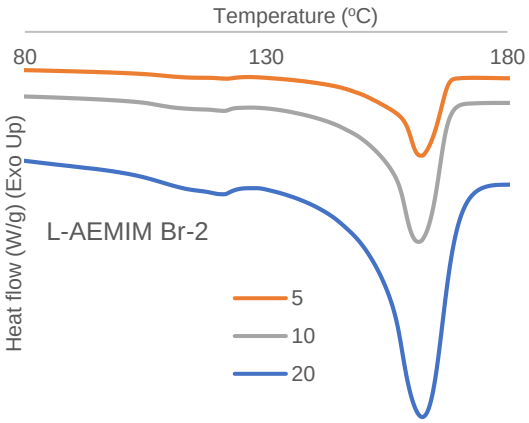

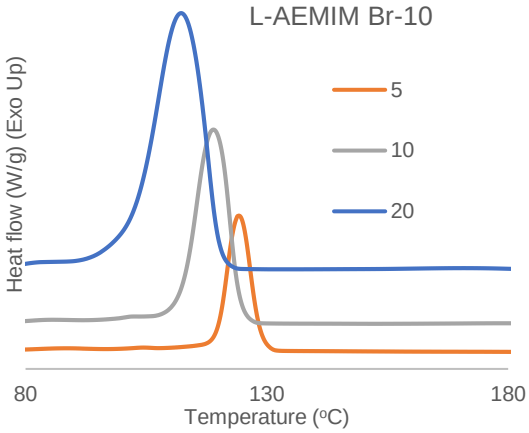

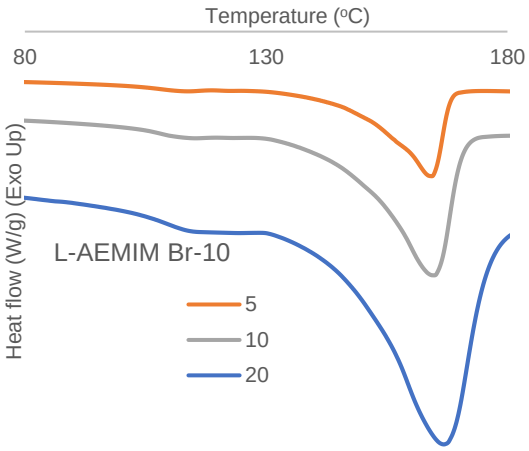

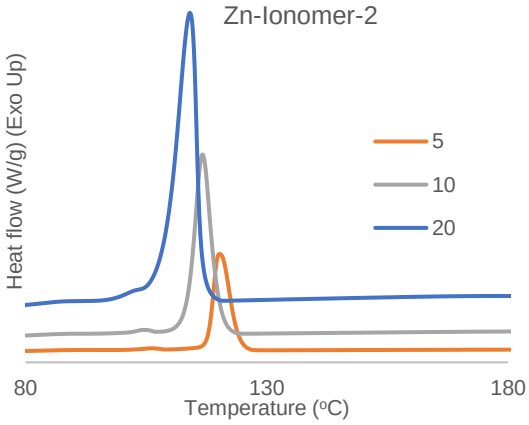

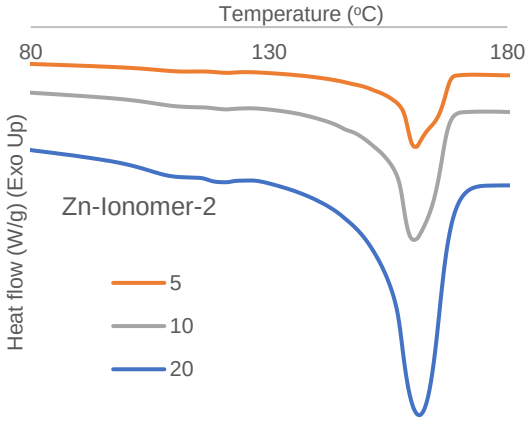

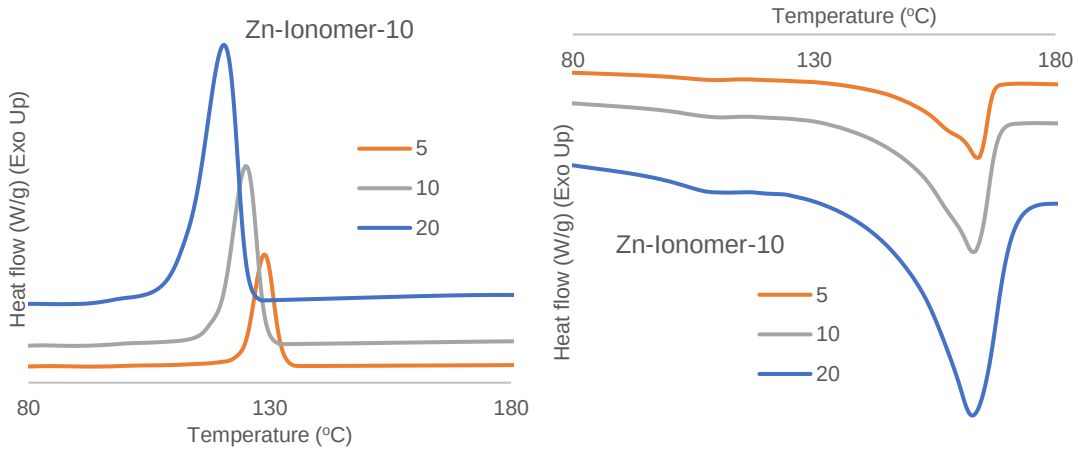

Figure S3- 5 The crystallization and melting curves at different heating and cooling rate run (5, 10, and 20 K·min^{-1}) under nitrogen atmosphere

3. The $ln[-ln(1-Xt)]$ vs lnt plots according to Jeziorny's Non-isothermal crystallization model

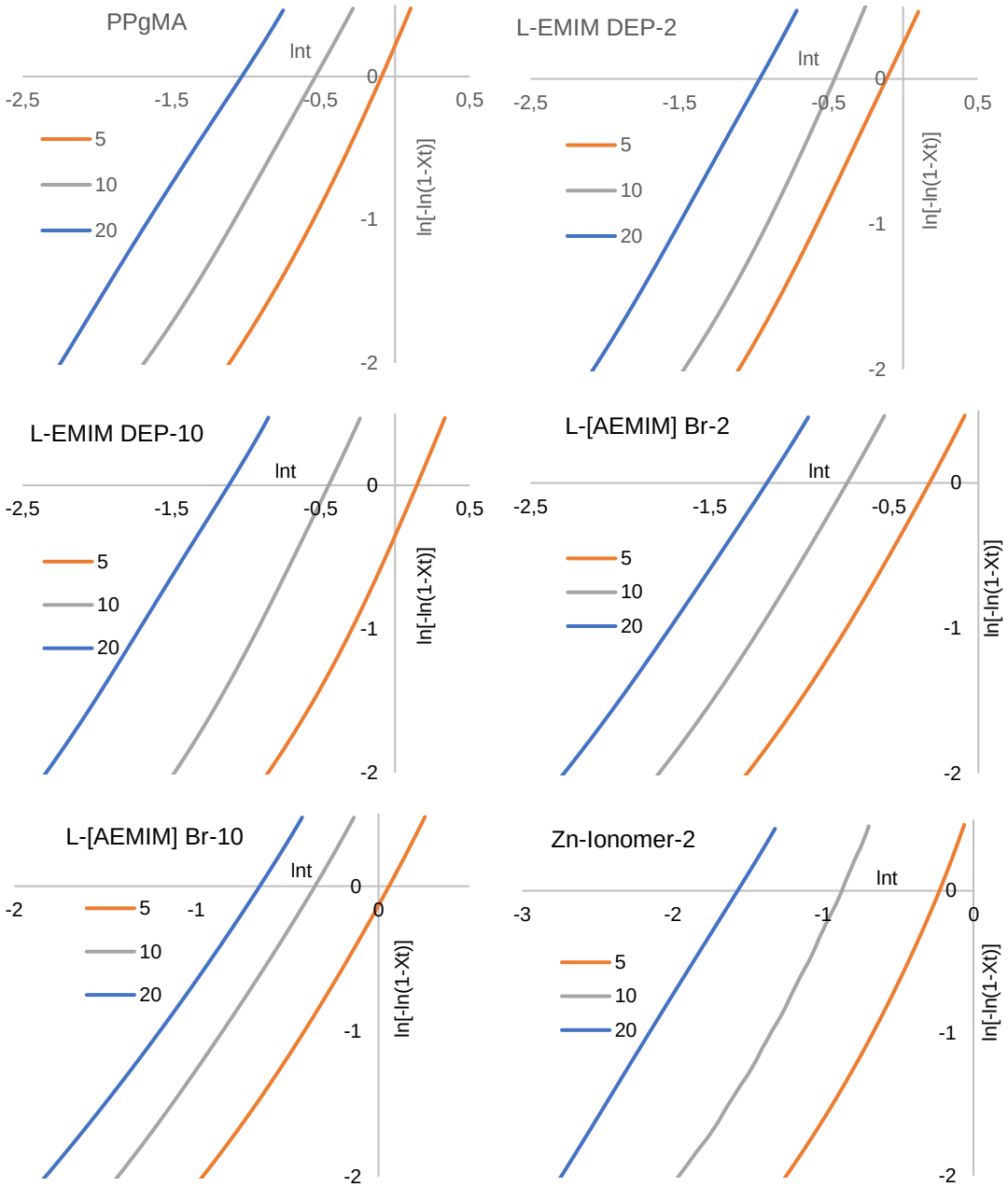

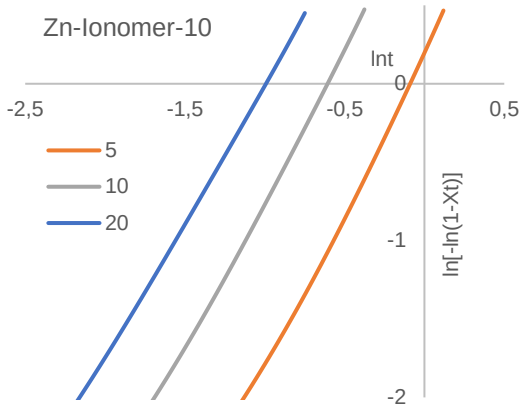

Figure S3- 6 $ln[-ln(1-Xt)]$ vs lnt plots based on Jeziorny's theory for PPgMA and its blends

4. The detailed parameters of non-isothermal crystallization process in accordance with Jeziorny's model

Table S3- 2 The parameters of non-isothermal crystallization process based on Jeziorny's model

Samples	φ	$t_{1/2}$(min)	n	Z_t	T_m(°C)	T_c(°C)	X_c(%)
PPgMA	5	0.77	2.01	1.17	159.0/165.6	116.1	34.1
	10	0.47	1.78	2.68	164.2	114.1	35.5
	20	0.28	1.65	5.55	164.5	109.5	31.6
L-EMIM DEP-2	5	0.72	1.98	1.33	162.9	124.6	36.8
	10	0.50	1.94	2.65	162.3	114.6	34.3
	20	0.31	1.81	5.66	163.4	111.0	33.2
L-EMIM DEP-10	5	0.87	2.04	0.92	161.6	118.0	35.3
	10	0.49	1.85	2.56	162.9	115.1	34.0
	20	0.28	1.69	5.98	162.2	110.2	33.4
L-[AEMIM] Br-2	5	0.64	2.00	0.53	162.2	122.7	36.4
	10	0.40	1.91	1.40	161.7	118.2	35.2
	20	0.25	1.78	2.10	162.5	113.8	34.4
L-[AEMIM] Br-10	5	0.89	2.01	-0.13	164.4	124.2	34.2
	10	0.58	1.89	0.65	164.8	118.9	34.2
	20	0.42	1.74	1.13	166.9	112.3	32.8
Zn-Ionomer-2	5	0.67	2.02	0.43	160.7	120.2	35.8
	10	0.35	1.91	1.64	160.4	116.7	35.4
	20	0.17	1.71	2.68	161.5	114.1	34.6
Zn-Ionomer-10	5	0.76	1.97	0.16	163.9	128.9	38.9
	10	0.45	1.87	1.13	163.0	125.1	38.6
	20	0.30	1.73	1.72	162.7	120.5	37.2

Note: φ: cooling rate (K·min^{-1}), T_m: melting temperature (°C), T_c: crystallization temperature (°C) and X_c: crystallinity (%)

Chapter 4: Fabrication of Maleic Anhydride-grafted Polypropylene containing LIonomers microcellular foaming with supercritical carbon dioxide

Table of contents

Chapter 4: Fabrication of Maleic anhydride-grafted Polypropylene-containing LIonomers microcellular foams with supercritical carbon dioxide

4.1 Introduction

For many years, polypropylene (PP) represents one of the most widely reported and used commercial polymers. Due to these numerous properties such as low density, chemical resistance, low melting point, excellent processability, and chemical resistance, as well as good mechanical performances and low cost, PP is really competitive for the production of foams compared to polystyrene or polyethylene ones [1–4], for a variety of applications ranging from protective equipment, insulation, cushions, damping to absorbers for acoustic and electromagnetic waves [5,6]. In addition, these foamed materials display many advantages including high impact strength, high toughness, high thermal stability, etc. [7–9]. However, the preparation of PP foams is not easy due to two major factors [10,2,11,12]. On the one hand, being a semi-crystalline polymer, the gases do not dissolve in the crystalline zones. Therefore, the control of the cellular structure of PP is more difficult compared to the foaming of an amorphous polymer. Meanwhile, due to the heterogeneity of the semi-crystalline polymer, cell nucleation is heterogeneous. On the other hand, according to the weak melting strength of PP, the cell walls separating cells do not have enough strength to stand the extensional force and several small cells may collapse into a big one during the foaming process.

Many strategies have been conducted to achieve outstanding PP foams, such as polymer blends [13] and composites [14,15]. Blending with polystyrene let improve the cell structure [16], since the second polymer could provide many uniformly dispersed heterogeneous cell nucleation sites favouring the foaming processing. The low activation energy at the interface of high-density polyethylene/PP blends contributes to the occurrence of cell nucleus [17]. Adding fillers (such as clay or $CaCO_3$) [18–21] could

also bring about great improvement of complex viscosity since these additives may act as the crosslinking points limiting the motions of polymer chains, avoiding the collapse of small cells. One other strategy is to use maleic anhydride modified polypropylene (PPgMA), well-known to be the most functionalized PP combining the low cost of maleic anhydride, and the effect of the resulting succinic anhydride part as well as a good processability. According to the literatures [22,23], PPgMA have low molecular weight compared to neat PP but it is the best strategy to improve the compatibility of PP with other polymers. Very recently, our group [24] have developed a new generation of polypropylene-based ionomers, called LIonomers, consisting in an association of Ionic Liquids (ILs) and maleic anhydride-grafted polypropylene. In this study, we have demonstrated a synergistic effect between COO^- groups from PPgMA and the cation or the counter anion of ILs inducing a percolated ionic species phase. Thus, the ion–ion/ion–dipolar interactions lead to a strong shear thinning behavior compared to neat PPgMA. As a consequence, a significant reduction of the chain mobility, resulting in a large increase of the melt viscosity was obtained.

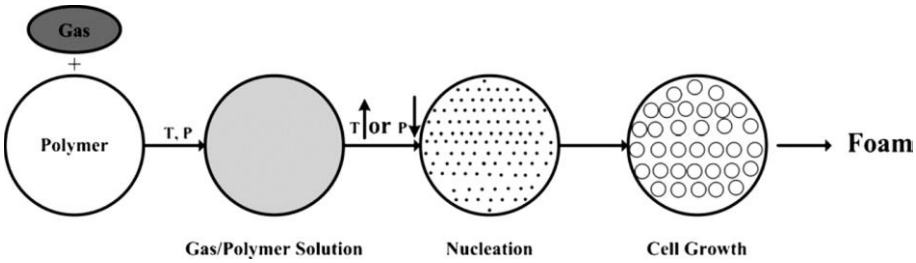

Figure 4- 1 Cellular foaming process

On the other side, supercritical carbon dioxide ($scCO_2$) is considered as the ideal environmentally friendly foaming agent as well as other strong advantages (for example: non-toxic, non-flammable, low price, low critical temperature and pressure) [25–29]. The basic principle of carbon dioxide in supercritical state is to be dissolved into the polymer at high pressure and temperature to form a polymer/CO_2 homogeneous saturated system. Then, by releasing pressure or increasing temperature, a phase separation occurs and triggers the generation as well as the growth of bubble nuclei,

and finally the end shape of the lightweight materials [5,7,9,30–38] (see Figure 4-1 [9]). Here, various LIonomers based on unreactive (imidazolium and phosphonium) or reactive ionic liquids [24,39] will be used in order to generate maleic anhydride-grafted polypropylene-based LIonomers as microcellular foams by using an environmentally friendly approach, *i.e.* using supercritical carbon dioxide as physical foaming agent [40–44]. The morphologies will be analysed in relationship with the mechanical performances under compression that will be investigated.

4.2 Experimental section

4.2.1 Materials

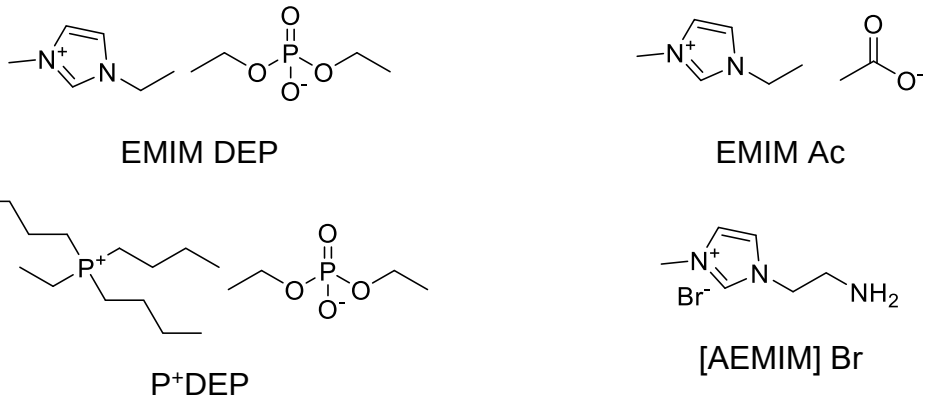

Scheme 4- 1 Chemical structures of ImILs and PhIL used in this study

PPgMA was received from Arkema (1 wt.%, OREVAC® CA 100). Two imidazolium-based ionic liquids (ImILs), *i.e.* 1-Ethyl-3-methylimidazolium acetate (EMIM Ac), 1-ethyl-3-methylimidazolium diethyl phosphate (EMIM DEP), and one phosphonium-based ionic liquid (PhIL), *i.e.* tributyl (ethyl) phosphonium diethyl phosphate (P^+DEP) are supplied from TCI. 1-aminoethyl-3-methylimidazolium bromide ([AEMIM] Br) and zinc acetate are produced by Chemfish Tokyo CO.,LTD and Sigma-Aldrich, respectively. Scheme 4-1 shows the chemical structure of ILs.

4.2.2 LIonomers preparation and characterizations

The PPgMA was dried at 70 ºC for 12 hours. The PPgMA/additive mixtures (10wt%) were blended into a DSM micro extruder at 180 ºC for 5 min and injected in a

mould at 30°C. Then, the specimen are collected at room temperature, the details of all materials are shown in Table 4-1.

Table 4- 1 LIonomers formulations considered in this study

Polymer	Additive	Content (wt%)	Abbreviation
PPgMA	P^+DEP	10	L-P^+DEP-10
	EMIM DEP	10	L-EMIM DEP-10
	EMIM Ac	10	L-EMIM Ac-10
	[AEMIM] Br	10	L-[AEMIM] Br-10
	Zinc acetate	10	Zn-Ionomer-10

4.2.3 Foaming under $scCO_2$ and foam characterization

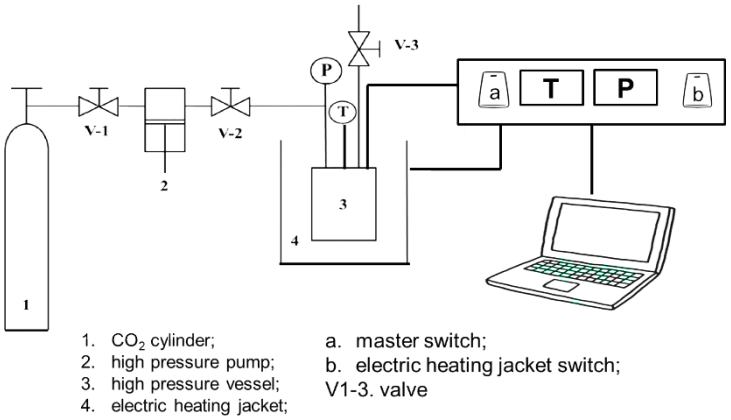

Figure 4- 2 Schematic diagram of $scCO_2$ batch foaming in this present

Batch foaming process (Figure 4-2) was conducted in a high-pressure in a stainless-steel autoclave having an internal volume of 0.3 L. According to the foaming processing conditions described in the literature [45], the sample was: *1)* immersed in $scCO_2$ for one hour at 158 °C ($T_{infiltration}$) and 150 bar ($P_{saturation}$); *2)* decreasing the temperature and pressure to 135 °C ($T_{foaming}$) and 135 bar ($P_{foaming}$), for one hour; *3)* CO_2 was quickly released (> 10bar/s) to induce foam nucleation and growth; *4)* the foamed sample was quickly transferred into liquid nitrogen to stabilize the cell structure. The schematic diagram of batch foaming and whole procedure is shown in Scheme 4-2.

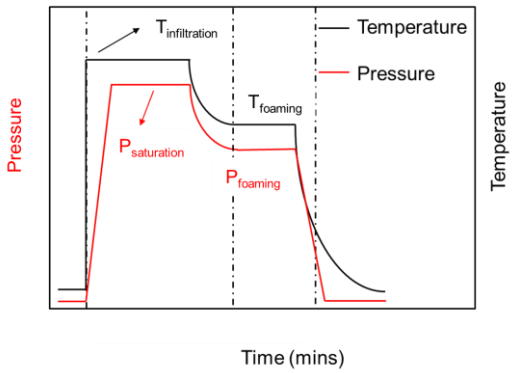

Scheme 4- 2 Batch foaming process ($P_{saturation}$ and $P_{foaming}$: saturation and foaming pressure, $T_{infiltration}$ and $T_{foaming}$: infiltration and foaming temperature) considered in this study

The volume expansion ration, R_V, [46] and porosity [47] of the foamed samples are determined according to Equations 4- 1 and 4- 2:

$$R_V = \frac{p^0}{p'} \quad \text{Equation 4- 1}$$

$$Porosity = 1 - \frac{1}{R_v} \quad \text{Equation 4- 2}$$

where p^0 and p' are the density of the unfoamed and foamed samples respectively. And the value (p') is defined via the drainage method following ASTM D792 (from Equation 4- 3):

$$p' = \frac{a}{a+b-c} \times p_w \quad \text{Equation 4- 3}$$

where p_w is the density of water at the testing temperature, a is the apparent mass of specimen in air without the sinker, while b is the apparent mass of completely immersed sinker (if used). c is apparent mass of specimen and sinker (if used) totally immersed in water.

The cell size and density are determined using scanning electron microscopy (SEM, ZEISS MERLIN COMPACT Munich, Germany). The average cell size is obtained with the help of Image J image analysis. The cell density, N, defined as the number of cells per unit volume with respect to the unfoamed polymer, is determined from Equation 4-4 [48]:

$$N = (\frac{nM^2}{A})^{3/2} R_V \quad \text{Equation 4- 4}$$

where n is the number of cells in the SEM microscopies, M is the magnification factor, and A is the area considered for determination.

The compression behaviours of LIonomers and Zn-Ionomers were determined at room temperature using an Instron machine operating with a sample of 5*5*5 mm^3. Each test has been repeated at least three times with a speed of 1mm·min^{-1}.

4.3 Results and discussion

4.3.1 Foamability of the LIonomers

Using supercritical carbon dioxide ($scCO_2$) as physical foaming agent, all IL/PPgMA combinations whatever the chemical nature of the ILs (as well with the addition of Zn^{2+} Ac) display an improved foamability compared to neat PPgMA. Especially, the LIonomer based on [AEMIM] Br displays the best foamability due to its highest viscosity in the molten state as well as its high absorption capability in supercritical carbon dioxide which could be attributed to the highest solubility of this ionic liquid.

The cell morphologies of LIonomers evaluated from SEM, and expansion ratio, average cell diameter as well as cell density are represented in Figures 4-3 and 4-4.

Let's consider the effect of foaming temperature on the resulting morphologies. The increase of foaming temperature leads to increase the average cell diameter and expansion ratio, and to decrease of cell density. The decrease of cell density and the increase of cell diameter can be associated to the collapse of small cells at higher foaming temperature [9,45,49,50].

Whatever the nature of additives added to PPgMA, *i.e.* ILs or Zn^{2+} Ac, the improved uniformity of cellular morphology, more homogeneous cell size and foam density are observed. These morphologies are linked to the high melt strength of the IL or Zn^{2+} Ac modified PPgMA systems. In fact, the high molten viscosity suppresses cell coalescence and rupture, as well as prevents the generation of higher cell sizes [51–54].

At the same time, during the growth of cells, the molten material undergoes the biaxial extension [55]. Therefore, the enhanced viscosity related to the formation of the PP ionic percolating force within polymer matrix plays the major role for improving foamability.

Regarding to LIonomers based on various ionic liquids, their foaming behavior could differ according to the nature of the ionic liquid. The effect of the ionic liquid relates to the absorption of CO_2 [56–61], since the absorption process of polymer-rich fraction could be completed within few minutes [62]. The strong interactions between CO_2 and [AEMIM] Br and EMIM Ac ILs could explain the high cell density of their LIonomers. As shown in Figure 4-5, the presence of amino group in [AEMIM] Br cation could allow better interactions, *i.e.* higher absorption of carbon dioxide [57–59]. In fact, high CO_2 dissolution could facilitate cell nucleation (and as a consequence, density increases) as it promotes bubble growth as well as vesicle walls extension [63]. Consequently, combination with the improvement of molten viscosity, the L-[AEMIM] Br-10 shows the best foaming performances, *i.e.* the highest cell density, the most uniform cell morphology, as well as the smallest average cell diameter. On the other hand, the LIonomer processed with EMIM Ac displays an interesting high cell density as the generation of the carbene-CO_2 adducts could promote the CO_2-absorption process [60]. Van der Waals force (vdW) may play a key role for the solubility of CO_2 in EMIM DEP [61,64]. However, the alkyl chains of P^+DEP cation account for the higher CO_2 solubilities than that in EMIM DEP with the same anion [56], because it facilitates the capture of more CO_2 molecules. Therefore, the LIonomer processed with P^+DEP displays the highest density morphology compared to EMIM DEP-based LIonomer.

In summary, ILs (P^+DEP, EMIM DEP, EMIM Ac, and [AEMIM] Br) and Zn^{2+} Ac could improve the foaming ability of PPgMA from enhancing their molten viscosity (especially their elongational viscosity) and by acting as nucleation sites. The average cell size is strongly related to the complex viscosity of PPgMA systems, while the density seems to be more dependent on the content of foaming agents as well as the nucleating sites. Compared to the conventional ionomers considering Zn^{2+} Ac as modifier, these ILs

contribute to the absorption of CO_2 increasing the solubility of foaming agents in the PPgMA systems [54,65–69]. Therefore, the final cell morphologies could be tailored from the cation/anion combinations of the considered ILs. The L-[AEMIM] Br-10 displays the higher cell density compared to Zn-Ionomer-10 material.

	PPgMA	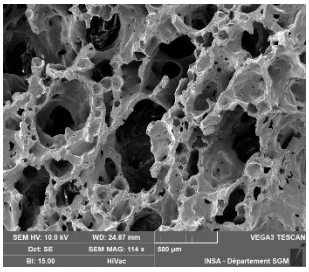	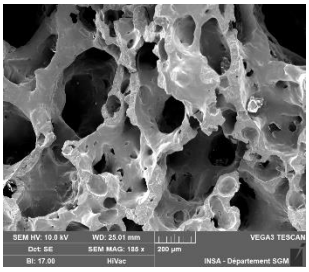
	L-P^{+}DEP-10	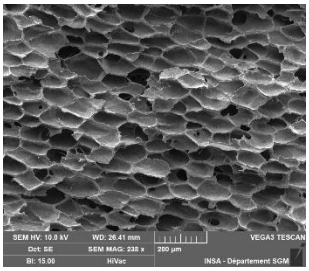	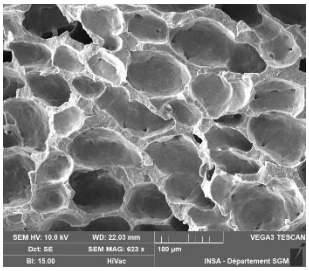
Foaming temperature: 130 °C	L-EMIM DEP-10	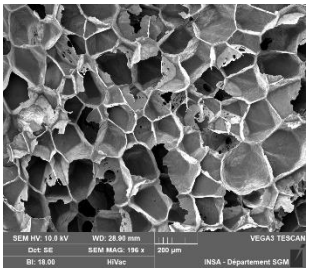	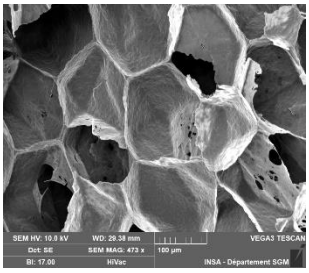
	L-EMIM Ac-10	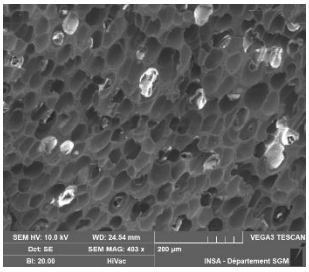	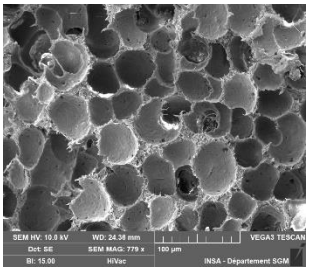
	L-[AEMIM] Br-10	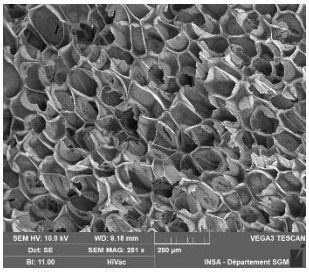	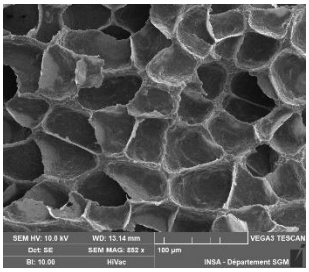

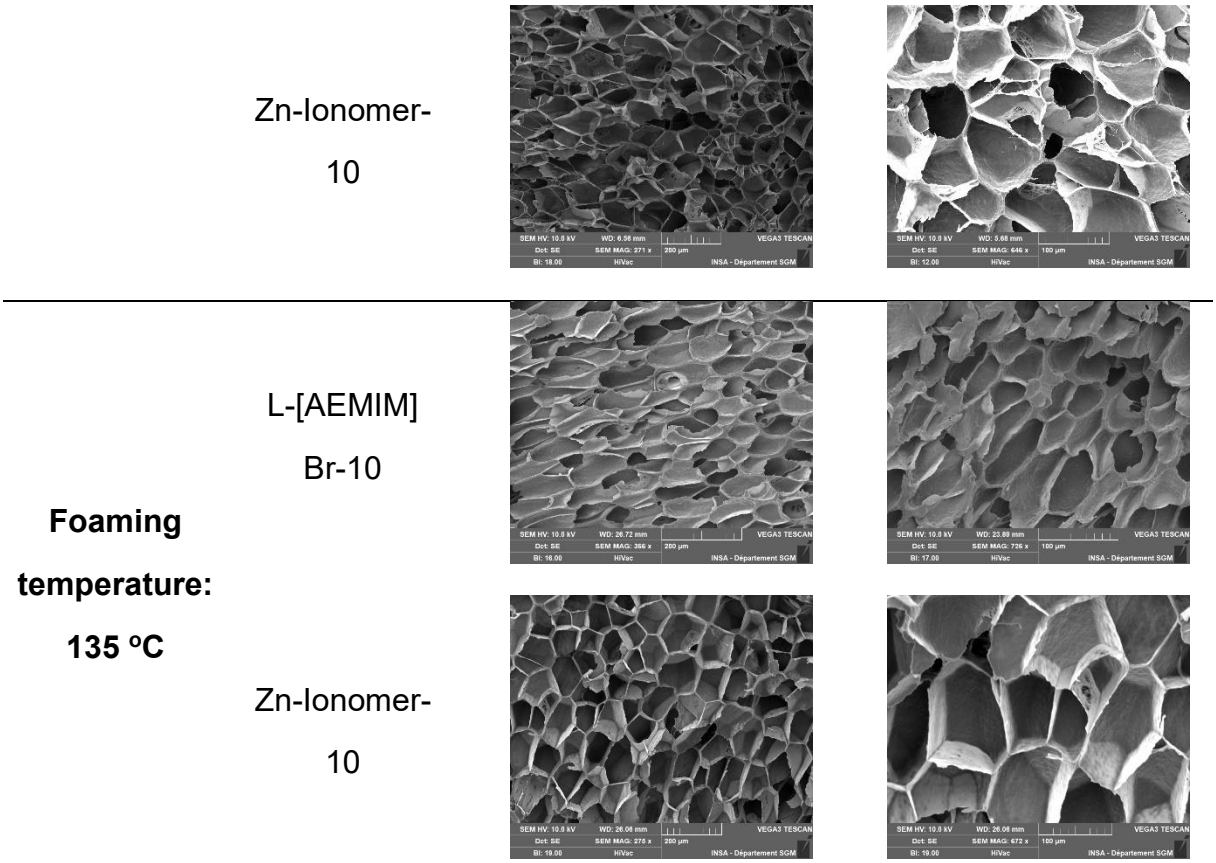

Figure 4- 3 Cell morphologies by Scanning Electron Microscopy (SEM) of PPgMA and LIonomers/Zn-Ionomers foamed materials

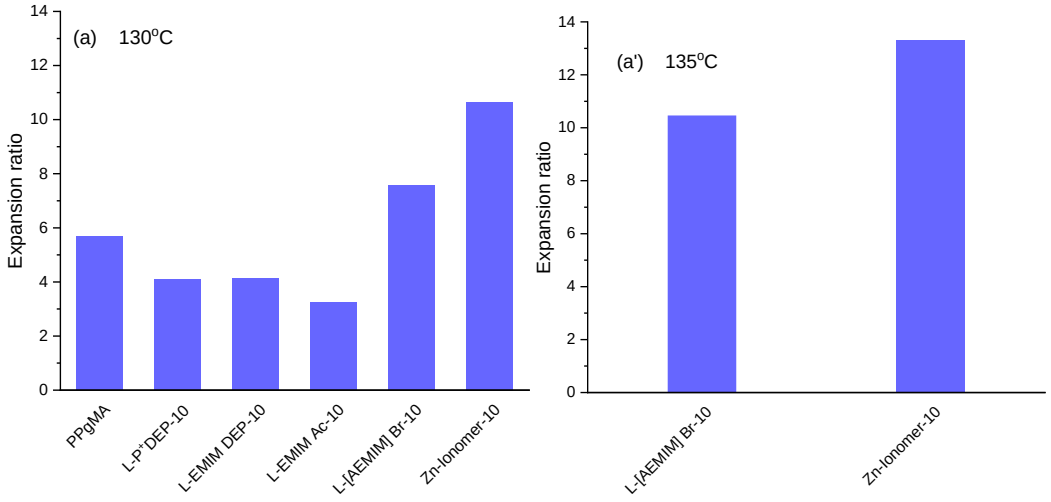

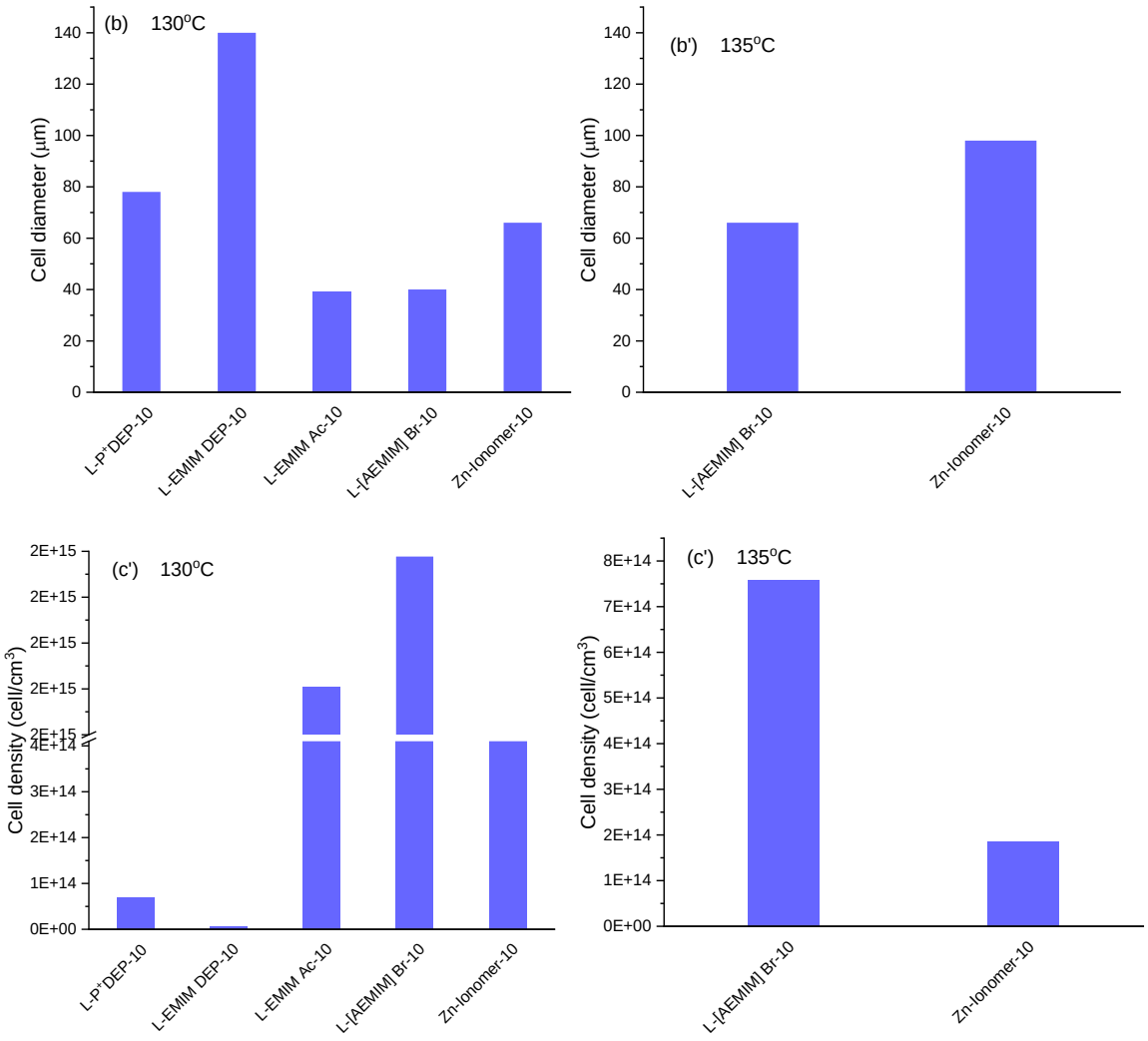

Figure 4- 4 (a) Cell expansion ratio, (b) cell diameter, and (c) cell density of the various foamed materials, *i.e.* PPgMA and related blends (cell diameters and density cannot be obtained for neat PPgMA due to its low foaming ability)

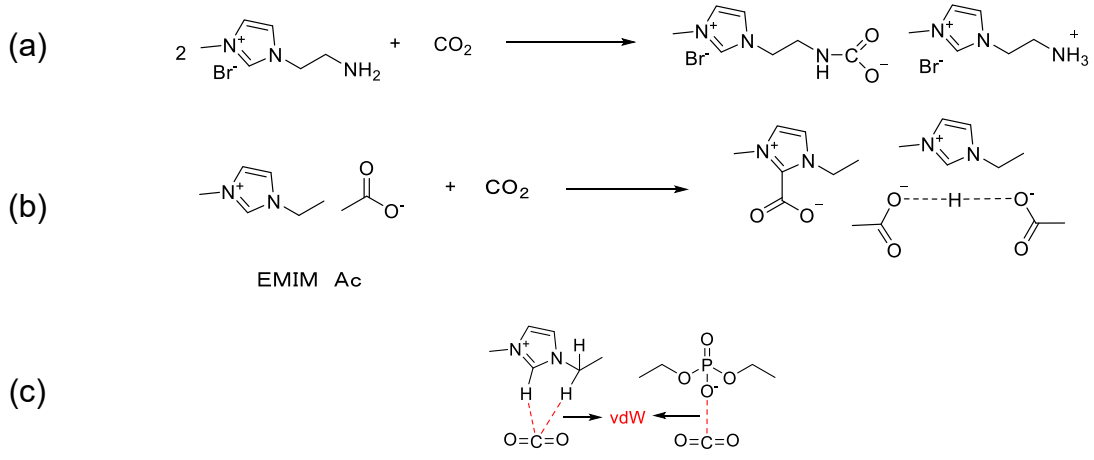

(d)

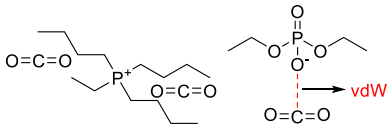

Figure 4- 5 Excepted interactions between ionic liquids and CO_2 (the number of CO_2 molecules close to a P^+DEP cation given as an example)

4.3.2 Compression behaviours of LIonomers foams

In accordance with the Gibson-Ashby's theory, the compression stress strain process can be divided into three stages: linear elastic stage, platform stage, and compressive stage [70,71]. The stage of elasticity phase is mainly govened by three parameters, *i.e.* cell edge bends, intracellular gas compression, and cell wall extension.

As the deformation increases, the foam collapse occurs first on the upper surface and the collapse gradually spreads over the thickness of the specimen. During the plateau phase, the stress remains constant or slightly increases as strain increases. This phase length is strongly associated with the energy absorption capacity of the material. The stress in this period is dependent on ***(a)*** the cell geometry, ***(b)*** the influence of the internal air, and ***(c)*** the stress strength behaviour [72]. As discussed previously, increasing the foaming temperature leads to a change of the cell size, foam density and cell walls thinner. From compressive stress-strain test (see Figure 4-6), the honeycomb cells (resulting from 135 °C) sustain lower compressive stress than the foam displaying the smallest pores (130 °C). Increasing foaming temperature leads to an increase in porosity (see Figure 4-7a) and a decrease in wall thickness, *i.e.* larger cells are produced and compression deformation becomes lesser. As excepted, foams with small cells also exhibit higher compressive strength [73]. For compression behaviour, small cells may exhibit uniform cell shrinkage to withstand external pressure, while the honeycomb cell foam is compacted at the top and slightly contracted at the bottom (see illustration in Figure 4-6a). Further increasing the compressive strain, the small cell size foam exhibits a steeper stress rise (shorter plateau zone), in contrast, the honeycomb foam has a mild compressive stress-strain curve rise (larger plateau

zone) [71]. Such displays increasing the foaming temperature leads to the enhancement of energy absorption capacity. In addition, comparing the compression tests of L-[AEMIM] Br-10 and Zn-Ionomer-10 at the same temperature (130 ºC or 135 ºC), the plateau length of the former is longer than the latter. This observation interprets the potential of L-[AEMIM] Br-10 to offer better vibration damping performance [71]. Furthermore, in contrast to the effective stress transfer and the increased compression resistance thanks to the small cells in the literature [42], herein, the L-[AEMIM] Br-10 displays lower compressive stress than L-P$^+$DEP-10, L-EMIM DEP-10 and L-EMIM Ac-10 at the same strain (see Figure 4-6c). Such observation is due to the low porosity of the later three kinds LIonomers (see Figure 4-7b). Low porosity means fewer compression bubbles, compression deformation becomes harder and therefore the length of the platform stage is shortened and the height in the plateau region becomes higher. Therefore, L-EMIM Ac-10 indicates the highest compressive stress as shown in Figure 4-6c.

At the last stage, the porous materials are compressed significantly and behaves like the solid, therefore the stress rises dramatically.

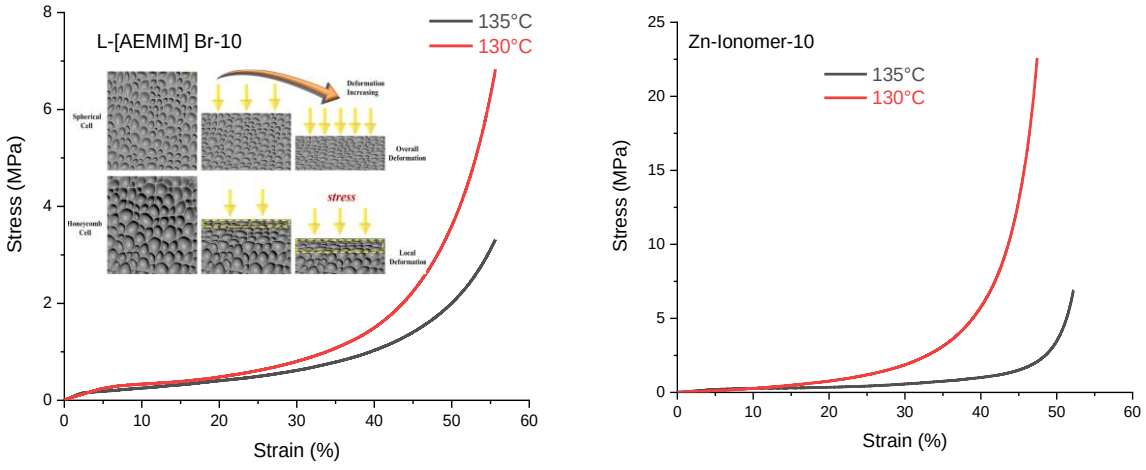

a b

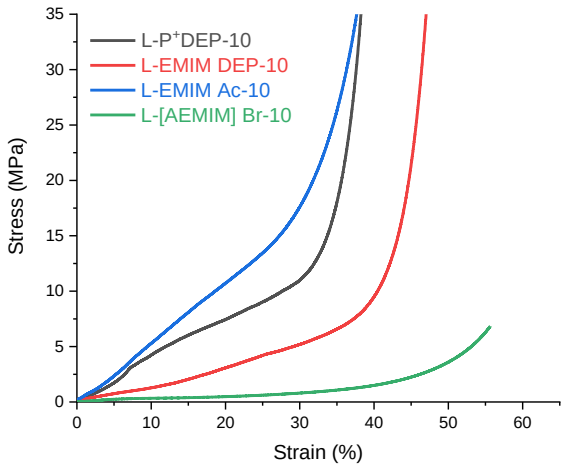

c

Figure 4- 6 Compression stress-strain curves of foamed PPgMA based (strain rate:1 mm·min^{-1}); a (L-[AEMIM] Br-10), b (Zn-Ionomer-10) as a function of foaming temperature, c based on various foamed materials

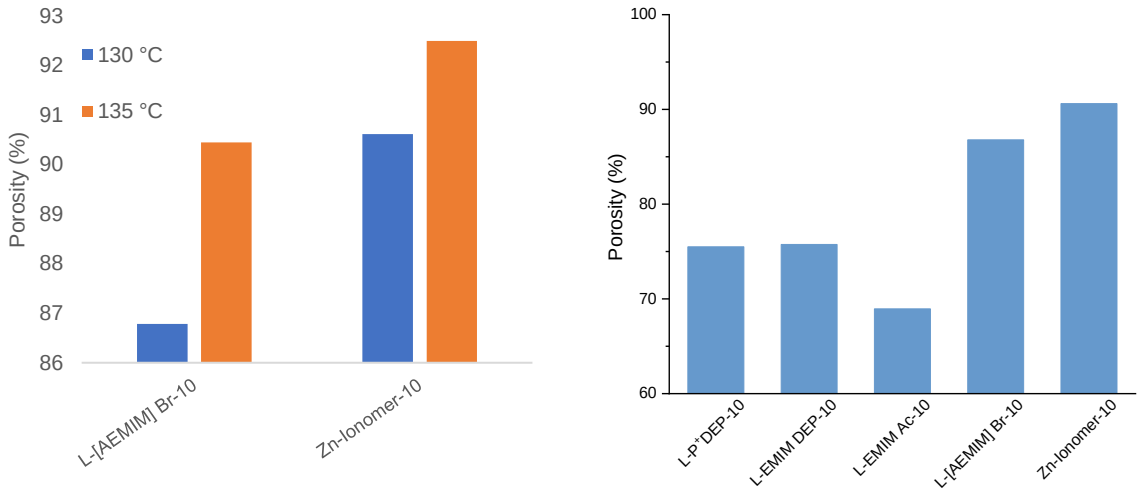

a b

Figure 4- 7 Porosity of foamed samples at different foaming temperatures (a), and for the various blends foamed at 130 ºC (b)

4.4 Conclusions

Based on the conclusions for previous chapters, several LIonomers exhibiting good physical properties have been selected as candidates to produce microcellular foams using supercritical carbon dioxide ($scCO_2$) foaming process which is a friendly

component for such a purpose compared to the industrial existing solutions. The results indicated the foamability of neat PPgMA could be considerably improved by the incorporation of ionic liquids or Zn^{2+} Acetate to form ionic-modified PP. The foaming morphology and compressive behavior vary with the foaming temperature, cation/anion combinations of ionic liquids as well as the additive type (IL or Zn^{2+}Ac). Increasing foaming temperature leads to the increased average cell size, thinner cell wall and seems to reinforce energy absorption capability. While the final cell morphology is very related to the nature of ionic liquids, due to the different CO_2 absorption capability as a result of the cation/anion pairs. The lowest porosity of L-EMIM Ac-10 is the major contributor to its highest compressive stress. While the LIonomers processed with [AEMIM] Br always displays the best vibration damping performance.

4.5 References

[1] Jiang X L, Liu T, Xu Z M, et al. Effects of crystal structure on the foaming of isotactic polypropylene using supercritical carbon dioxide as a foaming agent[J]. The Journal of Supercritical Fluids, 2009, 48(2): 167-175.

[2] Naguib H E, Park C B, Panzer U, et al. Strategies for achieving ultra low-density polypropylene foams[J]. Polymer Engineering & Science, 2002, 42(7): 1481-1492.

[3] Lee S H, Kontopoulou M, Park C B. Effect of nanosilica on the co-continuous morphology of polypropylene/polyolefin elastomer blends[J]. Polymer, 2010, 51(5): 1147-1155.

[4] Lee P C, Kaewmesri W, Wang J, et al. Effect of die geometry on foaming behaviors of high-melt-strength polypropylene with CO_2[J]. Journal of Applied Polymer Science, 2008, 109(5): 3122-3132.

[5] Krause B, Sijbesma H J P, Münüklü P, et al. Bicontinuous nanoporous polymers by carbon dioxide foaming[J]. Macromolecules, 2001, 34(25): 8792-8801.

[6] Doroudiani S, Park C B, Kortschot M T. Effect of the crystallinity and morphology on the microcellular foam structure of semicrystalline polymers[J]. Polymer Engineering & Science, 1996, 36(21): 2645-2662.

[7] Suh K W, Park C P, Maurer M J, et al. Lightweight cellular plastics[J]. Advanced Materials, 2000, 12(23): 1779-1789.

[8] Tomasko D L, Li H, Liu D, et al. A review of CO_2 applications in the processing of polymers[J]. Industrial & Engineering Chemistry Research, 2003, 42(25): 6431-6456.

[9] Xu Z M, Jiang X L, Liu T, et al. Foaming of polypropylene with supercritical carbon dioxide[J]. The Journal of Supercritical Fluids, 2007, 41(2): 299-310.

[10] Fu D, Chen F, Kuang T, et al. Supercritical CO_2 foaming of pressure-induced-flow processed linear polypropylene[J]. Materials & Design, 2016, 93: 509-513.

[11] Naguib H E, Park C B, Reichelt N. Fundamental foaming mechanisms governing the volume expansion of extruded polypropylene foams[J]. Journal of Applied Polymer Science, 2004, 91(4): 2661-2668.

[12] Pop-Iliev R, Rizvi G M, Park C B. The importance of timely polymer sintering while processing polypropylene foams in rotational molding[J]. Polymer Engineering & Science, 2003, 43(1): 40-54.

[13] Li H, Zhang X M, Zhu S Y, et al. Preparation of polypropylene and polystyrene with -NCO and -NH2 functional groups and their applications in polypropylene/polystyrene blends[J]. Polymer Engineering & Science, 2015, 55(3): 614-623.

[14] Kuo C C, Liu L C, Liang W C, et al. Preparation of polypropylene (PP) composite foams with high impact strengths by supercritical carbon dioxide and their feasible evaluation for electronic packages[J]. Composites Part B: Engineering, 2015, 79: 1-5.

[15] Gong W, Yu J, Fu H, et al. Strengthening and toughening mechanisms for polypropylene/glass fiber composite foams under three-phase coexistence[J]. Polimery, 2015, 60(7-8): 457-461.

[16] Huang H X, Xu H. Preparation of microcellular polypropylene/polystyrene blend foams with tunable cell structure[J]. Polymers for Advanced Technologies, 2011, 22: 822-829.

[17] Rachtanapun P, Selke S E M, Matuana L M. Relationship between cell morphology and impact strength of microcellular foamed high-density polyethylene/polypropylene blends[J]. Polymer Engineering and Science, 2004, 44(8): 1551-1560.

[18] Chen L, Sheth H, Kim R. Gas absorption with filled polymer systems[J]. Polymer Engineering & Science, 2001, 41(6): 990-997.

[19] Chen J, Liu T, Yuan W kang, et al. Solubility and diffusivity of CO_2 in polypropylene/micro-calcium carbonate composites[J]. The Journal of Supercritical Fluids, 2013, 77: 33-43.

[20] Nam P H, Maiti P, Okamoto M, et al. Foam processing and cellular structure of polypropylene/clay nanocomposites[J]. Polymer Engineering & Science, 2002, 42(9): 1907-1918.

[21] Zeng C, Han X, Lee L J, et al. Polymer–clay nanocomposite foams prepared using carbon dioxide[J]. Advanced Materials, 2003, 15(20): 1743-1747.

[22] Palacios J K, Sangroniz A, Eguiazabal J I, et al. Tailoring the properties of PP/PA6 nanostructured blends by the addition of nanosilica and compatibilizer agents[J]. European Polymer Journal, 2016, 85: 532-552.

[23] Feng J, Zhang G, MacInnis K, et al. Structure-property relationships of microporous membranes produced by biaxial orientation of compatibilized PP/Nylon 6 blends[J]. Polymer, 2018, 145: 148-156.

[24] Hou L, Livi S, Gérard J F, et al. LIonomers-New generation of ionomer: understanding of their interaction and structuration as a function of the tunability of cation and anion[J]. Polymers, 2023, 15(2): 370.

[25] Watkins J J, McCarthy T J. Polymerization in supercritical fluid-swollen polymers: a new route to polymer blends[J]. Macromolecules, 1994, 27(17): 4845-4847.

[26] Kung E, Lesser A J, McCarthy T J. Morphology and mechanical performance of polystyrene/polyethylene composites prepared in supercritical carbon dioxide[J]. Macromolecules, 1998, 31(13): 4160-4169.

[27] Kumar V, Suh N P. A process for making microcellular thermoplastic parts[J]. Polymer Engineering & Science, 1990, 30(20): 1323-1329.

[28] Arora K A, Lesser A J, McCarthy T J. Synthesis, characterization, and expansion of poly (tetrafluoroethylene-co-hexafluoropropylene)/polystyrene blends processed in supercritical carbon dioxide[J]. Macromolecules, 1999, 32(8): 2562-2568.

[29] Nalawade S P, Picchioni F, Janssen L. Supercritical carbon dioxide as a green solvent for processing polymer melts: Processing aspects and applications[J]. Progress in Polymer Science, 2006, 31(1): 19-43.

[30] Matuana L M, Park C B, Balatinecz J J. Structures and mechanical properties of microcellular foamed polyvinyl chloride[J]. Cellular polymers, 1998, 17(1): 1-16.

[31] Park C B, Behravesh A H, Venter R D. Low density microcellular foam processing in extrusion using CO_2[J]. Polymer Engineering & Science, 1998, 38(11): 1812-1823.

[32] Rodeheaver B A, Colton J S. Open-celled microcellular thermoplastic foam[J]. Polymer Engineering & Science, 2001, 41(3): 380-400.

[33] Reverchon E, Cardea S. Production of controlled polymeric foams by supercritical CO_2[J]. The Journal of Supercritical Fluids, 2007, 40(1): 144-152.

[34] Mills N J, Zhu H X. The high strain compression of closed-cell polymer foams[J]. Journal of the Mechanics and Physics of Solids, 1999, 47(3): 669-695.

[35] Liang M T, Wang C M. Production of engineering plastics foams by supercritical CO_2[J]. Industrial & Engineering Chemistry Research, 2000, 39(12): 4622-4626.

[36] Cooper A I. Recent developments in materials synthesis and processing using supercritical CO_2[J]. Advanced Materials, 2001, 13(14): 1111-1114.

[37] Okamoto M, Nam P H, Maiti P, et al. A house of cards structure in polypropylene/clay nanocomposites under elongational flow[J]. Nano Letters, 2001, 1(6): 295-298.

[38] Jin W, Xingguo C, Mingjun Y, et al. An investigation on the microcellular structure of polystyrene/LCP blends prepared by using supercritical carbon dioxide[J]. Polymer, 2001, 42(19): 8265-8275.

[39] Hou L, Gérard J F, Livi S, et al. Understanding and compressive investigation between conventional and the next generation of ionomers: Zn-Ionomer versus LIonomers[J]. ACS Applied Polymer Materials, 2023(in press).

[40] Bhamidipati M, Scurto A M, Detamore M S. The future of carbon dioxide for polymer processing in tissue engineering[J]. Tissue Engineering Part B: Reviews, 2013, 19(3): 221-232.

[41] White L J, Hutter V, Tai H, et al. The effect of processing variables on morphological and mechanical properties of supercritical CO_2 foamed scaffolds for tissue engineering[J]. Acta biomaterialia, 2012, 8(1): 61-71.

[42] Sheng S J, Hu X, Wang F, et al. Mechanical and thermal property characterization of poly-L-lactide (PLLA) scaffold developed using pressure-controllable green foaming technology[J]. Materials Science and Engineering: C, 2015, 49: 612-622.

[43] Montjovent M O, Mathieu L, Hinz B, et al. Biocompatibility of bioresorbable poly (L-lactic acid) composite scaffolds obtained by supercritical gas foaming with human fetal bone cells[J]. Tissue engineering, 2005, 11(11-12): 1640-1649.

[44] Dlouhá J, Suryanegara L, Yano H. The role of cellulose nanofibres in supercritical foaming of polylactic acid and their effect on the foam morphology[J]. Soft Matter, 2012, 8(33): 8704-8713.

[45] Ding J, Shangguan J, Ma W, et al. Foaming behavior of microcellular foam polypropylene/modified nano calcium carbonate composites[J]. Journal of Applied Polymer Science, 2013, 128(6): 3639-3651.

[46] Hani E. Naguib, Chul B. Park, Patrick C. Lee. Effect of Talc Content on the Volume Expansion Ratio of Extruded PP Foams[J]. Journal of Cellular Plastics, 2003, 39(6): 499-511.

[47] Kwon Y, Cooke R E, Park C. Representative unit-cell models for open-cell metal foams with or without elastic filler[J]. Materials Science and Engineering: A, 2003, 343: 63-70.

[48] Wang X, Max R Salick, Guo Y, et al. Interconnected porous poly(ε-caprolactone) tissue engineering scaffolds fabricated by microcellular injection molding[J]. Journal of Cellular Plastics, 2018, 54(2): 379-397.

[49] Corre Y M, Maazouz A, Duchet J, et al. Batch foaming of chain extended PLA with supercritical CO_2: Influence of the rheological properties and the process parameters on the cellular structure[J]. The Journal of Supercritical Fluids, 2011, 58(1): 177-188.

[50] Li Y, Yao Z, Chen Z hua, et al. Numerical simulation of polypropylene foaming process assisted by carbon dioxide: Bubble growth dynamics and stability[J]. Chemical Engineering Science, 2011, 66(16): 3656-3665.

[51] Zhai W, Wang H, Yu J, et al. Cell coalescence suppressed by crosslinking structure in polypropylene microcellular foaming[J]. Polymer Engineering & Science, 2008, 48(7): 1312-1321.

[52] Zheng W G, Lee Y H, Park C B. Use of nanoparticles for improving the foaming

behaviors of linear PP[J]. Journal of Applied Polymer Science, 2010, 117(5): 2972-2979.

[53] Park C B, Cheung L K. A study of cell nucleation in the extrusion of polypropylene foams[J]. Polymer Engineering & Science, 1997, 37(1): 1-10.

[54] Huang H X, Wang J K. Improving polypropylene microcellular foaming through blending and the addition of nano-calcium carbonate[J]. Journal of Applied Polymer Science, 2007, 106(1): 505-513.

[55] Arefmanesh A, Advani S G. Diffusion-induced growth of a gas bubble in a viscoelastic fluid[J]. Rheologica Acta, 1991, 30(3): 274-283.

[56] Mejía I, Stanley K, Canales R, et al. On the High-Pressure Solubilities of Carbon Dioxide in Several Ionic Liquids[J]. Journal of Chemical & Engineering Data, 2013, 58(9): 2642-2653.

[57] Sistla Y S, Khanna A. CO_2 absorption studies in amino acid-anion based ionic liquids[J]. Chemical Engineering Journal, 2015, 273: 268-276.

[58] Said R B, Kolle J M, Essalah K, et al. A Unified Approach to CO_2 –Amine Reaction Mechanisms[J]. ACS Omega, 2020, 5(40): 26125-26133.

[59] Huang Z. Study on Supported Triamino-functionalized Ionic Liquids for Carbon Dioxide Capture[D]. Schulich School of Engineering, 2021.

[60] Chen F F, Huang K, Fan J P, et al. Chemical solvent in chemical solvent: A class of hybrid materials for effective capture of CO_2[J]. AIChE Journal, 2018, 64(2): 632-639.

[61] Zhu R, Huang S, Gui C, et al. Capturing low-carbon alcohols from CO_2 gas with ionic liquids[J]. Chemical Engineering Science, 2022, 258: 117745.

[62] Wang J, Petit C, Zhang X, et al. Simultaneous measurement of CO_2 sorption and swelling of phosphate-based ionic liquid[J]. Green Energy & Environment, 2016, 1(3): 258-265.

[63] Low B T, Xiao Y, Chung T S, et al. Simultaneous occurrence of chemical grafting, cross-linking, and etching on the surface of polyimide membranes and their impact on

H_2 /CO_2 separation[J]. Macromolecules, 2008, 41(4): 1297-1309.

[64] Park Y. Specific interactions between phosphorus compounds and carbon dioxide: Ab initio approach[J]. The Journal of Supercritical Fluids, 2005, 36(2): 154-159.

[65] Li Y, Yao Z, Chen Z hua, et al. High melt strength polypropylene by ionic modification: Preparation, rheological properties and foaming behaviors[J]. Polymer, 2015, 70: 207-214.

[66] Jiang X L, Bao J B, Liu T, et al. Microcellular foaming of polypropylene/clay nanocomposites with supercritical carbon dioxide[J]. Journal of Cellular Plastics, 2009, 45(6): 515-538.

[67] Yu K, Jiang H, Zhou H, et al. Evolution of double crystal melting peak in polypropylene foam assisted by β-nucleating agent and supercritical CO_2[J]. Journal of Applied Polymer Science, 2018, 135(12): 46007.

[68] Livi S, Pham T N, Gérard J F, et al. Supercritical CO_2–ionic liquids: Green combination for preparing foams[J]. Chemical Engineering Journal, 2014, 240: 534-540.

[69] Livi S, C. Lins L, Sar G, et al. Supercritical CO_2 –Ionic Liquids: A Successful Wedding To Prepare Biopolymer Foams[J]. ACS Sustainable Chemistry & Engineering, 2016, 4(2): 461-470.

[70] Gibson L J, Ashby M F. Cellular solids: Structure and properties[M]. 2nd ed. Cambridge: Cambridge University Press, 1997.

[71] Song P, Zhang Y, Luo Y, et al. Design of lightweight silicone rubber foam for outstanding deformation recoverability based on supercritical CO_2 foaming technology[J]. Journal of Materials Science, 2022, 57(3): 2292-2304.

[72] Reglero Ruiz J A, Viot P, Dumon M. Microcellular foaming of polymethylmethacrylate in a batch supercritical CO_2 process: Effect of microstructure on compression behavior[J]. Journal of Applied Polymer Science, 2010, 118(1): 320-331.

[73] Ameli A, Nofar M, Wang S, et al. Lightweight polypropylene/stainless-steel fiber

composite foams with low percolation for efficient electromagnetic interference shielding[J]. ACS Applied Materials & Interfaces, 2014, 6(14): 11091-11100.

Chapter 5: Conclusions and Perspectives

This work aims to design new generation of ionomers (denoted LIonomers) for innovative foams. Based on this purpose, different ionic liquids (ILs) have been introduced into polypropylene grafted maleic anhydride (PPgMA) to realize the designing of LIonomers for the first time. Then several of them have been selected to foam using supercritical carbon dioxide ($scCO_2$) as the physical agent.

In the first experiment section, four tributyl phosphonium-based and four imidazolium-based ionic liquids are cooperated with PPgMA with different content. Based on their steric hindrance and reactivity with maleic anhydride group of polymer backbone, three LIonomers processed with tributyl (ethyl) phosphonium diethyl phosphate (P^+DEP), 1-ethyl-3-methylimidazolium diethyl phosphate (EMIM DEP) and 1-ethyl-3-methylimidazolium acetate (EMIM Ac) exhibit relatively good characteristics. This chapter demonstrates that grafted maleic anhydride is present as a 'head group' on the polypropylene backbone and that binding to ionic liquid pairs can lead to the formation of new nanostructures by generated ionic and polar interactions. Different morphologies can be devised, ranging from single (nano)-scale structures resulting from phase separation, such as the distribution of LIonomers composed of P^+DEP, to multi-scale structures, such as the use of EMIM DEP and EMIM Ac that bind ionophores and IL-rich separated phases. The smaller size of the isolated IL-rich phase makes it easier to establish stronger IL/polymer interactions. The binding of the imidazole cation to the acetate anion appears to be the most relevant IL to favor the interaction with the maleic anhydride group grafted onto the polymer backbone. The physical properties in both the molten and solid states appear to be strongly influenced by these interactions and ionic networks within polymer/ILs blends. Indeed, the increase in complex viscosity highlights the presence of IL/polymer interactions and the ability to form ionic networks in this case. In relation to their morphology, crystallinity and the presence of infiltrated ionic phases, LIonomers show better Young's modulus and the ability to withstand large strains prior to fracture.

In the second section, one functional imidazolium-based ionic liquid (1-aminoethyl-3-methylimidazolium Bromide ([AEMIM] Br)) has been used to prepare 2.0 generation of ionomer via the chemical reaction between terminated amino group of ionic liquid and the maleic anhydride group on the substrate backbone. The generated imide structure shows more stronger than the interactions within LIonomers prepared in the previous chapter. Such new group could act as the “head” of the new formed "liquid-like branches" while the cation/anion combination through its initial interactions as components. The reactivity of this amino functionalized IL enhances the compatibility with the PPgMA matrix and as a result dispersion, better than other LIonomers obtained previously. In addition, the value of complex viscosity (η^*) shows the following sequence: L-[AEMIM] Br-10 > L-EMIM Ac-10 > L-EMIM DEP-10, which reveals the interaction strength between polar group in PPgMA and various ILs at high temperature, and the ability to generate continuous ionic-network contributing to the molten viscosity. All ionic liquids prefer to be located in the amorphous phase, particularly in the rigid amorphous fraction (RAF) resulting in significantly promoted relaxation value. Comparing to the effect on PPgMA substrate caused by Zn^{2+} Acetate within traditional Zn-Ionomer, such ionic liquids combinations of ionic liquids could not only create β-phase crystalline but also realize an excellent compromise of stiffness and stretchability.

In the third part of this work, several LIonomers exhibiting outstanding performance (especially with high molten strength) have been chosen to foam considering supercritical carbon dioxide (CO_2) as the physical agent. The results indicate the foamability of pure PPgMA has been improved considerably by the addition of ionic liquid or Zn^{2+} Acetate. The foaming morphology and compressive behaviour vary with the foaming temperature and the change of cation or anion of ionic liquids, or additive kind (ionic liquid or Zn^{2+}Ac). Increasing foaming temperature seems to benefits to the energy absorption capability thanks to the enhanced porosity and cell size. Since the cation/anion combinations lead to different CO_2 uptake capacities, the final cell morphology is closely related to the nature of the ionic liquid. The lowest

porosity of L-EMIM Ac-10 is mainly responsible for its highest compressive stress. Whereas LIonomers treated with [AEMIM] Br consistently showed the best vibration damping properties.

Although we have achieved some progresses on the designing and tailoring of LIonomers-new generation of ionomers combining ILs and polypropylene grafted maleic anhydride, as well as the foaming parameters. In order to further deepen and broaden this newly developed topic, it should also be interesting and urgent to continue and complete this dissertation work along different directions.

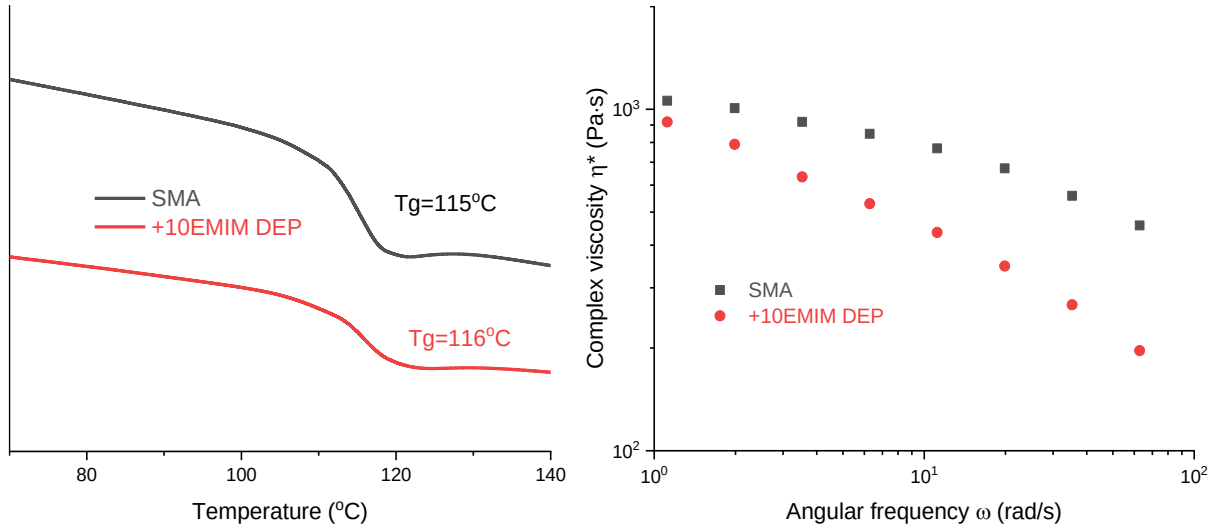

(a) (b)

Figure 5-1 Effect of EMIM DEP on the glass transition temperature (a) and rheology property (b) of SMA

(1) The emphasis of this thesis is the basic investigation of interactions and structurations effect mechanism of ILs on the polymer matrix, which is, of course, not the destination of the development of functional IL-based polymer composite materials. The understanding of their interaction and structuration as a function of the tunability of cation and anion combinations have been studied deeply. The cooperation of the class of ionic liquids should be adjusted according to desired properties of LIonomers. For example, 1-ethyl-3-methylimidazolium acetate (EMIM Ac) or 1-ethyl-3-methylimidazolium diethyl phosphate (EMIM DEP) may be applied when considering the compromise between stiffness and stretch-ability, while introducing 1-aminoethyl-

3-methylimidazolium Bromide when high modulus and molten strength are required. In addition, EMIM DEP has been proved a slight effect on SMA property (see Figure 5-1). Therefore, the applicability of these three ionic liquids in different matrices (for example, PEgMA, SMA, ABS-g-MA, SAN-g-MA, EVA-g-MA) or in the polymer/filler blends as well as polymer blends needs to be further considered.

(2) Facing with the desiring functional property, for instance hydrophobic surface, the combinations of different ionic liquids may be considered if the strong interactions could not be obtained between maleic anhydride with one lonely fluorinated Ionic liquid (like 1-butyl-3-methylimidazolium tetrafluoroborate, 1-butyl-3-methylimidazolium hexafluorophosphate).

(3) Developing new ionic liquids to broaden the LIonomers. Trying to design/synthesize the ionic liquid that each one could interact with two or more polymer groups in the polymer backbone, so that the stronger interaction strength between cation/anion combinations of ionic liquids and polar groups from polymer backbone could be realized to tune the final performances of LIonomers. In addition, the new generation of ionic liquids containing metal ions may be also considered.

(4) The absorption ability of ionic liquids on CO_2 should be further investigated, especially at high temperature and pressure. Because such ability is very related to the final property of prepared lightweight materials.

FOLIO ADMINISTRATIF

THESE DE L'INSA LYON, MEMBRE DE L'UNIVERSITE DE LYON

NOM : HOU
(avec précision du nom de jeune fille, le cas échéant)

DATE de SOUTENANCE : 19/07/2023

Prénoms : Liutong

TITRE : **Design of polymer materials for innovative foams**

NATURE : Doctorat

Numéro d'ordre : 2023ISAL0052

Ecole doctorale : ED34 (Matériaux de Lyon)

Spécialité : Matériaux Polymères et Composites

RESUME : En combinant le polypropylène greffé et les liquides ioniques (ILs), la nouvelle génération d'ionomères (appelés LIonomères) a été conçue et adaptée dans ce travail. Les LIonomères possédant les meilleures propriétés sont ensuite utilisés pour préparer des matériaux légers en utilisant le dioxyde de carbone supercritique ($scCO_2$) comme agent physique. Une série de LIonomères avec différentes structures sont préparés via le réglage des teneurs en anhydride maléique (MA) et la nature des ILs, la dispersion du ILs, et la longueur des "branches liquides" s'assemblant à partir des paires de cations/anions des ILs réactifs. La versatilité de la nature de l'IL sur les propriétés des LIonomères est mise en évidence et comparée à l'Ionomère de Zn conventionnel. Les spectroscopies RMN et FTIR sont utilisées et révèlent l'existence d'interactions ioniques-polaires/ioniques et/ou la création de liaisons chimiques en fonction de la nature chimique des ILs. Les propriétés rhéologiques mettent en évidence la présence de telles interactions entre les LIonomères à base des ILs, similaires aux interactions au sein des Zn-Ionomères traditionnels. Ces interactions et distributions multiples peuvent également influencer la dynamique moléculaire, en particulier dans la phase amorphe rigide. Grâce à l'existence d'interactions entre l'MA et les ILs et à la génération d'une forme β-cristalline ainsi que de diverses morphologies riches en ions, les LIonomères permettent d'obtenir un compromis exceptionnel entre rigidité et extensibilité. En considérant le CO_2 comme agent physique, la moussabilité du PPgMA pur a été considérablement améliorée grâce aux réseaux ioniques par la coopération des ILs ou $Zn^{2+}Ac$. La morphologie de la mousse et le comportement à la compression varient en fonction des combinaisons cation/anion des liquides ioniques ainsi que du type d'additif. Ces résultats offrent de nouvelles perspectives pour la conception de la génération 2.0 d'ionomères qui peuvent être utilisés dans des applications de moussage avec l'aide du CO_2.

MOTS-CLÉS : LIonomères, liquides ioniques, anhydride maléique greffé sur du polypropylène, mousses microcellulaires, CO_2 supercritique

Laboratoire (s) de recherche : Ingenierie des Matériaux Polyméres - UMR 5223

Directeur de thèse : DUCHET-RUMEAU Jannick
Co-directeur de thèse : GÉRARD Jean-François, LIVI Sébastien

Président de jury :

Composition du jury :
Prof. KOTEK Jiri ; Prof. NANNI Francesca ; Dr. LEROY Eric ; Prof. DUCHET-RUMEAU Jannick ; Prof. GÉRARD Jean-François ; Prof. LIVI Sébastien